UTS UNIVERSITY OF TECHNOLOGY SYDNEY

The Roles Played by Acetylcholine in Cardiac Regeneration

Subtitle- Insights from 3D modeling of the heart: exploring acetylcholine and cardiovascular disease scenarios

by Clara Liu Chung Ming

Thesis submitted in fulfilment of the requirements for the degree of

DOCTOR OF PHILOSOPHY

under the supervision of Dr Carmine Gentile, Professor Joanne, A/Prof Kristine McGrath, Professor Jeremy Crook, A/Prof Sean Lal and A/Prof Xiaowei Wang

University of Technology Sydney
Faculty of Engineering and IT

June 2024

CERTIFICATE OF ORIGINAL AUTHORSHIP

I, Clara Liu Chung Ming, declare that this thesis is submitted in fulfillment of the requirements for the award of Doctor of Philosophy in the School of Biomedical Engineering at the University of Technology Sydney.

This thesis is wholly my own work unless otherwise referenced or acknowledged. In addition, I certify that all information sources and literature used are indicated in the thesis.

This document has not been submitted for qualifications at any other academic institution

This research is supported by the Australian Government Research Training Program.

Signature: Production Note:
Signature removed prior to publication.

Date: 3/03/24

Acknowledgments

The author wishes to extend heartfelt gratitude to all those who contributed their support, time, and resources to make this PhD journey possible. This acknowledgment encompasses a wide array of contributors including donors (for blood donors and heart tissue donors), formal and informal reviewers, and the dedicated staff at UTS who facilitated every step of this academic endeavor. Each of you played a pivotal role in bringing this research to fruition; I am profoundly thankful for that.

Supervisory Teams

Principal supervisor: Dr Carmine Gentile, Senior lecturer at the University of Technology (School of Biomedical Engineering/Faculty of Engineering and IT) and affiliated with the Heart Research Institute

Co-supervisors: A/Prof Kristine McGrath (University of Technology Sydney, Faculty of Science)

External supervisors: A/Prof Sean Lal (University of Sydney), Professor Jeremy Crook (University of Sydney/ University of Wollongong), A/Prof Xiaowei Wang (Baker Heart and Diabetes Institute/ The University of Melbourne/Monash University), Professor Joanne Tipper (RMIT)

Declarations of the candidate

This thesis follows the format of a thesis by compilation. It includes content that the candidate has either already published or is currently undergoing peer review. As an introduction to each publication that is part of this thesis, the candidate has written an original summary paragraph that was not submitted or published elsewhere. Following each summary paragraph, the published article (or manuscript under review) is inserted in total (as published or submitted) without any modifications. Any accompanying materials related to the published work, including Supplementary Materials, Figures, and Videos, are included right after the respective article, either embedded directly or through hyperlinks that connect to the original files submitted alongside the manuscripts for the review process.

The following declarations of the candidate have been agreed with the candidate's PhD supervisor regarding the contribution made by the candidate:

The candidate wrote the following chapters to introduce and discuss the thesis. The content included in Chapters 1.2, 1.3 and 2.2 has been published, whereas the one in Chapters 1.4, 2.3, 3.2 and 3.3 are under review.

It is important to note that the content listed below may be similar to the ones present in published articles by the candidate:

- Part 1 – Thesis introduction, hypothesis and aims (Chapter 1.1), Closing remarks Part 1 (Chapter 1.5)
- Part 2 – Introduction and Relevance (Chapter 2.1), Closing Remarks Part 2 (Chapter 2.4)
- Part 3 – Introduction and Relevance (Chapter 3.1), Closing Remarks Part 3 (Chapter 3.4)
- Part 4 – Introduction and Relevance (Chapter 4.1), Thesis discussion (Chapter 4.2), Future

directions (Chapter 4.3), Thesis conclusion (Chapter 4.4), Thesis take-home message (Chapter 4.5)

Candidate contribution statements for each of these published/under review chapters are as follows:

1.2 – Considerations for Advanced Cardiac Models to Study Preeclampsia and Other Cardiovascular Diseases

Published article: **Liu Chung Ming, C.**, Sesperez, K., Ben-Sefer, E., Arpon, D., McGrath, K., McClements, L., and Gentile, C. **Considerations for Advanced Cardiac Models to Study Preeclampsia and Other Cardiovascular Diseases** (*Cells*: IF: 4.829).

Link: https://www.mdpi.com/2073-4409/10/4/899

Contribution: As the first author, the candidate researched this narrative review article and wrote the original draft alongside Kimberley Sesperez and Eitan Ben-Sefer. Her contribution to the paper was to write the introduction, cardiovascular models to mimic ischemic-reperfusion injury part, the tables, discussion and conclusion. The candidate worked on all revised drafts under the supervision of Carmine Gentile and Lana McClements.

1.3 - Stem Cell-based 3D Bioprinting for Cardiovascular Tissue Regeneration, Advanced Technologies in Cardiovascular Bioengineering

Published book chapter: **Liu Chung Ming, C.**, Ben-Sefer, E., and Gentile, C. **Stem Cell-based 3D Bioprinting for Cardiovascular Tissue Regeneration,** Advanced Technologies in Cardiovascular Bioengineering (Springer: IF: 2.495).

Link: https://link.springer.com/chapter/10.1007/978-3-030-86140-7_13

Contribution: As the first author, the candidate researched this narrative book chapter and wrote the introduction, cardiovascular regeneration using cell approaches, cell-free approaches, 3D bioprinting of heart tissue's section and discussion section. Clara Liu Chung Ming did all the schematic figures and worked on all revised drafts under the supervision of her supervisor, Carmine Gentile.

1.4 - Protective Role of Acetylcholine and the Cholinergic System in the Injured Heart

Under review: **Liu Chung Ming, C**., Wang, X., and Gentile, C, **Protective Role of Acetylcholine and the Cholinergic System in the Injured Heart** (*iScience*: IF: 6.01) (submitted 2/04/24).

Contribution: As the first author, the candidate researched this literature review article, wrote the original draft, created the figures and worked on all revised drafts under the supervision of her supervisors, Carmine Gentile and Xiaowei Wang.

2.2 – Biofabrication of Advanced *in vitro* 3D Models to Study Ischaemic and Doxorubicin-induced Myocardial Infarction Damage

Published article: Sharma, P., **Liu Chung Ming, C**., Wang, X., Bienvenu, L., Figtree, G., Boyle, A., and Gentile, C, **Biofabrication of Advanced *in vitro* 3D Models to Study Ischaemic and Doxorubicin-induced Myocardial Infarction Damage** (*Biofabrication*: IF: 8.3).

Link: https://iopscience.iop.org/article/10.1088/1758-5090/ac47d8/meta

Contribution: As a second author of this study, Clara Liu Chung Ming generated advanced *in*

vitro 3D models and mimicked ischemic-reperfusion injury and doxorubicin myocardial damage. Her contribution was also to help with the analyses of the *in vitro* models with the help of Poonam Sharma and Carmine Gentile. She also helped in the drafting of the paper and resubmission alongside Poonam Sharma, Xiaowei Wang and Carmine Gentile.

2.3.1 - *In vitro* Modelling of Cardiovascular Damage following Hypertensive Disorders of Pregnancy using Cardiac Spheroids and Patient-derived Plasma

Under review: **Liu Chung Ming, C**., Pienaar, D., Ghorbanpour, S., Chen, H., Roberts, LM., Cole, L., McGrath, K., Padula, M., Henry, A., Gentile, C., and McClements, L, ***In vitro* Modelling of Cardiovascular Damage following Hypertensive Disorders of Pregnancy using Cardiac Spheroids and Patient-derived Plasma** (Communications Biology : IF: 6.548) (Submitted on 12/01/2024).

Contribution: As the first co-author, the candidate's role was to develop the *in vitro* model and write the manuscript, that is, half of the introduction, half of the methods, the results (except the proteomic analysis), discussion and conclusion. This research utilized patient-derived plasma within a bioengineered CS heart tissue model to reveal specific mechanistic pathways leading to cardiac damage and CVD. Clara Liu Chung Ming also helped draft the paper alongside Carmine Gentile and Lana McClements, as well as with the resubmission of the paper.

3.2 - Acetylcholine-loaded nanoparticles protect against myocardial injury in *in vitro* cardiac spheroids and in an *in vivo* myocardial infarction murine model

Under review: **Liu Chung Ming, C**., Beck, D., Patil, R., Vettori, L., Lal, S., Wang, X., and Gentile, C, **Acetylcholine-mediated protection against I/R in 3D in vitro model and myocardial infarction in murine model** (*Advanced Functional Materials*: IF: 19) (submitted on 19/06/24)

Contribution: As the first author, the candidate proposed the idea of this project, and her primary supervisor, Carmine Gentile, helped with developing the project. Clara Liu Chung Ming led this article, which represents the role of acetylcholine against ischemic-reperfusion injury in a 3D *in vitro* model and myocardial infarction in mice. Clara Liu Chung Ming underwent training in the necessary lab techniques and did all the *in vitro* experiments. Rupali Patil and Xiaowei Wang collaborated to develop ACh-loaded nanoparticles at Baker Heart and Diabetes Institute, which were then shipped to the University of Technology Sydney. Clara assisted Carmine Gentile with inducing myocardial infarction in the mice and adding the treatment. The candidate underwent training with Xiaowei Wang for the cardiac imaging and analysis and did the *in vivo* analysis.

Sean Lal provided the human heart tissue, and Clara performed the *ex vivo* experiment. The cDNA extracted from the mice samples were sent to BGI for RNA sequencing, and Dominik Beck analyzed the genomics data. The candidate then drafted the whole paper as well as all the figures.

3.3 - Acetylcholine-loaded nanoparticles protect against doxorubicin-induced toxicity *in in vitro* cardiac spheroids

Under review: **Liu Chung Ming, C**., Patil, R., Wang, X., Lal, S., and Gentile, C, **Acetylcholine-loaded nanoparticles protect against doxorubicin-induced toxicity in *in vitro* cardiac spheroids** (Advanced Functional Materials: IF: 19) (submitted on 21/06/24)

Contribution: As the first author, the candidate proposed the idea of this project, and her principal supervisor, Carmine Gentile, helped with developing the project. Clara Liu Chung Ming led this project, which focusses on the protective role of acetylcholine against doxorubicin-induce toxicity in a 3D *in vitro* model. She underwent training in the necessary lab techniques and did all the *in vitro* experiments. Rupali Patil and Xiaowei Wang collaborated to develop ACh-loaded nanoparticles at Baker Heart and Diabetes Institute, which were then shipped to the University of Technology Sydney. Sean Lal provided the human heart tissue, and Clara performed the *ex vivo* experiment. The candidate then drafted the whole paper as well as all the figures.

Approved and signed by main supervisor: Dr Carmine gentile

Production Note:
Signature removed prior to publication.

The Roles Played by Acetylcholine in Cardiac Regeneration

Thesis Graphical Overview

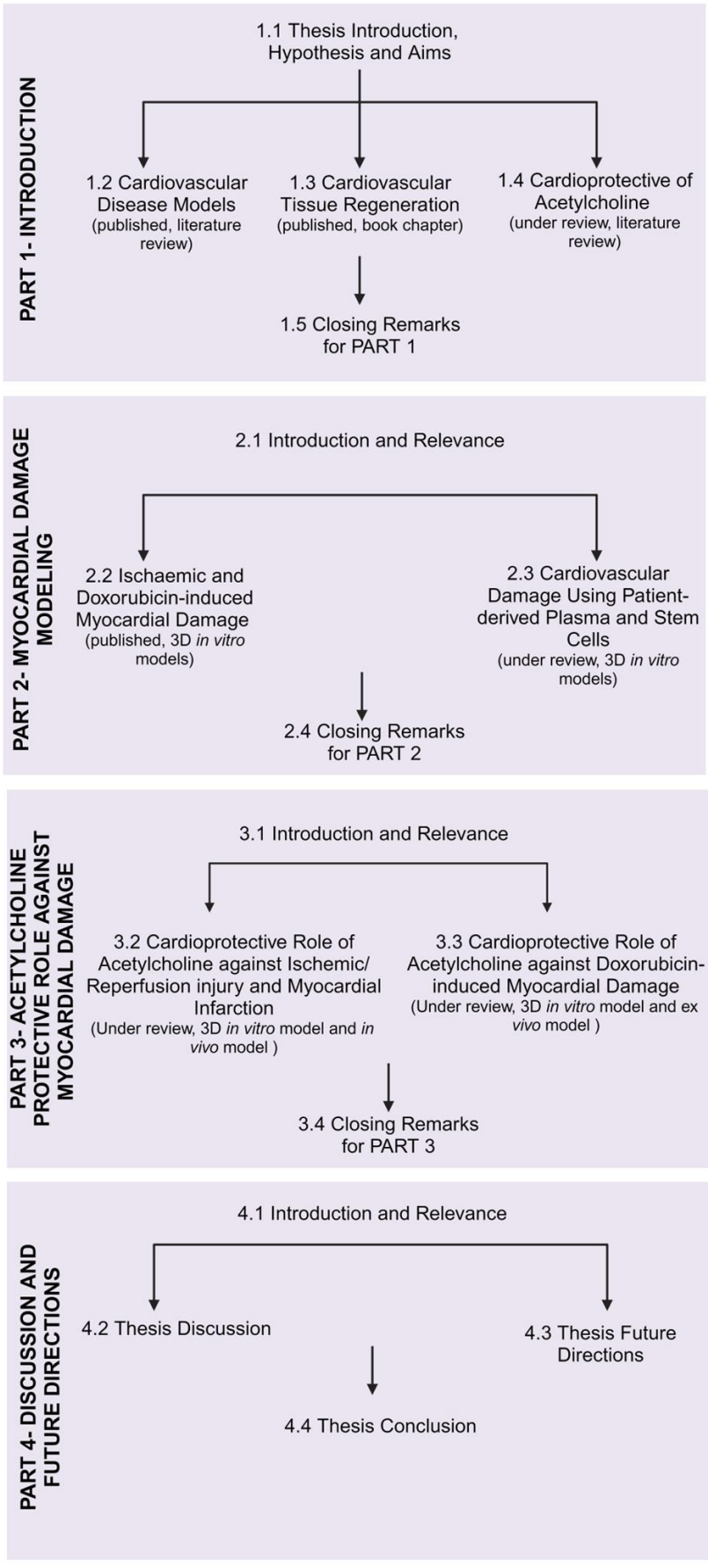

Contents

List of Figures and Tables

1.2 – Considerations for Advanced Cardiac Models to Study Preeclampsia and Other Cardiovascular Diseases

Liu Chung Ming, C., Sesperez, K., Ben-Sefer, E., Arpon, D., McGrath, K., McClements, L., and Gentile, C. Considerations for Advanced Cardiac Models to Study Preeclampsia and Other Cardiovascular Diseases (Cells: IF: 4.829).

Link: https://www.mdpi.com/2073-4409/10/4/899

Figures:

Tables:

1.3 - Stem Cell-based 3D Bioprinting for Cardiovascular Tissue Regeneration, Advanced Technologies in Cardiovascular Bioengineering

Liu Chung Ming, C., Ben-Sefer, E., and Gentile, C. Stem Cell-based 3D Bioprinting for Cardiovascular Tissue Regeneration, Advanced Technologies in Cardiovascular Bioengineering (Springer: IF: 2.495).

Link: https://link.springer.com/chapter/10.1007/978-3-030-86140-7_13

Figures:

1.4 - Protective Role of Acetylcholine and the Cholinergic System in the Injured Heart

Liu Chung Ming, C., Wang, X., and Gentile, C, Protective Role of Acetylcholine and the Cholinergic System in the Injured Heart (iScience) (Submitted 28/02/24).

Figures:

Figure 1: Schematic illustration of the cardiac neuronal cholinergic system in cardiomyocytes and cholinergic nerves.

Figure 2: Schematic illustration of therapeutic approaches to target and elevate ACh levels in the infarcted heart.

2.2 – Biofabrication of Advanced *in vitro* 3D Models to Study Ischaemic and Doxorubicin-induced Myocardial Infarction Damage

Sharma, P., **Liu Chung Ming, C**., Wang, X., Bienvenu, L., Figtree, G., Boyle, A., and Gentile, C, Biofabrication of Advanced *in vitro* 3D Models to Study Ischaemic and Doxorubicin-induced Myocardial Infarction Damage (Biofabrication: IF: 8.3).

Link: https://iopscience.iop.org/article/10.1088/1758-5090/ac47d8/meta

Figures:

Figure 1: Protocol for *in vitro* and *in vivo* myocardial damage models used in this study.

Figure 2: Intracellular O_2 concentration changes in I/R CSs.

Figure 3: Confocal imaging analyses for cell death and viability in I/R CSs.

Figure 4: Confocal imaging analyses for cell death and viability in DOX CSs.

Figure 5: 3D cell death analyses of confocal images of an I/R CS using Imaris software.

Figure 6: 3D cell death analyses of confocal images of DOX CS using Imaris software.

Figure 7: Decrease in contraction frequency and fractional shortening of CSs.

Figure 8: Difference in expression of cardiac genes in *in vivo* and *in vitro* models of myocardial I/R injury.

Figure 9: Difference in expression of cardiac genes in *in vitro* I/R and DOX mCSs.

Figure 10: Difference in expression of cardiac genes in *in vitro* I/R and DOX hCSs.

Tables

Table 1: Expression of cardiovascular genes following I/R injury.

Table 2: Expression of cardiovascular genes following DOX treatment.

2.3.1 - *In vitro* Modelling of Cardiovascular Damage following Hypertensive Disorders of Pregnancy using Cardiac Spheroids and Patient-derived Plasma

Liu Chung Ming, C., Pienaar, D., Ghorbanpour, S., Chen, H., Roberts, LM., Cole, L., McGrath, K., Padula, M., Henry, A., Gentile, C., and McClements, L, *In vitro* Modelling of Cardiovascular Damage following Hypertensive Disorders of Pregnancy using Cardiac Spheroids and Patient-derived Plasma (Hypotension AHA: IF: 10.2) (Submitted on 12/01/2024).

Figures:

Figure 1: Representative images of live and dead cells within cardiac spheroids and percentage of live cells remaining following exposure to human plasma from women with HDPs.

Figure 2: Effects of healthy, GH and PE plasma on cardiac spheroid contractile function.

Figure 3: Confocal images and protein expression analysis of the three cardiac cell type markers in control, GH and preeclampsia groups.

Figure 4: Confocal images and analysis of protein expression of FKBPL and α-SMA markers in control, GH and preeclampsia groups.

Figure 5: Confocal images and analysis of protein expression of Gal-3 and VE-Cadherin markers in control, GH and preeclampsia groups.

Figure 6: Differential expression analysis of grouped patient plasma for discovery/untargeted proteomics.

Tables:

Supplementary Table 1. Clinical characteristics of P4 participants subgroups.

Supplementary Table 2. Multiple group comparison for differential expression of plasma proteins.

3.2 - Acetylcholine-loaded nanoparticles protect against myocardial injury in *in vitro* cardiac spheroids and in an *in vivo* myocardial infarction murine model

Liu Chung Ming, C., Patil, R., Vettori, L., Couttas, T.A., Beck, D., Wang, X.[#], and Gentile,

C[#], Acetylcholine-loaded nanoparticles protect against myocardial injury in *in vitro* cardiac spheroids and in an *in vivo* myocardial infarction murine model (Advanced Functional Materials: IF: 19) (Submitted on 19/06/24)

Figures:

Figure 1: ACh's protective effect against I/R-induced CS.

Figure 2: Protective role of co-culture of ACh-producing IPSC-derived cholinergic nerves against I/R in CNs.

Figure 3: Protective role of ACh-nanoparticles against I/R-induced myocardial damage.

Figure 4: Protective role of ACh-loaded nanoparticle against MI mice model.

Figure 5: The transcriptomic profile of ACh-NPs against MI mice model. A) Principal component analysis of whole transcriptome expression levels.

Figure 6: Schematic illustration of *in vitro* and *in vivo* modeling for I/R and MI.

Supplementary Figure 1: Loading efficiency of ACH in PBCA nanoparticles. The mass ratio of PBCA to ACH taken was 2:1, 1:1 and 1:2 (n=1)

Tables:

Table 1: Significant changes in the relative expression of CS genes regulating cardiac remodeling, apoptosis and signal transduction.

Table 2: qPCR relative expression of significant changes for apoptotic genes and signal transduction genes.

Table 3: Ingenuity Pathway Analysis (IPA) on RNAseq identified molecular functions in MI treated with ACh-NPs.

Supplementary Table 1: Loading efficiency of ACH in PBCA-NPs.

Supplementary Table 2: Ingenuity canonical pathways.

Supplementary Table 3: Upstream of system development.

3.3 - Acetylcholine-loaded nanoparticles protect against doxorubicin-induced toxicity *in in vitro* cardiac spheroids

Liu Chung Ming, C., Patil, R., Lal, S., Wang, X., and Gentile, C, Acetylcholine-loaded nanoparticles protect against doxorubicin-induced toxicity in *in vitro* cardiac spheroids (Advanced Functional Materials: IF: 19) (Submitted on 21/06/24)

Figures:

Figure 1: Protective role of addition of ACh against DOX CS.

Figure 2: Protective role of co-culture of ACh-producing IPSC-derived cholinergic nerves against DIC in CNs.

Figure 3: Protective role of ACh-loaded nanoparticle against DOX CS.

Figure 4: Effect of ACh on nitric oxide synthase through the eNOS pathway.

Figure 5: Schematic illustration of *in vitro* DOX-induced CS modeling.

Supplementary Figure 1: Loading efficiency of ACH in PBCA nanoparticles. The mass ratio of PBCA to ACH taken was 2:1, 1:1 and 1:2 (n=1)

Supplementary Figure 2: Confocal image analyses of fluorescent intensity of DAF-FM to look at nitric oxide production.

Supplementary Figure 3: eNOS pathway in human heart tissue *ex vivo*.

Tables:

Table 1: Significant changes in the relative expression of CS genes regulating cardiac remodeling, apoptosis and signal transduction.

Table 2: qPCR relative expression of significant changes for apoptotic genes and signal transduction genes.

Supplementary Table 1: Loading efficiency of ACH in PBCA-NPs.

List of Abbreviations

2D or 3D – Two or three-dimensional

ACh – Acetylcholine

ACh-NPs – Acetylcholine-loaded nanoparticles

aSMA – smooth muscle alpha-actin

CO_2 – Carbon dioxide

CD31 – Cluster of Differentiation 31

CF – Contraction frequency

CMs/icells – Human induced pluripotent stem cell-derived cardiomyocytes/ Cardiomyocytes

CS - Cardiac spheroids

CTE – Cardiac tissue engineering

CVD - Cardiovascular diseases

DCM- Dilated cardiomyopathy

DIC – Doxorubicin-induced heart toxicity

DMEM – Dulbecco's Modified Eagle Medium

DOX – Doxorubicin

EC – Endothelial cells

ECM - Extracellular matrix

EF – Ejection fraction

EOPE - Early-onset preeclampsia

FKBPL - FK506-binding protein-like

GH - Gestational hypertension

HCAEC- Human coronary artery endothelial cells

HCF – Human cardiac fibroblast

HDP - Hypertensive disorders of pregnancy

HF – Heart failure

IHD - Ischemic heart disease

IPSC- Induced pluripotent stem cell

IPSC-CMs- Induced pluripotent stem cell-derived cardiomyocytes

IPSC-ECs- Induced pluripotent stem cell-derived endothelial cells

I/R or IR- Ischemic reperfusion injury

LV – Left ventricle

LVEF – Left ventricle ejection fraction

LOPE - Late-onset preeclampsia

MI – Myocardial infarction

mRNA- Messenger ribonucleic acid

Nanoparticles - NPs

N – Nitrogen

NO – Nitric oxide

O_2 – Oxygen

PBCA - Poly-butylcyanoacrylate

PE – Preeclampsia

qPCR- Quantitative polymerase chain reaction

RNA - Ribonucleic acid

ROS – Reactive oxygen species

VEGF – vascular endothelial growth factor

List of publications, presentations, awards, and collaborations

Manuscripts

1. Sharma, P., Wang, X., **Liu Chung Ming, C**., Vettori, L., Figtree, G., Boyle, A., and Gentile, C. Considerations for the Bioengineering of Advanced Cardiac in vitro Models of Myocardial Infarction, Advanced in vitro Models for Replacement of Animal Experiments (Small: *IF: 11.459*).
   Link: https://onlinelibrary.wiley.com/doi/abs/10.1002/smll.202170067
2. Polonchuk, L., Surija, L., Lee, M. H., Sharma, P., **Liu Chung Ming, C.**, Richter, F., Ben-Sefer, E., Rad, M. A., Mahmodi Sheikh Sarmast, H., Shamery, W. A., Tran, H. A., Vettori, L., Haeusermann, F., Filipe, E. C., Rnjak-Kovacina, J., Cox, T., Tipper, J., Kabakova, I., & Gentile, C. Engineering Heart tissues from Bioprinted Cardiac Spheroids (IOP Publishing: *IF: 7.343*).
   Link: https://iopscience.iop.org/article/10.1088/1758-5090/ac14ca/meta
3. Richards, C., Sesperez, K., Chhor, M., Ghorbanpour, S., Rennie, C., **Ming, C. L. C**., Evenhuis, C., Nikolic, V., Orlic, N. K., Mikovic, Z., Stefanovic, M., Cakic, Z., McGrath, K., Gentile, C., Bubb, K., & McClements, L. Characterisation of cardiac health in the reduced uterine perfusion pressure model and a 3D cardiac spheroid model, of preeclampsia (Biology of Sex Differences: *IF: 3.267*).
   Link: https://pubmed.ncbi.nlm.nih.gov/33879252/
4. **Liu Chung Ming, C**., Sesperez, K., Ben-Sefer, E., Arpon, D., McGrath, K., McClements, L., and Gentile, C. Considerations for Advanced Cardiac Models to Study Preeclampsia and Other Cardiovascular Diseases (Cells: *IF: 4.829*).
   Link: https://www.mdpi.com/2073-4409/10/4/899
5. **Liu Chung Ming, C.,** Ben-Sefer, E., and Gentile, C. Stem Cell-based 3D Bioprinting for Cardiovascular Tissue Regeneration, Advanced Technologies in Cardiovascular Bioengineering (Springer: *IF: 2.495*).
   Link: https://link.springer.com/chapter/10.1007/978-3-030-86140-7_13
6. Sharma, P., **Liu Chung Ming, C.,** Wang, X., Bienvenu, L., Figtree, G., Boyle, A., and Gentile, C, Biofabrication of Advanced *in vitro* 3D Models to Study Ischaemic and Doxorubicin-induced Myocardial Infarction Damage (Biofabrication: *IF: 8.3*).
   Link: https://iopscience.iop.org/article/10.1088/1758-5090/ac47d8/meta
7. Sharma, P., **Liu Chung Ming**, **C.,** and Gentile, C, In vitro Modeling of Myocardial Ischaemia/Reperfusion Injury using 3D Cardiac Spheroids (STAR Protocols: IF: 66.850).
   Link: https://www.sciencedirect.com/science/article/pii/S2666166722006311
8. Bahrami, H., Vettori, L., **Liu Chung Ming, C.**, Puppo, E., Perry, S., Gentile, C., and Pietroni, N, Physically based simulation of elastic-plastic fusion of 3D bioprinted spheroids (Biofabrication: *IF: 8.3*).
   Link: https://iopscience.iop.org/article/10.1088/1758-5090/acf2cb/meta
9. Vettori, L., Tran, A.H., Mahmodi Sheikh Sarmast, H., Filipe, E.C., Wyllie, K., **Liu Chung Ming, C.**, Cox, T.R., Tipper, J., Kabakova, I.V., Rnjak-Kovacina, J., and Gentile, C, Silk fibroin increases the elasticity of alginate gelatin hydrogels and regulates cardiac cell contractile function in cardiac bioinks (Biofabrication: *IF: 8.3*).

Link: https://pubmed.ncbi.nlm.nih.gov/38776895/

10. **Liu Chung Ming, C**., Pienaar, D., Ghorbanpour, S., Chen, H., Roberts, LM., Cole, L., McGrath, K., Padula, M., Henry, A., Gentile, C., and McClements, L, *In vitro* Modelling of Cardiovascular Damage following Hypertensive Disorders of Pregnancy using Cardiac Spheroids and Patient-derived Plasma (Hypotension AHA: *IF: 10.2*). (Submitted on 12/01/2024)
11. **Liu Chung Ming, C**., Wang, X*., and Gentile, C*, Protective Role of Acetylcholine and the Cholinergic System in the Injured Heart (iScience: *IF: 6.17*; submitted on 2/04/2024)
12. Tarsitano, M., **Liu Chung Ming, C**., Bennar, L., Mahmodi, H, Wylie, K., Paolino, D., Cox, T.R., Kabakova, I.V., Ralph, P., and Gentile, C, Chlorella-enriched hydrogels protect against myocardial damage and reactive oxygen species production in an *in vitro* ischemia/reperfusion model using cardiac spheroids (Biofabrication: *IF: 8.3;* under review – submitted 10/03/2024).
13. Johansen, M.[#], **Liu Chung Ming, C**.[#], Hansbro, P., Gentile, C, Modelling the Complex Microenvironment for SARS-CoV-2 Infection using 3D *in vitro* Cardiac Spheroids (Biofabrication: *IF: 8.3;* submitted 17/06/24).
14. **Liu Chung Ming, C**., Patil, R., Vettori, L., Couttas, T.A., Beck, D., Wang, X.[*], and Gentile, C[*], Acetylcholine-loaded nanoparticles mediated protection against I/R in 3D *in vitro* model and myocardial infarction in murine model (Advanced Functional Materials: *IF: 19*; under review – submitted 19/06/24).
15. **Liu Chung Ming, C**.[#], Patil, R., Lal, S., Wang, X., and Gentile, C[*], Acetylcholine-mediated exerts cardiac protection against Doxorubicin-induced cardiotoxicity (Advanced Functional Materials: *IF: 19*; under review – submitted 21/06/24).

Presentations

1. *International Society of Biofabrication, Online, 27-29th Sept 2021*. Multimedia poster and pre-recorded oral presentation. In vitro Modelling of the Complex Human Heart Pathophysiology using Vascularised Cardiac Spheroids.
2. *Cardiovascular Research Network for Heart Foundation, Online, Sept 2021.* Heart pitch Heats. Reversing heart attack and heart failure damage in mini hearts.
3. *Sydney Cardiovascular Symposium 2021, Online, 9-10th Dec 2021*. Flash Talks. *In vitro* Modelling of Human Heart Hypoxia/Reoxygenation- and Drug-induced Myocardial Damage.
4. *Australasian Society for Biomaterials and Tissue Engineering 2022*, *Melbourne,* 20-22 April 2022. Rapid Fire Presentation. *In vitro* 3D Modelling of Human Heart Myocardial Damage using Cardiac Spheroids.
5. *Royal Society New South Wales 2023*, Sydney, 15th March 2023. *A New Hope For Heart Failure Patients: Bioengineered Heart Tissues*.
6. *Australasian Society for Biomaterials and Tissue Engineering 2023*, New Zealand, 11-13th April 2022. Poster Presentation. *Acetylcholine-mediated protection against myocardial damage in in vitro human vascularised cardiac spheroids*.

7. *American Heart Association 2023*, Boston, 1-3rd August 2023. Poster Presentation. *Personalized care using patient-derived cardiac spheroids for heart failure patients*.
8. *Australian Atherosclerosis Society (AAS), the Australian and New Zealand Microcirculation Society (ANZMS) and the Australian Vascular Biology Society (AVBS) Joint Meeting 2023*, Adelaide, 29th Oct- 1st November 2023. PhD Rising Stars. *Acetylcholine-mediated protection against myocardial damage in in vitro human vascularised cardiac spheroids*.
9. *Heart Research Institute (HRI),* HRI Seminar 2024, Sydney, 28th Feb 2024. *Acetylcholine-mediated protection against myocardial damage.*

Awards

2021 Vice Chancellor's Conference Fund (VCCF) awards

2021 FEIT HDR Women in Engineering and IT awards

2022 Australasian Society for Biomaterials and Tissue Engineering (ASBTE) Conference Travel Award 2022

2022 ASBTE Rapid Fire Presentation Award 2022

2022 NSW Education Waratah Scholarship

2022 Royal Society New South Wales Scholarship

2023 Australian Atherosclerosis Society (ASM) Joint Travel Grant

2023 Vice Chancellor's Conference Fund (VCCF) awards

2023 Australian Atherosclerosis Society (ASM) PhD Rising Star

2023 2023 TERMIS-AP Virtual Student Paper Contest

Collaborations

Dr Lana McClements and Dr Kristine McGrath (Faculty of Science, UTS)

- Facilitated cell culture growth for their students.
- Spearheaded the development of a pioneering 3D cardiac spheroid model to prevent future cardiovascular disease in preeclampsia patients (DOI: 10.1186/s13293-021-00376-1). This groundbreaking research holds promise in preventing future cardiovascular complications in individuals affected by preeclampsia.

Paul Brown and Linda Dement (NSW Artists)

- Cultured cells and look at CSs contractility for their mini-sculpture 'Last Breaths,' displayed at ISEA (International Symposium on Electronic Arts) 2022 in Barcelona. The ISEA exhibition runs from 9-30th June in multiple venues.

Link: https://isea2022.isea-international.org/event/artwork-last-breaths/

A/Prof Louise Cole (Director of Microbial Imaging Facility (MIF), UTS)

- Shared and helped Louise with her presentation as co-authors at the 2023 ASMI (Australian Society of Molecular Imaging) at UNSW on the 6th of October, 2023.
- Shared and helped Louise with her presentation as co-authors at the 2024 ELMI (European Light Microscopy Initiative) in Liverpool, UK.

Abstract (Whole thesis)

Cardiovascular disease (CVD) is the leading cause of death worldwide. However, existing therapeutic interventions are limited, as they only delay the progression to chronic heart failure (HF) and do not regenerate the damaged heart tissue. Acetylcholine (ACh) is a well-known neurotransmitter that controls cardiac function, and its production is significantly reduced following myocardial damage. Increasing ACh in the infarcted heart reduces infarct size in *in vivo* models, activates anti-inflammatory pathways, and promotes cell survival. Nonetheless, the protective role of ACh against myocardial damge remains underexplored as current approaches to increasing ACh levels are invasive and unsafe for patients. Furthermore, current *in vitro* and *in vivo* models fail to fully recapitulate the complex scenario of human pathophysiology, leading to poor translation of findings from the bench to the bedside. We developed 3D *in vitro* cardiac spheroid (CS) models, comprising of stem cells-derived cardiomyocytes, fibroblast and endothelial cells that better mimic the molecular, cellular, and extracellular features typical of the human cardiac microenvironment compared to existing models.

In this project, we first develop *in vitro* models using bioengineered CSs for *1*) myocardial injury following ischemic-reperfusion (I/R) and doxorubicin (DOX) treatment and for *2*) hypertensive disorder pregnancy (HDP)-induced CVD.–We then investigate the protective role of ACh against I/R- and DOX-induced injury using our models mentioned above. Three different methods to deliver ACh are explored: *i*) freely-dissolved 100µM ACh, *ii*) ACh-producing cholinergic nerves (CNs), and *iii*) ACh-loaded nanoparticles (ACh-NPs). Our results show that ACh significantly attenuates cell death and restores contractile activity against I/R and DOX-induced myocardial damage. Our qPCR analyses show that ACh also protects against the I/R- and DOX-induced decrease of genes regulating contractile function, ATPase activity, cell cycle and survival. To translate our findings from *in vitro* to *in vivo* studies, we also investigate the protective effects of ACh-NPs in a myocardial infarction (MI) mouse model. Our results show that ACh-NPs attenuate MI-induced left ventricle dysfunction and remodeling and increase cell cycle and cell proliferation. Overall, our findings underscore the potential use of ACh-NPs to target deliver ACh and protect against myocardial injury.

CHAPTER 1 – INTRODUCTION

1.1 Thesis Introduction, Hypothesis and Aims

Introduction

Cardiovascular disease (CVD) is the leading cause of mortality and disability worldwide, responsible for an estimated 17.9 million deaths each year, according to the World Health Organization (2021). CVD can be caused by hypertensive disorders of pregnancy (HDP), which affect 2-8% of all pregnancies and are a leading cause of mortality and morbidity in pregnancy (Brown et al., 2018, Chappell et al., 2021). HDP is characterized by pregnancy hypertension (defined as blood pressure ≥140/90 mmHg). This includes gestational hypertension (GH) (new-onset at ≥20 weeks gestation) and preeclampsia (PE), which is characterized by abnormal placental development or dysfunction (Brown et al., 2018). Individuals affected by HDP have an increased risk of developing CVD, up to 7-fold higher than those who had normotensive pregnancies (Arnott et al., 2020). Among 1 452 926 records of singleton pregnancies, Jarvie et al. (2018) showed that women with HDP had double the risk of developing acute myocardial infarction (MI) or heart failure (HF). Even though the epidemiological link between HDP and future CVD is well-established, there is currently no treatment to prevent cardiometabolic HDP complications as the causal mechanisms and its direct correlation to CVD remain unclear (Chen et al., 2022, Liu Chung Ming et al., 2021).

MI occurs when blood flow is obstructed in one or more coronary arteries, resulting in a reduced supply of oxygen and nutrients to the myocardium (Bhandari et al., 2021). Therapeutic strategies such as percutaneous coronary intervention (PCI) mitigate ischemic injury by reinstating perfusion. However, this reperfusion is associated with the generation of reactive oxygen species (ROS) at the occlusion site, further exacerbating cell death (Sebastião et al., 2019). Ischemic-reperfusion (I/R) injury is irreversible and leads to ischemic HF (Brandt et al., 2019).

Another cause of CVD is doxorubicin (DOX); DOX is an antineoplastic agent extensively employed in treating various cancers, such as leukemia, lymphoma, and others (Volkova and Russell, 2011, Christidi and Brunham, 2021). However, it is estimated that up to 65% of oncology patients may experience DOX-induced cardiotoxicity (DIC), leading to adverse cardiac outcomes, including reduced left ventricular ejection fraction, ventricular wall thickening, arrhythmias, and congestive HF (Christidi and Brunham, 2021, Prathumsap et al., 2022).

As the adult human heart is not able to regenerate, cardiac injury is irreversible and current pharmacological treatments primarily serve to delay the progression of HF, rather than offering a curative solution (Lui et al., 2014, Brandt et al., 2019). The gold standard treatment for end-stage HF remains a heart transplant, which is available to less than 0.1% of HF patients (Gerbin and Murry, 2015).

Numerous studies demonstrated that ACh possesses cardioprotective properties against various CVD manifestations, including MI (Bezerra et al., 2017, Buchholz et al., 2012), I/R injury (Intachai et al., 2022, Kakinuma et al., 2012, Kakinuma et al., 2013, Katare et al., 2009), DOX-induced cardiotoxicity (Guo et al., 2022, Prathumsap et al., 2022, Siripakkaphant et al., 2023) and heart failure (De Ferrari et al., 2010, Gold et al., 2016). These protective effects are achieved through mechanisms involving the restoration of autonomic balance, enhancement of heart rate variability, mitigation of mitochondrial dysfunction, and activation of anti-inflammatory responses (Borovikova et al., 2000, Calvillo et al., 2011, Intachai et al., 2022). Despite that, vagus nerve stimulation (VNS) or cholinesterase inhibitors are currently used to increase ACh levels. VNS is invasive, and clinical trials have demonstrated mixed results (Capilupi et al., 2020). Moreover, cholinesterase inhibitors are commonly used for Alzheimer's disease (Birks and Harvey, 2018) and dementia (Battle et al., 2021, Jian et al., 2020) patients and culminating studies have demonstrated their effectiveness in combating CVD (Issotina Zibrila et al., 2021, Khuanjing et al., 2021, Khuanjing et al., 2020, Nordström et al., 2013). However, the benefit-to-harm ratio of cholinesterase inhibitors remains a crucial issue for clinical trials in CVD patients as cholinesterase inhibitors lead to adverse drug reactions such as vomiting, diarrhea, panic, muscle tension, speech difficulty, and involuntary tremors (Li et al., 2020a).

Additionally, the inadequacies of current *in vitro* and *in vivo* models of the human heart fail to capture the intricate pathophysiological landscape and therapeutic findings in model animals often cannot be translated to CVD patients. This fully underscores the necessity for advanced modeling techniques to test therapeutic approaches against CVD (Liu Chung Ming et al., 2022, Liu Chung Ming et al., 2021). In this project, we have pioneered a groundbreaking model to generate viable and functional heart tissues using stem cell-derived cardiac cells and 3D cell culture. Previous studies have shown that bioengineered heart tissue, also known as human cardiac spheroids (CSs), better mimic the human heart microenvironment; this includes molecular, cellular, and extracellular components typical of the human heart, including the vascular network and contractile activity. CSs are made of endothelial cells, fibroblast and

induced pluripotent stem cells derived-cardiomyocytes and are embedded in a hydrogel, which provides the extracellular matrix (ECM) environment to those cells (Polonchuk et al., 2021, Polonchuk et al., 2017). Additionally, CSs are used as an improved pathophysiological model to help bridge the gap between previously available 2D *in vitro*, animal *in vivo* models and *in vivo* human hearts (Polonchuk et al., 2017, Polonchuk et al., 2021, Sharma et al., 2022).

Project Description and Hypothesis

The main objective of my thesis is to evaluate ACh's cardioprotective roles in cardiac regeneration. However, the complexity of human CVD may not be fully replicated in either currently available monolayer *in vitro* cultures or *in vivo* animal models. Hence, the thesis's first objective centers around the development of advanced 3D *in vitro* bioengineered heart tissue (cardiac spheroid, CS) models to mimic human heart pathophysiology, such as I/R injury and drug-induced cardiotoxicity using DOX and as a patient-derived CVD model using HDP-patient plasma. Furthermore, as animal models are poor predictors of drug safety in humans, the second objective of the thesis is to explore the suitability and application of *in vitro* advanced CS disease models for drug screening and to further our understanding of the protective role of ACh against I/R and DOX-induced cardiovascular damage.

To evaluate the protective roles of ACh against myocardial damage, three distinct administration strategies to elevate ACh levels were tested: 1) addition of freely-dissolved 100μM ACh in CSs, 2) co-culturing ACh-producing iPSC-derived cholinergic neurons (CNs) with CSs, and 3) addition of ACh-encapsulated nanoparticles (ACh-NPs) to CSs. As ACh hydrolyses rapidly *in vivo* and has multitarget effects in the human body, coupled with the variability of current approaches to increase ACh levels (Zafeiropoulos et al., 2023, Kröger et al., 2015). We developed a novel therapeutic approach to deliver ACh in small doses and target the injured area. ACh-NPs are developed by encapsulating ACh in poly-butyl cyanoacrylate (PBCA). PBCA-NPs have been thoroughly developed as a drug delivery system for cancer chemotherapy (Evangelatov et al., 2016, Sulheim et al., 2016) and to pass through the brain-blood barrier (Rempe et al., 2011, Reukov et al., 2011). Previous studies demonstrated that PBCA-NPs are safe, non-toxic, stable and can release the encapsulated drug in primary rat aortic endothelial cells to treat atherosclerosis (Wang et al., 2024, Mehta et al., 2022).

The overall hypothesis of my PhD project is that **acetylcholine protects against myocardial damage.** This hypothesis will be tested via the following specific aims:

Aim & Objectives:

Specific-Aim 1: To model myocardial damage using advanced *in vitro* models.

Sub aims

1.1: To establish ischemic-reperfusion myocardial damage in bioengineered heart tissues.

1.2: To establish doxorubicin myocardial damage in bioengineered heart tissues.

1.3: To establish hypertensive disorders of pregnancy-induced myocardial damage tissues.

Specific-Aim 2: To evaluate the effects of acetylcholine on ischemic-reperfusion myocardial damage, bioengineered heart tissues, and myocardial infarction *in vivo*.

Sub aims

2.1: To evaluate the protective effect of acetylcholine on ischemic-reperfusion myocardial damage in bioengineered heart tissues.

2.2: To evaluate the protective effect of cholinergic nerve cells producing acetylcholine on ischemic-reperfusion myocardial damage in bioengineered heart tissues.

2.3: To evaluate the protective effect of acetylcholine nanoparticles on ischemic-reperfusion myocardial damage in bioengineered heart tissues.

2.4: To evaluate the protective effect of cholinergic innervation on myocardial infarction *in vivo*.

Specific-Aim 3: To evaluate the effects of acetylcholine on doxorubicin myocardial damage bioengineered heart tissues and *ex vivo* human heart biopsies.

Sub aims

3.1: To evaluate the protective effect of acetylcholine on doxorubicin myocardial damage in bioengineered heart tissues.

3.2: To evaluate the protective effect of cholinergic nerve cells producing acetylcholine on doxorubicin myocardial damage in bioengineered heart tissues.

3.3: To evaluate the protective effect of acetylcholine nanoparticles on doxorubicin myocardial damage in bioengineered heart tissues.

3.4: To evaluate the protective effect of acetylcholine on *ex vivo* human heart biopsies.

Breakdown of the project's components and goals:

Chapter 1 introduces critical background information, including 1) The considerations to model heart disease in women with PE and CVD, including MI, I/R and HF (**Chapter 1.2**). 2) Current approaches of cardiovascular regeneration using tissue engineering, which is a crucial part of my project as it describes the types of cardiovascular tissue engineering and the importance of using 3D *in vitro* cell culture models, including CS model (**Chapter 1.3**). 3) An overview of ACh's cardioprotective properties, the various delivery techniques currently used to administer ACh, and alternative approaches for more targeted and effective delivery (**Chapter 1.4**).

Chapter 2 focuses on Aim 1, that is, the applications of the CS model to mimic different aspects of heart diseases. This includes CVD modeling, Drug-induced toxicity modeling and patient-specific models.

CVD modeling and drug-induced toxicity modeling (sub aims 1.1 and 1.2)

Chapter 2.2 includes the biofabrication of advanced *in vitro* 3D models to study I/R and DOX-induced myocardial damage. We assessed the CS model's ability to replicate key features of cardiac pathophysiologies, such as I/R-mimic conditions through oxygen (O2) level changes. Additionally, we evaluated the CS model as a toxicological model by inducing DOX, which is a well-known cardiotoxic drug (Mitry and Edwards, 2016, Sharma et al., 2022). We demonstrated that the CS model could mimic I/R and DOX-induced conditions similar to *in vivo* studies.

Patient-specific models (sub aim 1.3)

In **Chapter 2.3**, we establish an advanced CS model to evaluate individual patient cardiac function alterations after HDP. While writing the first literature review in **Chapter 1.2** about PE and CVD, we encountered a pressing and unanswered question for the field of CVD and *in vitro* modeling. In pregnant women, the causes of HDP-induced cardiac dysfunction are still unknown, which is mainly due to the lack of optimal models to recapitulate this complex disease in the laboratory (Liu Chung Ming et al., 2021). This presents an opportunity to understand the mechanism between post-HDP and CVD using our CS models. But also, to develop more effective management and treatments for women post-HDP that could diagnose the incidence of cardiovascular risk in patients. We demonstrated that CSs could convey a unique way to explore that underlying correlation of CVD in post-HDP patients. This was done by taking the patient's blood and extracting the patient-derived plasma to test on CSs. The results identified GH and PE-mediated cardiovascular damage five years post-partum for

GH and PE patients.

In **Chapter 3**, we used the CS model to evaluate the efficacy and safety of pharmacological interventions as well as the protective effect of increasing ACh levels against myocardial damage, including I/R and DOX-induced myocardial damage. We used three therapeutic delivery methods to deliver ACh. We looked at the effect of i) adding freely-dissolved ACh, ii) ACh-derived from CNs and iii) ACh-NPs delivery in cardiac cells in I/R and DOX-induced CS models. To validate our *in vitro* findings, we also investigated the protective role of ACh-NPs on MI *in vivo* models. **Chapter 3.2** investigates the cardioprotective role of ACh against *in vitro* I/R-induced CS model and MI *in vivo* MI mice model (Aim 2). **Chapter 3.3** investigates the cardioprotective role of ACh against DOX-induced myocardial damage in *in vitro* CS model and *ex vivo* heart human tissue (Aim 3). Our findings provide novel evidence of the protective roles of ACh against myocardial damage.

Chapter 4 delves into the discoveries articulated throughout this thesis, exploring their significance (**Chapter 4.2**) and proposing future directions (**Chapter 4.3**). This section underscores the potential role of bioengineered CSs as an advanced model to mimic cardiac pathophysiology and for the early identification of changes in cardiac function. More importantly, it also highlights the protective effects of ACh against against I/R injury in *in vitro* and *in vivo* models for Aim 2 (**Chapter 3.2**) and the role of ACh against DOX-induced injury in *in vitro* CSs for Aim 3 (**Chapter 3.3**).

Overall, my project provides novel insights into the applications of bioengineered CSs that could benefit existing *in vitro* models and fill the gaps in the translation of research and drug discovery in patients. Foremost, my thesis explores the regenerative properties of ACh with a focus on a unique combination of state-of-the-art technologies, such as organoids, nanoparticles, stem cells and advanced *in vitro* disease modelling.

1.2 Cardiovascular Disease Models

Summary:

The following literature review, published on 14 April 2021 in Cells Journal, encompasses the study of PE and its correlation with CVD. The chapter highlights the increased risk of conditions such as MI and HF in both mothers and their offspring. It offers an insightful overview of PE and CVD alongside a comparative analysis of the current MI, I/R and HF model systems employed in research. The novelty of this review stems from its objective to evaluate and propose novel model systems designed to replicate CVD in PE patients accurately. This initiative aims to mirror better the complex molecular and physiological scenarios observed in human hearts affected by these conditions. By focusing on developing and validating these innovative model systems, the review opens new pathways for understanding the intricate relationship between PE and CVD. For the overall thesis, this chapter emphasizes the current models for HDP and CVD and their limitations.

cells

MDPI

Review

Considerations to Model Heart Disease in Women with Preeclampsia and Cardiovascular Disease

Clara Liu Chung Ming [1], Kimberly Sesperez [2], Eitan Ben-Sefer [1], David Arpon [1], Kristine McGrath [2], Lana McClements [2] and Carmine Gentile [1,3,4,*]

[1] School of Biomedical Engineering/FEIT, University of Technology Sydney, Sydney, NSW 2007, Australia; clara.liuchungming@student.uts.edu.au (C.L.C.M.); Eitan.B.Ben-Sefer@student.uts.edu.au (E.B.-S.); David.arpon@gmail.com (D.A.)
[2] School of Life Sciences, Faculty of Science, University of Technology Sydney, Sydney, NSW 2007, Australia; kimberly.sesperez@student.uts.edu.au (K.S.); Kristine.McGrath@uts.edu.au (K.M.); lana.mcclements@uts.edu.au (L.M.)
[3] Sydney Medical School, The University of Sydney, Sydney, NSW 2000, Australia
[4] Beth Israel Deaconess Medical Center, Harvard Medical School, Boston, MA 02115, USA
* Correspondence: Carmine.Gentile@uts.edu.au; Tel.: +61-(2)-9514-4502

Abstract: Preeclampsia is a multifactorial cardiovascular disorder diagnosed after 20 weeks of gestation, and is the leading cause of death for both mothers and babies in pregnancy. The pathophysiology remains poorly understood due to the variability and unpredictability of disease manifestation when studied in animal models. After preeclampsia, both mothers and offspring have a higher risk of cardiovascular disease (CVD), including myocardial infarction or heart attack and heart failure (HF). Myocardial infarction is an acute myocardial damage that can be treated through reperfusion; however, this therapeutic approach leads to ischemic/reperfusion injury (IRI), often leading to HF. In this review, we compared the current in vivo, in vitro and ex vivo model systems used to study preeclampsia, IRI and HF. Future studies aiming at evaluating CVD in preeclampsia patients could benefit from novel models that better mimic the complex scenario described in this article.

Keywords: preeclampsia; cardiovascular disease; heart failure; ischemic/reperfusion injury; in vivo model system; in vitro model system; ex vivo model system

Citation: Liu Chung Ming, C.; Sesperez, K.; Ben-Sefer, E.; Arpon, D.; McGrath, K.; McClements, L.; Gentile, C. Considerations to Model Heart Disease in Women with Preeclampsia and Cardiovascular Disease. *Cells* **2021**, *10*, 899. https://doi.org/10.3390/cells10040899

Academic Editor: Gabriella Minchiotti

Received: 25 March 2021
Accepted: 12 April 2021
Published: 14 April 2021

1. Introduction

Preeclampsia is a multifactorial and dangerous disorder of pregnancy associated with increased risk of developing cardiovascular disease (CVD) in women post-partum; the risk of myocardial infarction or heart attack and heart failure (HF) is at least doubled [1]. However, its pathophysiology remains poorly understood, arising from both scarcity of patient samples from the early stages of placental development, and the variability and unpredictability of disease manifestation in existing animal models. This impedes the development of reliable monitoring and treatment strategies and limits the transferability of findings to human applications [2,3].

Currently, the main phenotypes of preeclampsia are defined as early-onset preeclampsia diagnosed before 34 weeks' gestation, and late-onset preeclampsia diagnosed from 34 weeks' gestation. Early-onset preeclampsia is more closely associated with abnormal placentation occurring in the early stages of pregnancy where impaired spiral uterine artery (SUA) remodeling plays a significant role, whereas late-onset preeclampsia is linked to senescence of the placenta and underlying maternal cardiovascular and metabolic disorders [4,5]. Although mechanisms of this association are still poorly understood, a recent integrative bioinformatics study identified overlapping inflammatory, angiogenesis and metabolic pathways between preeclampsia, hypertension and HF with preserved ejection fraction (HFpEF) [3]. Based on transcriptome analysis, preeclampsia phenotypes have been

defined also as: (i) "maternal", (ii) "canonical" or (iii) "immunologic" (depending on the presence of a healthy placenta and term delivery, typical features of preeclampsia or severe growth restriction and maternal antifetal rejection, respectively) [6].

Myocardial infarction leads to myocardial tissue damage, with loss of cardiomyocytes [7]. Ischemic cardiomyopathy is the most common cause of heart failure and occurs when blood flow to the myocardium is decreased or blocked to a section of the heart [8]. The effective therapeutic intervention is immediate myocardial reperfusion such as percutaneous coronary intervention (PCI) by restoring the blood flow. However, this process can increase the oxygen level in the heart at a toxic rate, leading to ischemia-reperfusion injury (IRI), and induce further cardiomyocyte death [9,10]. The current treatments are successful in reducing immediate mortality, but there is no effective therapy preventing myocardial reperfusion injury, including subsequent scarring and the necrosis of the heart muscle leading to chronic HF.

HF is characterized by the irreversible damage to the ventricular muscle wall [11]. This is often hallmarked by changes in heart shape and size, cardiac remodeling, increased ventricular myocardial mass, hypertrophy, increased collagenous scar tissue and fibrosis [12,13]. HF is considered a chronic phase of cardiac impairment, secondary to other CVDs, rapidly growing in both confirmed and suspected undiagnosed cases, including in the presence of and post preeclampsia [14,15]. At present, prevention and treatment of the underlying CVD factors remain the only way to treat HF, while its prevalence is estimated to have doubled from 27 million cases worldwide to over 50 million cases, with a one in five lifetime risk of developing HF [11,15,16]. Over the past few decades, a better understanding of IRI and HF pathogenesis has been made possible due to several representative in vitro and in vivo models. However, these models have limitations for treating IRI and HF [17–21], which will be discussed below.

In pregnant women, the causes of preeclampsia-induced cardiac dysfunction are still unknown, mainly due to the lack of optimal models to recapitulate this complex disease in the laboratory. Nevertheless, what has been identified is that systemic oxidative stress, inflammation and irregular angiogenesis present in preeclampsia can lead to cardiac fibrosis, apoptosis, diastolic and systolic dysfunction, and subsequent HF post-partum [4,5]. The mechanisms of these aberrant processes that lead to HF following preeclampsia require more reliable disease models to further explore the mechanisms of onset and progression as well as provide an advanced platform for treatment development [22,23].

Advancements in the field of tissue engineering have elevated in vitro models to the point that they are now a promising alternative to in vivo models—that is, animal experimentation [24–26]. The choice of the most appropriate methodology will depend on multiple factors including the specific research question, availability of equipment and skills, budget and time restrictions. This review will primarily compare and contrast the existing in vivo and in vitro experimental models for preeclampsia, IRI and HF, outlining their strengths and limitations. Subsequently, the development of future models linking these disease entities together will be discussed.

2. Preeclampsia Models

2.1. In Vivo Models

The most reliable animal model of preeclampsia should closely mimic the pathogenesis of the disease and the clinical signs and symptoms. Preeclampsia is currently difficult to study due to its multifactorial nature and a lack of suitable patient samples because taking placental samples during pregnancy is invasive and can increase the risk of miscarriage. The commonly used laboratory species do not develop spontaneous preeclampsia. Mouse models display variable and unpredictable disease manifestation, with limited transferability to human applications. Currently, there are numerous animal models that have been developed to simulate these characteristics, however all representing different features of preeclampsia.

2.1.1. Animal Trophoblast Invasion Model

The unique process of placentation in humans makes it challenging to establish a reliable animal model recapitulating human trophoblast invasion. Inappropriate placental development is a fundamental feature in the preeclampsia pathogenesis, where the role of the trophoblast cells in remodeling the maternal uterine vasculature to support growth and development of the fetus is impaired [4]. Some species possess hemochorial placentation where the trophoblasts infiltrate the uterus and create intimate connections with the maternal vasculature, or endotheliochorial placentation, which is less invasive [3,27,28]. This is commonly seen in mammals including rodents, primates, insectivore and bats. Other species possess epitheliochorial placentation where there is a separation between the trophoblastic tissue and maternal tissue in ruminants, pigs and other domesticated animals [3,28,29].

Rodents are good models of preeclampsia as they display interstitial and endovascular trophoblast invasion leading to maternal artery remodeling, and also possess hemochorial placental types similar to humans [3,29]. These models have enabled a better understanding of the pathophysiology of the disease, however all of these models are induced and are not able to recapitulate different phenotypes of preeclampsia. Preeclampsia can be induced in rodents surgically, environmentally, genetically or immunologically [30].

2.1.2. Utero-Placental Ischemia Model

Utero-placental ischemia is another key feature in the pathogenesis of preeclampsia, particularly early onset preeclampsia, leading to hallmark complications including high blood pressure, vasoconstriction, and endothelial dysfunction [31]. Early models of this kind mainly focus on abruptio placentae in animals such as baboons, rabbits, rhesus monkeys, and dogs. This type of model of preeclampsia is induced by either a temporary or permanent ligation of uterine arteries and/or aorta to induce high blood pressure and proteinuria during pregnancy [32–35]. The method has been modernized many times over the years to the most utilized method now being the reduced uterine perfusion pressure (RUPP) model developed by Granger et al., [28,36]. Based on the murine model developed by DJ Eder and MT McDonald [37], the method was modified to assess how hypoxic conditions correlate to cardiovascular and renal dysfunction [28,37]. RUPP models have been used to study and evaluate hallmark features of preeclampsia including elevated blood pressure, proteinuria, fetal growth restrictions, intrauterine growth restrictions, histopathological placental aberrations, reduced placental and embryo weight, and glomerular endotheliosis [28].

2.1.3. Anti-Angiogenic Response Model

One of the key underlying processes in preeclampsia include angiogenic imbalance. The most well studied angiogenic factors, vascular endothelial growth factor (VEGF) and pregnancy induced growth factor (PIGF), are often decreased, whilst anti-angiogenic factors such as soluble fms-like tyrosine kinases (sFlt-1) and soluble endoglin (sEng) increased. Novel angiogenesis-related pathways implicated in preeclampsia have also emerged, including the FKBPL-CD44 pathway [38]. This angiogenic imbalance where anti-angiogenic proteins are increased and pro-angiogenic proteins are reduced often leads to endothelial dysfunction [39].

VEGF is responsible for the production of nitric oxide and other vasodilatory molecules, which are key in maintaining low vascular tone and blood pressure, hence facilitating appropriate glomerular function [38–40]. To study this, models have been developed that focus on administering exogenous anti-angiogenic factors (such as sFlt-1 and sEng) in pregnant rats to induce a preeclampsia-like phenotype [39–42]. Administration of sFlt-1 adenovirus in pregnant rats is capable of generating the preeclampsia phenotype, including decreased levels of VEGF and PIGF, with sFlt-1 having a direct impact on maternal endothelium [39,40]. Similarly, sEng is associated with a reduction in endothelial nitric oxide synthase (eNOS) activity and vascular tone that can lead to vascular damage and

dysfunction [40,42]. These models are best utilized for studying the downstream effects, pathophysiology and treatment options for preeclampsia as opposed to its underlying causes [3].

2.1.4. Immune Models

Several models investigating the immune response in preeclampsia pathogenesis have also been developed. Both TNF-α and IL-6 are inflammatory cytokines elevated in the presence of preeclampsia, a feature recapitulated in animals' models that also exhibit the typical preeclamptic features, including elevated blood pressure, proteinuria, and elevated sFlt-1 and sEng levels [43–47]. Conversely, IL-10 knockout mice in hypoxic conditions in pregnancy displayed preeclamptic symptoms, yet fetal growth restrictions were only seen in wild-type mice exposed to hypoxic conditions [48].

Some women with preeclampsia also display autoantibodies to phospholipids and angiotensin II type I receptors increasing the disease risk. Immunization against these antigens has been used to create other types of immune models of preeclampsia [49,50]. These types of models have suggested a pathophysiological association between immune factors and hypoxic conditions [50]. Hypoxia has been shown to decrease the number of trophoblast cells by causing cell death and as a result of a maternal allogenic immune response induced by shedding of paternal antigens from the placenta into maternal circulation [51].

2.2. In Vitro Models

As described above, one of the key biological processes in pregnancy includes placental development; irregular placental development and growth have been closely associated with preeclampsia [52]. A unique feature in human placentation is endovascular invasion, where trophoblast cells invade the decidua and myometrium to remodel the spiral uterine arteries. Trophoblast invasion is a complex process involving interactions with numerous different cells including endothelial, immune, stem and other stromal cells in the body, making it challenging to study. Furthermore, there is high variability in placentation between species, hence a lack of good animal models to recapitulate early human trophoblast invasion and development [3,52]. Due to these limitations, a wide range of in vitro models have been developed using trophoblast, endothelial, immune and recently mesenchymal stem cells to study mechanisms leading to inappropriate placentation that could lead to preeclampsia [4,23]. These models of placental development and growth have been utilized to investigate the mechanisms of development of different trophoblast cell lineages, invasion and differentiation of trophoblast cells, the formation of syncytia, morphogenesis, placental development, endocrine function, maternal immune response, metabolism and transport, and disease adaptation. Important diagnostic biomarkers and/or potential therapeutic agents have also been identified and developed using these models [28].

2.2.1. Models of Trophoblast Cells

Many in vitro models used to study preeclampsia are based on using trophoblast cells [52–56]. These cells can be obtained through a culture of primary villous and extravillous trophoblasts as well as trophoblast cell lines obtained from the placenta. Fresh isolation of primary trophoblasts is challenging and difficult to obtain, and is often representative of term placental trophoblasts rather than first trimester trophoblasts important for SUA remodeling and appropriate placental developments. Trophoblasts are dynamic cells, which undergo many rounds of differentiation and interact with various cells at different gestational points during placental development. Several freshly isolated first trimester trophoblasts have been transfected with the virus, acquiring the advantage of longer proliferation in cell culture than primary cells [4].

There is controversy around the types of cell lines that should be used to study the role of trophoblasts in SUA remodeling and placental development. The optimal in vitro model would utilize freshly isolated first trimester (primary cytotrophoblast) trophoblast cells; however, when primary cells are newly isolated and cultured, they fuse impulsively,

forming syncytiotrophoblasts [53]. Further limitations include their inability to divide, their limited lifespan, and ethical considerations in the difficulty in obtaining human placental tissue to isolate these cells, especially early in pregnancy [54]. The vast majority of trophoblast cells are isolated from the term placentae following delivery of the baby, which is not reflective of their role in placental development. Inadequate function of trophoblasts in remodeling SUA and placental development is one of the key processes leading to preeclampsia.

The many different cell lines used in placental research include choriocarcinoma (trophoblastic cancer of the placenta) cell lines (JEG-3, BeWo, and JAR), utilized for their villous and extravillous trophoblast features (VTs and EVTs). However, the gene expression profile of choriocarcinoma cell lines inadequately reflects VTs and EVTs due to their inconsistencies in the transcriptome profile, malignant behavior, high passage via hamster cheek pouch, and atypical chromosome count [52,55]. Still, choriocarcinoma cells prove useful to study particular facets of trophoblast immunobiology. JAR cells were found to be beneficial in the investigations of the fusion of the syncytial VT layer and JEG-3 have been beneficial in identifying EVT HLA class-1 molecules [55,57].

HTR-8/SVneo cell lines contain a combination of EVTs transfected with a retrovirus plasmid (simian virus 40) aimed at acquiring the advantage of longer proliferation in cell culture (56), which are frequently used to study EVT invasion, proliferation, and regulation. HTR-8/SVneo is now considered outdated in its attributes to EVTs [57]. A more appropriate trophoblast cell line appears to be the ACH-3P cell line, which was developed by fusing freshly isolated primary first trimester cells with a human choriocarcinoma cell line (AC1-1) [58]. These cells have been shown to closely mimic primary trophoblasts, express trophoblast markers including cytokeratin-7, integrins and matrix metalloproteinases, and display appropriate invasion potential and primary trophoblast transcriptome profile. Interestingly, this cell line contains both VT and EVTs, which can be separated by the presence of HLA-G on the cell surface. When a range of cells were compared to healthy term and first trimester placentae, chromosome 19 miRNA cluster (C19MC) and C14MC that correlate with gestational age were expressed accordingly in HTR-8/SVneo and ACH-3Ps and were absent from choriocarcinoma cells, questioning their reliability for use in trophoblast studies [59]. Furthermore, when functional aspects of choriocarcinoma cells (BeWo, JAR JEG-3) and ACH-3Ps were compared, BeWo cells were determined as the most suitable model of syncytial fusion, whereas ACH-3P and JEG-3 were representative of primary cells in terms of barrier function; overall, ACH-3Ps were deemed the most reliable for placental nanoparticle transport studies [60].

2.2.2. Placental Explants

The use of placental explants involves obtaining a small section of placental tissue to be cultured ex vivo in a dish. This method is used to study trophoblast proliferation and invasion where the cells are maintained in their adequate cellular environment. In the past, placental explants have been used to study placental functions and mechanisms including cellular uptake and interactions, disease mechanisms through secretome profiling and genetic manipulations, as well as drug effects and toxicity. The most common use of this technique nowadays is in relation to trophoblast function. The main advantages of placental explant models are that the trophoblasts are conditioned in a co-cultured environment with appropriate cells, enabling investigations of function and behavior. The main limitations of this model include an inability to separate functions, mechanisms and responses of individual cell types given that placental tissue is multicellular. Furthermore, the explants are generally obtained from term pregnancies, preventing identification of processes implicated in early placental development, which are closely associated with preeclampsia. Extensive degradation of the cells is also observed within as little as 4 h and cell death can occur within 48 h [53,61].

2.2.3. Microfluidics Models

Microfluidic-based assays recapitulate cell–cell and cell–stroma interactions and can monitor cellular and molecular changes in real-time. This facilitates profiling of the secretome in real-time and not just at one point in time. These models allow for the control and manipulation of physical and chemical factors, which are involved in processes at the microenvironment level [52]. The main advantages are the ability to generate chemical gradient profiles, identify chemotactic factors associated with different cell types and observe individual cell migration and morphology while utilizing a cost-effective method [62]. In relation to the study of preeclampsia, this model captures critical features of the maternal–fetal interface, structural placental characteristics, and some physiological features [63]. The device is limited by the amount of stress that can be induced in this model in comparison to what is endured during pregnancy and preeclampsia. It is limited in size to replicate the shear force that is observed in fetal capillaries under physiological conditions [63]. A microfluidics model of placental vasculature and growth incorporating three different cell types (fibroblasts, endothelial cells and pericytes) was recently developed, capable of demonstrating the inflammation-mediated vascular leakage and leukocyte infiltration of the placenta, processes associated with preeclampsia [64]. Another microfluidics model more closely resembling the placenta was developed to include human choriocarcinoma trophoblast cells (JEG-3) and human umbilical cord endothelial cells (HUVECs) seeded between extracellular matrix membrane under dynamic flow conditions illustrating epithelial and endothelial layers within the placenta [63].

2.2.4. In Vitro Models of Endothelial Dysfunction in Preeclampsia

Endothelial dysfunction is another key underlying cause of preeclampsia induced by increased levels of antiangiogenic factors, sFlt-1 and sEng, and a reduction in angiogenic factors, PIGF and VEGF [65]. Another likely cause of endothelial dysfunction includes placental hypoxia or ischemia-reperfusion, leading to oxidative stress, inflammation and endothelial dysfunction [66]. Endothelin 1 (ET-1) and vascular cell adhesion molecule 1 (VCAM-1) are markers of endothelial dysfunction that are also elevated in preeclampsia. ET-1 is a powerful vasoconstrictor released from endothelial cells and VCAM-1 is a cell surface adhesion molecule involved in leukocyte-endothelial cell signal transduction [67]. Both of these molecules, when elevated in preeclampsia, can lead to hypertension and a reduction in blood flow to the major organs. If left untreated, end organ damage likely follows. Research investigating therapeutic options for endothelial dysfunction utilizes either HUVECs or uterine microvascular endothelial cells treated with combination therapy to help restore angiogenic balance and hence ameliorate endothelial dysfunction in preeclampsia [65,67]. Brownfoot et al. [68] previously identified metformin and sulfasalazine as each individually reducing secretion levels of endothelial sFlt-1 and sEng [69]. Recently, they utilized a combination therapy of metformin and sulfasalazine, demonstrating a reduction in sFlt-1 and overexpression of VEGF-α from the placenta. Individual low dose administration led to a reduction in sEng and an increase in PIGF; however, no additive effect was observed from the combination therapy. Moderate effects were noted on reducing markers of endothelial dysfunction with some reduction in ET-1 observed and no change to VCAM-1. The researchers suggest that this low dose treatment was potentially too low and higher doses may be required for the desired effects [65]. In a similar study, proton pump inhibitors were shown to be able to ameliorate TNF-α-induced endothelial dysfunction of HUVECs and uterine microvascular cells, by blocking VCAM-1 expression, leukocytes adhesion to endothelium and irregular tube formation [70]. Other pregnancy-safe medicines including pravastatin were also investigated for the same purpose and showed promising results in restoring endothelial functional dysfunctions [67,71,72].

Co-culture models with trophoblast and endothelial cells are also utilized to mimic the interaction between these two cell types during SUA remodeling that leads to the replacement of maternal endothelial cells to establish high-caliber, low-resistance vessels that enable increased blood flow to the developing feto-placental interface. In this context,

a recent study showed the importance of integrins α1β1 in trophoblast and endothelial cell interaction. Human uterine myometrial endothelial and trophoblast cells (HTR-8/SVneo) were labelled with different fluorescent stains; HTR-8/SVneo were pre-treated with various neutralizing integrin antibodies before co-culturing with endothelial cell networks formed in Matrigel. Trophoblast integration into the endothelial cell network was assessed and the expression of various invasive pathways was determined, identifying galectin-1, TIMP-1, PAI-1, MMP-2, and MMP-9 as key in this process [73].

Despite the great utility of in vitro models, the multifactorial nature of the disease involving many different organs in addition to the placenta limits their use in recapitulating all features of preeclampsia. For this reason, the development of reliable in vivo models is also important [3].

2.3. Additional Considerations of Current In Vivo and In Vitro Models

In summary, abnormalities of cellular and molecular origins in preeclampsia occur between weeks 8 and 18 of pregnancy. It is very difficult and rare to obtain samples of placental tissue during this early stage of pregnancy, which is a major obstacle in the study of the disease [74]. Most methods rely upon placental specimens obtained after delivery. This is limiting in terms of the knowledge that can be obtained within this field, often representative of consequences of preeclampsia rather than pathogenesis. Inherent complications with in vitro and in vivo models require the development of novel model systems that are low-risk, low-cost and reproducible [28]. Since there is no model that can comprehensively replicate the complexities of the disease, a range of in vivo and in vitro systems and preeclampsia-like models are currently necessary to be used in parallel to elucidate the pathophysiology of preeclampsia [3].

3. Cardiovascular Models to Mimic Ischemic-Reperfusion Injury

3.1. In Vivo Models of Ischaemic Heart Disease

While animal models have been extensively used to assess various parameters of cardiac cell physiology and electrophysiology within a living organism, as they integrate the complexity of the whole organism and allow long-term studies, they also display several limitations (Table 1). In addition to ethical considerations, these models do not fully emulate human physiology, are expensive and need experienced personnel [17,75].

Table 1. Major advantages and disadvantages of in vivo models of ischemic heart diseases.

Model	Typical Features	Advantages	Disadvantages	References
Large Nonhuman mammals (dogs, sheep, pigs or nonhuman primates)	-They capture the process of hypoxia-reoxygenation but does not fully model the clinical setting. - Interactions between various cell types.	-Pigs are the closest analogues to humans, followed by sheeps and dogs (comparable heart size and heart rate to humans).	- Difficult and expensive to work with. - Ethical considerations.	[17,19,76–78]
Small mammals (rodents, mice, rabbits)	-They capture the process of hypoxia-reoxygenation but does not fully model the clinical setting. -Interactions between various cell types.	- Physiologically relevant. -Cheaper compared to big animals. -Easier to genetically manipulate compared to larger animals. -Effective to evaluate therapeutic approaches to regenerate the heart after injury.	-Effectiveness and safety for humans remain to be determined. -Rodent hearts have a much higher intrinsic beating rate, higher cardiac basal metabolism and different electrophysiology compared with the human heart. - Ethical considerations.	[76,79,80]

Myocardial IRI is induced in animals by using a suture to temporarily occlude the left descending coronary artery for the designated ischemic time, which is then subsequently released to allow reperfusion [75,76]. This approach captures the process of hypoxia-reoxygenation typical of IRI. However, it does not fully recapitulate the clinical setting, perhaps due to the vessel stenosis or occlusion of an atherosclerotic artery by dislodged plaque, and the reperfusion by the PCI in humans. The ischemic time, ischemic preconditioning and the duration of the reperfusion may depend on the species and other factors, including gender, age and temperature [77,81]. For example, the ischemic time for animal models spans between 30–40 min (mice, rats and rabbits) and 60–180 min (dogs, pigs and monkeys), whereas in humans it is around 198–411 min [81]. Moreover, animal hearts have physiologically different hearts that can affect their response to IRI [75].

3.1.1. Small Mammals Models

Small mammalian animal models, including mice, rats, hamsters and rabbits, have been extensively used to identify effective therapeutic interventions to regenerate the heart following injury [17,82]. Mice are frequently utilized for IRI experiments, as they are genetically malleable, have a rapid breeding cycle and are cheaper compared to other bigger animals [83]. However, they fail to fully replicate human pathophysiology and morphology [8,21]. For example, rodents and mice have a higher heart rate, and different cardiac basal metabolism and electrophysiology compared to humans [75,83,84]. Furthermore, myocardial ischemia develops faster in rodents and is completed after 30 min of coronary occlusion [81]. Using small mammals for IRI allows the examination of the interactions of various cell types, testing of drug effects in the whole organism by analyzing the cell biological and molecular mechanisms as well as genetic modification of the animals. Despite this, the implications for drug efficacy and safety in humans remain to be determined, and while large animal models are considered closer to the clinical settings of IRI in humans, smaller animals are preferred for early testing of feasibility and safety [8,19].

3.1.2. Large Non-Human Mammals Models

Large animals including dogs, sheep, pigs or primates have been used for testing preclinical therapeutic approaches [8,19]. Pigs are the closest analogues to humans and have gained an increasing relevance in recent years as models of IRI since they have a comparable heart size, heart rate, and do not present with resistance against infarction that is typical of primates [75,81,85]. Studies using dogs, sheep, and pigs focusing on the evaluation of novel stem cell therapy approaches to treat ischemic heart disease have been shown to be relevant to humans with a better translation into the clinic [84]. Despite this, preclinical large animal models fail at mimicking remote ischemic conditioning and the inflammatory response [85]. Furthermore, patients with IRI and frequently observed co-morbidities, including diabetes, hypertension and renal failure, are routinely treated with other drugs, hence masking some of the effects of IRI in research animals [84].

3.2. Ex Vivo Models of Ischemic Heart Disease

A Langendorff preparation used to mimic IRI ex vivo involves the isolation of the whole heart from an animal and its perfusion to simulate blood flow [82]. This model allows the evaluation of cardiac function for a more physiological simulation of IRI and for the study of the effects of several drugs to protect against IRI [82,86]. The benefits of this model are that it is low cost, simple to prepare, reproducible and can examine the heart in isolation from the other organ systems and independently of the exocrine control. However, the absence of the reduction-oxidation (redox) signaling and other paracrine factors besides the use of animal cells limits the translation of these studies into humans [17,86]. Additionally, a Langendorff preparation might be viable for only several hours, and around 5–10% of deterioration in the chronotropic and contractile function is developed per hour [86,87].

3.3. In Vitro Models of Ischaemic Heart Disease

In vitro models of myocardial IRI are essential to study the direct effect of reperfusion on individual cardiac cells including cardiomyocytes and to identify potential novel therapeutic targets to prevent the subsequent irreversible cardiac damage [76]. These can be used to control and identify individual external factors that may be involved in IRI and are commonly divided into two-dimensional (2D) and three-dimensional (3D) cell-culture models, as shown in Table 2.

Table 2. Major advantages and disadvantages of in vitro models of ischemic heart diseases.

Model	Typical Features	Advantages	Disadvantages	References
2D Cultures (monocellular and multicellular cell layers)	-High control of various confounding factors (temperature, pH, CO_2). -Widely used to study pathways of IRI and test the candidate therapeutic options.	Monocellular cultures -Testing of the electromechanical properties of individual cardiomyocytes (cardiac physiology). -Individual cardiomyocytes can be controlled by numerous factors such as stress, strain, stiffness. -Effective technique for expanding cell lines Multicellular cultures -Can examine cardiomyocytes culture electrically using microelectrode arrays. -Optimal control over environmental parameters.	Monocellular cultures -Isolated cardiomyocytes can behave differently and show different responses to drugs from cells that are cultured with other cells. -Limited maturity. Multicellular cultures -No cell to cell interaction in 3D and static conditions. - Response to drugs, toxins or signalling modifiers may be misleading.	[8,25,76]
3D Cultures (cardiac spheroids, scaffold-based approaches and organ-on-a-chip models)	-Useful to evaluate more physiologically relevant mechanisms for the prevention and treatment of ischemia/reperfusion injury -Rely on isolated cardiomyocytes from animals, immortalised cell lines, or HiPS-CMs	-Prolonged viability and retain contractile properties. - Mimic key aspects of the phenotypical and cellular heterogeneity as well as microenvironmental aspects. -Cardiac tissue engineering uisng hiPS-CMs aims at promoting cardiac cell maturation and developing a more predictive human tissue model of IRI as well as be patient-specific.	-Expensive cultures. -Tissue culture skills optimal for these cultures are required. -Cell phenotype can be dramatically affected by the culture geometry.	[8,88–92]

3.3.1. Cardiomyocytes Cell Culture (2D Culture)

The 2D in vitro models based on cell monolayers using either freshly isolated primary cardiomyocytes or cell lines in a non-physiological setting induce ischemia with hypoxic conditions and reperfusion with reoxygenation [8]. While freshly isolated cardiomyocytes are more relevant to cardiac cell lines, repeated experimental observations cannot be carried out using the same primary cells [93]. The models primarily rely on isolated cardiomyocytes from animals, immortalized cell lines, or human induced-pluripotent stem cells (hiPSCs). The advantage of studying isolated cardiomyocytes is that it allows precise control of the cellular and extracellular conditions, without the influences of other cell types, notably endothelial cells, fibroblasts, inflammatory/immune cells and platelets as well as circulating factors including hormones, cytokines and neurotransmission [8,88,89,93]. Two-dimensional cardiomyocyte cell culture models offer the advantage to identify the effects of therapeutic agents on cardiomyocytes to elucidate molecular signaling pathways, assess drug-induced cardiotoxicity and achieve targeted manipulation of gene expression

involved in IRI in order to determine disease mechanisms [19]. However, isolated cardiomyocytes in in vitro 2D cultures are removed from their surroundings, that is, syncytial neighbors, blood vessels and extracellular matrix. This leads to the loss of important cues for the optimal pathophysiological scenario typical of IRI [93,94]. Therefore, findings of studies conducted at a cellular level may not necessarily predict what the response would be if the same drug, toxin or signaling agent is tested in in vivo models. Nevertheless, the most attractive cell source for IRI studies are cardiomyocytes derived from hiPSCs (hiPSC-CMs) as they can be cultured to generate human IRI model system, with potential for personalized medicine and be patient-specific [76,95]. This personalized model could be applied for prediction and drug screening of women's heart disease in high-risk women post-preeclampsia given that there is a substantial inter-patient variability for the future risk of CVD.

3.3.2. Three-Dimensional (3D) Cultures

Tissue engineering employed for the purpose of investigating cardiac modelling facilitates the generation of 3D structures from cardiomyocytes alone or in co-cultures with other cell types including endothelial cells and fibroblasts [89,96]. Cardiac cells can be grown in scaffolds, scaffold-free or matrix environments aiming to mimic the extracellular matrix (ECM) aspects of the heart. For example, scaffolds made of collagen and fibrin provide a 3D environment for cells to attach onto, interact with other cells and conduct electrical signals [25].

Engineered heart tissues (EHT) comprised of cardiomyocytes embedded within fibrin-based constructs have been used in numerous in vitro and in vivo studies [90,97–100]. In particular, EHTs have been used to study features typical of IRI and is a promising model to study cardiac function in vitro [90]. The advantages of using EHT are that they are easy to fabricate and can provide reproducible results within a short timeframe [90]. EHTs can be used for real-time measurements of the contractile function and may represent a promising tool for advancing the treatment and prevention of IRI [76].

Scaffold-free approaches using spheroids in hanging drop cultures provide similar advantages to EHTs and do not require the addition of foreign material for the fabrication of the cardiac tissue [88,101]. For instance, Jeong et al.'s [102] research showed that genetically engineered antigen-1-positive cardiac stem cells (Sca-1$^+$ CSC lines) secrete paracrine factors such as SDF-1α and have cardioprotective roles described using in vitro spheroids. SDF-1α has demonstrated to protect the ischemic cardiomyocytes by inducing the signaling pathway for cell growth, survival, and protein synthesis in the 3D IRI spheroid heart model [102].

Interestingly, hiPS-CMs retain a fetal phenotype and are more resistant to IRI hence limiting the translation of findings using these cells into humans [76,95,103]. Tissue engineering approaches using bioreactors or microfluidics devices allow further maturation of hiPS-CMs into a more adult phenotype, but more progress needs to be made as they cannot recapitulate complex features typical of the in vivo microenvironment, such as adult cardiomyocyte function [10,91]. Bioreactors or microfluidic "organ-on-chips" devices provide precise control and better recapitulate the cellular microenvironment of IRI of the heart compared to other in vitro systems, including the monitoring of critical parameters such as pH and oxygen levels [76,104]. However, these cultures do not fully represent the complexity and tissue architecture of the heart due to the absence of different cell types such as fibroblast, endothelial cells and immune cells [91]. Co-culturing cardiomyocytes with other cell types found in the human heart improves the representation of the key aspects of the phenotypical and cellular heterogeneity as well as microenvironmental cues, hence leading to a more reliable model of IRI in the human heart [104]. Therefore, future studies aiming at better engineering strategies of the human heart microenvironment are needed to improve translation of the findings using IRI in vitro models into patients.

3.4. Additional Considerations of Current In Vitro and In Vivo Models

A common criticism of preclinical IRI studies (both cell culture and animal models) is that testing is performed using a homogenous, young and healthy population, while myocardial infarction primarily affects a diverse older population with different comorbidities, including diabetes and cardiac hypertrophy [76]. These additional factors affect the cardiomyocyte response, including their susceptibility to reperfusion injury and the effectiveness of treatments, and further considerations are needed to better translate preclinical studies into humans [95,103,104].

4. Cardiovascular Models to Mimic Heart Failure

Although it is not clear whether endothelial dysfunction is a cause or consequence of preeclampsia, longitudinal studies reported that endothelial dysfunction can persist for 10–20 years following preeclampsia in pregnancy [105]. Epidemiological evidence shows a strong association between preeclampsia and future CVD including HF; however, the mechanisms are poorly understood. In a recent bioinformatics study based on publicly available datasets, 76 overlapping biomarkers which translated into 29 shared pathogenic pathways were identified between preeclampsia, hypertension and heart failure with preserved ejection fraction (HFpEF) [105]. Nevertheless, there are limited studies that investigate the pathogenic mechanisms between preeclampsia and HF, and this area of research is also lacking reliable in vitro and in vivo models.

4.1. In Vivo Models

Animal models seek to mimic both the pathological features of HF and the clinical scenario of patients with HF. The use of animals for this type of modelling can range from multi-organ level (e.g., nervous input to the cardiovascular system) to cellular level (e.g., variable expression of cell-specific genes) [106]. In vivo models exhibit a range of unique advantages including physiological relevance in large animals and reliable standardized protocols in small animals, features that in vitro models are still tackling [20]. Small animal models typically utilize either mice or rats to perform a surgical procedure and induce HF [107]. One of the most frequently used methods is the transverse aortic constriction surgical procedure (TAC). Originally developed by Rockman et al. [108], this widely used method reliably induces HF via increased left-ventricular (LV) afterload, resulting in a sharp increase in LV mass as early as two weeks [108,109]. The disadvantages of these models include the inability to induce progressive features of HF, and they are therefore mainly used for testing the role of specific proteins involved in cardiac dysfunction and genetic mechanisms via transgenic mice [110,111]. Other less common surgical procedures in rats, including a left coronary ligation (LCL) and ascending aortic constriction (AAC), offer a relatively simple procedure with low cost, allowing for a greater number of subjects without damaging large volumes of myocardial tissue [112,113]. LCL induces HF via MI while AAC induces HF via a pressure overload in the ventricles; unlike TAC, this pressure is gradual as opposed to acute. However, these models typically require expensive equipment for analyses, and results are less likely to be reproduced in the clinic. This also posits the challenge of inducing only a specific phenotype of HF, which may be characterized by either a reduced (HFrEF) or HFpEF.

The suitability of large animal models is dependent on the research question being addressed. Spannbauer et al. [114] postulated that the use of large animal models in studies requiring genetic manipulations is limited due to their long gestational periods. Additionally, the development of transgenic species requires highly skilled researchers and the use of expensive specialized facilities that may be a limitation from a resource perspective. However, large animal models have a better translational potential to human clinical studies [20]. Furthermore, these models are considered optimal for studies requiring implantation of sensors and data gathering in a non-anesthetized state related to long term outcomes and medical device development [18,115]. Similar to small animal models, aortic constructions resulting in LV remodeling and hypertrophy are commonly utilized to induce

HF, though there are other methods not utilized in mice and rats [106,115]. Pacing-induced tachycardia has been recognized as a method of HF modelling in large animals via the onset of dilated cardiomyopathy [116]. This model reliably results in progressive and reversible human HF hallmarks such as mechanical, structural and hormonal alterations that has previously been used for testing pharmacological therapies, though it does not result in myocyte hypertrophy or fibrosis and is reversible unlike human HF [117,118].

4.2. In Vitro Models

Modelling HF in vitro has been particularly challenging for researchers due to the nature of the disease and limited options compared to IRI models. As HF is largely related to cardiac output, current methodologies to model and study this aspect are limited. The advent of iPSC-derived cardiac myocytes has propelled in vitro models forward via a reliable source of human cardiac myocytes [26].

Two-dimensional cultures have typically fewer representative models of clinical outcomes but are cost-effective, with access to high throughput assays. This is largely due to the availability of transformed cell lines that, although they may have lower resemblance to in vivo counterparts, allow for unrestricted proliferation. For this reason, transformed cells are often used for drug discovery and cardiotoxicity studies, while iPSC-derived cells are used for genetic and functional studies [25,119]. This is achieved by treating cells with ET-1 to induce cardiac hypertrophy, one of the major risk factors for HF [120].

While useful for investigating certain biochemical or genetic changes, 2D cell cultures ultimately lack important physiological aspects including cell–cell and cell-ECM interactions [102]. An emerging trend that has been rapidly gaining recognition for its potential to model diseases that addresses the drawbacks of 2D cultures is the use of 3D cell cultures of spheroids. Cardiac myocytes cultured within 3D environment often employ a biomaterial such as a hydrogel or biocompatible polymer to mimic the ECM, providing a 3D architecture for cell spheroids to interact in all spatial dimensions both with other cells and their environment. Various ECM are employed for fine-tuning of the microenvironment by modifying properties including elasticity, stiffness, conductivity and porosity [25]. This is a promising advancement for HF modelling as reports have demonstrated the utility of 3D cell models capable of simulating blood flow with modified ejection fractions, observing contractile forces and relaxation velocity in cardiac myocytes as well as variable mechanical cues to simulate increased afterload [121–123].

With the increase in controllable parameters, there is also an increase in complexity. Lack of standardized protocols compared to 2D cell models means that experimental design is more demanding and without high-throughput testing. Additionally, direct induction of HF is still a challenge for disease modelling. The primary methods of modelling in vivo HF rely on replicating the disease by primarily using either cardiovascular high-risk factors including hypertension and MI. Additionally, HF can be induced by mimicking its phenotypic presentation, such as reduced ejection fraction (to simulate the heart as a failing blood pump). Though useful strategies, these approaches restrict studying complex presentations such as HFpEF and long-term disease state.

Overall, in vitro models have great utility as they provide a platform for fundamental biology in drug development, biochemical, genetic and pathophysiology studies, free of ethical concerns for animal use with the potential to reduce the number of animals used in these experiments. Challenges remain in the generation of high-throughput methods for 3D cell analysis and maturation of iPSC-derived cardiac myocytes beyond the neonatal phenotype that is commonly observed.

4.3. Additional Considerations of Current In Vivo and In Vitro Models

In vivo models provide information regarding HF pathophysiology and progression that cannot be replaced until in vitro technologies are developed further. Although there are ethical concerns with animal use, relatively cheap small animal models are still the primary source of data for studying signal cascades and biological processes, while large

animals are paramount for studying contractile function that cannot be replicated in small animals due to biological differences in functional activity. Further information on the advantages and limitations of various in vitro and in vivo models of HF are presented in Table 3.

Table 3. Major advantages and disadvantages of in vitro and in vivo models of heart failure (HF).

Model	Typical Features	Advantages	Disadvantages	References
In Vitro 2D Cell Culture	- Monolayer cell cultures of cardiac cells (either transformed cell lines or iPSC-derived cardiac myocytes) can be co-cultured with other cardiac cells to better recapitulate the in vivo cardiac environment. (commonly employed for genetic studies and drug discovery). - Treatment with endothelin-1 is commonly used as a positive control for cardiac hypertrophy (the largest risk factor for heart failure).	- Culturing cells in 2D is significantly cost-effective when using immortallised cell lines. -Both transformed cells and iPSC-derived cells could be human derived. -Extensive literature using transformed cell lines for drug discovery and cardiotoxic effects. - Cardiac myocytes can be employed for studies of genetic mutations in response to hypertension and cardiac hypertrophy.	-Transformed cells have fundamentally altered genomes. - Two-dimensional culturing lacks the full 3D architecture present in vivo (i.e.,interactions with other cells and the ECM). -They cannot fully recapitulate the human heart pathophysiology.	[23,113,117,119,124]
In Vitro *3D* Cell Culture	- Often including a biomaterial (i.e., a hydrogel or biocompatible polymer) for optimal stiffness and electrical signals.	- Improved models of the in vivo physiological, morphological, biochemical and genetic profile. - Engineered 3D environments also use structural features not present in 2D to mimic mechanical cues (i.e., increased afterload).	-Increased complexity of experimental design. -Directly inducing heart failure is still a challenge for in vitro models when compared to in vivo counterparts.	[22,115–117]
Small Animal In Vivo	- Transverse aortic constriction (TAC) surgery (greater pressure in the left ventricle and subsequently cardiac hypertrophy, fibrosis as well as cardiac output dysfunction).-In periods of up to 4–6 weeks, this progresses to clinical heart failure.	-TAC procedure is a well established method (it can be easily replicated with consistent results). - Can use transgenic mice-Low maintenance costs when compared to in vivo models in large animals.	-Translatability of results is challenging in small animals. - Features of the heart are functionally different when compared to the human heart. - Slight variations can result in greater pathological stimuli than intended. - Ethical considerations.	[106,107,109–111]
Large Animal In Vivo	- A progressive aortic constriction in dogs, sheeps and pigs, is induced in a similar fashion to small animals. - Another method involves tachycardia-induced cardiomyopathy that results in heart failure after several weeks of continuation.	- Increased translatability to human physiology. - Allows live monitoring.	-Research facilities are rarely equipped for significant large animal studies. - Higher costs compared to small animals; - Multidisciplinary teams required for handling. - Ethical considerations.	[18,20,24,106,115,116,125]

5. Discussion

As discussed above, different types of models currently used for preeclampsia, IRI and HF have provided knowledge in understanding some of the pathophysiology and the mechanisms of these CVDs and have been utilized extensively for drug screening. However, none of the current models could fully replicate all the pathophysiological mechanisms for human applications. Following such an extensive list of models in preeclampsia, IRI and GF, we could not identify a model that fully recapitulates the link between preeclampsia and future CVD in laboratory models, which is critical to further address the heterogeneity typical of the preeclampsia phenotypes described in the Introduction. A wide range of in vitro, ex vivo and in vivo model systems of individual diseases have helped in the discovery and validation of novel therapeutic targets and disease mechanisms. However,

there are still large gaps in the knowledge or technology impeding successful translation of the findings from preclinical into human studies. While the etiology of preeclampsia is still not fully uncovered, there is evidence that the fetal environment plays a major role [126]. Among the plethora of potential biomarkers identified in previous studies, future studies will be critical for the identification of better markers for improved classification and potential prevention and therapeutic approaches [127,128].

The approach used to mimic IRI in in vitro and in vivo model systems does not fully recapitulate the occlusion and the reopening of the blood vessels. Furthermore, most tests are performed using a homogenous, young and healthy population without the inclusion of comorbidities. In terms of HF, the current model systems are unable to induce progressive features of HF. The advent of iPSCs could generate in vitro models with potential for personalized medicine [76,95]. Preeclampsia is more complex to replicate in a model, because it starts to develop between 8 and 18 weeks of pregnancy and sampling of the placental tissue is challenging during this stage [74]. There are no current models that mimic the complexities and pathophysiology of the disease.

In vitro models are useful for investigating biochemical or genetic changes, but 2D cultures lack important physiological aspects including cell–cell and cell-ECM interactions [101]. The advancement of 3D cultures has propelled in vitro models forward and could potentially fully replicate the microenvironment and physiology of human heart however further improvements in research are still needed. The most efficient models remain in vivo animal models, especially with large animals that have translation potential towards human clinical studies. However, the reliability of these models still remains unclear, as they do not fully mimic the pathogenesis of the disease, clinical signs, and symptoms.

The pathophysiology of preeclampsia still remains poorly understood, impeding the development of much needed monitoring and treatment strategies for human applications [2,3]. Moreover, preeclampsia is associated with higher risk of subsequent hypertension, MI and HF, leading causes of death in women [129]. The mechanisms of this association are poorly understood due to the lack of available models of disease. Hence, it is critical that further research is carried out that can lead to the development of new platforms and to shed a better light on the pathophysiology leading to the subsequent development of CVD post preeclampsia.

6. Conclusions

The existence of multiple disease models for preeclampsia, IRI and HF illustrates the inherent complexity of these diseases. As discussed above, none of these models encompass all the key pathophysiological mechanisms. However, our increasing knowledge, the diversity of techniques and approaches of each pathology would allow us to develop a unique model that could demonstrate the link between preeclampsia and the subsequent development of CVD. Three-dimensional personalized models based on patients' own cells and iPCSs could better recapitulate the complex cardiovascular scenario typical of preeclampsia and be developed further for testing novel therapies, which is particularly challenging in human pregnancy (Figure 1).

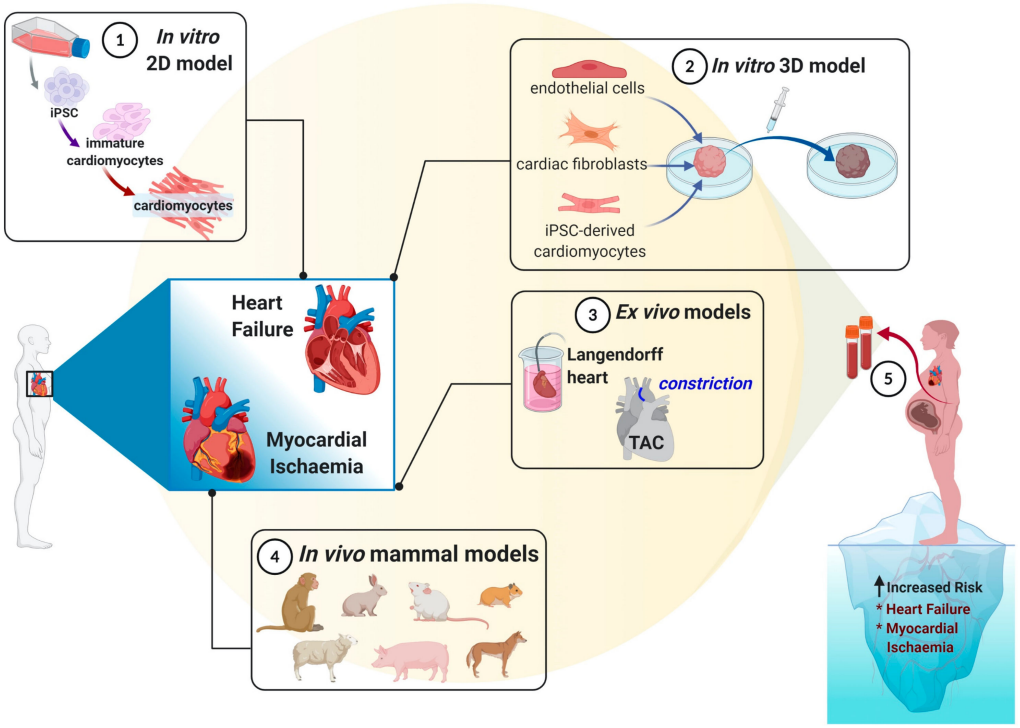

Figure 1. Modeling cardiovascular complications in preeclampsia women. Despite the several in vivo, ex vivo and in vitro models to mimic cardiovascular complications, future studies utilizing personalized approaches, such as patient-derived cells, may benefit to further advance the development of novel therapeutics to both prevent and treat preeclampsia-associated cardiovascular disease in women.

Author Contributions: Writing—original draft preparation, C.L.C.M., K.S., E.B.-S.; writing—review and editing, C.L.C.M., D.A., C.G., K.M., L.M.; visualization, C.G., K.M., L.M.; supervision, C.G., K.M., L.M.; funding acquisition, C.G. All authors have read and agreed to the published version of the manuscript.

Funding: This work was supported by a UTS Seed Grant, a Catholic Archdiocese of Sydney 2019 Grant for Adult Stem Cell Research, and a Sydney Medical School Foundation Cardiothoracic Surgery Research Grant to C.G.

Institutional Review Board Statement: Not applicable.

Informed Consent Statement: Not applicable.

Data Availability Statement: Not applicable.

Conflicts of Interest: The authors declare no conflict of interest.

References

1. Bellamy, L.; Casas, J.P.; Hingorani, A.D.; Williams, D.J. Pre-eclampsia and risk of cardiovascular disease and cancer in later life: Systematic review and meta-analysis. *BMJ* **2007**, *335*, 974. [CrossRef]
2. Marshall, S.A.; Hannan, N.J.; Jelinic, M.; Nguyen, T.P.H.; Girling, J.E.; Parry, L.J. Animal models of preeclampsia: Translational failings and why. *Am. J. Physiol. Regul. Integr. Comp. Physiol.* **2018**, *314*, R499–R508. [CrossRef]
3. Pennington, K.A.; Schlitt, J.M.; Jackson, D.L.; Schulz, L.C.; Schust, D.J. Preeclampsia: Multiple approaches for a multifactorial disease. *Dmm Dis. Models Mech.* **2012**, *5*, 9–18. [CrossRef] [PubMed]
4. McNally, R.; Alqudah, A.; Obradovic, D.; McClements, L. Elucidating the Pathogenesis of Pre-eclampsia Using In Vitro Models of Spiral Uterine Artery Remodelling. *Curr. Hypertens. Rep.* **2017**, *19*, 93. [CrossRef] [PubMed]
5. Burton, G.J.; Redman, C.W.; Roberts, J.M.; Moffett, A. Pre-eclampsia: Pathophysiology and clinical implications. *BMJ* **2019**, *366*, l2381. [CrossRef]
6. Leavey, K.; Benton, S.J.; Grynspan, D.; Kingdom, J.C.; Bainbridge, S.A.; Cox, B.J. Unsupervised Placental Gene Expression Profiling Identifies Clinically Relevant Subclasses of Human Preeclampsia. *Hypertension* **2016**, *68*, 137–147. [CrossRef]

7. Hansen, T.; Saleh, S.; Figtree, G.A.; Gentile, C. The Role of Redox Signalling in Cardiovascular Regeneration. In *Oxidative Stress in Heart Diseases*; Chakraborti, S., Dhalla, N.S., Ganguly, N.K., Dikshit, M., Eds.; Springer: Singapore, 2019; pp. 19–37. [CrossRef]
8. Lindsey, M.L.; Bolli, R.; Canty, J.M., Jr.; Du, X.J.; Frangogiannis, N.G.; Frantz, S.; Gourdie, R.G.; Holmes, J.W.; Jones, S.P.; Kloner, R.A.; et al. Guidelines for experimental models of myocardial ischemia and infarction. *Am. J. Physiol. Heart Circ. Physiol.* **2018**, *314*, H812–H838. [CrossRef] [PubMed]
9. Hausenloy, D.J.; Yellon, D.M. Myocardial ischemia-reperfusion injury: A neglected therapeutic target. *J. Clin. Investig.* **2013**, *123*, 92–100. [CrossRef]
10. Sebastião, M.J.; Serra, M.; Pereira, R.; Palacios, I.; Gomes-Alves, P.; Alves, P.M. Human cardiac progenitor cell activation and regeneration mechanisms: Exploring a novel myocardial ischemia/reperfusion in vitro model. *Stem Cell Res. Ther.* **2019**, *10*, 77. [CrossRef]
11. Ferreira, J.P.; Kraus, S.; Mitchell, S.; Perel, P.; Piñeiro, D.; Chioncel, O.; Colque, R.; de Boer, R.; Gomez-Mesa, J.E.; Grancelli, H. World Heart Federation Roadmap for Heart Failure. *Glob. Heart* **2019**, *14*, 197. [CrossRef]
12. Mann, D.L.; Bristow, M.R. Mechanisms and models in heart failure: The biomechanical model and beyond. *Circulation* **2005**, *111*, 2837–2849. [CrossRef]
13. McMurray, J.J.; Pfeffer, M.A. steady increase, age-adjusted rates of admission for heart failure seem to have reached a plateau, or even decreased. *Lancet* **2005**, *365*, 1877–1889. [CrossRef]
14. Ambrosy, A.P.; Fonarow, G.C.; Butler, J.; Chioncel, O.; Greene, S.J.; Vaduganathan, M.; Nodari, S.; Lam, C.S.; Sato, N.; Shah, A.N. The global health and economic burden of hospitalizations for heart failure: Lessons learned from hospitalized heart failure registries. *J. Am. Coll. Cardiol.* **2014**, *63*, 1123–1133. [CrossRef]
15. Ziaeian, B.; Fonarow, G.C. Epidemiology and aetiology of heart failure. *Nat. Rev. Cardiol.* **2016**, *13*, 368–378. [CrossRef]
16. Bui, A.L.; Horwich, T.B.; Fonarow, G.C. Epidemiology and risk profile of heart failure. *Nat. Rev. Cardiol.* **2011**, *8*, 30. [CrossRef]
17. Black, S.C. In vivo models of myocardial ischemia and reperfusion injury: Application to drug discovery and evaluation. *J. Pharmacol. Toxicol. Methods* **2000**, *43*, 153–167. [CrossRef]
18. Dixon, J.A.; Spinale, F.G. Large animal models of heart failure: A critical link in the translation of basic science to clinical practice. *Circ. Heart Fail.* **2009**, *2*, 262–271. [CrossRef] [PubMed]
19. Garbern, J.C.; Mummery, C.L.; Lee, R.T. Model systems for cardiovascular regenerative biology. *Cold Spring Harb. Perspect. Med.* **2013**, *3*, a014019. [CrossRef]
20. Janssen, P.M.; Elnakish, M.T. Modeling heart failure in animal models for novel drug discovery and development. *Expert Opin. Drug Discov.* **2019**, *14*, 355–363. [CrossRef] [PubMed]
21. Verdouw, P.D.; van den Doel, M.A.; de Zeeuw, S.; Duncker, D.J. Animal models in the study of myocardial ischaemia and ischaemic syndromes. *Cardiovasc. Res.* **1998**, *39*, 121–135. [CrossRef]
22. Aryan, L.; Medzikovic, L.; Umar, S.; Eghbali, M. Pregnancy-associated cardiac dysfunction and the regulatory role of microRNAs. *Biol. Sex Differ.* **2020**, *11*, 14. [CrossRef] [PubMed]
23. Suvakov, S.; Bonner, E.; Nikolic, V.; Jerotic, D.; Simic, T.P.; Garovic, V.D.; Lopez-Campos, G.; McClements, L. Overlapping pathogenic signalling pathways and biomarkers in preeclampsia and cardiovascular disease. *Pregnancy Hypertens.* **2020**, *20*, 131–136. [CrossRef] [PubMed]
24. Oh, J.G.; Kho, C.; Hajjar, R.J.; Ishikawa, K. Experimental models of cardiac physiology and pathology. *Heart Fail. Rev.* **2019**, *24*, 601–615. [CrossRef] [PubMed]
25. Novakovic, G.V.; Eschenhagen, T.; Mummery, C. Myocardial tissue engineering: In Vitro models. *Cold Spring Harb. Perspect. Med.* **2014**, *4*, a014076. [CrossRef]
26. Davis, R.P.; van den Berg, C.W.; Casini, S.; Braam, S.R.; Mummery, C.L. Pluripotent stem cell models of cardiac disease and their implication for drug discovery and development. *Trends Mol. Med.* **2011**, *17*, 475–484. [CrossRef]
27. Pijnenborg, R.; Vercruysse, L.; Pijnenborg, R.; Brosens, I.; Romero, R. Animal models of deep trophoblast invasion. In *Placental Bed Disorders*; Brosens, I., Pijnenborg, R., Romero, R., Eds.; Cambridge University Press: Cambridge, UK, 2010; pp. 127–139.
28. Martinez-Fierro, M.L.; Hernndez-Delgadillo, G.P.; Flores-Morales, V.; Cardenas-Vargas, E.; Mercado-Reyes, M.; Rodriguez-Sanchez, I.P.; Delgado-Enciso, I.; Galvn-Tejada, C.E.; Galvn-Tejada, J.I.; Celaya-Padilla, J.M.; et al. Current model systems for the study of preeclampsia. *Exp. Biol. Med.* **2018**, *243*, 576–585. [CrossRef] [PubMed]
29. Carter, A.M. Animal Models of Human Placentation—A Review. *Placenta* **2007**, 28. [CrossRef]
30. Verlohren, S.; Geusens, N.; Morton, J.; Verhaegen, I.; Hering, L.; Herse, F.; Dudenhausen, J.W.; Muller, D.N.; Luft, F.C.; Cartwright, J.E.; et al. Inhibition of Trophoblast-Induced Spiral Artery Remodeling Reduces Placental Perfusion in Rat Pregnancy. *Hypertension* **2010**, *56*, 304–310. [CrossRef]
31. Aardema, M.W.; Oosterhof, H.; Timmer, A.; van Rooy, I.; Aarnoudse, J.G. Uterine artery Doppler flow and uteroplacental vascular pathology in normal pregnancies and pregnancies complicated by pre-eclampsia and small for gestational age fetuses. *Placenta* **2001**, *22*, 405–411. [CrossRef]
32. Cavanagh, D.; Rao, P.S.; Tung, K.S.; Gaston, L. Eclamptogenic toxemia: The development of an experimental model in the subhuman primate. *Am. J. Obstet. Gynecol.* **1974**, *120*, 183–196. [CrossRef]
33. Myers, R.E.; Fujikura, T. Placental changes after experimental abruptio placentae and fetal vessel ligation of rhesus monkey placenta. *Am. J. Obstet. Gynecol.* **1968**, *100*, 946–951. [CrossRef]
34. Haynes, D.M. Experimental abruptio placentae in the rabbit. *Am. J. Obstet. Gynecol.* **1963**, *85*, 626–645. [CrossRef]

35. Howard, B.K.; Goodson, J.H. Experimental placental abruption. *Obstet. Gynecol.* **1953**, *2*, 442–446. [CrossRef]
36. Granger, J.P.; LaMarca, B.B.; Cockrell, K.; Sedeek, M.; Balzi, C.; Chandler, D.; Bennett, W. Reduced uterine perfusion pressure (RUPP) model for studying cardiovascular-renal dysfunction in response to placental ischemia. *Methods Mol. Med.* **2006**, *122*, 383–392. [CrossRef]
37. Eder, D.J.; McDonald, M.T. A Role for Brain Angiotensin II in Experimental Pregnancy-Induced Hypertension in Laboratory Rats. *Clin. Exp. Hypertens. Part B Hypertens. Pregnancy* **1987**, *6*, 431–451. [CrossRef]
38. Todd, N.; McNally, R.; Alqudah, A.; Jerotic, D.; Suvakov, S.; Obradovic, D.; Hoch, D.; Hombrebueno, J.R.; Campos, G.L.; Watson, C.J.; et al. Role of A Novel Angiogenesis FKBPL-CD44 Pathway in Preeclampsia Risk Stratification and Mesenchymal Stem Cell Treatment. *J. Clin. Endocrinol. Metab.* **2020**, *106*, 26–41. [CrossRef]
39. Maynard, S.E.; Min, J.-Y.; Merchan, J.; Lim, K.-H.; Li, J.; Mondal, S.; Libermann, T.A.; Morgan, J.P.; Sellke, F.W.; Stillman, I.E.; et al. Excess placental soluble fms-like tyrosine kinase 1 (sFlt1) may contribute to endothelial dysfunction, hypertension, and proteinuria in preeclampsia. *J. Clin. Investig.* **2003**, *111*, 649–658. [CrossRef]
40. McCarthy, F.P.; Kingdom, J.C.; Kenny, L.C.; Walsh, S.K. Animal models of preeclampsia; Uses and limitations. *Placenta* **2011**, *32*, 413–419. [CrossRef]
41. Bergmann, A.; Ahmad, S.; Cudmore, M.; Gruber, A.D.; Wittschen, P.; Lindenmaier, W.; Christofori, G.; Gross, V.; Gonzalves, A.C.d.C.; Gröne, H.-J.; et al. Reduction of circulating soluble Flt-1 alleviates preeclampsia-like symptoms in a mouse model. *J. Cell Mol. Med.* **2010**, *14*, 1857–1867. [CrossRef]
42. Venkatesha, S.; Toporsian, M.; Lam, C.; Hanai, J.I.; Mammoto, T.; Kim, Y.M.; Bdolah, Y.; Lim, K.H.; Yuan, H.T.; Libermann, T.A.; et al. Soluble endoglin contributes to the pathogenesis of preeclampsia. *Nat. Med.* **2006**, *12*, 642–649. [CrossRef]
43. Benyo, D.F.; Smarason, A.; Redman, C.W.; Sims, C.; Conrad, K.P. Expression of inflammatory cytokines in placentas from women with preeclampsia. *J. Clin. Endocrinol. Metab.* **2001**, *86*, 2505–2512. [CrossRef]
44. Kupferminc, M.J.; Peaceman, A.M.; Wigton, T.R.; Rehnberg, K.A.; Socol, M.L. Tumor necrosis factor-alpha is elevated in plasma and amniotic fluid of patients with severe preeclampsia. *Am. J. Obstet. Gynecol.* **1994**, *170*, 1752–1757, discussion 1757–1759. [CrossRef]
45. Vince, G.S.; Starkey, P.M.; Austgulen, R.; Kwiatkowski, D.; Redman, C.W. Interleukin-6, tumour necrosis factor and soluble tumour necrosis factor receptors in women with pre-eclampsia. *Br. J. Obstet. Gynaecol.* **1995**, *102*, 20–25. [CrossRef]
46. Faas, M.M.; Schuiling, G.A.; Baller, J.F.; Visscher, C.A.; Bakker, W.W. A new animal model for human preeclampsia: Ultra-low-dose endotoxin infusion in pregnant rats. *Am. J. Obstet. Gynecol.* **1994**, *171*, 158–164. [CrossRef]
47. Aneman, I.; Pienaar, D.; Suvakov, S.; Simic, T.P.; Garovic, V.D.; McClements, L. Mechanisms of Key Innate Immune Cells in Early- and Late-Onset Preeclampsia. *Front. Immunol.* **2020**, *11*. [CrossRef] [PubMed]
48. Lai, Z.; Kalkunte, S.; Sharma, S. A critical role of interleukin-10 in modulating hypoxia-induced preeclampsia-like disease in mice. *Hypertension* **2011**, *57*, 505–514. [CrossRef]
49. Redman, C.W.; Sargent, I.L. Immunology of pre-eclampsia. *Am. J. Reprod. Immunol.* **2010**, *63*, 534–543. [CrossRef]
50. Wenzel, K.; Rajakumar, A.; Haase, H.; Geusens, N.; Hubner, N.; Schulz, H.; Brewer, J.; Roberts, L.; Hubel, C.A.; Herse, F.; et al. Angiotensin II Type 1 Receptor Antibodies and Increased Angiotensin II Sensitivity in Pregnant Rats. *Hypertension* **2011**, *58*, 77–84. [CrossRef] [PubMed]
51. Johansen, M.; Redman, C.W.; Wilkins, T.; Sargent, I.L. Trophoblast deportation in human pregnancy—Its relevance for pre-eclampsia. *Placenta* **1999**, *20*, 531–539. [CrossRef]
52. Abbas, Y.; Turco, M.Y.; Burton, G.J.; Moffett, A. Investigation of human trophoblast invasion in vitro. *Hum. Reprod. Update* **2020**. [CrossRef]
53. Abou-Kheir, W.; Barrak, J.; Hadadeh, O.; Daoud, G. HTR-8/SVneo cell line contains a mixed population of cells. *Placenta* **2017**, *50*, 1–7. [CrossRef]
54. Li, Z.; Kurosawa, O.; Iwata, H. Establishment of human trophoblast stem cells from human induced pluripotent stem cell-derived cystic cells under micromesh culture. *Stem. Cell Res. Ther.* **2019**, *10*, 245. [CrossRef]
55. Apps, R.; Murphy, S.P.; Fernando, R.; Gardner, L.; Ahad, T.; Moffett, A. Human leucocyte antigen (HLA) expression of primary trophoblast cells and placental cell lines, determined using single antigen beads to characterize allotype specificities of anti-HLA antibodies. *Immunology* **2009**, *127*, 26–39. [CrossRef]
56. Apps, R.; Sharkey, A.; Gardner, L.; Male, V.; Trotter, M.; Miller, N.; North, R.; Founds, S.; Moffett, A. Genome-wide expression profile of first trimester villous and extravillous human trophoblast cells. *Placenta* **2011**, *32*, 33–43. [CrossRef] [PubMed]
57. Mi, S.; Lee, X.; Li, X.-P.; Veldman, G.M.; Finnerty, H.; Racie, L.; LaVallie, E.; Tang, X.-Y.; Edouard, P.; Howes, S.; et al. Syncytin is a captive retroviral envelope protein involved in human placental morphogenesis. *Nature* **2000**, *403*, 785–789. [CrossRef]
58. Hiden, U.; Wadsack, C.; Prutsch, N.; Gauster, M.; Weiss, U.; Frank, H.-G.; Schmitz, U.; Fast-Hirsch, C.; Hengstschläger, M.; Pötgens, A.; et al. The first trimester human trophoblast cell line ACH-3P: A novel tool to study autocrine/paracrine regulatory loops of human trophoblast subpopulations—TNF-α stimulates MMP15 expression. *BMC Dev. Biol.* **2007**, *7*, 137. [CrossRef] [PubMed]
59. Morales-Prieto, D.M.; Chaiwangyen, W.; Ospina-Prieto, S.; Schneider, U.; Herrmann, J.; Gruhn, B.; Markert, U.R. MicroRNA expression profiles of trophoblastic cells. *Placenta* **2012**, *33*, 725–734. [CrossRef]
60. Rothbauer, M.; Patel, N.; Gondola, H.; Siwetz, M.; Huppertz, B.; Ertl, P. A comparative study of five physiological key parameters between four different human trophoblast-derived cell lines. *Sci. Rep.* **2017**, *7*, 5892. [CrossRef]

61. Miller, R.K.; Genbacev, O.; Turner, M.A.; Aplin, J.D.; Caniggia, I.; Huppertz, B. Human placental explants in culture: Approaches and assessments. *Placenta* **2005**, *26*, 439–448. [CrossRef]
62. Sackmann, E.K.; Fulton, A.L.; Beebe, D.J. The present and future role of microfluidics in biomedical research. *Nature* **2014**, *507*, 181–189. [CrossRef] [PubMed]
63. Lee, J.S.; Romero, R.; Han, Y.M.; Kim, H.C.; Kim, C.J.; Hong, J.S.; Huh, D. Placenta-on-A-chip: A novel platform to study the biology of the human placenta. *J. Matern. Fetal Neonatal Med.* **2016**, *29*, 1046–1054. [CrossRef] [PubMed]
64. Haase, K.; Gillrie, M.R.; Hajal, C.; Kamm, R.D. Pericytes Contribute to Dysfunction in a Human 3D Model of Placental Microvasculature through VEGF-Ang-Tie2 Signaling. *Adv. Sci.* **2019**, *6*, 1900878. [CrossRef]
65. Brownfoot, F.C.; Hastie, R.; Hannan, N.J.; Cannon, P.; Nguyen, T.V.; Tuohey, L.; Cluver, C.; Tong, S.; Kaitu'u-Lino, T.J. Combining metformin and sulfasalazine additively reduces the secretion of antiangiogenic factors from the placenta: Implications for the treatment of preeclampsia. *Placenta* **2020**, *95*, 78–83. [CrossRef] [PubMed]
66. Wu, F.; Tian, F.J.; Lin, Y.; Xu, W.M. Oxidative Stress: Placenta Function and Dysfunction. *Am. J. Reprod. Immunol.* **2016**, *76*, 258–271. [CrossRef] [PubMed]
67. De Alwis, N.; Beard, S.; Mangwiro, Y.T.; Binder, N.K.; Kaitu'u-Lino, T.J.; Brownfoot, F.C.; Tong, S.; Hannan, N.J. Pravastatin as the statin of choice for reducing pre-eclampsia-associated endothelial dysfunction. *Pregnancy Hypertens.* **2020**, *20*, 83–91. [CrossRef] [PubMed]
68. Brownfoot, F.C.; Hastie, R.; Hannan, N.J.; Cannon, P.; Tuohey, L.; Parry, L.J.; Senadheera, S.; Illanes, S.E.; Kaitu'u-Lino, T.J.; Tong, S. Metformin as a prevention and treatment for preeclampsia: Effects on soluble fms-like tyrosine kinase 1 and soluble endoglin secretion and endothelial dysfunction. *Am. J. Obstet. Gynecol.* **2016**, *214*, 356.e1. [CrossRef]
69. Brownfoot, F.C.; Hannan, N.J.; Cannon, P.; Nguyen, V.; Hastie, R.; Parry, L.J.; Senadheera, S.; Tuohey, L.; Tong, S.; Kaitu'u-Lino, T.J. Sulfasalazine reduces placental secretion of antiangiogenic factors, up-regulates the secretion of placental growth factor and rescues endothelial dysfunction. *EBioMedicine* **2019**, *41*, 636–648. [CrossRef]
70. Onda, K.; Tong, S.; Beard, S.; Binder, N.; Muto, M.; Senadheera, S.N.; Parry, L.; Dilworth, M.; Renshall, L.; Brownfoot, F.; et al. Proton Pump Inhibitors Decrease Soluble fms-Like Tyrosine Kinase-1 and Soluble Endoglin Secretion, Decrease Hypertension, and Rescue Endothelial Dysfunction. *Hypertension* **2017**, *69*, 457–468. [CrossRef]
71. Beckman, J.A.; Creager, M.A. The nonlipid effects of statins on endothelial function. *Trends Cardiovasc. Med.* **2006**, *16*, 156–162. [CrossRef]
72. Zhou, Q.; Liao, J.K. Statins and cardiovascular diseases: From cholesterol lowering to pleiotropy. *Curr. Pharm. Des.* **2009**, *15*, 467–478. [CrossRef]
73. Xu, B.; Shanmugalingam, R.; Chau, K.; Makris, A.; Hennessy, A. Galectin-1–Related Modulation of Trophoblast Endothelial Interactions by Integrins α1 and β1. *Reprod. Sci.* **2020**, *27*, 1097–1109. [CrossRef]
74. Steegers, E.A.P.A. Pre-eclampsia. *Lancet* **2010**, *376*, 631–644. [CrossRef]
75. Chen, T.; Vunjak-Novakovic, G. Human Tissue-Engineered Model of Myocardial Ischemia–Reperfusion Injury. *Tissue Eng. Part A* **2019**, *25*, 711–724. [CrossRef] [PubMed]
76. Chen, T.; Vunjak-Novakovic, G. In vitro Models of Ischemia-Reperfusion Injury. *Regen. Eng. Transl. Med.* **2018**, *4*, 142–153. [CrossRef] [PubMed]
77. Lawson, C.S.; Downey, J.M. Preconditioning: State of the art myocardial protection. *Cardiovasc. Res.* **1993**, *27*, 542–550. [CrossRef]
78. Van der Spoel, T.I.G.; Jansen of Lorkeers, S.J.; Agostoni, P.; van Belle, E.; Gyöngyösi, M.; Sluijter, J.P.G.; Cramer, M.J.; Doevendans, P.A.; Chamuleau, S.A.J. Human relevance of pre-clinical studies in stem cell therapy: Systematic review and meta-analysis of large animal models of ischaemic heart disease. *Cardiovasc. Res.* **2011**, *91*, 649–658. [CrossRef]
79. Xu, Z.; McElhanon, K.E.; Beck, E.X.; Weisleder, N. A Murine Model of Myocardial Ischemia-Reperfusion Injury. *Methods Mol. Biol.* **2018**, *1717*, 145–153. [CrossRef]
80. Luther, D.J.; Thodeti, C.K.; Meszaros, J.G. Injury models to study cardiac remodeling in the mouse: Myocardial infarction and ischemia-reperfusion. *Methods Mol. Biol.* **2013**, *1037*, 325–342.
81. Skyschally, A.; van Caster, P.; Iliodromitis, E.K.; Schulz, R.; Kremastinos, D.T.; Heusch, G. Ischemic postconditioning: Experimental models and protocol algorithms. *Basic Res. Cardiol.* **2009**, *104*, 469–483. [CrossRef]
82. Vidavalur, R.; Swarnakar, S.; Thirunavukkarasu, M.; Samuel, S.M.; Maulik, N. Ex vivo and in vivo approaches to study mechanisms of cardioprotection targeting ischemia/reperfusion (i/r) injury: Useful techniques for cardiovascular drug discovery. *Curr. Drug Discov. Technol.* **2008**, *5*, 269–278. [CrossRef]
83. Bohl, S.; Medway, D.J.; Schulz-Menger, J.; Schneider, J.E.; Neubauer, S.; Lygate, C.A. Refined approach for quantification of in vivo ischemia-reperfusion injury in the mouse heart. *Am. J. Physiol. Heart Circ. Physiol.* **2009**, *297*, H2054–H2058. [CrossRef]
84. O'Hara, T.; Rudy, Y. Quantitative comparison of cardiac ventricular myocyte electrophysiology and response to drugs in human and nonhuman species. *Am. J. Physiol. Heart Circ. Physiol.* **2012**, *302*, H1023–H1030. [CrossRef]
85. Baehr, A.; Klymiuk, N.; Kupatt, C. Evaluating Novel Targets of Ischemia Reperfusion Injury in Pig Models. *Int. J. Mol. Sci.* **2019**, *20*, 4749. [CrossRef] [PubMed]
86. Bell, R.M.; Mocanu, M.M.; Yellon, D.M. Retrograde heart perfusion: The Langendorff technique of isolated heart perfusion. *J. Mol. Cell. Cardiol.* **2011**, *50*, 940–950. [CrossRef]
87. Sutherland, F.J.; Hearse, D.J. THE ISOLATED BLOOD AND PERFUSION FLUID PERFUSED HEART. *Pharmacol. Res.* **2000**, *41*, 613–627. [CrossRef]

88. Figtree, G.A.; Bubb, K.J.; Tang, O.; Kizana, E.; Gentile, C. Vascularized cardiac spheroids as novel 3D in vitro models to study cardiac fibrosis. *Cells Tissues Organs* **2017**, *204*, 191–198. [CrossRef]
89. Polonchuk, L.; Chabria, M.; Badi, L.; Hoflack, J.-C.; Figtree, G.; Davies, M.J.; Gentile, C. Cardiac spheroids as promising in vitro models to study the human heart microenvironment. *Sci. Rep.* **2017**, *7*, 1–12. [CrossRef] [PubMed]
90. Katare, R.G.; Ando, M.; Kakinuma, Y.; Sato, T. Engineered heart tissue: A novel tool to study the ischemic changes of the heart in vitro. *PLoS ONE* **2010**, *5*, e9275. [CrossRef]
91. Roche, C.D.; Brereton, R.J.; Ashton, A.W.; Jackson, C.; Gentile, C. Current challenges in three-dimensional bioprinting heart tissues for cardiac surgery. *Eur. J. Cardio-Thorac. Surg.* **2020**, *58*, 500–510. [CrossRef]
92. Valdés, G. Preeclampsia and cardiovascular disease: Interconnected paths that enable detection of the subclinical stages of obstetric and cardiovascular diseases. *Integr. Blood Press Control* **2017**, *10*, 17–23. [CrossRef] [PubMed]
93. Diaz, R.J.; Wilson, G.J. Studying ischemic preconditioning in isolated cardiomyocyte models. *Cardiovasc. Res.* **2006**, *70*, 286–296. [CrossRef]
94. Piper, H.; Garcña-Dorado, D.; Ovize, M. A fresh look at reperfusion injury. *Cardiovasc. Res.* **1998**, *38*, 291–300. [CrossRef]
95. Hidalgo, A.; Glass, N.; Ovchinnikov, D.; Yang, S.-K.; Zhang, X.; Mazzone, S.; Chen, C.; Wolvetang, E.; Cooper-White, J. Modelling ischemia-reperfusion injury (IRI) in vitro using metabolically matured induced pluripotent stem cell-derived cardiomyocytes. *APL Bioeng.* **2018**, *2*, 026102. [CrossRef]
96. Kanazawa, H.; Tseliou, E.; Malliaras, K.; Yee, K.; Dawkins, J.F.; De Couto, G.; Smith, R.R.; Kreke, M.; Seinfeld, J.; Middleton, R.C.; et al. Cellular postconditioning: Allogeneic cardiosphere-derived cells reduce infarct size and attenuate microvascular obstruction when administered after reperfusion in pigs with acute myocardial infarction. *Circ. Heart Fail.* **2015**, *8*, 322–332. [CrossRef]
97. Song, H.; Yoon, C.; Kattman, S.J.; Dengler, J.; Massé, S.; Thavaratnam, T.; Gewarges, M.; Nanthakumar, K.; Rubart, M.; Keller, G.M.; et al. Interrogating functional integration between injected pluripotent stem cell-derived cells and surrogate cardiac tissue. *Proc. Natl. Acad. Sci. USA* **2010**, *107*, 3329–3334. [CrossRef]
98. Naito, H.; Melnychenko, I.; Didié, M.; Schneiderbanger, K.; Schubert, P.; Rosenkranz, S.; Eschenhagen, T.; Zimmermann, W.H. Optimizing engineered heart tissue for therapeutic applications as surrogate heart muscle. *Circulation* **2006**, *114*, I72–I78. [CrossRef] [PubMed]
99. Zimmermann, W.H.; Melnychenko, I.; Wasmeier, G.; Didié, M.; Naito, H.; Nixdorff, U.; Hess, A.; Budinsky, L.; Brune, K.; Michaelis, B.; et al. Engineered heart tissue grafts improve systolic and diastolic function in infarcted rat hearts. *Nat. Med.* **2006**, *12*, 452–458. [CrossRef]
100. Shimizu, T.; Sekine, H.; Yamato, M.; Okano, T. Cell sheet-based myocardial tissue engineering: New hope for damaged heart rescue. *Curr. Pharm. Des.* **2009**, *15*, 2807–2814. [CrossRef] [PubMed]
101. Gentile, C. Filling the Gaps between the In Vivo and In Vitro Microenvironment: Engineering of Spheroids for Stem Cell Technology. *Curr. Stem Cell Res. Ther.* **2016**, *11*, 652–665. [CrossRef] [PubMed]
102. Jeong, H.S.; Park, C.-Y.; Kim, J.-H.; Joo, H.J.; Choi, S.-C.; Choi, J.-H.; Lim, I.R.; Park, J.H.; Hong, S.J.; Lim, D.-S. Cardioprotective effects of genetically engineered cardiac stem cells by spheroid formation on ischemic cardiomyocytes. *Mol. Med.* **2020**, *26*, 15. [CrossRef]
103. Wang, Y.; Zhang, L.; Li, Y.; Chen, L.; Wang, X.; Guo, W.; Zhang, X.; Qin, G.; He, S.-h.; Zimmerman, A.; et al. Exosomes/microvesicles from induced pluripotent stem cells deliver cardioprotective miRNAs and prevent cardiomyocyte apoptosis in the ischemic myocardium. *Int. J. Cardiol.* **2015**, *192*, 61–69. [CrossRef]
104. Sebastião, M.J.; Gomes-Alves, P.; Reis, I.; Sanchez, B.; Palacios, I.; Serra, M.; Alves, P.M. Bioreactor-based 3D human myocardial ischemia/reperfusion in vitro model: A novel tool to unveil key paracrine factors upon acute myocardial infarction. *Transl. Res.* **2020**, *215*, 57–74. [CrossRef]
105. Shahul, S.; Rhee, J.; Hacker, M.R.; Gulati, G.; Mitchell, J.D.; Hess, P.; Mahmood, F.; Arany, Z.; Rana, S.; Talmor, D. Subclinical left ventricular dysfunction in preeclamptic women with preserved left ventricular ejection fraction: A 2D speckle-tracking imaging study. *Circ. Cardiovasc. Imaging* **2012**, *5*, 734–739. [CrossRef]
106. Houser, S.R.; Margulies, K.B.; Murphy, A.M.; Spinale, F.G.; Francis, G.S.; Prabhu, S.D.; Rockman, H.A.; Kass, D.A.; Molkentin, J.D.; Sussman, M.A. Animal models of heart failure: A scientific statement from the American Heart Association. *Circ. Res.* **2012**, *111*, 131–150. [CrossRef]
107. Patten, R.D.; Hall-Porter, M.R. Small animal models of heart failure: Development of novel therapies, past and present. *Circ. Heart Fail.* **2009**, *2*, 138–144. [CrossRef] [PubMed]
108. Rockman, H.A.; Ross, R.S.; Harris, A.N.; Knowlton, K.U.; Steinhelper, M.E.; Field, L.J.; Ross, J.; Chien, K.R. Segregation of atrial-specific and inducible expression of an atrial natriuretic factor transgene in an in vivo murine model of cardiac hypertrophy. *Proc. Natl. Acad. Sci. USA* **1991**, *88*, 8277–8281. [CrossRef]
109. Richards, D.A.; Aronovitz, M.J.; Calamaras, T.D.; Tam, K.; Martin, G.L.; Liu, P.; Bowditch, H.K.; Zhang, P.; Huggins, G.S.; Blanton, R.M. Distinct phenotypes Induced by three Degrees of transverse Aortic Constriction in Mice. *Sci. Rep.* **2019**, *9*, 1–15. [CrossRef] [PubMed]
110. Irion, C.I.; John-Williams, K.; Chahdi, A.; Yousefi, K.; Fernandez, Y.R.; Hatzistergos, K.E.; Hare, J.M.; Webster, K.; Shehadeh, L.A. Osteopontin Regulates Adult Cardiomyocyte Division in a Mouse Model of Pressure Overload Induced Heart Failure. *Circ. Res.* **2019**, *125*, A123. [CrossRef]

111. Veeraveedu, P.T.; Sanada, S.; Okuda, K.; Fu, H.Y.; Matsuzaki, T.; Araki, R.; Yamato, M.; Yasuda, K.; Sakata, Y.; Yoshimoto, T. Ablation of IL-33 gene exacerbate myocardial remodeling in mice with heart failure induced by mechanical stress. *Biochem. Pharmacol.* **2017**, *138*, 73–80. [CrossRef]
112. Weinberg, E.O.; Schoen, F.J.; George, D.; Kagaya, Y.; Douglas, P.S.; Litwin, S.E.; Schunkert, H.; Benedict, C.R.; Lorell, B.H. Angiotensin-converting enzyme inhibition prolongs survival and modifies the transition to heart failure in rats with pressure overload hypertrophy due to ascending aortic stenosis. *Circulation* **1994**, *90*, 1410–1422. [CrossRef]
113. Pfeffer, M.A.; Pfeffer, J.M.; Fishbein, M.C.; Fletcher, P.J.; Spadaro, J.; Kloner, R.A.; Braunwald, E. Myocardial infarct size and ventricular function in rats. *Circ. Res.* **1979**, *44*, 503–512. [CrossRef] [PubMed]
114. Spannbauer, A.; Traxler, D.; Zlabinger, K.; Gugerell, A.; Winkler, J.; Mester-Tonczar, J.; Lukovic, D.; Müller, C.; Riesenhuber, M.; Pavo, N.; et al. Large Animal Models of Heart Failure With Reduced Ejection Fraction (HFrEF). *Front. Cardiovasc. Med.* **2019**, 6. [CrossRef] [PubMed]
115. Shinbane, J.S.; Wood, M.A.; Jensen, D.N.; Ellenbogen, K.A.; Fitzpatrick, A.P.; Scheinman, M.M. Tachycardia-induced cardiomyopathy: A review of animal models and clinical studies. *J. Am. Coll. Cardiol.* **1997**, *29*, 709–715. [CrossRef]
116. Dandamudi, G.; Rampurwala, A.Y.; Mahenthiran, J.; Miller, J.M.; Das, M.K. Persistent left ventricular dilatation in tachycardia-induced cardiomyopathy patients after appropriate treatment and normalization of ejection fraction. *Heart Rhythm* **2008**, *5*, 1111–1114. [CrossRef] [PubMed]
117. McMahon, W.S.; Mukherjee, R.; Gillette, P.C.; Crawford, F.A.; Spinale, F.G. Right and left ventricular geometry and myocyte contractile processes with dilated cardiomyopathy: Myocyte growth and β-adrenergic responsiveness. *Cardiovasc. Res.* **1996**, *31*, 314–323.
118. Spinale, F.G.; Tomita, M.; Zellner, J.L.; Cook, J.C.; Crawford, F.A.; Zile, M.R. Collagen remodeling and changes in LV function during development and recovery from supraventricular tachycardia. *Am. J. Physiol. Heart Circ. Physiol.* **1991**, *261*, H308–H318. [CrossRef]
119. Watkins, S.J.; Borthwick, G.M.; Arthur, H.M. The H9C2 cell line and primary neonatal cardiomyocyte cells show similar hypertrophic responses in vitro. *Vitr. Cell. Dev. Biol. Anim.* **2011**, *47*, 125–131. [CrossRef] [PubMed]
120. Carlson, C.; Koonce, C.; Aoyama, N.; Einhorn, S.; Fiene, S.; Thompson, A.; Swanson, B.; Anson, B.; Kattman, S. Phenotypic Screening with Human iPS Cell–Derived Cardiomyocytes: HTS-Compatible Assays for Interrogating Cardiac Hypertrophy. *J. Biomol. Screen.* **2013**, *18*, 1203–1211. [CrossRef]
121. Hirt, M.N.; Sörensen, N.A.; Bartholdt, L.M.; Boeddinghaus, J.; Schaaf, S.; Eder, A.; Vollert, I.; Stöhr, A.; Schulze, T.; Witten, A. Increased afterload induces pathological cardiac hypertrophy: A new in vitro model. *Basic Res. Cardiol.* **2012**, *107*, 307. [CrossRef] [PubMed]
122. Bouten, C.; Dankers, P.; Driessen-Mol, A.; Pedron, S.; Brizard, A.; Baaijens, F. Substrates for cardiovascular tissue engineering. *Adv. Drug Deliv. Rev.* **2011**, *63*, 221–241. [CrossRef]
123. Wang, Y.; Hill, J.A. Electrophysiological remodeling in heart failure. *J. Mol. Cell. Cardiol.* **2010**, *48*, 619–632. [CrossRef] [PubMed]
124. Yarbrough, W.M.; Spinale, F.G. Large animal models of congestive heart failure: A critical step in translating basic observations into clinical applications. *J. Nucl. Cardiol.* **2003**, *10*, 77–86. [CrossRef] [PubMed]
125. Ye, L.; Chang, Y.H.; Xiong, Q.; Zhang, P.; Zhang, L.; Somasundaram, P.; Lepley, M.; Swingen, C.; Su, L.; Wendel, J.S.; et al. Cardiac repair in a porcine model of acute myocardial infarction with human induced pluripotent stem cell-derived cardiovascular cells. *Cell Stem Cell* **2014**, *15*, 750–761. [CrossRef]
126. Nomura, Y.; John, R.M.; Janssen, A.B.; Davey, C.; Finik, J.; Buthmann, J.; Glover, V.; Lambertini, L. Neurodevelopmental consequences in offspring of mothers with preeclampsia during pregnancy: Underlying biological mechanism via imprinting genes. *Arch. Gynecol. Obstet.* **2017**, *295*, 1319–1329. [CrossRef] [PubMed]
127. Carty, D.M.; Delles, C.; Dominiczak, A.F. Novel biomarkers for predicting preeclampsia. *Trends Cardiovasc. Med.* **2008**, *18*, 186–194. [CrossRef]
128. Eastabrook, G.; Aksoy, T.; Bedell, S.; Penava, D.; de Vrijer, B. Preeclampsia biomarkers: An assessment of maternal cardiometabolic health. *Pregnancy Hypertens.* **2018**, *13*, 204–213. [CrossRef]
129. Melchiorre, K.; Sutherland, G.R.; Liberati, M.; Thilaganathan, B. Preeclampsia Is Associated With Persistent Postpartum Cardiovascular Impairment. *Hypertension* **2011**, *58*, 709–715. [CrossRef] [PubMed]

1.3 Cardiovascular Tissue Regeneration

Summary:

The following book chapter was published on 2 May 2022 by Springer International Publishing. It provides a comprehensive overview of the cutting-edge strategies for promoting cardiovascular regeneration, focusing on cell-based, cell-free therapies and cardiac tissue engineering techniques to promote cardiac function and prevent HF in adults. It delves into the therapeutic potential of paracrine factors, cellular therapies utilizing stem cells, and a variety of 3D bioengineering technologies, including engineered heart tissues (EHTs), tissue organoids, and cell sheets. Additionally, it discusses the application of 3D bioengineered cardiac tissues as substitutes for traditional research model systems in disease modeling, drug discovery, and toxicity testing. The novelty of this paper lies in its integration of the latest advancements in 3D bioprinting technology with cell-based therapies to create a multidimensional approach to cardiac regeneration. This innovative perspective not only offers a detailed analysis of the potential mechanisms and benefits of these regenerative strategies but also highlights the transformative impact of 3D bioprinting on the development of more accurate and practical models for cardiovascular research. By bridging the gap between traditional regenerative techniques and cutting-edge bioprinting technologies, this chapter sets a new precedent for the future of cardiovascular disease treatment and research, opening new avenues for personalized medicine and the development of targeted therapies. For the overall thesis, this chapter highlights the types of 3D *in vitro* models for CVD research, including the CS model and their applications as a substitute for current *in vitro* and *in vivo* models.

Stem Cell-Based 3D Bioprinting for Cardiovascular Tissue Regeneration

Clara Liu Chung Ming, Eitan Ben-Sefer, and Carmine Gentile

1 Introduction

Cardiovascular disease (CVD) represents the single greatest cause of death in the world, especially in the aging population [1–3]. The increased incidence of CVD has been more recently associated with co-morbidity with other chronic diseases, such as kidney failure and type II diabetes [3–6]. In the last decade, CVD accounted for nearly one third of all deaths worldwide [1, 3, 7]. The global disease burden caused by CVD is estimated to include up to 400 deaths per 100,000 in developed countries and is further driven by an unprecedented growing and aging population, with notable increases in ischaemic heart disease (IHD), stroke and heart failure (HF) [1, 2, 7]. IHD and strokes are caused by a lack of blood supply and oxygen to the heart or brain, respectively, and are the main CVD contributions to the global disease burden accounting for 8–10% of all deaths in Europe [2, 3, 8]. Their treatments have greatly advanced over the past three decades, resulting in improved survival rates [1, 5, 8]. Multiple therapeutic interventions including drugs (such as, cholesterol modifiers and anti-hypertensives) and surgical procedures aiming at repairing or bypassing damaged arteries, have greatly reduced the mortality of CVD

1.4 Cardioprotective Role of Acetylcholine (ACh)

Summary:

The literature review is currently under review for publication in the iScience Journal, submitted on 02 April 2024. This chapter delves into the physiological significance of ACh and explores current approaches to increase ACh levels against CVD in both pre-clinical and clinical studies. Additionally, it offers an overview of various ACh delivery mechanisms and presents a comprehensive overview of alternative strategies for targeted ACh delivery in affected areas. The novelty of this review lies in its comprehensive synthesis of recent advancements in ACh delivery technology and its potential for targeted therapeutic applications. It highlights emerging methodologies that could revolutionize the precision and effectiveness of CVD treatments, providing a fresh perspective on integrating biochemical and biomedical engineering approaches in the field. This innovative angle not only bridges existing gaps in the literature but also sets the stage for future research directions that could lead to significant breakthroughs in cardiovascular therapy. To the overall thesis, this chapter describes the protective role of ACh against CVD and the limitations of current approaches such as VNS and cholinesterase inhibitors. Hence, there is a need to develop new therapeutic strategies aiming to deliver ACh directly to the infarcted area in low doses sufficient to confer protective effects while minimizing the side effects.

Protective Role of Acetylcholine and the Cholinergic System in the Injured Heart

Clara Liu Chung Ming[1], Xiaowei Wang[2,3,4*], Carmine Gentile[1,5*].

1. School of Biomedical Engineering, Faculty of Engineering and Information Technology, University of Technology Sydney, Sydney, NSW, Australia.
2. Molecular Imaging and Theragnostic Laboratory, Baker Heart and Diabetes Institute, Melbourne, VIC 3004, Australia.
3. Department of Medicine, Monash University, Melbourne, VIC 3800, Australia.
4. Department of Cardiometabolic Health, University of Melbourne, Melbourne, VIC 3010, Australia.
5. Cardiovascular Regeneration Group, Heart Research Institute, Newtown, NSW 2042, Australia.

***Corresponding authors:** Dr Carmine Gentile, School of Biomedical Engineering, Faculty of Engineering and IT, University of Technology Sydney, Ultimo, NSW; email: carmine.gentile@uts.edu.au

A/Prof Xiaowei Wang, Molecular Imaging and Theragnostic Laboratory, Baker Heart and Diabetes Institute, Melbourne, VIC; email: xiaowei.wang@baker.edu.au

Abstract

This review explores the roles of the cholinergic system in the heart, comprising the neuronal and non-neuronal cholinergic systems. Both systems are essential for maintaining cardiac homeostasis by regulating the release of acetylcholine (ACh). A reduction in ACh release is associated with the early onset of cardiovascular diseases (CVD), and increasing evidence supports the protective roles of ACh against CVD. We address the challenges and limitations of current strategies to elevate ACh levels, including vagus nerve stimulation and pharmacological interventions such as cholinesterase inhibitors. Additionally, we introduce novel strategies to increase ACh in the heart, such as stem cell therapy, gene therapy, microRNAs, and nanoparticle drug delivery methods. These findings offer new insights into advanced treatments for regenerating the injured human heart.

1. Introduction

Cardiovascular diseases (CVD) are a leading contributor to global mortality and morbidity, responsible for an estimated 17.9 million deaths each year, as reported by World Health Organisation [1]. In the early phases of CVD, an imbalance occurs within the autonomic system, marked by an increase in the sympathetic activity and a decrease in the parasympathetic system. This disequilibrium is associated with an increase of norepinephrine and a reduction in the release of acetylcholine (ACh), contributing to higher rates of cardiac mortality and hindering myocardial regeneration [2-4]. Early studies reported that an increase in sympathetic activation and parasympathetic inhibition in dogs leads to tachycardia-induced heart failure [5]. Additionally, Mahmoud et al. [2] demonstrated that inhibition of the cholinergic nerve during cardiac injury in neonatal mice and zebrafish leads to incomplete heart regeneration, causing a significant decrease in neonatal cardiac cell proliferation. In clinical trials, such as the Autonomic Tone and Reflexes After Myocardial Infarction study (ATRAMI) and Cardiac Insufficiency Bisoprolol Study II (CIBIS II), reduced cardiac vagal activity is associated with increased heart rate and higher mortality rates in HF patients [6, 7]. In preclinical studies, Guimarães [8] demonstrated that mice with a long-term cholinergic deficit exhibit increased norepinephrine levels and heightened sympathetic activity, resulting in cardiotoxicity. However, the correlation between CVD and autonomic dysfunction is still not well understood.

Several studies have reported that a decrease in ACh release, stemming from reduced cholinergic activity, is linked with various CVD, including arrhythmias [9], atherosclerosis [10, 11], myocardial infarction (MI) [12, 13], ischemic-reperfusion injury (I/R) [14, 15], doxorubicin (DOX)-induced cardiotoxicity [16] and heart failure (HF) [17]. Additionally, increasing ACh secretion restores the imbalance of the autonomic system, improves heart rate viability, regulates mitochondrial function, suppresses reactive oxygen species (ROS) production and alleviates inflammatory responses [8, 18]. Several studies have shown that the cholinergic system in the heart plays a pivotal role in guiding cardiac regeneration in the injured heart in mice, rats, rabbits, swine and canine [19-23]. Nonetheless, these pre-clinical findings have not been successfully translated to clinical studies, potentially due to the variability in ACh delivery methods across studies and more broadly to the multitarget effects of ACh in the human body. Therefore, a better understanding of the potential protective roles of ACh against myocardial injury as well as the mechanisms regulating this process will facilitate the development of new therapeutic targets against cardiac damage.

This review provides an overview of the cholinergic system in the heart, categorizing it into the neuronal and non-neuronal cholinergic systems (NNCS). Both systems are interconnected and essential for regulating the release of ACh, which binds to muscarinic and/or nicotinic ACh receptors to activate various signaling pathways, thereby maintaining cardiac homeostasis. We discuss the role of ACh-derived from both systems in the heart and its therapeutic potential through muscarinic and/or nicotinic ACh receptors against CVD. The review also examines the limitations and constraints of current methods used to increase ACh levels in pre-clinical and clinical trials, such as vagus nerve stimulation and cholinesterase inhibitors. Finally, we highlight alternative approaches to target the cholinergic system for more targeted and less invasive therapeutic strategies.

2. The cholinergic system of the heart

The autonomic system is comprized of the sympathetic and parasympathetic nervous systems, which work in opposition to each other to balance heart activity. The parasympathetic nervous system, also known as the neuronal cholinergic system encompasses molecules responsible for the synthesis, storage, release, signaling, and degradation of ACh, collectively regulating extracellular ACh concentrations within the presynaptic terminal [18]. As a neurotransmitter, ACh is employed to modulate cardiac activity through muscarinic ACh receptors (mAChRs) to regulate heart dynamics [8] and through nicotinic ACh receptors (nAChRs) to modulate inflammatory pathways and cardiac hemodynamic [24].

As outlined in **Figure 1**, ACh synthesis is catalyzed by choline acetyltransferase (ChAT), leading to its release and subsequent action in the cardiac extracellular space. The latter combines choline, supplied by high-affinity choline transporter (CHT1) with acetyl-CoA [18, 25]. ACh is stored within synaptic vesicles, which are acidified *via* an energy-dependent pump (H-ATPase) and mediated *via* vesicular acetylcholine transporter (VAChT) [26]. Upon depolarization, calcium influx triggers exocytosis, wherein ACh-filled synaptic vesicles fuse with the cellular membrane, releasing ACh in the synaptic cleft [4]. Once released into the extracellular space, neuronal-derived ACh binds to mAChRs and nAChRs to activate various signalling pathway in the cardiovascular system [27] . The degradation of ACh occurs rapidly by cholinesterase including acetylcholinesterase (AChE) found on the surface of the postsynaptic cell surface [27] and are anchored to red blood cells [28], and butyrylcholinesterase (BChE), a soluble enzyme largely found in blood [29, 30]. BChE is

significantly present in the heart, while both BChE and AChE hydrolyse ACh in choline and acetate [30]. CHT1 then transports Choline to the presynaptic terminal [4].

Over the past two decades, a few studies have supported an additional intrinsic cholinergic machinery in heart cells, also known as the non-neuronal cholinergic system (NNCS) (which includes cardiomyocytes [14], endothelial cells [31], and leukocytes [31, 32]). Recently, Tarnawski et al. [31] showed that ACh-derived T cells regulate vascular endothelial function and blood pressure *via* promoting endothelial nitric oxide synthase activity, vasorelaxation and reducing vascular endothelial activation. Although leukocytes and endothelial cells have been shown to have the components of cholinergic machinery, their contribution to the total pool of ACh in the heart is low and remains unexplored [4, 33].

In this review, we focus on cardiomyocyte cholinergic machinery and the role played by cardiomyocyte-derived ACh in the heart. Cardiomyocytes can synthesize, transport, and release ACh, as they contain enzymes and transporters for ACh synthesis (ChAT), storage (VAChT), degradation (AChE), and reuptake of choline for synthesis (CHT1) (**Figure 1**) [34]. Roy et al. [35] suggested that cardiomyocyte-derived ACh functions through similar second messenger systems and binds to mAChRs or nAChRs similar to neuronal-derived ACh. Additionally, studies have found that cardiomyocyte-derived ACh was detected intracellularly and extracellularly using cholinesterase inhibitors such as donepezil, pyridostigmine, and physostigmine [36, 37]. Hence, NNCS in cardiomyocytes comprises those components to regulate ACh homeostasis and acts in an auto-/ paracrine manner to mediate signalling [18]. This concludes that both neuronal and NNCS cross-talk with each other to mediate and regulate homeostasis heart activity.

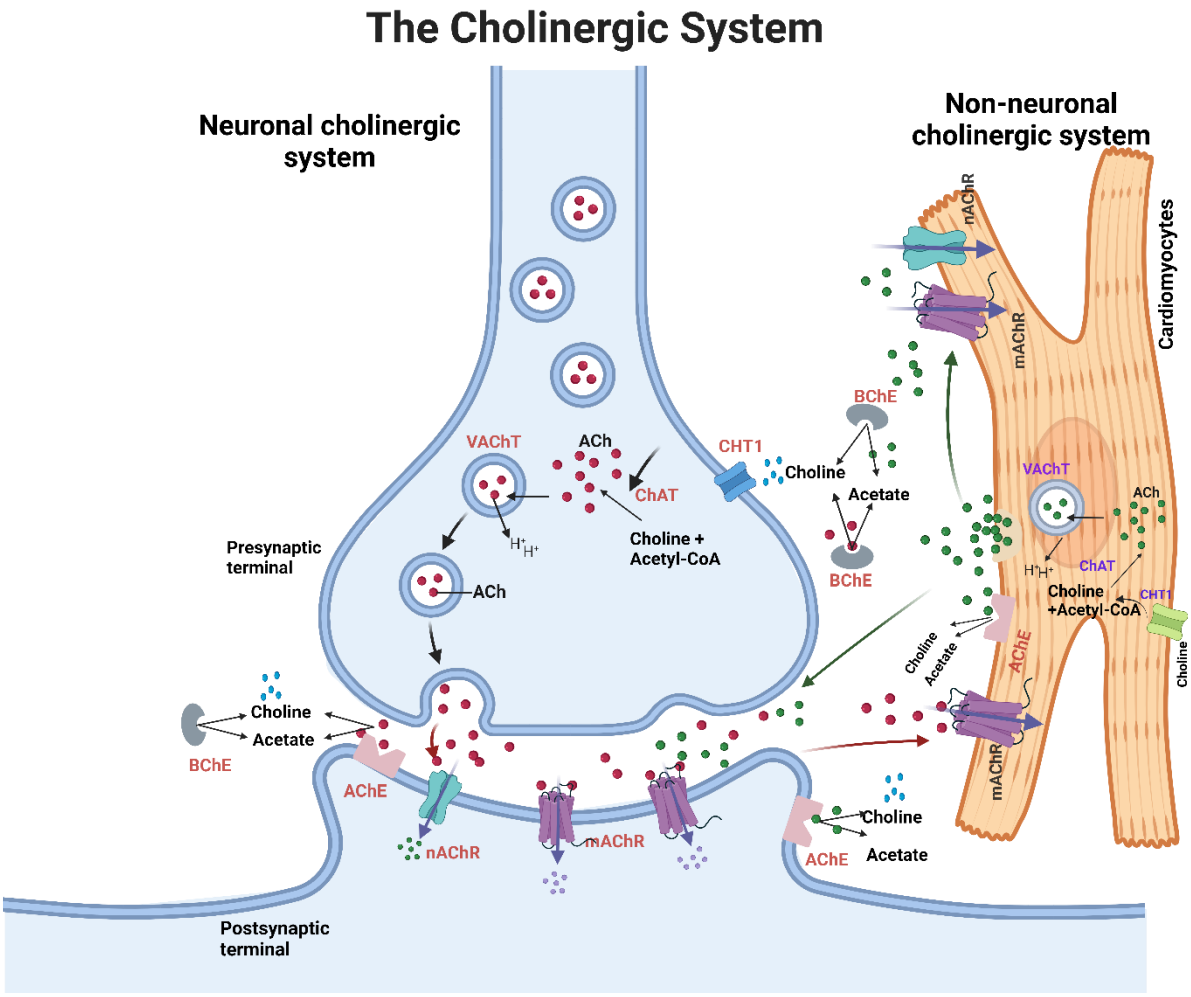

Figure 1. Schematic illustration of the cardiac neuronal cholinergic system in both cardiomyocytes and cholinergic nerves. ACh (red) is synthesized by choline acetyltransferase (ChAT) from the reaction between acetyl-CoA and choline within neurons. ACh is stored and released by vesicular acetylcholine transporter (VAChT) upon stimulation. ACh binds to ligand-gated ion channels nicotinic or G protein-coupled muscarinic ACh receptors (nAChRs and mAChRs, respectively) at the postsynaptic terminal and on cardiomyocytes. For cardiomyocytes, ACh (green) is released from cardiomyocytes and ACh binds to mAChRs and nAChRs expressed on their membrane to mediate signalling and at the postsynaptic terminal. Acetylcholinesterase (AChE) present on postsynaptic terminal and cardiomyocytes, and butyrylcholinesterase (BChE) present in the extracellular space degrade ACh to choline and acetate. High-affinity choline transporters (CHT1) present in cholinergic neurons and cardiomyocytes, are responsible for the reuptake of free choline for ACh synthesis.

3. The role of cardiomyocytes-derived acetylcholine in the heart

While both the neuronal and NNCS operate concurrently to regulate cardiac homeostasis, cardiomyocyte-derived ACh plays a crucial role in the heart and offers protection against CVD. ACh-derived from cardiac NNCS sustains or enhances neuronal cholinergic effects, regulates heart rate, counteracts hypertrophic signals, maintains action potential propagation, and regulates cardiac energy metabolism [26, 35, 36, 38-40]. For instance, Roy et al. [40] found that lowering the levels of cardiomyocyte-derived ACh using ChAT and VAChT knockout mice models resulted in increased heart rate and cardiovascular dysfunction. This suggests that a reduction in cardiomyocyte-derived ACh levels could potentially cause long-term changes in heart function, including ventricular cardiomyocyte hypertrophy, cardiac remodeling, and an increase in ROS [40]. Similar to neuronal-derived ACh, cardiomyocyte-derived ACh is crucial for maintaining cardiac homeostasis and regulating critical signaling pathways to maintain normal heart activity. Furthermore, Kakinuma et al. [41] demonstrated that ChAT deletion in murine atrial myocardial cells increased oxygen consumption, mitochondrial activity and reduction of ATP levels. As a result, cardiac NNCS plays a protective role in cardiomyocytes and the entire heart by maintaining physiological ATP levels and inhibiting oxygen consumption [42].

NNCS is also crucial for maintaining the balance between parasympathetic and sympathetic heart innervation and could amplify the protective effects of the parasympathetic nervous system [4, 43]. Few studies have shown that cardiomyocyte-derived ACh could modulate the central nervous system via the afferent vagal nerve, initiating cross-talk with other organs such as the brain, liver and others [44]. Increasing cardiac NNCS signaling through genetic approach and/or pyridostigmine a cholinesterase inhibitor, leads to protective immunomodulatory effects, such as a reduction in CCL2/7 chemokines expression and a decrease of proinflammatory CCR2+ monocytes in the heart following cardiac injury [45]. This supports the cardioprotective role of cardiomyocyte-derived ACh *via* the modulation of the innate immune system.

Despite the fact that cardiac NNCS could be a potential target for therapeutic intervention, the detailed mechanisms that trigger the release of cardiomyocyte-derived ACh are still unclear. While Rocha-Resende et al. [26] proposed that adrenergic stimulation can induce cholinergic gene expression in cardiomyocytes. Roy et al. [35] suggested that cardiomyocyte-derived ACh may be regulated by sympathetic activity and the intrinsic cholinergic machinery, to regulate

heart rate after stress and exercise. However, further studies are needed to identify the factors that activate NNCS in cardiomyocytes.

3.1 The role of cardiomyocyte-derived ACh against CVD

In this sub-section, we explore the potential therapeutic role of targeting cardiac NNCS and the protective role of cardiomyocyte-derived ACh against CVD. The current methods to increase cardiac NNCS activity are cholinesterase inhibitors including pyridostigmine [26, 45] and donepezil [36], siRNA targeting AChE to increase ACh level [26] and overexpression of ChAT gene [34, 42] or VAChT gene [45]. Numerous studies have demonstrated that cardiac NNCS reduces oxygen demand and improves oxygen supply during ischemic injury, thereby preventing ischemia-induced cardiac dysfunction [42, 45] as well as preventing type 1 diabetes-induced heart diseases [46].

To elucidate the cardioprotective function of the NNCS in ischemic heart disease, Kakinuma et al. [42] generated a heart-specific ChAT transgenic (ChAT-tg) mouse model that express ChAT exclusively in the heart and effectively synthesise ACh in cardiomyocytes. The findings revealed that cardiomyocyte-derived ACh plays an evident role in regulating myocardial energy metabolism through the activation of myocardial glucose utilization and angiogenesis in the infarcted area. Additionally, after 14 days, ChAT-tg mice exhibited increased resistance to MI and a higher survival rate compared to wild-type mice. This could be linked to the fact that cardiomyocyte-derived ACh activates HIF-1α, a non-hypoxic mechanism as well as efficiently preventing energy depletion in the heart [47].

Moreover, cardiomyocyte-derived ACh increases cellular ATP levels. By monitoring ATP levels in real-time, Oikawa et al. [48] demonstrated that IGF-1R and Glut-1 protein expressions were upregulated together with an increase of ACh-derived cardiomyocytes, leading to a rise in glucose uptake and utilisation. This mechanism preserves cellular ATP levels during oxidative stress and suppresses ROS production [14]. Therefore, overexpression of cardiomyocyte ChAT activates cardiac ACh-HIF-1α cascade and improves cell survival after myocardial I/R. Moreover, Kakinuma et al. [42] found that upregulation of cardiomyocyte ChAT activates the cardiac ACh-HIF-1α cascade to improve cells in ChAT-tg myocardial I/R mice. Hence, loss of cardiac ACh-HIF-1α transcriptional pathway leads to cardiac dysfunction, which could be due to the synergistic effect of hypovascularity, calcium mishandling, and decreased myocardial energy [14].

While increase of sympathetic activity and norepinephrine is associated with arrhythmogenesis, cardiotoxicity, and impaired parasympathetic function, no link has been established between cardiomyocyte-derived ACh and cardiac norepinephrine levels [8]. Consequently, the specific molecular mechanisms by which cardiomyocyte-derived ACh influences the cardiac cholinergic system remain unknown, underscoring the need for additional research. For instance, Kakinuma et al. [36] suggested that cardiomyocytes increase the transcriptional activity of ChAT gene through mAChRs and ChAT protein expression to increase ACh level in the cholinergic system. Furthermore, studies have shown that the NNCS enhances vagus nerve activity by increasing the release of nitric oxide from cardiomyocytes, contributing to beneficial cardiac effects [42, 44] as well as extracardiac effect [49]. Oikawa et al. [49] reported that ChAT-tg mice increase production of ventricular cardiomyocytes-derived ACh which acts as vagus nerve stimulation (VNS). Hence, NNCS is involved in anti-inflammatory responses in the brain and plays a significant role in regulating higher brain functions, including mood or stress, and the blood-brain barrier (BBB) [44, 49]. Therefore, it is crucial to conduct further investigations to fully understand the true clinical potential of targeting the cardiac NNCS and its effects on peripheral organs. Future research should also focus on determining the optimal strategies for enhancing NNCS-derived ACh levels in the heart.

4. Cardioprotective roles of ACh via muscarinic and nicotinic ACh receptors

Impairments in ACh signaling from both neuronal and NNCS sources can result in cellular death, heart dysfunction, and suppression of anti-inflammatory pathways, mediated by mAChRs and nAChRs [50, 51]. Stimulation of mAChRs, which are G protein-coupled receptors, leads to a decrease in heart rate and reduced cardiac conductivity [52, 53]. mAChRs regulate ventricular function both directly, by counteracting β-adrenergic stimulation, and indirectly, by inhibiting L-type calcium channels [54, 55]. nAChRs are cholinergic ligand-gated ion channels permeable to Na^+, K^+, and Ca^{2+} [10] and have a central role in the cholinergic anti-inflammatory pathway by maintaining immune homeostasis through the activation and differentiation of immune T cells and reducing pro-inflammatory cytokines [56]. Moreover, alpha 7 nicotinic ACh receptor subunit (α7nAChR) regulates blood flow, cardiac hemodynamics [24], and enhances ACh release [57, 58]. While mAChRs and nAChRs trigger

distinct signaling cascades across various cell types, they operate synergistically. Targeting both mAChRs and nAChRs through vagus nerve stimulation or cholinesterase inhibitors improves left ventricular systolic function, prevents progressive left ventricular enlargement, and modulates the inflammatory response [51, 59]. The following sub-sections outline the cardioprotective effects of ACh in mitigating CVD through actions on muscarinic and nicotinic receptors.

4.1 Muscarinic ACh receptors

Type 2 muscarinic ACh receptors (M_2AChR) is the most commonly present receptor in the mammalian heart that activates several cardioprotective signalling pathways [60]. Previous studies have shown that elevated ACh secretion in an injured heart promotes cardiomyocyte proliferation, suppresses ROS production, and prevents heart injury exacerbation via M_2AChR [61-64]. Activation of M_2AChR also reduces mitochondrial oxidative damage in a DOX-induced rat model. This effect is mediated by Synapsin I, leading to heightened mitochondrial dynamics, while concurrently mitigating sympathetic activity and diminishing cardiac cell death, and necroptosis [16, 65]. ACh prevents cell apoptosis by inhibiting the action of angiotensin II (Ang II), and inhibits ROS production as well as cardiac hypertrophy by the activation of sirtuin 3/AMP-activated protein kinase (SIRT3-AMPK) signaling [66-68]. ACh also prevents the progression of HF and cardiac remodeling through its inhibition of Ang II, improving survival rates in HF animal models including mice, rats, and canines [9, 39, 69, 70]. Furthermore, ACh has the ability to activate superoxide dismutase (SOD), a crucial ROS-detoxifying enzyme in mitochondria and cytoplasm, which suppresses ROS production and protects against oxidative stress in ischaemia/reperfusion (I/R) injury [71, 72].

Several studies have indicated that an increase in ACh levels activates cell survival mechanisms in the heart against I/R [73]. ACh protects cardiomyocytes from ischemia through the transcription factor hypoxia-inducible factor (HIF-1α) and downstream gene expression for cell survival. However further studies need to be performed to fully identify these signalling pathways [74, 75]. Additionally, type 3 muscarinic ACh receptor (M_3AChR) is found abundantly in cardiac fibroblast and plays a critical role in fibroblast proliferation. The activation of M_3AChR during cardiac fibrosis leads to the inhibition of mitogen-activated protein kinase (MAPK) signaling pathway including p38MAPK and ERK1/2 associated with reduced collagen production and cardiac fibrosis [76].

4.2 Nicotinic ACh receptors

In the injured heart, ACh also binds to α7nAChR on various cell types including cardiomyocytes, monocytes, macrophages, endothelial cells and others involved in immune responses [10], thereby regulating systemic inflammatory responses in CVD patients [77]. ACh inhibits the production of inflammatory cytokines such as tumour necrosis factor (TNF), interleukin (IL)-6, IL-1β and IL-18), which are responsible for activating T cells [4, 21, 65, 78, 79]. Additionally, ACh stimulates macrophages through paracrine signaling, resulting in a reduction in the release of pro-inflammatory cytokines, the uptake of oxidized LDL, and the build-up of cholesterol within macrophages [10, 80].

Through α7nAChR, ACh attenuates endothelial dysfunction and promotes vasodilation, improving blood flow to the injured heart [65]. Li et al. [80] showed that vascular injury in α7nAChR knockout mice led to vascular remodeling, arterial inflammation and chemokines induction and increased oxidative vascular stress. Activation of α7nAChR can enhance tissue repair as well as reduce cardiac fibrosis damage [10, 81]. As cardiac fibrosis originates from endothelial cells through a process known as endothelial-to-mesenchymal transition [82], α7nAChR has the ability to significantly inhibit IL-1β-induced endothelial-to-mesenchymal transition, NF-κB and the induction of autophagy leading to the attenuation of cardiac fibrosis [13, 75].

In addition, ACh plays a significant role in cardiac angiogenesis via the α7nAChR during cardiac hypertrophy and MI. Elevating ACh levels in MI mice enhances angiogenesis through vascular endothelial growth factor (VEGF), leading to increased coronary arterial wall thickness and tube formation [67, 83]. Moreover, α7nAChR activation also plays a critical role in attenuating ROS by promoting mitochondrial fusion via upregulation of mitofusins (1-2) and thus inhibiting DOX-induced autophagy [16].

The cardioprotective function of ACh is intricate, involving various downstream pathways mediated by mAChRs and nAChRs to prevent cell death and avert cardiac dysfunction in the injured human heart. Thus, further research is required to identify and evaluate therapeutic approaches aimed at increasing ACh levels and enhancing the activation of mAChRs and nAChRs without adverse effects.

5. Challenges and constraints to translate current strategies to clinical studies and alternative approaches

ACh has exhibited protective effects in various *in vivo* animal myocardial damage models. However, these benefits have been poorly translated into clinical trials. The primary challenge in translating ACh's attributes to clinical trials is its rapid hydrolysis in the presence of cholinesterase and the widespread distribution of ACh receptors throughout the body. Moreover, in 1985, Shepherd and Vanhoutte [84] found that ACh can detect coronary artery spasms (CAD). The current method for identifying CAD in patients is through intracoronary injection of ACh (ACh-provocation test). This technique is highly sensitive and specific for detecting various types of CAD, including epicardial coronary spasm, microvascular spasm, microvascular dysfunction and coronary stenosis [85, 86]. Abnormal vascular responses to ACh, such as ischemic electrocardiogram (ECG) changes, may be a consequence of endothelial dysfunction and hyperconstriction of vascular smooth muscle. The ACh-provocation test holds potential for tailoring treatment for CAD patients, as it is considered safe with irreversible non-fatal complications. However, it is crucial to note that injecting large doses of ACh (>100μg) into the right coronary artery of CAD patients may lead to bradycardia lasting up to 45 minutes [87, 88].

Several methods are commonly employed to elevate ACh levels in the neuronal cholinergic system, such as VNS via implanted stimulators or electrical stimulation, and vagal efferent/afferent stimulation. Additionally, ACh levels can be increased in both neuronal and NNCS through pharmacological interventions including cholinesterase inhibitors. This section discusses current pre-clinical and clinical studies aimed at elevating ACh levels using VNS and cholinesterase inhibitors, examining their limitations and constraints, including the invasiveness of VNS and the adverse drug reactions (ADRs) associated with cholinesterase inhibitors. Furthermore, we explore potential alternative strategies to enhance ACh levels in the heart, including stem cell therapy, gene therapy, miRNA therapy, and the use of nanoparticles, highlighting the need for more targeted and less invasive approaches.

5.1 Vagus nerve stimulation (VNS)

VNS is frequently used to elevate myocardial ACh levels within the neuronal cholinergic system, suggesting its potential as a therapeutic strategy to restore the autonomic balance and its anti-inflammatory effect [89]. Numerous studies have demonstrated that VNS reduces

infarct size, improves ventricular function, attenuates ROS production, and decreases ventricular fibrillation in I/R animal models [73, 74, 90], in hypotension and heart failure models [91] as well for a DOX-induced rat model [92, 93] through MAChRs and nAChRs. Uitterdijk et al. [94] demonstrated that stimulating VNS in an ischemic swine model, 5 minutes before reperfusion and continuing for 15 minutes post-reperfusion, resulted in a significant reduction in infarct size. This intervention also led to a decrease in macrophages and neutrophils within the infarct area and a mitigation of no-reflow phenomenon through nAChRs [95, 96]. VNS exhibits protective effects against cardiomyocyte necrosis and microvascular obstruction which could prevent reperfusion injury through both muscarinic and nicotinic pathways [64, 97]. Furthermore, Li et al. [98] demonstrated that 6 weeks of VNS in HF mice prevented long-term remodeling and improved overall survival.

Despite the evident promise of VNS as a therapeutic strategy against I/R, Buchholz et al. [23] showed that continuous VNS for 10 minutes before ischemia significantly increased the infarct size in a rabbit MI heart model. This opposite effect to what is reported above could be due to differences in VNS protocols and model species [99]. Moreover, implanting electrodes to stimulate VNS is invasive and the optimal electrical dosage remain uncertain [100]. For instance, Sun et al. [101] initially employed an electrical voltage of 10Hz for 0.5ms, which was subsequently fine-tuned to achieve a 10% reduction in heart rate in rats. This approach significantly constrained infarct size through the mAChRs pathway, mitigating cardiac dysfunction via the nAChRs pathway, and extending their survival. While Shao et al. [102] used a pulse frequency of 4Hz and an intensity of 6V to stimulate both right and left vagus nerves, ameliorating the myocardial function in rats by decreasing tumor necrosis factor-alpha (TNF-α) level, arrhythmia score and increasing the expression of α7nAChR. Xue et al. [103] used electrical voltage from 2 to 4V to achieve a 10% decrease in the baseline heart rate. This method regulated metabolic homoeostasis, modulated mitochondrial function and endoplasmic reticulum stress, and prevented myocardial necrosis and contractile dysfunction during MI in rats. This indicates that the effectiveness of VNS is significantly influenced by factors such as the electrical voltage pulses, stimulation duration, timing, and electrode positioning. These findings underscore the importance of carefully considering these parameters in pre-clinical trials to aim at safeguarding the myocardium against cardiac injury.

Among existing clinical trials, the first pilot study of VNS using CardioFit implantable system showed that VNS may improve quality of life and left ventricle function in chronic HF patients [104]. However, large cohort clinical studies have shown mixed results [105]. For

instance, the INOVATE-HF clinical trial evaluated the impact of VNS in patients with HF, involving 390 individuals who received implants. Within 90 days, 46 complications occurred in 37 patients and after 16 months, VNS failed to demonstrate efficacy in reducing the mortality rate or HF-related events. Furthermore, it did not induce reverse remodeling or increase the left ventricle ejection fraction in this cohort [106]. The ANTHEM-HF study investigated the impact of continuous cyclic stimulation on both the left and right vagus nerves in HF patients. One patient passed away 3 days after experiencing an embolic stroke during implantation while in the remaining 59 patients, the devices were successfully implanted. At the six-month mark, the patients showed improvements in left ventricular ejection fraction, left ventricular end-systolic diameter, time-domain of heart rate variability, and high-sensitivity C-reactive protein levels. These findings indicate potential autonomic and anti-inflammatory effects of the treatment [107]. Hence, it is crucial to acknowledge that VNS is an invasive procedure, and uncertainties persist regarding its safety and potential effects on the human heart.

Despite that, VNS is FDA-approved for pharmaco-resistant depression, epilepsy and stroke rehabilitation, the device implantation involves perioperative risks. Potential adverse effects include bradyarrhythmias, development of peritracheal hematoma, dyspnea and respiratory complications [108, 109]. Furthermore, the establishment of an appropriate protocol for VNS in ischemic and HF patients remains unresolved, necessitating optimal techniques and future studies are needed to discern the impact of long-term VNS on acute and chronic myocardial damage [3]. Given the invasive nature of VNS and the perioperative risks associated with device implantation, alternative methods to modulate the cholinergic system must be considered. For instance, the application of transcutaneous VNS (tVNS) could provide the best clinical outcome and overcome surgical VNS limitations [110]. tVNS device is either placed on the anterior wall of the outer ear canal (tragus) or the cymba conchae and it is inexpensive, low-risk and easy to administer. For instance, Choudhary et al. [100] demonstrated that tVNS improves cardiac function and reduces MI area in rats. A 6 months clinical study from Stavrakis et al. [111] demonstrated that tVNS device reduce atrial fibrillation burden, TNF-α level and suppressed inflammation in patients with paroxysmal atrial fibrillation. However, there is a relative paucity of literature surrounding tVNS operation, functionality, and its therapeutic effects [112]. Future research is needed to identify the most efficient and safest approaches to enhance acetylcholine levels in the heart and reduce side effects to the patients.

5.2 Cholinesterase inhibitors

A non-invasive pharmacological treatment could serve as a potential alternative to chronic VNS therapy, offering a means to target both the neuronal and NNCS. Donepezil, rivastigmine, pyridostigmine and galantamine are reversible noncompetitive cholinesterase inhibitors. Donepezil is commonly used to prevent progressive neuronal damage [113, 114], improve cognitive function and delay the progression of Alzheimer's disease [115] and vascular dementia [116, 117]. Clinical trials and meta-analyses suggest that cholinesterase inhibitors, particularly donepezil, may be beneficial in combating CVD due to their anti-inflammatory properties and their ability to increase ACh levels in the heart, as observed in Alzheimer's disease and dementia patients with CVD [118-120]. Ongnok et al. [114] reported that the administration of donepezil significantly mitigates brain pathologies caused by cardiac I/R. This treatment led to increase expression of blood-brain barrier junction proteins, reduce brain inflammation and oxidative stress, improve mitochondrial function and dynamics, and alleviate amyloid-β accumulation and microglial activation. Furthermore, the cohort study by Nordström et al. [121] indicated that the use of cholinesterase inhibitors was associated with 35% reduced risk of MI and death in 7073 individuals diagnosed with Alzheimer’s disease. However, the study was observational, and the patients had no prior history of CVD. Additionally, healthier patients received higher doses of cholinesterase inhibitors, which was more effective than the standard dose [122]. Another cohort study found that dementia patients receiving cholinesterase inhibitors have a significantly lower risk of acute coronary syndrome. Consequently, donepezil may protect endothelial cells and improve cardiac vagal activity [119].

Donepezil has demonstrated favourable cardioprotective effects in animal models against DOX-induced cardiotoxicity [16, 65], MI [123], I/R [124] and HF [17]. Additionally, Kakinuma et al. [35] demonstrated that donepezil acts as an amplifier of NNCS activity by enhancing ACh synthesis through upregulating ChAT promoter activity in cardiomyocytes [35] and cholinergic nerve cells [96]. This could indicate that donepezil increases mAChRs and nAChRs activity by preventing ACh degradation and providing cardioprotective effects against CVD. Despite the impact of cholinesterase inhibitors on CVD, the benefit to harm ratio remains a crucial issue for clinical trials. Adverse effects of cholinesterase inhibitors are significant, Kröger et al. [125] analysis showed that the ADRs are neuropsychiatric (31.4%), gastrointestinal (15.9%), and cardiovascular disorders were 11.7% found in 18 955 reports (out

of 43 753 ADRs). Cardiovascular disorders include a significant increase in the risk of bradycardia [126], hypotension [127, 128], cardiac arrhythmia [129, 130], and syncope [131]. While a recent meta-analysis study found no association between donepezil and those cardiovascular disorders [132], donepezil still leads to ADRs such as tiredness, panic, sweating, diarrhoea, vomiting, muscle tension, speech difficulty, and involuntary tremors [133]. Hence, further research is needed to clarify the protective effects and ADRs of cholinesterase inhibitors against CVD.

5.3 Alternative approaches to target the cholinergic system

Multiple pieces of evidence strongly support the cardioprotective effects of ACh against CVD. Nevertheless, therapeutic approaches to target the cholinergic system remain uncertain and limited, warranting further exploration and investigation. This section proposes alternative approaches for future research, including ACh receptor stimulation, stem cell therapy, gene therapy, microRNA therapy and nanoparticle drug delivery (**Figure 2**).

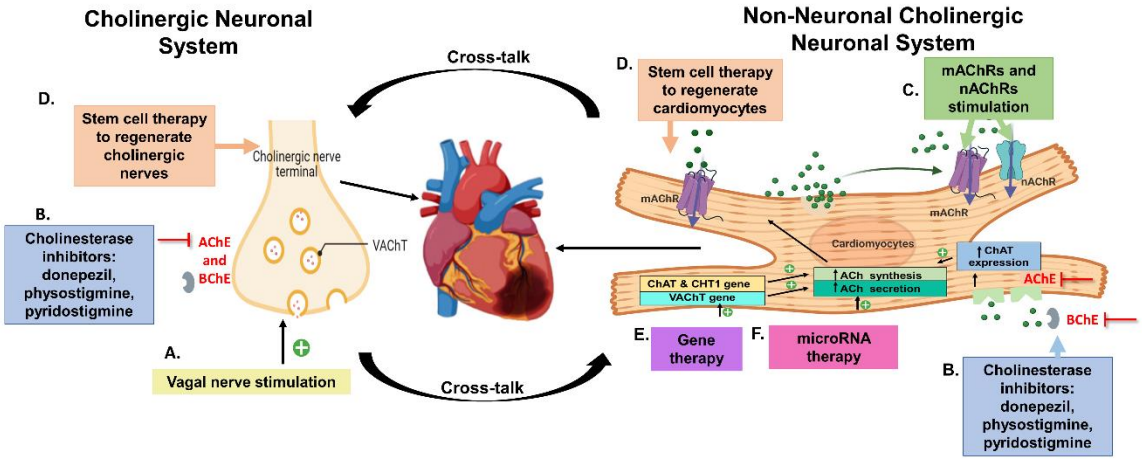

Figure 2. Schematic illustration of therapeutic approaches to target and elevate ACh levels in the infarcted heart. This includes, A) Vagal/vagus nerve stimulation to produce and secrete ACh. B) The other approach is through cholinesterase inhibitors to attenuate the degradation of ACh and prolong ACh effect in the extracellular space. Donepezil can simultaneously inhibit cholinesterase enzymes and increase ChAT expression. C) A third approach could include a positive allosteric modulator to stimulate mAChRs and nAChRs activity. D) An alternative approach would be the use of stem cell therapies to either repopulate

cholinergic neurons or replace damaged cardiomyocytes respectively. E) Gene therapy could be a therapeutic strategy to increase the expression of the cholinergic genes such as ChAT, CHT1, and VAChT that are responsible for ACh synthesis and secretion. F) Another possibility is targeting the cardiac miRNAs by diminishing levels of miRNAs that promote ACh degradation. Acetylcholine (ACh); acetylcholinesterase (AChE) choline acetyltransferase (ChAT); high-affinity choline transporter (CHT1); muscarinic acetylcholine receptors (mAChRs); vesicular acetylcholine transporter (VAChT).

Stem cell therapy offers a promising avenue for replenishing cholinergic neurons and fostering the regeneration of new, functional cardiomyocytes in hearts damaged by disease or injury. This approach could enhance self-repair mechanisms and improve the functionality of the damaged heart [18]. While replenishing cholinergic neurons through stem cells has not been extensively studied due to the complexity of the human nervous system, cardiac cell-based therapies, such as bone marrow stem cells, embryonic stem cells (ESCs), and induced pluripotent stem cells (IPSCs), have been explored for their potential to regenerate cardiomyocytes that synthesize ACh [134-136]. For instance, the transplantation of bone marrow-derived mononuclear cells has been shown to significantly elevate left ventricular ejection fraction in patients with non-ischaemic dilated cardiomyopathy and acute MI. However, it has not led to myocardial regeneration [134, 137]. Moreover, in large phase II randomized controlled trials, stem cell therapy yielded modest results, which could be due to the poor quality of transplanting stem cells [138, 139]. Additionally, there are concerns with ESCs and IPSCs, such as high survival rates potentially leading to teratoma formation [140, 141]. Despite these challenges, further exploration into stem cell therapy could lead to significant advancements in achieving cardiac regeneration and restoring cardiac function.

Another potential approach could be gene therapy, which aims to deliver the appropriate gene to be expressed and rescue the ischemic heart by increasing ACh synthesis or secretion pathways in cardiomyocytes. However, there are different types of vectors (non-viral and viral vectors) for gene delivery, and the selection of these vectors depends on the pathological condition of CVD patients. Different types of vectors lead to different durations of cardiac expression and transfection efficiency [142, 143]. Cholinergic markers, including ChAT [34, 42] or VAChT [45], could be considered new targets to increase ACh and restore the balance between the sympathetic and cholinergic systems in the ischemic heart. As mentioned above, ChAt-tg and VAChT-tg models provide cardioprotective effects against myocardial damage and ChAt-tg model also acts as a VNS. Moreover, increasing the overexpression of mAChRs

and nAChRs could be another approach. Liu et al. [144] showed that cardiac-specific M3-mAChR-tg mice significantly attenuated the hypertrophic response by reducing the expression of atrial natriuretic peptide and β-myosin heavy chain induced by angiotensin II. Nevertheless, the selection of the type of vector needs to be thoroughly considered and studied as the main disadvantage of these vectors is that this technique could induce an inflammatory response [142]. Therefore, additional research is required to find an effective *in vivo* delivery method, the duration of gene expression in the ischemic heart, and any potential toxicity effects in CVD patients.

MicroRNAs (miRNAs) are essential regulators of gene expression. miRNA therapy could potentially target mRNA to inhibit translation or inhibit the degradation of ACh. For example, Oikawa et al. [145] demonstrated that the expression of miR-345 was a regulator of the expression of ChAT mRNA in murine hearts. A synthetic inhibitor for miR-345 could be designed to increase ChAT protein expression and ACh synthesis [18]. However, further validation is needed to confirm which miRNAs could directly target ChAT, VAChT, and AChE. The effective delivery method and potential toxicity effects of miRNA therapy remain unclear. More studies are required to find the ideal approach, determine the duration of its effects, and assess its toxicity effects on the heart and other parts of the body. To conclude, targeting the cardiac NNCS through gene or miRNA therapy seems to be the next step.

Furthermore, BChE is predominantly found in plasma and the liver [146], and AChE is present in various conducting tissues such as nerves, muscles, central and peripheral tissues, and motor and sensory fibers [147]. AChE subunits also produce glycosylphosphatidylinositol (GPI)-anchored dimers and are anchored to red blood cells [28]. Given their widespread presence and their rapid and efficient hydrolysis of ACh in these tissues, optimal delivery and dosing of ACh require careful consideration. Under normal conditions, BChE does not actively hydrolyze ACh, but it becomes active when AChE activity is inhibited [146]. For instance, increased BChE levels in monkeys [148] and mice [149] protected against the toxicity of nerve agents, such as organophosphorus poisoning and cocaine. While AChE inhibition in mice led to BChE-mediated hydrolysis of ACh and inhibition of both BChE and AChE in mice caused an excess of ACh and overstimulation of ACh receptors. This results to ACh toxicity, including lacrimation, salivation, tremors, loss of motor activity, hypothermia, and tonic convulsions [148]. Therefore, delivering ACh at small doses and targeting the infarcted area using nanoparticles could be a novel therapeutic approach. This strategy could potentially enhance the therapeutic effects while minimizing systemic side effects, offering a more precise and

effective treatment for conditions requiring cholinergic modulation. Various nanocarriers such as dendrimers, nanometals, nano gels, liposomes, nano-emulsions, polymeric nanoparticles and nano suspensions have been studied to deliver drugs at small doses. Nanometal and liposomes nanocarriers have proven to be suitable to deliver ACh, a positively charged and hydrophilic molecule. Studies utilizing silver or gold nanoparticles, as well as chitosan nanoparticles demonstrated neuroprotective effects against alleviating Alzheimer's disease [150-152]. However, these approaches are not currently being explored for CVD. Future research should investigate the potential of these nanocarriers for targeted ACh delivery in CVD, which could open new avenues for therapeutic interventions.

6. Conclusions and future directions

While inhibition of the cholinergic system leads to an increased heart rate, loss of cardiomyocytes [2], and increase of production of ROS [30], there is evidence that the physiological role of both the neuronal and non-neuronal cholinergic systems protects the heart against ischemic and chronic myocardial damage [3, 14, 19, 47]. For instance, the cholinergic system prevents cell apoptosis, inhibits ROS production and cardiac hypertrophy [61-63], and prevents the progression of HF and cardiac remodeling [9, 38, 64, 65]. Moreover, the cholinergic system provides beneficial immunomodulatory effects following heart tissue injury, such as stimulating macrophages, inhibiting the release of pro-inflammatory cytokines [10, 75], attenuating endothelial dysfunction [60] and activating cardiac angiogenesis [67]. However, the relationship between the neuronal and NNCS remains to be fully understood. Understanding the precise mechanisms and interactions between the neuronal and NNCS will also be vital for designing effective treatments.

Additionally, excessive production of ACh and its synthesis can lead to toxicity and bradycardia. Therefore, it is crucial to identify optimal methods for enhancing ACh levels in the heart. VNS and cholinesterase inhibitors are commonly employed to elevate ACh levels in the heart in pre-clinical and clinical studies. However, VNS is invasive, and cholinesterase inhibitors can cause ADRs. Hence, future research should focus on developing targeted and controlled delivery systems to increase ACh in cardiac tissues without causing adverse effects. This includes exploring the use of stem cell therapy, gene therapy, miRNA therapy, and the use of nanoparticle to support and enhance the cholinergic system's protective functions in the heart. In **Figure 2**, we also mention the potential use of positive allosteric modulators to selectively target specific subtypes of mAChRs and/or nAChRs, potentially increasing receptor

affinity for ACh [153]. However, current positive allosteric modulators lack specificity and often interact with multiple subtypes, leading to major ADRs such as increased heart rate and drowsiness due to the varied functions of each subtype and subunit of ACh receptors [154, 155]. Future research should focus on developing more targeted approaches for increasing ACh levels in the heart. This could involve the use of nanoparticle delivery systems or gene therapy to selectively enhance ACh production in cardiac tissue.

More importantly, it is crucial to understand the systemic interactions between the cardiac cholinergic system and other organs, as this will help elucidate the broader physiological impacts of modulating the cholinergic system in the heart. Moreover, long-term studies are necessary to evaluate the safety and efficacy of these novel approaches, the long-term effects and safety of enhancing ACh levels in the heart, including the chronic impacts on cardiac function and potential off-target effects. Exploring the potential benefits of combining cholinergic modulation with other therapeutic approaches, such as anti-inflammatory treatments or antioxidants, could provide a more comprehensive protective strategy against heart diseases. Addressing these future directions will help harness the full therapeutic potential of the cholinergic system for cardiovascular health and pave the way for innovative treatments for CVD.

7. References

[1] Cardiovascular Diseases (CVDs), 2021. https://www.who.int/news-room/fact-sheets/detail/cardiovascular-diseases-(cvds). (Accessed 3 January 2022).
[2] A.I. Mahmoud, C.C. O'Meara, M. Gemberling, L. Zhao, D.M. Bryant, R. Zheng, J.B. Gannon, L. Cai, W.-Y. Choi, G.F. Egnaczyk, C.E. Burns, C.G. Burns, C.A. MacRae, K.D. Poss, R.T. Lee, Nerves Regulate Cardiomyocyte Proliferation and Heart Regeneration, Developmental cell 34(4) (2015) 387-399.
[3] K. Intachai, S. C. Chattipakorn, N. Chattipakorn, K. Shinlapawittayatorn, Revisiting the Cardioprotective Effects of Acetylcholine Receptor Activation against Myocardial Ischemia/Reperfusion Injury, International Journal of Molecular Sciences 19(9) (2018) 2466.
[4] C. Rocha-Resende, A.M.d. Silva, M.A.M. Prado, S. Guatimosim, Protective and anti-inflammatory effects of acetylcholine in the heart, American Journal of Physiology-Cell Physiology 320(2) (2021) C155-C161.
[5] H. Ishise, H. Asanoi, S. Ishizaka, S. Joho, T. Kameyama, K. Umeno, H. Inoue, Time course of sympathovagal imbalance and left ventricular dysfunction in conscious dogs with heart failure, Journal of Applied Physiology 84(4) (1998) 1234-1241.
[6] M.T.L. Rovere, J.T. Bigger, F.I. Marcus, A. Mortara, P.J. Schwartz, Baroreflex sensitivity and heart-rate variability in prediction of total cardiac mortality after myocardial infarction, The Lancet 351(9101) (1998) 478-484.

[7] P. Lechat, J.-S. Hulot, S. Escolano, A. Mallet, A. Leizorovicz, M. Werhlen-Grandjean, G. Pochmalicki, H. Dargie, Heart Rate and Cardiac Rhythm Relationships With Bisoprolol Benefit in Chronic Heart Failure in CIBIS II Trial, Circulation 103(10) (2001) 1428-1433.
[8] D.A. Guimarães, N.S.S. Aquino, C. Rocha-Resende, I.C.G. Jesus, M.M. Silva, S.A. Scalzo, R.C. Fonseca, M.T. Durand, V. Pereira, G.C.S.V. Tezini, A. Oliveira, V.F. Prado, I. Stefanon, H.C. Salgado, M.A.M. Prado, R.E. Szawka, S. Guatimosim, Neuronal cholinergic signaling constrains norepinephrine activity in the heart, American Journal of Physiology-Cell Physiology 322(4) (2022) C794-C801.
[9] X. An, H. Cho, Increased GIRK channel activity prevents arrhythmia in mice with heart failure by enhancing ventricular repolarization, Scientific Reports 13(1) (2023) 22479.
[10] I. Vieira-Alves, L.M.C. Coimbra-Campos, M. Sancho, R.F. da Silva, S.F. Cortes, V.S. Lemos, Role of the α7 Nicotinic Acetylcholine Receptor in the Pathophysiology of Atherosclerosis, Frontiers in Physiology 11 (2020).
[11] G.S. Werner, V. Wiegand, H. Kreuzer, Effect of acetylcholine on arterial and venous grafts and coronary arteries in patients with coronary artery disease, Eur Heart J 11(2) (1990) 127-37.
[12] O.C. Bezerra, C.M. França, J.A. Rocha, G.A. Neves, P.R.M. Souza, M. Teixeira Gomes, C. Malfitano, T.C.A. Loleiro, P.M. Dourado, S. Llesuy, K. de Angelis, M.C.C. Irigoyen, L. Ulloa, F.M. Consolim-Colombo, Cholinergic Stimulation Improves Oxidative Stress and Inflammation in Experimental Myocardial Infarction, Scientific Reports 7(1) (2017) 13687.
[13] X. Li, X. Zhu, B. Li, B. Xia, H. Tang, J. Hu, R. Ying, Loss of α7nAChR enhances endothelial-to-mesenchymal transition after myocardial infarction via NF-κB activation, Experimental Cell Research 419(1) (2022) 113300.
[14] F. Braczko, J. Reinders, H.R. Lieder, G. Heusch, P. Kleinbongard, Non-neuronal acetylcholine is causal for cardioprotection by hypoxic preconditioning in adult rat cardiomyocytes, European Heart Journal 44(Supplement_2) (2023).
[15] L. Calvillo, E. Vanoli, E. Andreoli, A. Besana, E. Omodeo, M. Gnecchi, P. Zerbi, G. Vago, G. Busca, P.J. Schwartz, Vagal stimulation, through its nicotinic action, limits infarct size and the inflammatory response to myocardial ischemia and reperfusion, J Cardiovasc Pharmacol 58(5) (2011) 500-7.
[16] N. Prathumsap, B. Ongnok, T. Khuanjing, A. Arinno, C. Maneechote, N. Apaijai, T. Chunchai, B. Arunsak, K. Shinlapawittayatorn, S.C. Chattipakorn, N. Chattipakorn, Acetylcholine receptor agonists provide cardioprotection in doxorubicin-induced cardiotoxicity via modulating muscarinic M2 and α7 nicotinic receptor expression, Translational Research 243 (2022) 33-51.
[17] T. Handa, R.G. Katare, Y. Kakinuma, M. Arikawa, M. Ando, S. Sasaguri, F. Yamasaki, T. Sato, Anti-Alzheimer's Drug, Donepezil, Markedly Improves Long-Term Survival After Chronic Heart Failure in Mice, Journal of Cardiac Failure 15(9) (2009) 805-811.
[18] E.L. Saw, Y. Kakinuma, M. Fronius, R. Katare, The non-neuronal cholinergic system in the heart: A comprehensive review, Journal of Molecular and Cellular Cardiology 125 (2018) 129-139.
[19] T. Fujii, M. Mashimo, Y. Moriwaki, H. Misawa, S. Ono, K. Horiguchi, K. Kawashima, Expression and Function of the Cholinergic System in Immune Cells, Frontiers in Immunology 8(1085) (2017).
[20] T. Fujii, M. Mashimo, Y. Moriwaki, H. Misawa, S. Ono, K. Horiguchi, K. Kawashima, Physiological functions of the cholinergic system in immune cells, Journal of Pharmacological Sciences 134(1) (2017) 1-21.
[21] L.V. Borovikova, S. Ivanova, D. Nardi, M. Zhang, H. Yang, M. Ombrellino, K.J. Tracey, Role of vagus nerve signaling in CNI-1493-mediated suppression of acute inflammation, Auton Neurosci 85(1-3) (2000) 141-7.

[22] G.B. Koelle, The histochemical localization of cholinesterases in the central nervous system of the rat, Journal of Comparative Neurology 100(1) (1954) 211-235.
[23] B. Buchholz, M. Donato, V. Perez, F.C. Ivalde, C. Höcht, E. Buitrago, M. Rodríguez, R.J. Gelpi, Preischemic efferent vagal stimulation increases the size of myocardial infarction in rabbits. Role of the sympathetic nervous system, International journal of cardiology 155(3) (2012) 490-491.
[24] K. Targosova, M. Kucera, T. Fazekas, Z. Kilianova, T. Stankovicova, A. Hrabovska, α7 nicotinic receptors play a role in regulation of cardiac hemodynamics, Journal of Neurochemistry 168(4) (2024) 414-427.
[25] O. Ojiakor, R. Rylett, Modulation of sodium-coupled choline transporter CHT function in health and disease, Neurochemistry international 140 (2020) 104810.
[26] C. Rocha-Resende, A. Roy, R. Resende, M.S. Ladeira, A. Lara, E.R. de Morais Gomes, V.F. Prado, R. Gros, C. Guatimosim, M.A. Prado, Non-neuronal cholinergic machinery present in cardiomyocytes offsets hypertrophic signals, Journal of molecular and cellular cardiology 53(2) (2012) 206-216.
[27] C. Sam, B. Bordoni, Physiology, acetylcholine, (2020).
[28] J. Massoulié, The Origin of the Molecular Diversity and Functional Anchoring of Cholinesterases, Neurosignals 11(3) (2002) 130-143.
[29] A. Chatonnet, O. Lockridge, Comparison of butyrylcholinesterase and acetylcholinesterase, Biochem J 260(3) (1989) 625-34.
[30] A. Roy, S. Guatimosim, V.F. Prado, R. Gros, M.A.M. Prado, Cholinergic Activity as a New Target in Diseases of the Heart, Molecular Medicine 20(1) (2014) 527-537.
[31] L. Tarnawski, V.S. Shavva, E.J. Kort, Z. Zhuge, I. Nilsson, A.L. Gallina, D. Martínez-Enguita, B. Heller Sahlgren, M. Weiland, A.S. Caravaca, Cholinergic regulation of vascular endothelial function by human ChAT+ T cells, Proceedings of the National Academy of Sciences 120(14) (2023) e2212476120.
[32] C.-R.C. Eduardo, T.-I.G. Alejandra, D.-R.K.J. Guadalupe, V.-R.G. Herminia, P. Lenin, B.-V. Enrique, B.M. Evandro, B. Oscar, G.-P.M. Iván, Modulation of the extraneuronal cholinergic system on main innate response leukocytes, Journal of Neuroimmunology 327 (2019) 22-35.
[33] Y. Kakinuma, Non-neuronal cholinergic system in the heart influences its homeostasis and an extra-cardiac site, the blood-brain barrier, Frontiers in Cardiovascular Medicine 11 (2024) 1384637.
[34] E.L. Saw, J.T. Pearson, D.O. Schwenke, P.E. Munasinghe, H. Tsuchimochi, S. Rawal, S. Coffey, P. Davis, R. Bunton, I. Van Hout, Y. Kai, M.J.A. Williams, Y. Kakinuma, M. Fronius, R. Katare, Activation of the cardiac non-neuronal cholinergic system prevents the development of diabetes-associated cardiovascular complications, Cardiovascular Diabetology 20(1) (2021) 50.
[35] A. Roy, W.C. Fields, C. Rocha-Resende, R.R. Resende, S. Guatimosim, V.F. Prado, R. Gros, M.A.M. Prado, Cardiomyocyte-secreted acetylcholine is required for maintenance of homeostasis in the heart, FASEB journal : official publication of the Federation of American Societies for Experimental Biology 27(12) (2013) 5072-5082.
[36] Y. Kakinuma, T. Akiyama, T. Sato, Cholinoceptive and cholinergic properties of cardiomyocytes involving an amplification mechanism for vagal efferent effects in sparsely innervated ventricular myocardium, The FEBS Journal 276(18) (2009) 5111-5125.
[37] O.R. Rana, P. Schauerte, R. Kluttig, J.W. Schröder, R.R. Koenen, C. Weber, K.W. Nolte, J. Weis, R. Hoffmann, N. Marx, E. Saygili, Acetylcholine as an age-dependent non-neuronal source in the heart, Autonomic Neuroscience 156(1) (2010) 82-89.
[38] M. Gavioli, A. Lara, P.W. Almeida, A.M. Lima, D.D. Damasceno, C. Rocha-Resende, M. Ladeira, R.R. Resende, P.M. Martinelli, M.B. Melo, Cholinergic signaling exerts protective

effects in models of sympathetic hyperactivity-induced cardiac dysfunction, PloS one 9(7) (2014) e100179.
[39] A. Lara, D.D. Damasceno, R. Pires, R. Gros, E.R. Gomes, M. Gavioli, R.F. Lima, D. Guimaraes, P. Lima, C.R. Bueno, Dysautonomia due to reduced cholinergic neurotransmission causes cardiac remodeling and heart failure, Molecular and cellular biology 30(7) (2010) 1746-1756.
[40] A. Roy, M. Dakroub, G.C. Tezini, Y. Liu, S. Guatimosim, Q. Feng, H.C. Salgado, V.F. Prado, M.A. Prado, R. Gros, Cardiac acetylcholine inhibits ventricular remodeling and dysfunction under pathologic conditions, The FASEB Journal 30(2) (2016) 688-701.
[41] Y. Kakinuma, T. Akiyama, K. Okazaki, M. Arikawa, T. Noguchi, T. Sato, A non-neuronal cardiac cholinergic system plays a protective role in myocardium salvage during ischemic insults, PLoS One 7(11) (2012).
[42] Y. Kakinuma, M. Tsuda, K. Okazaki, T. Akiyama, M. Arikawa, T. Noguchi, T. Sato, Heart-specific overexpression of choline acetyltransferase gene protects murine heart against ischemia through hypoxia-inducible factor-1α-related defense mechanisms, J Am Heart Assoc 2(1) (2013) e004887.
[43] C. Reardon, G.S. Duncan, A. Brüstle, D. Brenner, M.W. Tusche, P.S. Olofsson, M. Rosas-Ballina, K.J. Tracey, T.W. Mak, Lymphocyte-derived ACh regulates local innate but not adaptive immunity, Proc Natl Acad Sci U S A 110(4) (2013) 1410-5.
[44] S. Oikawa, Y. Kai, M. Tsuda, H. Ohata, A. Mano, N. Mizoguchi, S. Sugama, T. Nemoto, K. Suzuki, A. Kurabayashi, Non-neuronal cardiac cholinergic system influences CNS via the vagus nerve to acquire a stress-refractory propensity, Clinical Science 130(21) (2016) 1913-1928.
[45] C. Rocha-Resende, C. Weinheimer, G. Bajpai, L. Adamo, S.J. Matkovich, J. Schilling, P.M. Barger, K.J. Lavine, D.L. Mann, Immunomodulatory role of nonneuronal cholinergic signaling in myocardial injury, JCI insight 4(14) (2019).
[46] P.E. Munasinghe, E.L. Saw, M. Reily-Bell, D. Tonkin, Y. Kakinuma, M. Fronius, R. Katare, Non-neuronal cholinergic system delays cardiac remodelling in type 1 diabetes, Heliyon 9(6) (2023) e17434.
[47] F. Braczko, J. Reinders, H. Lieder, G. Heusch, P. Kleinbongard, The Non-Neuronal Cholinergic System is Causal for Cardioprotection by Hypoxic Preconditioning in Isolated Adult Rat Cardiomyocytes, The FASEB Journal 35(S1) (2021).
[48] S. Oikawa, M. Iketani, Y. Kakinuma, A non-neuronal cholinergic system regulates cellular ATP levels to maintain cell viability, Cellular Physiology and Biochemistry 34(3) (2014) 781-789.
[49] S. Oikawa, Y. Kai, A. Mano, S. Sugama, N. Mizoguchi, M. Tsuda, K. Muramoto, Y. Kakinuma, Potentiating a non-neuronal cardiac cholinergic system reinforces the functional integrity of the blood brain barrier associated with systemic anti-inflammatory responses, Brain, Behavior, and Immunity 81 (2019) 122-137.
[50] D. McAreavey, J. Neilson, D. Ewing, D. Russell, Cardiac parasympathetic activity during the early hours of acute myocardial infarction, Heart 62(3) (1989) 165-170.
[51] T. Khuanjing, S. Palee, S.C. Chattipakorn, N. Chattipakorn, The effects of acetylcholinesterase inhibitors on the heart in acute myocardial infarction and heart failure: From cells to patient reports, Acta Physiologica 228(2) (2020) e13396.
[52] C. LaCroix, J. Freeling, A. Giles, J. Wess, Y.-F. Li, Deficiency of M2 muscarinic acetylcholine receptors increases susceptibility of ventricular function to chronic adrenergic stress, American Journal of Physiology-Heart and Circulatory Physiology 294(2) (2008) H810-H820.

[53] H.A. Tettelbaum, J.E.O. Newton, W.H. Gantt, Cardiovascular responses to acetylcholine: Effects of pentobarbital and autonomic blocking agents, Conditional Reflex : A Pavlovian Journal of Research & Therapy 6(2) (1971) 101-118.
[54] J.M. Hare, J.F. Keaney, J.-L. Balligand, J. Loscalzo, T.W. Smith, W.S. Colucci, Role of nitric oxide in parasympathetic modulation of beta-adrenergic myocardial contractility in normal dogs, The Journal of clinical investigation 95(1) (1995) 360-366.
[55] R.J. Henning, I.R. Khalil, M.N. Levy, Vagal stimulation attenuates sympathetic enhancement of left ventricular function, American Journal of Physiology-Heart and Circulatory Physiology 258(5) (1990) H1470-H1475.
[56] C. Ren, Y.L. Tong, J.C. Li, Z.Q. Lu, Y.M. Yao, The Protective Effect of Alpha 7 Nicotinic Acetylcholine Receptor Activation on Critical Illness and Its Mechanism, Int J Biol Sci 13(1) (2017) 46-56.
[57] K.A. Petrov, S.E. Proskurina, E. Krejci, Cholinesterases in Tripartite Neuromuscular Synapse, Frontiers in Molecular Neuroscience 14 (2021).
[58] A. Osipov, A. Averin, E. Shaykhutdinova, I. Dyachenko, V. Tsetlin, Y. Utkin, Muscarinic and nicotinic acetylcholine receptors in the regulation of the cardiovascular system, Russian Journal of Bioorganic Chemistry 49(1) (2023) 1-18.
[59] M.J. Capilupi, S.M. Kerath, L.B. Becker, Vagus Nerve Stimulation and the Cardiovascular System, Cold Spring Harb Perspect Med 10(2) (2020).
[60] Y.-D. Fei, M. Chen, S. Guo, A. Ueoka, Z. Chen, M. Rubart-von der Lohe, T.H. Everett, Z. Qu, J.N. Weiss, P.-S. Chen, Simultaneous activation of the small conductance calcium-activated potassium current by acetylcholine and inhibition of sodium current by ajmaline cause J-wave syndrome in Langendorff-perfused rabbit ventricles, Heart Rhythm 18(1) (2021) 98-108.
[61] Y. Kakinuma, M. Ando, M. Kuwabara, R.G. Katare, K. Okudela, M. Kobayashi, T. Sato, Acetylcholine from vagal stimulation protects cardiomyocytes against ischemia and hypoxia involving additive non-hypoxic induction of HIF-1α, FEBS Letters 579(10) (2005) 2111-2118.
[62] T. Soeki, T. Niki, E. Uematsu, S. Bando, T. Matsuura, K. Kusunose, T. Ise, Y. Ueda, N. Tomita, K. Yamaguchi, Ghrelin protects the heart against ischemia-induced arrhythmias by preserving connexin-43 protein, Heart and vessels 28(6) (2013) 795-801.
[63] T. Tsutsumi, T. Ide, M. Yamato, W. Kudou, M. Andou, Y. Hirooka, H. Utsumi, H. Tsutsui, K. Sunagawa, Modulation of the myocardial redox state by vagal nerve stimulation after experimental myocardial infarction, Cardiovascular research 77(4) (2008) 713-721.
[64] W. Nuntaphum, W. Pongkan, S. Wongjaikam, S. Thummasorn, P. Tanajak, J. Khamseekaew, K. Intachai, S.C. Chattipakorn, N. Chattipakorn, K. Shinlapawittayatorn, Vagus nerve stimulation exerts cardioprotection against myocardial ischemia/reperfusion injury predominantly through its efferent vagal fibers, Basic Res Cardiol 113(4) (2018) 22.
[65] T. Khuanjing, B. Ongnok, C. Maneechote, N. Siri-Angkul, N. Prathumsap, A. Arinno, T. Chunchai, B. Arunsak, S.C. Chattipakorn, N. Chattipakorn, Acetylcholinesterase inhibitor ameliorates doxorubicin-induced cardiotoxicity through reducing RIP1-mediated necroptosis, Pharmacological Research 173 (2021) 105882.
[66] J.-J. Liu, D.-L. Li, J. Zhou, L. Sun, M. Zhao, S.-S. Kong, Y.-H. Wang, X.-J. Yu, J. Zhou, W.-J. Zang, Acetylcholine prevents angiotensin II-induced oxidative stress and apoptosis in H9c2 cells, Apoptosis 16(1) (2011) 94-103.
[67] M. Xu, R.-Q. Xue, Y. Lu, S.-Y. Yong, Q. Wu, Y.-L. Cui, X.-T. Zuo, X.-J. Yu, M. Zhao, W.-J. Zang, Choline ameliorates cardiac hypertrophy by regulating metabolic remodelling and UPRmt through SIRT3-AMPK pathway, Cardiovascular Research 115(3) (2018) 530-545.

[68] R.-Q. Xue, M. Zhao, Q. Wu, S. Yang, Y.-L. Cui, X.-J. Yu, J. Liu, W.-J. Zang, Regulation of mitochondrial cristae remodelling by acetylcholine alleviates palmitate-induced cardiomyocyte hypertrophy, Free Radical Biology and Medicine 145 (2019) 103-117.
[69] R.G. Katare, M. Ando, Y. Kakinuma, M. Arikawa, T. Handa, F. Yamasaki, T. Sato, Vagal nerve stimulation prevents reperfusion injury through inhibition of opening of mitochondrial permeability transition pore independent of the bradycardiac effect, The Journal of Thoracic and Cardiovascular Surgery 137(1) (2009) 223-231.
[70] J. Sun, Y. Lu, Y. Huang, N. Wugeti, Unilateral vagus nerve stimulation improves ventricular autonomic nerve distribution and functional imbalance in a canine heart failure model, Int J Clin Exp Med 8(6) (2015) 9334-9340.
[71] Z. Wang, G. Zhao, A.I. Zibrila, Y. Li, J. Liu, W. Feng, Acetylcholine ameliorated hypoxia-induced oxidative stress and apoptosis in trophoblast cells via p38 MAPK/NF-κB pathway, Molecular Human Reproduction 27(8) (2021).
[72] K. Intachai, S.C. Chattipakorn, N. Chattipakorn, K. Shinlapawittayatorn, Acetylcholine exerts cytoprotection against hypoxia/reoxygenation-induced apoptosis, autophagy and mitochondrial impairment through both muscarinic and nicotinic receptors, Apoptosis 27(3) (2022) 233-245.
[73] K. Shinlapawittayatorn, K. Chinda, S. Palee, S. Surinkaew, S. Kumfu, S. Kumphune, S. Chattipakorn, B.H. KenKnight, N. Chattipakorn, Vagus nerve stimulation initiated late during ischemia, but not reperfusion, exerts cardioprotection via amelioration of cardiac mitochondrial dysfunction, Heart Rhythm 11(12) (2014) 2278-2287.
[74] J. Zhang, Y. Yong, X. Li, Y. Hu, J. Wang, Y.-q. Wang, W. Song, W.-t. Chen, J. Xie, X.-m. Chen, X. Lv, L.-l. Hou, K. Wang, J. Zhou, X.-r. Wang, J.-g. Song, Vagal modulation of high mobility group box-1 protein mediates electroacupuncture-induced cardioprotection in ischemia-reperfusion injury, Scientific Reports 5(1) (2015) 15503.
[75] Z. Li, X. Li, Y. Zhu, Q. Chen, B. Li, F. Zhang, Protective effects of acetylcholine on hypoxia-induced endothelial-to-mesenchymal transition in human cardiac microvascular endothelial cells, Molecular and Cellular Biochemistry 473(1) (2020) 101-110.
[76] L. Zhao, T. Chen, P. Hang, W. Li, J. Guo, Y. Pan, J. Du, Y. Zheng, Z. Du, Choline Attenuates Cardiac Fibrosis by Inhibiting p38MAPK Signaling Possibly by Acting on M3 Muscarinic Acetylcholine Receptor, Frontiers in Pharmacology 10 (2019).
[77] R. Lampert, J.D. Bremner, S. Su, A. Miller, F. Lee, F. Cheema, J. Goldberg, V. Vaccarino, Decreased heart rate variability is associated with higher levels of inflammation in middle-aged men, Am Heart J 156(4) (2008) 759.e1-7.
[78] L.V. Borovikova, S. Ivanova, M. Zhang, H. Yang, G.I. Botchkina, L.R. Watkins, H. Wang, N. Abumrad, J.W. Eaton, K.J. Tracey, Vagus nerve stimulation attenuates the systemic inflammatory response to endotoxin, Nature 405(6785) (2000) 458-62.
[79] W.R. Parrish, M. Rosas-Ballina, M. Gallowitsch-Puerta, M. Ochani, K. Ochani, L.H. Yang, L. Hudson, X. Lin, N. Patel, S.M. Johnson, S. Chavan, R.S. Goldstein, C.J. Czura, E.J. Miller, Y. Al-Abed, K.J. Tracey, V.A. Pavlov, Modulation of TNF release by choline requires alpha7 subunit nicotinic acetylcholine receptor-mediated signaling, Mol Med 14(9-10) (2008) 567-74.
[80] D.-J. Li, H. Fu, J. Tong, Y.-H. Li, L.-F. Qu, P. Wang, F.-M. Shen, Cholinergic anti-inflammatory pathway inhibits neointimal hyperplasia by suppressing inflammation and oxidative stress, Redox Biology 15 (2018) 22-33.
[81] J.M. Huston, K.J. Tracey, The pulse of inflammation: heart rate variability, the cholinergic anti-inflammatory pathway and implications for therapy, J Intern Med 269(1) (2011) 45-53.

[82] E.M. Zeisberg, O. Tarnavski, M. Zeisberg, A.L. Dorfman, J.R. McMullen, E. Gustafsson, A. Chandraker, X. Yuan, W.T. Pu, A.B. Roberts, Endothelial-to-mesenchymal transition contributes to cardiac fibrosis, Nature medicine 13(8) (2007) 952-961.
[83] C. Hao, Z.H. Huang, S.W. Song, Y.Q. Shi, X.W. Cheng, T. Murohara, W. Lu, D.F. Su, J.L. Duan, Arterial Baroreflex Dysfunction Impairs Ischemia-Induced Angiogenesis, Journal of the American Heart Association 3(3) (2014) e000804.
[84] J.T. Shepherd, P.M. Vanhoutte, Spasm of the Coronary Arteries: Causes and Consequences (the Scientist's Viewpoint), Mayo Clinic Proceedings 60(1) (1985) 33-46.
[85] S. Suzuki, K. Kaikita, E. Yamamoto, H. Jinnouchi, K. Tsujita, Role of acetylcholine spasm provocation test as a pathophysiological assessment in nonobstructive coronary artery disease, Cardiovascular Intervention and Therapeutics 36 (2021) 39-51.
[86] M. Ishii, K. Kaikita, K. Sato, T. Tanaka, K. Sugamura, K. Sakamoto, Y. Izumiya, E. Yamamoto, K. Tsujita, M. Yamamuro, S. Kojima, H. Soejima, S. Hokimoto, K. Matsui, H. Ogawa, Acetylcholine-Provoked Coronary Spasm at Site of Significant Organic Stenosis Predicts Poor Prognosis in Patients With Coronary Vasospastic Angina, Journal of the American College of Cardiology 66(10) (2015) 1105-1115.
[87] T. Isogai, H. Yasunaga, H. Matsui, H. Tanaka, T. Ueda, H. Horiguchi, K. Fushimi, Serious cardiac complications in coronary spasm provocation tests using acetylcholine or ergonovine: analysis of 21 512 patients from the diagnosis procedure combination database in Japan, Clin Cardiol 38(3) (2015) 171-7.
[88] S.R. Erickson, M.J. Yousuf, Hypotension and bradycardia possibly associated with intraocular injection of acetylcholine, Dicp 25(11) (1991) 1178-80.
[89] J. Hadaya, J.L. Ardell, Autonomic modulation for cardiovascular disease, Frontiers in physiology 11 (2020) 617459.
[90] B. Buchholz, M. Donato, V. Perez, A.C.R. Deutsch, C. Höcht, J.S. Del Mauro, M. Rodríguez, R.J. Gelpi, Changes in the loading conditions induced by vagal stimulation modify the myocardial infarct size through sympathetic-parasympathetic interactions, Pflügers Archiv - European Journal of Physiology 467(7) (2015) 1509-1522.
[91] G.L. Cavalcante, F. Brognara, L.V.d.C. Oliveira, R.M. Lataro, M.d.T. Durand, A.P. de Oliveira, A.C.L. da Nóbrega, H.C. Salgado, J.P.J. Sabino, Benefits of pharmacological and electrical cholinergic stimulation in hypertension and heart failure, Acta Physiologica 232(3) (2021) e13663.
[92] F. Guo, Y. Wang, J. Wang, Z. Liu, Y. Lai, Z. Zhou, Z. Liu, Y. Zhou, X. Xu, Z. Li, M. Wang, F. Yu, R. Hu, L. Zhou, H. Jiang, Choline Protects the Heart from Doxorubicin-Induced Cardiotoxicity through Vagal Activation and Nrf2/HO-1 Pathway, Oxidative Medicine and Cellular Longevity 2022 (2022) 4740931.
[93] C. Siripakkaphant, B. Ongnok, N. Prathumsap, T. Khuanjing, T. Chunchai, B. Arunsak, P. Pantiya, N. Chattipakorn, S.C. Chattipakorn, Vagus Nerve Stimulation Provides Neuroprotection Against Doxorubicin-induced Chemobrain Via Activations of Both Muscarinic and Nicotinic Acetylcholine Receptors, Alzheimer's & Dementia 19(S13) (2023) e073548.
[94] A. Uitterdijk, T. Yetgin, M. te Lintel Hekkert, S. Sneep, I. Krabbendam-Peters, H.M.M. van Beusekom, T.M. Fischer, R.N. Cornelussen, O.C. Manintveld, D. Merkus, D.J. Duncker, Vagal nerve stimulation started just prior to reperfusion limits infarct size and no-reflow, Basic Research in Cardiology 110(5) (2015) 51.
[95] G. Galasso, S. Schiekofer, C. D'Anna, G.D. Gioia, R. Piccolo, T. Niglio, R.D. Rosa, T. Strisciuglio, P. Cirillo, F. Piscione, B. Trimarco, No-reflow phenomenon: pathophysiology, diagnosis, prevention, and treatment. A review of the current literature and future perspectives, Angiology 65(3) (2014) 180-9.

[96] B.G. Schwartz, R.A. Kloner, Coronary no reflow, J Mol Cell Cardiol 52(4) (2012) 873-82.
[97] M. Zhao, X. He, X.Y. Bi, X.J. Yu, W. Gil Wier, W.J. Zang, Vagal stimulation triggers peripheral vascular protection through the cholinergic anti-inflammatory pathway in a rat model of myocardial ischemia/reperfusion, Basic Res Cardiol 108(3) (2013) 345.
[98] M. Li, C. Zheng, T. Sato, T. Kawada, M. Sugimachi, K. Sunagawa, Vagal nerve stimulation markedly improves long-term survival after chronic heart failure in rats, Circulation 109(1) (2004) 120-124.
[99] C. Liu Chung Ming, K. Sesperez, E. Ben-Sefer, D. Arpon, K. McGrath, L. McClements, C. Gentile, Considerations to Model Heart Disease in Women with Preeclampsia and Cardiovascular Disease, Cells 10(4) (2021) 899.
[100] R.C. Choudhary, U. Ahmed, M. Shoaib, E. Alper, A. Rehman, J. Kim, K. Shinozaki, B.T. Volpe, S. Chavan, S. Zanos, K.J. Tracey, L.B. Becker, Threshold adjusted vagus nerve stimulation after asphyxial cardiac arrest results in neuroprotection and improved survival, Bioelectronic Medicine 8(1) (2022) 10.
[101] P. Sun, J. Wang, S. Zhao, Z. Yang, Z. Tang, N. Ravindra, J. Bradley, J.P. Ornato, M.A. Peberdy, W. Tang, Improved Outcomes of Cardiopulmonary Resuscitation in Rats Treated With Vagus Nerve Stimulation and Its Potential Mechanism, Shock 49(6) (2018) 698-703.
[102] W.J. Shao, T.T. Shu, S. Xu, L.C. Liang, J.M.L. Grange, Y.R. Zhou, H. Huang, Y. Cai, Q. Zhang, P. Sun, Left-sided vagus nerve stimulation improves cardiopulmonary resuscitation outcomes in rats as effectively as right-sided vagus nerve stimulation, World J Emerg Med 12(4) (2021) 309-316.
[103] R.-Q. Xue, L. Sun, X.-J. Yu, D.-L. Li, W.-J. Zang, Vagal nerve stimulation improves mitochondrial dynamics via an M3 receptor/CaMKKβ/AMPK pathway in isoproterenol-induced myocardial ischaemia, J Cell Mol Med 21(1) (2017) 58-71.
[104] G.M. De Ferrari, H.J.G.M. Crijns, M. Borggrefe, G. Milasinovic, J. Smid, M. Zabel, A. Gavazzi, A. Sanzo, R. Dennert, J. Kuschyk, S. Raspopovic, H. Klein, K. Swedberg, P.J. Schwartz, f.t.C.M.T. Investigators, Chronic vagus nerve stimulation: a new and promising therapeutic approach for chronic heart failure, European Heart Journal 32(7) (2010) 847-855.
[105] S. Zafeiropoulos, U. Ahmed, A. Bikou, I.T. Mughrabi, S. Stavrakis, S. Zanos, Vagus nerve stimulation for cardiovascular diseases: Is there light at the end of the tunnel?, Trends Cardiovasc Med (2023).
[106] M.R. Gold, D.J.V. Veldhuisen, P.J. Hauptman, M. Borggrefe, S.H. Kubo, R.A. Lieberman, G. Milasinovic, B.J. Berman, S. Djordjevic, S. Neelagaru, P.J. Schwartz, R.C. Starling, D.L. Mann, Vagus Nerve Stimulation for the Treatment of Heart Failure, Journal of the American College of Cardiology 68(2) (2016) 149-158.
[107] R.K. Premchand, K. Sharma, S. Mittal, R. Monteiro, S. Dixit, I. Libbus, L.A. DiCarlo, J.L. Ardell, T.S. Rector, B. Amurthur, B.H. KenKnight, I.S. Anand, Autonomic Regulation Therapy via Left or Right Cervical Vagus Nerve Stimulation in Patients With Chronic Heart Failure: Results of the ANTHEM-HF Trial, Journal of Cardiac Failure 20(11) (2014) 808-816.
[108] J. Dawson, C.Y. Liu, G.E. Francisco, S.C. Cramer, S.L. Wolf, A. Dixit, J. Alexander, R. Ali, B.L. Brown, W. Feng, L. DeMark, L.R. Hochberg, S.A. Kautz, A. Majid, M.W. O'Dell, D. Pierce, C.N. Prudente, J. Redgrave, D.L. Turner, N.D. Engineer, T.J. Kimberley, Vagus nerve stimulation paired with rehabilitation for upper limb motor function after ischaemic stroke (VNS-REHAB): a randomised, blinded, pivotal, device trial, The Lancet 397(10284) (2021) 1545-1553.
[109] J.Y.Y. Yap, C. Keatch, E. Lambert, W. Woods, P.R. Stoddart, T. Kameneva, Critical Review of Transcutaneous Vagus Nerve Stimulation: Challenges for Translation to Clinical Practice, Front Neurosci 14 (2020) 284.

[110] A.B.A. Elamin, K. Forsat, S.S. Senok, N. Goswami, Vagus Nerve Stimulation and Its Cardioprotective Abilities: A Systematic Review, J Clin Med 12(5) (2023).
[111] S. Stavrakis, A. Stoner Julie, B. Humphrey Mary, L. Morris, A. Filiberti, C. Reynolds Justin, K. Elkholey, I. Javed, N. Twidale, P. Riha, S. Varahan, J. Scherlag Benjamin, M. Jackman Warren, W. Dasari Tarun, S. Po Sunny, TREAT AF (Transcutaneous Electrical Vagus Nerve Stimulation to Suppress Atrial Fibrillation), JACC: Clinical Electrophysiology 6(3) (2020) 282-291.
[112] M.F. Butt, A. Albusoda, A.D. Farmer, Q. Aziz, The anatomical basis for transcutaneous auricular vagus nerve stimulation, J Anat 236(4) (2020) 588-611.
[113] H. Wiendl, C. Elger, H. Förstl, H.-P. Hartung, W. Oertel, H. Reichmann, S. Schwab, Gaps Between Aims and Achievements in Therapeutic Modification of Neuronal Damage ("Neuroprotection"), Neurotherapeutics 12(2) (2015) 449-454.
[114] B. Ongnok, T. Khuanjing, T. Chunchai, S. Kerdphoo, T. Jaiwongkam, N. Chattipakorn, S.C. Chattipakorn, Donepezil provides neuroprotective effects against brain injury and Alzheimer's pathology under conditions of cardiac ischemia/reperfusion injury, Biochimica et Biophysica Acta (BBA) - Molecular Basis of Disease 1867(1) (2021) 165975.
[115] J.S. Birks, R.J. Harvey, Donepezil for dementia due to Alzheimer's disease, Cochrane Database Syst Rev 6(6) (2018) Cd001190.
[116] C.E. Battle, A.H. Abdul-Rahim, S.D. Shenkin, J. Hewitt, T.J. Quinn, Cholinesterase inhibitors for vascular dementia and other vascular cognitive impairments: a network meta-analysis, Cochrane Database of Systematic Reviews (2) (2021).
[117] W.-x. Jian, Z. Zhang, J.-h. Zhan, S.-f. Chu, Y. Peng, M. Zhao, Q. Wang, N.-h. Chen, Donepezil attenuates vascular dementia in rats through increasing BDNF induced by reducing HDAC6 nuclear translocation, Acta Pharmacologica Sinica 41(5) (2020) 588-598.
[118] J. Kazmierski, C. Messini-Zachou, M. Gkioka, M. Tsolaki, The Impact of a Long-Term Rivastigmine and Donepezil Treatment on All-Cause Mortality in Patients With Alzheimer's Disease, American Journal of Alzheimer's Disease & Other Dementias® 33(6) (2018) 385-393.
[119] P.-H. Wu, Y.-T. Lin, P.-C. Hsu, Y.-H. Yang, T.-H. Lin, C.-T. Huang, Impact of acetylcholinesterase inhibitors on the occurrence of acute coronary syndrome in patients with dementia, Scientific Reports 5(1) (2015) 15451.
[120] A.T. Isik, P. Soysal, B. Stubbs, M. Solmi, C. Basso, S. Maggi, P. Schofield, N. Veronese, C. Mueller, Cardiovascular Outcomes of Cholinesterase Inhibitors in Individuals with Dementia: A Meta-Analysis and Systematic Review, J Am Geriatr Soc 66(9) (2018) 1805-1811.
[121] P. Nordström, D. Religa, A. Wimo, B. Winblad, M. Eriksdotter, The use of cholinesterase inhibitors and the risk of myocardial infarction and death: a nationwide cohort study in subjects with Alzheimer's disease, European Heart Journal 34(33) (2013) 2585-2591.
[122] H. Wang, Y. Zong, Y. Han, J. Zhao, H. Liu, Y. Liu, Compared of efficacy and safety of high-dose donepezil vs standard-dose donepezil among elderly patients with Alzheimer's disease: a systematic review and meta-analysis, Expert Opinion on Drug Safety 21(3) (2022) 407-415.
[123] M. Li, C. Zheng, T. Kawada, K. Uemura, S. Yokota, H. Matsushita, K. Saku, Donepezil attenuates progression of cardiovascular remodeling and improves prognosis in spontaneously hypertensive rats with chronic myocardial infarction, Hypertension Research (2024) 1-11.
[124] T. Khuanjing, S. Palee, S. Kerdphoo, T. Jaiwongkam, A. Anomasiri, S.C. Chattipakorn, N. Chattipakorn, Donepezil attenuated cardiac ischemia/reperfusion injury through balancing mitochondrial dynamics, mitophagy, and autophagy, Translational Research 230 (2021) 82-97.

[125] E. Kröger, M. Mouls, M. Wilchesky, M. Berkers, P.-H. Carmichael, R. van Marum, P. Souverein, T. Egberts, M.-L. Laroche, Adverse Drug Reactions Reported With Cholinesterase Inhibitors:An Analysis of 16 Years of Individual Case Safety Reports From VigiBase, Annals of Pharmacotherapy 49(11) (2015) 1197-1206.
[126] R. Morris, H. Luboff, R.P. Jose, K. Eckhoff, K. Bu, M. Pham, D. Rohlsen-Neal, F. Cheng, Bradycardia Due to Donepezil in Adults: Systematic Analysis of FDA Adverse Event Reporting System, J Alzheimers Dis 81(1) (2021) 297-307.
[127] P. Bordier, S. Garrigue, S. Lanusse, J. Margaine, F. Robert, L. Gencel, A. Lafitte, Cardiovascular effects and risk of syncope related to donepezil in patients with Alzheimer's disease, CNS drugs 20 (2006) 411-417.
[128] Z. Pu, W. Xu, Y. Lin, J. Shen, Y. Sun, Donepezil decreases heart rate in elderly patients with Alzheimer's disease, International Journal of Clinical Pharmacology and Therapeutics 57(2) (2019) 94.
[129] T. Suleyman, P. Tevfik, G. Abdulkadir, S. Ozlem, Complete atrioventricular block and ventricular tachyarrhythmia associated with donepezil, Emergency medicine journal 23(8) (2006) 641-642.
[130] Y. Hadano, H. Ogawa, T. Wakeyama, T. Iwami, M. Kimura, M. Mochizuki, S. Akashi, Y. Miyazaki, T. Nakashima, A. Shimizu, Donepezil-induced torsades de pointes without QT prolongation, Journal of cardiology cases 8(2) (2013) e69-e71.
[131] B.H. Malik, P. Hamid, S. Khan, D. Gupta, M. Islam, Correlation between donepezil and QTc prolongation and torsades de pointes: a very rare phenomenon, Cureus 11(12) (2019).
[132] T. Nham, M.C. Garcia, K.L.J. Tsang, J.M. Silva, T. Schneider, J. Deng, S. Lohit, L. Mbuagbaw, A. Holbrook, Proarrhythmic major adverse cardiac events with donepezil: A systematic review with meta-analysis, Journal of the American Geriatrics Society n/a(n/a).
[133] H.-C. Li, K.-X. Luo, J.-S. Wang, Q.-X. Wang, Extrapyramidal side effect of donepezil hydrochloride in an elderly patient: a case report, Medicine 99(11) (2020) e19443.
[134] Y. Wen, J. Ding, B. Zhang, Q. Gao, Bone marrow-derived mononuclear cell therapy for nonischaemic dilated cardiomyopathy—A meta-analysis, European Journal of Clinical Investigation 48(4) (2018) e12894.
[135] B.A. Nasseri, W. Ebell, M. Dandel, M. Kukucka, R. Gebker, A. Doltra, C. Knosalla, Y.H. Choi, R. Hetzer, C. Stamm, Autologous CD133+ bone marrow cells and bypass grafting for regeneration of ischaemic myocardium: the Cardio133 trial, Eur Heart J 35(19) (2014) 1263-74.
[136] C. Liu Chung Ming, E. Ben-Sefer, C. Gentile, Stem Cell-Based 3D Bioprinting for Cardiovascular Tissue Regeneration, Advanced Technologies in Cardiovascular Bioengineering, Springer2022, pp. 281-312.
[137] R. Delewi, A. Andriessen, J.G. Tijssen, F. Zijlstra, J.J. Piek, A. Hirsch, Impact of intracoronary cell therapy on left ventricular function in the setting of acute myocardial infarction: a meta-analysis of randomised controlled clinical trials, Heart (2012).
[138] E. Nollet, V.Y. Hoymans, A.H.V. Craenenbroeck, C.J. Vrints, E.M.V. Craenenbroeck, Improving stem cell therapy in cardiovascular diseases: the potential role of microRNA, American Journal of Physiology-Heart and Circulatory Physiology 311(1) (2016) H207-H218.
[139] M.R. Afzal, A. Samanta, Z.I. Shah, V. Jeevanantham, A. Abdel-Latif, E.K. Zuba-Surma, B. Dawn, Adult bone marrow cell therapy for ischemic heart disease: evidence and insights from randomized controlled trials, Circulation research 117(6) (2015) 558-575.
[140] M.I. Nasser, X. Qi, S. Zhu, Y. He, M. Zhao, H. Guo, P. Zhu, Current situation and future of stem cells in cardiovascular medicine, Biomedicine & Pharmacotherapy 132 (2020) 110813.

[141] Y. An, T. Sekinaka, Y. Tando, D. Okamura, K. Tanaka, Y. Ito-Matsuoka, A. Takehara, N. Yaegashi, Y. Matsui, Derivation of pluripotent stem cells from nascent undifferentiated teratoma, Developmental biology 446(1) (2019) 43-55.
[142] M.Y. Rincon, T. VandenDriessche, M.K. Chuah, Gene therapy for cardiovascular disease: advances in vector development, targeting, and delivery for clinical translation, Cardiovascular research 108(1) (2015) 4-20.
[143] M. Xu, J. Song, Targeted therapy in cardiovascular disease: A precision therapy era, Frontiers in Pharmacology 12 (2021) 623674.
[144] Y. Liu, S. Wang, C. Wang, H. Song, H. Han, P. Hang, Y. Jiang, L. Wei, R. Huo, L. Sun, X. Gao, Y. Lu, Z. Du, Upregulation of M3 muscarinic receptor inhibits cardiac hypertrophy induced by angiotensin II, Journal of Translational Medicine 11(1) (2013) 209.
[145] S. Oikawa, Y. Kai, A. Mano, H. Ohata, T. Nemoto, Y. Kakinuma, Various regulatory modes for circadian rhythmicity and sexual dimorphism in the non-neuronal cardiac cholinergic system, Journal of cardiovascular translational research 10(4) (2017) 411-422.
[146] O. Lockridge, Review of human butyrylcholinesterase structure, function, genetic variants, history of use in the clinic, and potential therapeutic uses, Pharmacology & Therapeutics 148 (2015) 34-46.
[147] E. Pytel, B. Bukowska, M. Koter-Michalak, M. Olszewska-Banaszczyk, P. Gorzelak-Pabiś, M. Broncel, Effect of intensive lipid-lowering therapies on cholinesterase activity in patients with coronary artery disease, Pharmacological Reports 69(1) (2017) 150-155.
[148] C.A. Broomfield, D. Maxwell, R. Solana, C. Castro, A. Finger, D. Lenz, Protection by butyrylcholinesterase against organophosphorus poisoning in nonhuman primates, Journal of Pharmacology and Experimental Therapeutics 259(2) (1991) 633-638.
[149] V. Murthy, Y. Gao, L. Geng, N.K. LeBrasseur, T.A. White, R.J. Parks, S. Brimijoin, Physiologic and metabolic safety of butyrylcholinesterase gene therapy in mice, Vaccine 32(33) (2014) 4155-4162.
[150] M. Sankar, R. Karthikeyan, S. Vigneshkumar, Synthesis and Characterization of Chitosan Acetylcholine Nanoparticles for Neural Disorders Associated with Cancer Treatment, Journal of Inorganic and Organometallic Polymers and Materials 33(8) (2023) 2465-2484.
[151] G.M. Abdelwahab, A. Mira, Y.B. Cheng, T.A. Abdelaziz, M.F.I. Lahloub, A.T. Khalil, Acetylcholine esterase inhibitory activity of green synthesized nanosilver by naphthopyrones isolated from marine-derived Aspergillus niger, PLoS One 16(9) (2021) e0257071.
[152] A.E. Alami, F. Lagarde, Q. Huo, T. Zheng, M. Baitoul, P. Daniel, Acetylcholine and acetylcholinesterase inhibitors detection using gold nanoparticles coupled with dynamic light scattering, Sensors International 1 (2020) 100007.
[153] D.J. Foster, P.J. Conn, Allosteric Modulation of GPCRs: New Insights and Potential Utility for Treatment of Schizophrenia and Other CNS Disorders, Neuron 94(3) (2017) 431-446.
[154] K.-E. Andersson, Antimuscarinics for treatment of overactive bladder, The Lancet Neurology 3(1) (2004) 46-53.
[155] P. Naicker, S. Anoopkumar-Dukie, G.D. Grant, J.J. Kavanagh, Anticholinergic activity in the nervous system: Consequences for visuomotor function, Physiology & behavior 170 (2017) 6-11.

7. Acknowledgments

CG was supported by a University of Sydney Kick-Start Grant, CDIP Grant, Cardiothoracic Surgery Research Grant, UTS Seed Funding and Catholic Archdiocese of Sydney Grant for Adult Stem Cell Research, the Heart Research Institute. XW was supported by National Heart Foundation Future Leader Fellowship and Baker Fellowship. CLCM was supported by UTS seeding fund and NSW Waratah Scholarship.

1.5 Closing Remarks for Part 1

The introductory section of this thesis highlights three critical reviews that collectively delved into the types of CVD and their current model systems (1.2), explored innovative strategies for cardiovascular regeneration as well as advanced techniques for disease modeling and drug testing (1.3) and shed light on the protective role of ACh against CVD (1.4).

Despite a clear understanding that an imbalance in the autonomic system is a precursor of CVD, the therapeutic elevation of ACh levels has been confined to pre-clinical studies, showing promise but facing significant hurdles for clinical studies. One of the primary challenges in ACh delivery is its capacity to detect coronary artery spasms and ACh's broad activity, alongside the disadvantages of current methods to increase ACh levels (1.4). Moreover, as explored in the first literature review (1.2), existing model systems of CVD fail to fully replicate the complex scenario of human cardiac pathophysiology, and drug findings in animal models are poorly translated into clinical trials. This limitation underscores the necessity for alternative CVD modeling strategies, a theme further examined in the subsequent review (1.3), which introduces the CS model, a novel technique that could evaluate ACh's protective role in the human heart.

Drawing upon the insights obtained, this thesis aims to look at the applications of the CS model. **Chapter 2** pioneers the use of human CS to mimic myocardial damage, including I/R and DOX-induced cardiotoxicity and using patient-derived plasma model for the early identification of changes in cardiac function.

Building on the foundational research regarding the protective role of ACh in cardiovascular health (1.4), **Chapter 3** delved into the investigation of ACh's effectiveness against I/R and DOX-induced myocardial damage in CSs models. Additionally, we explored the potential of ACh-NPs as a targeted therapeutic strategy in *in vitro* and *in vivo* models, aiming to answer the hypothesis that ACh protects against myocardial damage.

To conclude, this introduction compiles three valuable articles that provide an essential understanding of the basis of the rest of the thesis. Each article brings together disparate strands of research to forge a comprehensive knowledge of both the potential and the challenges associated with ACh-related therapies for CVD patients. By integrating insights on ACh's protective effects, the limitations of current heart disease models, and the forefront of regeneration and modeling technologies, these articles provide a foundational knowledge base for the thesis. They highlight gaps in the existing literature but also set the stage for this thesis

to explore uncharted territories in cardiovascular research, making a significant contribution to the field.

CHAPTER 2 – MYOCARDIAL DAMAGE MODELING

2.1 Introduction and Relevance

Current *in vitro* and *in vivo* models only mimic a few aspects of the intricate pathophysiology of CVD in patients, which hampers the translation of research discoveries to clinical applications. In this chapter, we assess the utilization of 3D *in vitro* bioengineered heart tissue (CSs) as an alternative option to study CVD pathophysiology. CS is composed of human coronary artery endothelial cells (HCAECs), human cardiac fibroblast (HCFs) and human induced pluripotent stem cells-derived cardiomyocytes (CMs) at ratios approximating those present *in vivo*. By co-culturing these three primary cell types found in the human heart with hydrogel, the bioengineered model successfully recreates the extracellular matrix, vascular network, and contractile functions characteristic of human cardiac tissue.

To evaluate our hypothesis that ACh protects against myocardial damage, we first assess how to model myocardial damage using advanced *in vitro* models (Aim 1).

Specific aim for aim 1:

1.1: Establishment of ischemic-reperfusion myocardial damage in CSs.

1.2: Establishment of doxorubicin myocardial damage in CSs.

1.3: Establishment of hypertensive disorders of pregnancy (HDP)-induced CVD in CSs.

Chapter 2.2 demonstrated that human 3D *in vitro* CSs could be an alternative option for studying I/R and DOX-induced myocardial damage (sub aims 1.1 and 1.2). Current models only mimic a few aspects of the complex pathophysiology of I/R and drug-induced toxicity, such as DOX. This leads to a poor translation of findings from the bench to the bench side. We mimicked I/R through changes in oxygen (O_2) levels and administered DOX to replicate DOX-induced cardiotoxicity. The analyses performed were:

- Cell death analysis,
- 3D rendering analyses
- Contractility assay
- mRNA level changes of cardiac damage-related genes

We found that *in vitro* CSs recapitulated major features typical of *in vivo* I/R and DOX-induced cardiac damages. As a result, we established I/R and DOX-like conditions in the CS model.

To reinforce the feasibility of human 3D bioengineered CSs as an alternative *in vitro* model system, the other critical component that we evaluated is using the CS model for patient-specific CVD models related to HDP (sub aim 1.3). Despite the well-documented epidemiological connection between HDP and an increased risk of CVD later in life, the underlying mechanisms of this link remain largely unexplored.

In **Chapter 2.3**, we evaluated the role of *in vitro* bioengineered CSs as advanced models to mimic HDP-induced CVD using. We added patient-derived plasma, five years post-HDP to the CSs and analyzed it through live cell analysis, CVD biomarkers, contractile assay, and proteomic analyses. We found novel discoveries that could link post-HDP to CVD. Hence, CSs could be useful in assessing early changes in cardiac function.

2.2 Ischemic-reperfusion and Doxorubicin-Induced Myocardial Damage

Summary:

This chapter is on *in vitro* modeling of I/R and DOX myocardial damage in CSs and was published in Biofabrication Journal on 24 January 2022. This publication set a foundation for modeling I/R and DOX-induced myocardial damage using bioengineered CS model. These pioneering myocardial damage models used patient-induced pluripotent stem cell-derived cardiomyocytes (CMs), offering a novel avenue for replicating human heart pathophysiology and its implications. The highlight of the paper is the inaugural direct comparison between *in vivo* I/R models and our *in vitro* bioengineered CS models, which accurately replicated I/R characteristics. Regarding intracellular alterations to O_2 concentration changes, increase in cell death and change in mRNA expression levels for genes regulating sarcomere structure, calcium transport, cell cycle, cardiac remodeling and signal transduction. Additionally, we demonstrated that DOX-induced cardiac damage which underscores the versatility of our CS model as a comprehensive platform for assessing drug-induced cardiac effects. DOX-induced toxicity also led to an increase in cell death for all cell types and expression of heart failure markers similar to previous *in vivo* studies.

Altogether, these findings demonstrated the utility of CSs as models to understand cardiac pathophysiology and to test drug toxicity. For the overall thesis, we will use our I/R and DOX-induced myocardial damage CSs to evaluate the protective effect of ACh against myocardial damage.

Biofabrication of advanced *in vitro* 3D models to study ischaemic and doxorubicin-induced myocardial damage

Biofabrication

PAPER

Biofabrication of advanced *in vitro* 3D models to study ischaemic and doxorubicin-induced myocardial damage

Poonam Sharma[1,2,3,4], **Clara Liu Chung Ming**[4], **Xiaowei Wang**[5,6,7], **Laura A Bienvenu**[5,7], **Dominik Beck**[4], **Gemma Figtree**[2,3], **Andrew Boyle**[1] and **Carmine Gentile**[2,3,4,*]

[1] The University of Newcastle, Newcastle, NSW 2308, Australia
[2] University of Sydney, Sydney, NSW 2000, Australia
[3] Kolling Institute of Medical Research, Royal North Shore Hospital, Sydney, NSW 2065, Australia
[4] University of Technology, Sydney, NSW 2007, Australia
[5] Molecular Imaging and Theranostics Laboratory, Baker Heart and Diabetes Institute, Melbourne, VIC 3004, Australia
[6] Monash University, Melbourne, , VIC 3800, Australia
[7] University of Melbourne, Melbourne, VIC 3010, Australia
[*] Author to whom any correspondence should be addressed.

E-mail: carmine.gentile@uts.edu.au

Keywords: *in vitro* advanced cardiac models, myocardial infarction, reperfusion injury, cardiac spheroids, I/R

Supplementary material for this article is available online

OPEN ACCESS

RECEIVED
1 December 2021

ACCEPTED FOR PUBLICATION
4 January 2022

PUBLISHED
24 January 2022

Abstract

Current preclinical *in vitro* and *in vivo* models of cardiac injury typical of myocardial infarction (MI, or heart attack) and drug induced cardiotoxicity mimic only a few aspects of these complex scenarios. This leads to a poor translation of findings from the bench to the bedside. In this study, we biofabricated for the first time advanced *in vitro* models of MI and doxorubicin (DOX) induced injury by exposing cardiac spheroids (CSs) to pathophysiological changes in oxygen (O_2) levels or DOX treatment. Then, contractile function and cell death was analyzed in CSs in control verses I/R and DOX CSs. For a deeper dig into cell death analysis, 3D rendering analyses and mRNA level changes of cardiac damage-related genes were compared in control verses I/R and DOX CSs. Overall, *in vitro* CSs recapitulated major features typical of the *in vivo* MI and drug induced cardiac damages, such as adapting intracellular alterations to O_2 concentration changes and incubation with cardiotoxic drug, mimicking the contraction frequency and fractional shortening and changes in mRNA expression levels for genes regulating sarcomere structure, calcium transport, cell cycle, cardiac remodelling and signal transduction. Taken together, our study supports the use of I/R and DOX CSs as advanced *in vitro* models to study MI and DOX-induced cardiac damge by recapitulating their complex *in vivo* scenario.

1. Introduction

Cardiovascular disease (CVD) (including myocardial infarction (MI) and drug-induced cardiotoxicity) is the major cause of death worldwide [1, 2]. MI is characterized by prolonged ischaemia (on average longer than 20 min) due to the blockage of coronary arteries causing cardiac cell death, inflammatory response, fibroblast infiltration and fibrosis [3]. Prompt myocardial reperfusion is necessary to maintain a healthy and functional ischaemic myocardium following an MI event [4]. However, restoration of blood flow following ischaemia is characterized by the release of high oxygen-led toxic compounds to the myocardium, including reactive oxygen (O_2) and nitrogen species, known as myocardial 'ischaemia/reperfusion (I/R) injury' [5]. Cancer is the largest killer globally [6]. The current therapies using doxorubicin (DOX) which is a widely used anticancer drug for leukemia, lymphoma and breast cancer patients, is related to delayed cardiotoxic effects in these patients (up to 17 years following their treatment). While several mechanisms have been identified for DOX-induced myocardial damage, including cell-specific effects in *in vitro* cardiac spheroids (CSs), its complex scenario is poorly recapitulated

in currently available *in vitro* models using human cardiac cells in monolayer cultures [7, 8]. As a consequence, there is a lack of thorough understanding of the mechanisms regulating myocardial damage following I/R injury and DOX treatment, and a limited translation of findings from the bench to the bedside, with serious consequences for CVD patients [9].

One of the primary reasons for the poor translation of currently used *in vitro* models for cardiovascular research is their limited recapitulation of the *in vivo* heart microenvironment and pathophysiology [10, 11]. In order to overcome this, advanced *in vitro* pathophysiological models of the human heart employing 3D cultures of cardiac cells have recently emerged [2, 12–14]. These include human cardiac organoids and 3D cultures of cardiac cells grown in a bioreactor, used to model MI and drug induced cardiotoxicity cues, such as a gradient for O_2 and nutrient and extracellular matrix deposition closer to the *in vivo* heart microenvironment [15]. Mimicking *in vivo*-like MI conditions is critical for the optimal *in vitro* modeling of myocardial damage. In the case of ischaemic damage, it is crucial to consider the concentration of O_2 required to generate pathophysiological hypoxia and reoxygenation in *in vivo* conditions, which may differ *in vitro*. Physiological O_2 concentration in the heart ranges between 3% and 5% *in vivo*, whereas most *in vitro* cardiac models are exposed to 20% O_2 in the incubator [16]. These are critical considerations for the recapitulation of the pathophysiology typical of an MI event. In case of drug-induced myocardial damage, the concentration of the drug is dependent on the thickness and the presence of cellular-extracellular components that make up the 3D cardiac microenviroment [8, 17, 18]. Our previous studies showed that *in vitro* 3D human cardiac spheroids (hCSs) better recapitulate the heart microenvironment by their comparison with *ex vivo* human heart biopsies [8]. Similarly, CSs have been generated from rodent cells as well [19]. CSs are generated by co-culturing cardiac endothelial cells, myocytes and fibroblasts at ratios found in the human heart and present morphological, biochemical and pathophysiological features typical of the *in vivo* microenvironment. Based on their unique features to better recapitulate the human heart microenvironment, they have been used to test toxicity of DOX and to model cardiac fibrosis *in vitro,* which is the stiffening of the heart typical of myocardial damage [8, 19]. While other studies attempted at recapitulating cardiac fibrosis *in vitro* as well, this has been successfully modelled in CSs by exposing them to TGF-beta 1 and DOX [19]. Therefore, the hypothesis of this study is that CSs can be used as advanced *in vitro* models to study myocardial injury typical of an *in vivo* MI event, as well as following DOX-treatment.

2. Material and methods

2.1. Mouse cardiac cell isolation and generation of mouse cardiac spheroids (mCSs)

Neonatal cardiac cells were isolated from mice between the age of one and five days. Neonatal mouse hearts were isolated following protocol approval from the Animal Ethics Committee at the Northern Sydney Local Health District (St Leonards, NSW, Australia). Briefly, murine hearts were isolated from one to five-day old mice, then chopped into smaller pieces and enzymatically digested with the Miltenyi Biotech GentleMACS dissociator. Single cells were then isolated using a 0.2-micron cell strainer on top of the 50 ml tube. The enzyme reaction is blocked by adding complete DMEM, containing 10% (v/v) FBS + 1% (v/v) pen/strep + 1%(v/v) L-glutamine, centrifuged at 300 g, for 5 min at 4 °C. Cell pellet thus obtained is resuspended into complete DMEM. CSs were generated by co-culturing 30 000 mice cardiac cells (immediately after their isolation) in 15 μl hanging drop cultures containing complete DMEM, using Perfecta 3D® 384-well hanging drop plates (3D Biomatrix, Ann Arbor, MI, USA) (figure 1). Media was replaced every 2–3 d.

2.2. Generation of human cardiac spheroids (hCSs)

hCSs were generated according to our previously published protocol [18]. Briefly, human induced pluripotent stem cell-derived cardiomyocytes (hiPSCs-CMs) (iCells, Fujifilm Cellular Dynamics, Inc.) were cultured in fibronectin pre-coated culture flasks following the manufacturer's instruction manual. HiPSCs-CMs were then isolated from culture flasks and mixed with primary human cardiac fibroblasts (HCFs) (Cell Applications, San Diego, CA, USA) and primary human coronary artery endothelial cells (Cell Applications, San Diego, CA, USA) in 2:1:1 ratio by plating 10 000 hiPSCs-CMs, 5000 HCFs and 5000 HCAECs per hanging drop culture containing 20 μl of CS medium into each well of the 384 well HDC. HCS media was prepared by mixing iCells Maintenance Medium, Human Cardiac Fibroblast Medium and Meso Endo Growth Medium in 2:1:1 ratio. HCS media was replaced every 2–3 d (figure 1).

2.3. *In vivo* mouse myocardial I/R injury

Left ventricular specimens of adult mice that have undergone myocardial I/R injury were kindly donated for mRNA isolation by A/Prof Xiaowei Wang (Molecular Imaging and Theranostics Laboratory, Baker Heart and Diabetes Institute, Melbourne, Australia). Briefly, adult male mice (6 weeks old) were divided into the following groups: (a) control (no injury); and (b) ischaemia/reperfusion (I/R) injury. I/R injury was induced by endoluminal occlusion of the left anterior descending (LAD) coronary

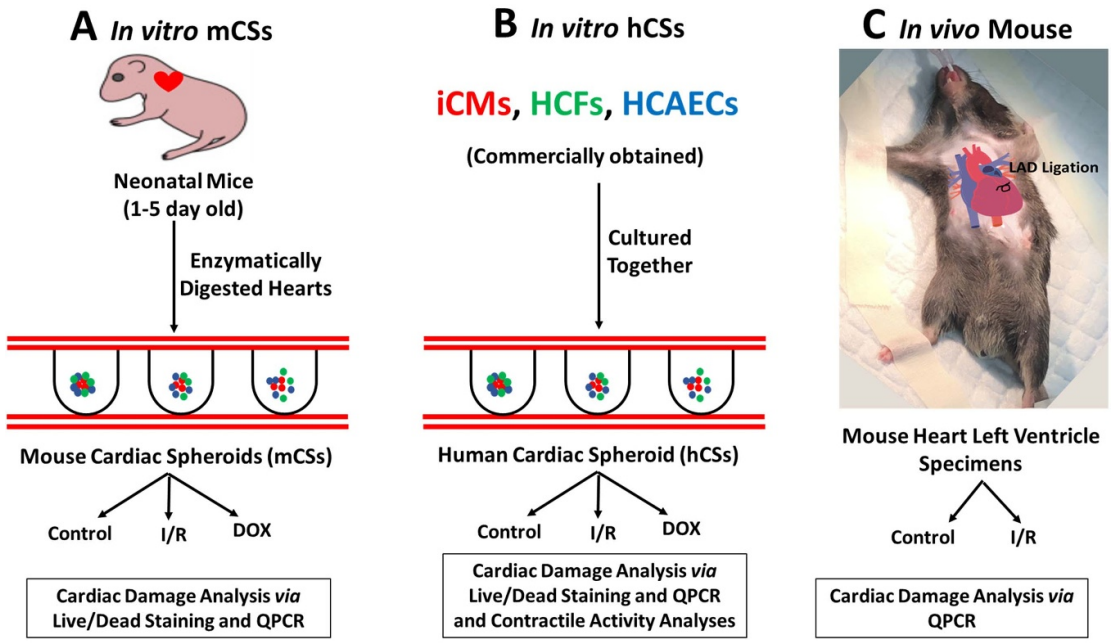

Figure 1. Protocol for *in vitro* and *in vivo* myocardial damage models used in this study. A schematic representing the procedures and analyses performed for I/R injury and DOX-induction in *in vitro* mCSs (A) and hCSs (B), and for *in vivo* I/R injury in adult mouse (C).

artery for 60 min, followed by reperfusion and recovery (figure 1). Hearts were collected 3 d later [20, 21]. Cellular damage was evaluated by qPCR analysis described above and compared with *in vitro* studies.

2.4. Establishment of the myocardial I/R injury in CSs using EVOS FL auto system

In vitro modeling of the hypoxic/normoxic-driven cardiac damage was achieved by culturing CSs at varying oxygen concentrations while evaluating changes in intracellular O_2 concentrations in a live imaging system (EVOS FL Auto system, Life Technologies). First, Image-iT (a reversible hypoxic fluorescent dye sensible to changes in intracellular O_2 levels, Thermo Fisher Scientific,AU) was added to CSs. Then, labeled CSs were moved to the live imaging gas chamber where they were cultured at 5% O_2 for 24 h to mimic *in vivo* normoxic conditions. To mimic the hypoxia typical of the ischemic event, CSs were then exposed to hypoxic conditions (0% O_2) for 20 h Reoxygenation of CSs was performed by increasing the O_2 concentrations again to 5% from T20 to T37.

2.5. Doxorubicin-mediated toxicity in CSs

HCSs were treated with 10 μM DOX (based on the previously established protocol for cell death in CSs) and incubated for 18 h at 37 °C, 5% CO_2 [8, 18]. Control hCSs contained media without any DOX. After 18 h of treatment, hCSs were evaluated for cellular damage and contractile function.

2.6. Cell viability and death analyses

Cell viability and death were evaluated by incubating CSs with calcein-AM and ethidium homodimer (staining live and dead cells, respectively) as previously described (Invitrogen LIVE/DEAD Viability/Cytotoxicity Kit) [8, 17]. Nuclei were stained with Hoechst stain. Stained CSs were imaged using a Zeiss LSM 800 Laser Confocal Microscope (Carl Zeiss AG, Oberkochen, Germany). Optical sectioning along the *Z* axis was performed, and the images collapsed into a single focal plane using the manufacturer's software. Images were processed using Adobe Photoshop CC (Adobe Systems, Inc., San Jose, CA) and NIH ImageJ software to obtain black and white ratios of the CSs, which were then used for fluorescence quantification.

2.7. CS staining, confocal imaging and 3D rendering analyses

CSs were first stained for ethidium homodimer, fixed with 4% paraformaldehyde for an hour at room temperature, permeabilized in PBS/0.01% sodium azide (PBSA) containing 0.02% Triton-X-100 for 60 min, blocked with a 3% bovine serum albumin/PBSA solution, and then incubated with appropriate primary (15 μg ml^{-1}) and secondary (10 μg ml^{-1}) antibodies at 4 °C (18 h). Endothelial cells were identified by immunostaining for CD31 with primary mouse anti-human CD31 (BD Pharmingen, San Diego, CA, USA) and secondary Cy3-conjugated donkey anti-mouse (Jackson Immunological Research Laboratories) antibodies, based on previously established protocols. CSs were also stained with mouse monoclonal

[1C11] anti-human cardiac troponin T and mouse monoclonal [V9] to vimentin (Alexa 488) antibodies.

Confocal imaging was performed on stained CSs using a Leica Stellaris WL confocal imaging system. Images were processed using NIH Fiji software and Adobe Photoshop 2021 (Adobe Systems, In., San Jose, CA, USA). For 3D rendering analyses, confocal images of stained CSs were processed using Imaris v 9.2 software (Bitplane, Concord, MA, USA).

2.8. Fractional shortening and contractile frequency measurements

Human CS movements ($n > 8$ for each condition) were analyzed using an Olympus microscope and the contractility of each CS was recorded using Olympus Cellsens software. The fractional shortening percentage and the frequency of contractions for each CS was measured for I/R versus control and DOX versus control, respectively. This was done, by measuring the total number of contractions of the CS, and by measuring the total length of each CS through the CS contractility/movement for each video.

2.9. mRNA isolation and qPCR analyses

Isolation of mRNA from CSs was performed using RNeasy Plus Mini Kit (Qiagen) following the manufacturer's guidelines. mRNA quality was measured using a Nanodrop device. Reverse transcription was performed on the mRNA obtained using RT2 First Strand Kit, and the resulting cDNA (20 μl) was diluted with 91 μl of water and used as polymerase chain reaction (PCR) template. Diluted cDNA was then mixed with 2 $\times$ RT2 SYBR Green Mastermix (Qiagen) and water and then transferred on the mouse and human CVD PCR array (PAMM-174Z and PAHS-174Z, Qiagen). qPCR analysis was performed using Quantstudio 12 K Flex PCR machine with a 384 block. Ct values were exported and analyzed using Qiagen web-based analysis tools. Four biological repeats were used.

The normalized differentially expressed fold change values (log2 fold change $\geqslant |1|$, adjusted $P < 0.05$) of all the genes of the array obtained from Qiagen web-based analysis were used to perform principal component analysis (PCA) to produce an unsupervised hierarchical clustering heat map in Partek Genomics Suite software (version 7.0) (Partek Inc., St. Louis, MO, USA).

2.10. Statistical analysis

Data were analyzed using Graphpad Prism software to calculate mean $\pm$ standard deviation (SD) and perform appropriate unpaired t-test according to distribution and sample variance. One-way ANOVA with Tukey post-hoc test was used for comparisons of multiple groups. Significance was set to $p < 0.05$. For single gene expression analysis, fold changes were calculated as $2^{\wedge}(-\text{Avg.}\Delta\Delta Ct)$ and analyzed based on the online software from Qiagen. A minimum of $n = 3$ biological replicates was used per group.

3. Results

3.1. Establishment of I/R injury in *in vitro* CSs

CSs stained with reversible hypoxic fluorescent dye were analyzed by assessing the overtime change in fluorescence intensity following the changes in intracellular O_2 concentration. An increase in the fluorescence intensity was observed when CSs were exposed to hypoxic conditions (0% O_2) for 20 h (T1-T20) following the exposure to 5% O_2 for 24 h (T0). A decrease in fluorescence intensity was observed after switching the O_2 concentration back to physiological levels (5%) for 17 h (T21-37) (figure 2(A)). Our quantification of the Image-iT fluorescence was statistically significant between T0, T20 and T37, confirming a change in intracellular O_2 levels in our model (figure 2(B)).

3.2. Increased cell death in I/R and DOX CSs

To quantify the extent of loss in cell viability in CSs, toxicity ratios were calculated by measuring the fluorescence between dead and live cells figures 3(A)–(P)). Our statistical analyses of toxicity ratios between control and I/R CSs from either mouse or human origin (mCSs and hCS, respectively) confirmed a statistically significant increase in cell death in I/R conditions compared to control (figures 3(Q) and (R)).

DOX-treated hCSs were also incubated with calcein-AM, ethidium homodimer and Hoechst stain to measure the toxicity ratio (figures 4(A)–(H)). Similar to what we have observed in I/R CSs, DOX significantly increased the toxicity ratio compared to control cultures (figure 4(I)).

3.3. Cardiac cell types were differently affected by I/R- and DOX-induced damage as shown by confocal microscopy analyses

In order to evaluate which cells died following I/R conditions, hCSs were incubated with ethidium homodimer, and cell type-specific antibodies against CD31, cTNT and vimentim (staining cardiac endothelial cells, myocytes and fibroblasts, respectively). Our 3D rendering analyses of confocal microscopy images from I/R hCS showed that most of the cardiomyocytes died following I/R injury, whereas endothelial cells and fibroblasts would partially die (figures 5(A)–(H), videos 1 and 2 available online at stacks.iop.org/BF/14/025003/mmedia).

3D rendering analyses of DOX-treated hCSs analyzed in a similar way showed that cardiomyocytes were more susceptible to DOX-induced cell death in comparison to fibroblasts and endothelial cells, but not all of them would die (figures 6(A)–(G), video 1 and 3).

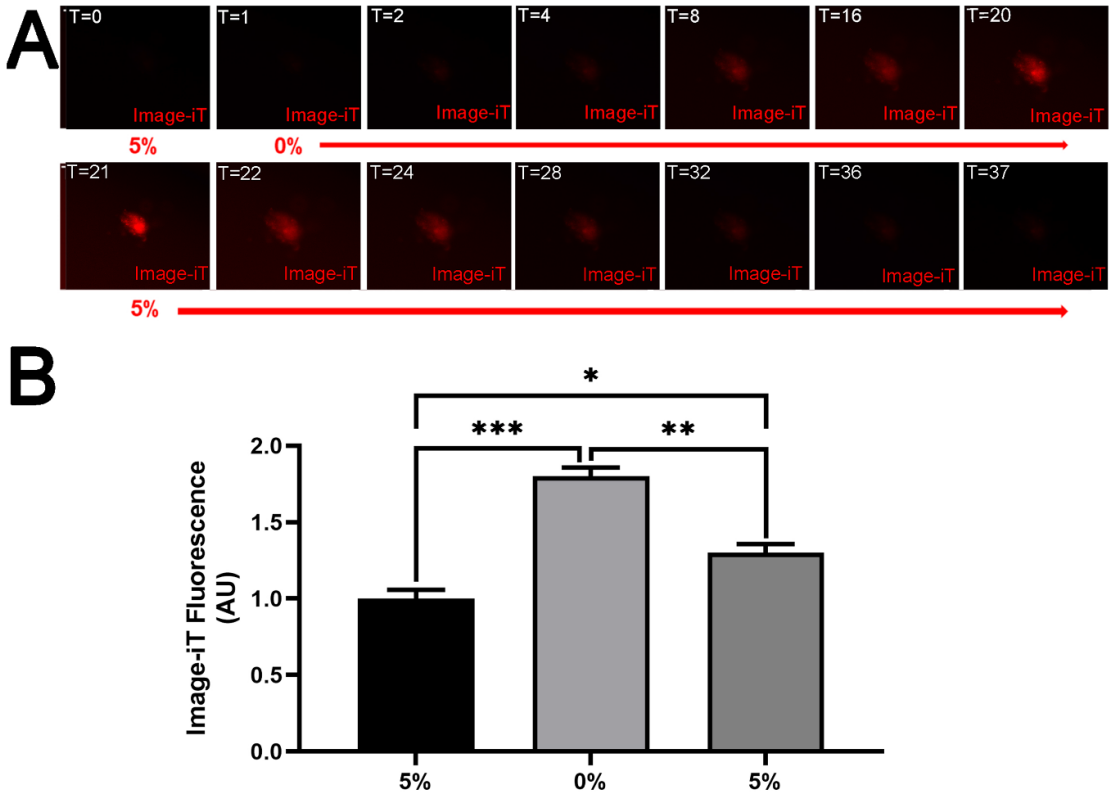

Figure 2. Intracellular O_2 concentration changes in I/R CSs. (A) Epifluorescence images of a representative CS treated with Image-iT (red) that was pre-incubated at 5% O2 ($T = 0$), and then exposed to 0% O2 for 20 h ($T = 20$) and 5% O_2 for additional 17 h ($T = 37$). (B) Statistical analysis of changes in Image-iT fluorescence between 5% ($T = 0$), 0% ($T = 20$) and 5% ($T = 37$). One-way ANOVA with Tukey post-hoc test was used for comparison of all groups. $p<0.01 = **$ and $p<0.001 = ***$. Error bars represent the mean ± SD ($n = 3$).

3.4. Decreased contraction frequency and fractional shortening in CSs following I/R injury and DOX-treatment

To evaluate the contractile activity of the hCSs following the I/R and DOX treatment, we assessed the changes in contraction frequency and fractional shortening of hCSs. We observed that while control hCS showed approximately 40 contractions per minute, I/R hCSs stopped contracting (figure 7(A)). Similarly, fractional shortening was only observed in control hCSs (figure 7(B)). Overall, it was observed a complete cessation in contractile activity in hCSs following an I/R injury (figures 7(A) and (B), videos 4 and 5).

DOX-treated CSs showed a significant decrease in contractile function and fractional shortening compared with control CSs. However, DOX CSs did not lose their contraction frequency and fractional shortening completely (figures 7(A) and (B), videos 4 and 6).

3.5. Changes in relative expression of cardiovascular genes during I/R and DOX-induced myocardial damage

To further evaluate whether *in vitro* I/R CSs mimic changes in mRNA expression levels typical of the *in vivo* I/R injury, we compared changes of cardiac damage-related genes (table 1) [22, 23]. The fold change values of all the genes from both human (*in vitro*) and mouse (*in vivo/in vitro*) CVD array was used to perform PCA. The heat maps obtained from PCA support that *in vitro* hCSs better mimic the *in vivo* I/R injury in comparison to *in vitro* mCSs (figure 8, supplementary figures 1–7).

DOX-treated CSs were analyzed for gene expression of cardiac damage-related genes via qPCR. Our PCA demonstrates that both DOX CSs (mCSs and hCSs) showed diference in gene expressions compared to I/R CSs (mCSs and hCSs) (figures 9 and 10, table 2, supplementary figures 8–14). However, it is important to further identify differences between gene families as well, as detailed below.

3.5.1. Sarcomeric genes were consistently regulated following an I/R injury and DOX treatment

Sarcomeric proteins control cardiac cell function and their expression levels change following I/R injury [24–27]. Our statistical analysis showed a similar trend in mRNA expression levels following injury in *in vivo* and *in vitro* In particular, actin alpha cardiac muscle 1 (Actc1), myosin heavy chain 6 (Myh6, cardiac muscle specific), cardiac troponin I (Tnni3), cardiac troponin T2 (Tnnt2) were all significantly downregulated in I/R CSs for both human

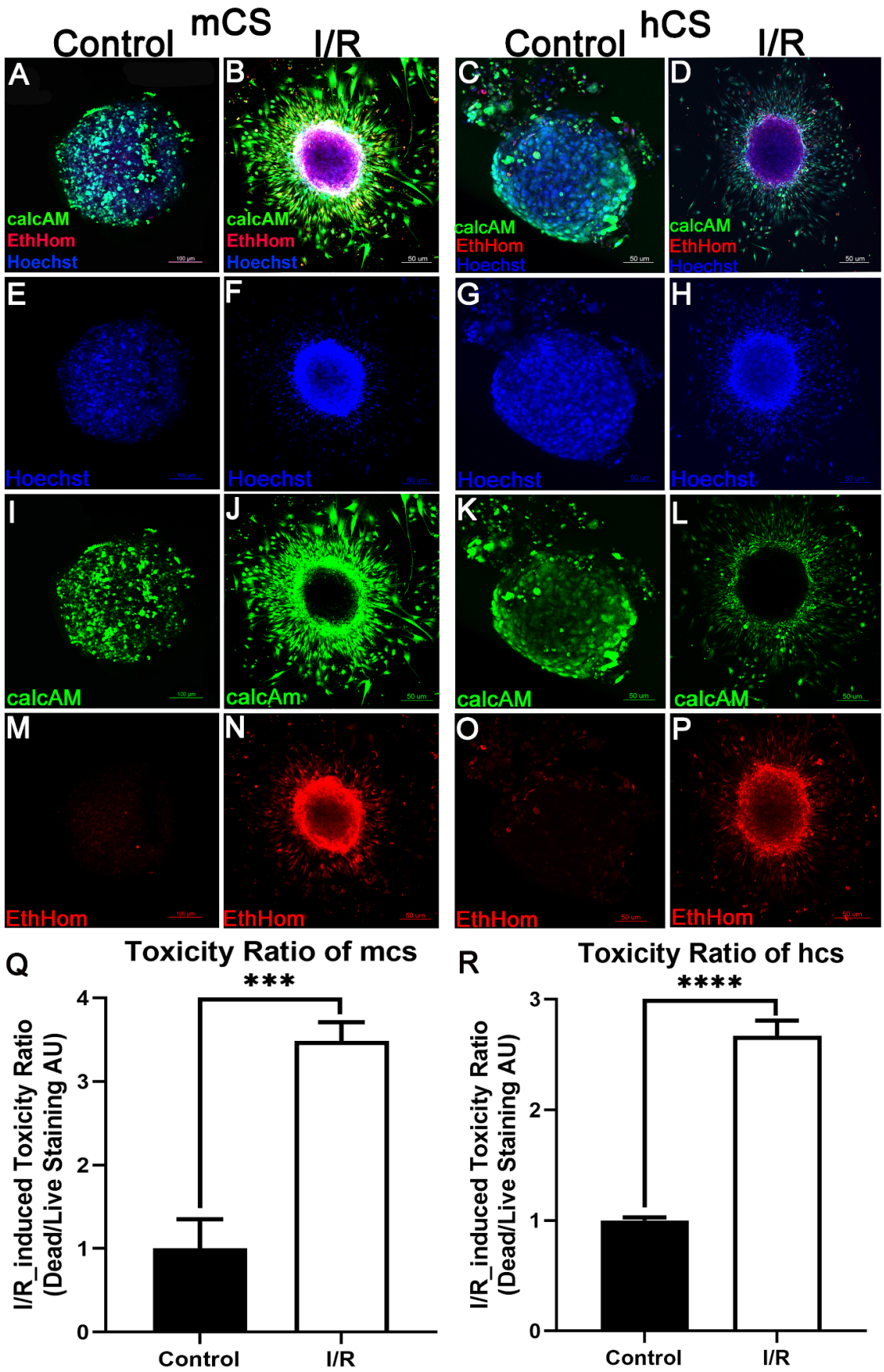

Figure 3. Confocal imaging analyses for cell death and viability in I/R CSs. (A)–(P) Collapsed z-stacks of laser scanning confocal images of control and I/R mCSs and hCSs stained with calcein-AM (green), ethidium homodimer (red) and Hoechst stain (blue), staining live, dead, and total cells, respectively. (A), (B), (C) and (D) overlays of Hoechst (E), (F), (G) and (H), calcein- AM (I), (J), (K) and (L) and ethidium homodimer (M), (N), (O) and (P) collapsed Z-stacks of control and I/R CSs. (Q) and (R) Statistical analyses of toxicity ratios for control and I/R mCSs (Q) and hCSs (R) using unpaired t-test. $p<0.001 = ***$ and $p < 0.0001 = ****$. Error bars represent the mean ± SD for $n = 3$.

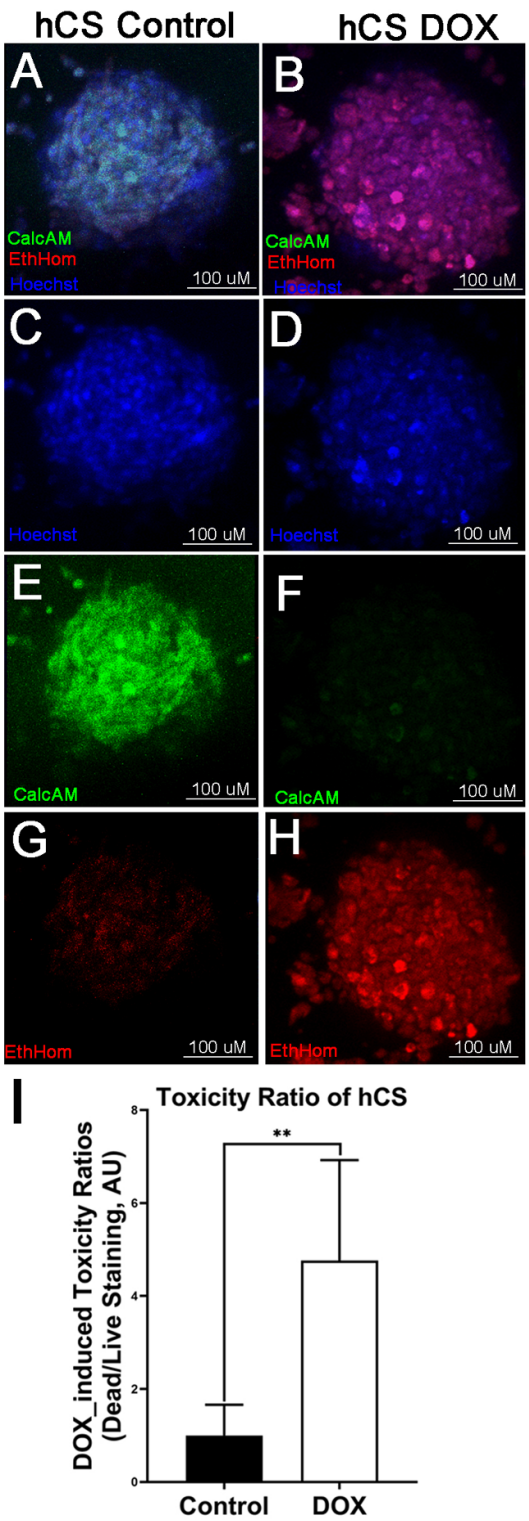

Figure 4. Confocal imaging analyses for cell death and viability in DOX CSs. (A)–(H) Collapsed z-stacks of laser scanning confocal images of control and DOX hCSs stained with calcein-AM (green), ethidium homodimer (red) and Hoechst stain (blue), staining live, dead, and total cells, respectively. (A), and (E) overlays of Hoechst (B) and (F), calcein-AM (C) and (G) and ethidium homodimer (D) and (H) collapsed Z-stacks of control and DOX CSs. (I) Statistical analyses of toxicity ratios for control and DOX hCSs using unpaired t-test. $p < 0.001 = ***$ and $p < 0.0001 = ****$. Error bars represent the mean ± SD for $n = 6$.

and murine origin when compared to control. This trend was similar to the changes measured in the *in vivo* mouse model. Similarly, myosin heavy chain 10 non-muscle (Myh10) was upregulated in both *in vitro* and *in vivo* I/R injury models (table 1).

Our statistical analysis of mRNA expression levels following DOX treatment in *in vitro* CSs showed that Actc1, Tnni3, Tnnt2 were significantly downregulated in CSs from either human or murine origin compared to control, except for Myh6 (not significant in case of hCSs). While Myh10 was significantly upregulated in both conditions compared to control, similar to what observed in our I/R injury model and constiistent with previous studies focusing on dysfunction of sarcomeric proteins post DOX-exposure (table 2) [28–30].

3.5.2. Calcium ion transport genes were downregulated in I/R and DOX CSs

Calcium ion transport genes, such as ATPase, Ca^{2+} transporting, cardiac muscle, slow twitch 2 (Atp2a2) and ATP synthase, H^+ transporting, mitochondrial F1 complex, alpha subunit 1 (Atp5a1) regulate contractile activity in cardiac myocytes [31, 32]. Both Atp2a2 and Atp5a1 were significantly downregulated in *in vivo* and *in vitro* I/R injury models compared to control, consistent with the ATP deficiency that follows an MI event (table 1) [32, 33].

Atp2a2 and Atp5a1 were significantly downregulated following DOX treatment in both mCSs and hCSs compared to controls (table 2). A similar response on calcium transporting genes was previously showed in rats during DOX treatment [34].

3.5.3. I/R injury and DOX-treatment induces overexpression of cell cycle genes

Infarcted heart tissues present a change in the expression of cell cycle controlling genes, including cyclin D1 (Ccnd1) and retinoic acid receptor responder (Rarres1) [35]. In our CS model, these two cell cycle regulatory genes were significantly upregulated in *in vivo* and *in vitro* compared to controls (table 1).

Our gene expression analysis of Ccnd1 and Rarres1 following DOX treatment showed that they were significantly upregulated in mCSs and hCSs compared to controls (table 2). These results are consistent with previous studies reporting the DOX-mediated overexpression of both genes in adult mice hearts and zebrafish [36, 37].

3.5.4. Cardiac remodeling genes were upregulated following I/R injury and DOX-treatment

In *in vivo* I/R injury models, infarcted myocardial tissue goes through extensive cardiac remodeling [38]. In our model, angiotensin-I-converting enzyme (Ace), matrix metallopeptidase 13 (Mmp13)

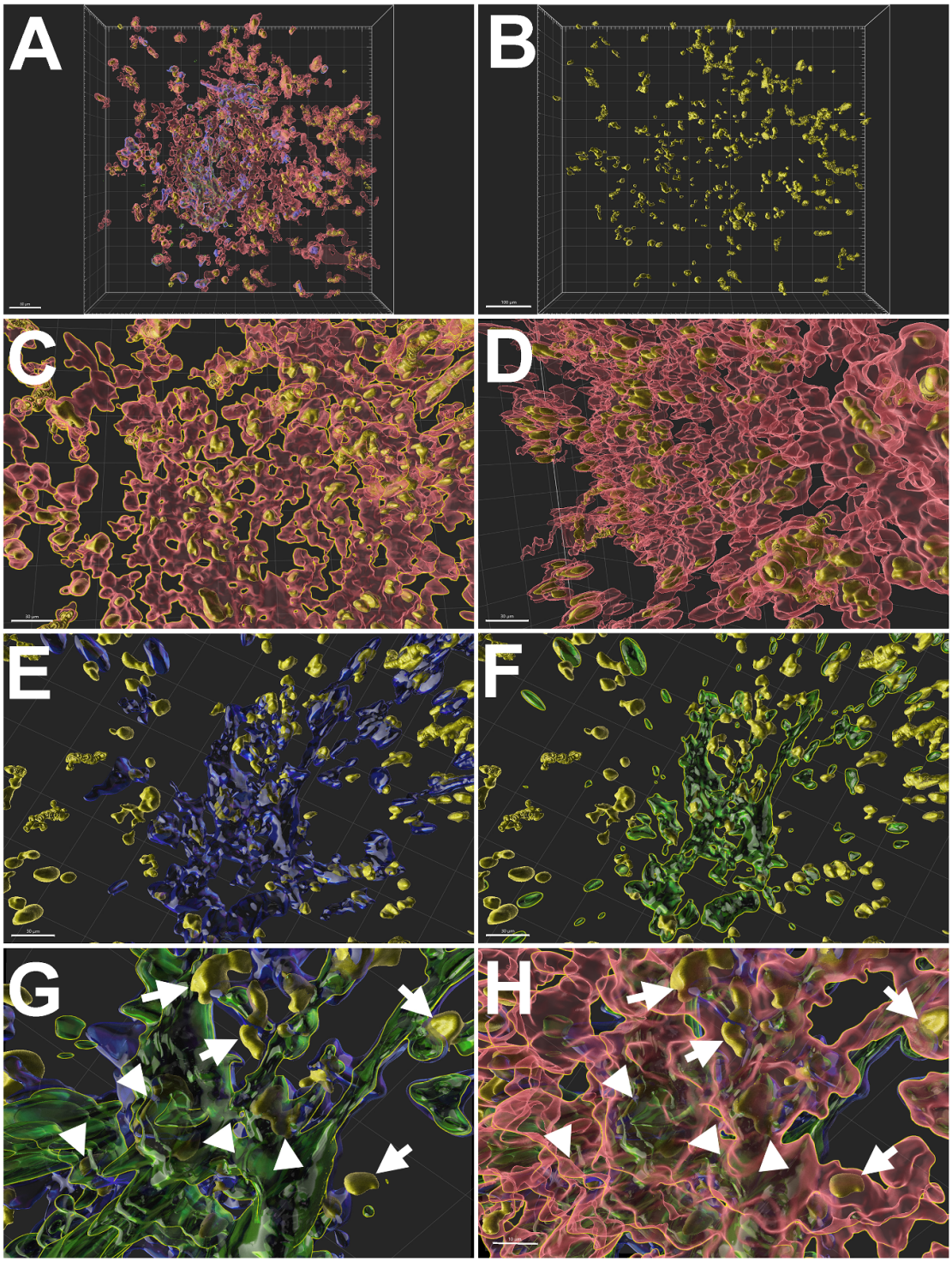

Figure 5. 3D cell death analyses of confocal images of an I/R CS using Imaris software. Confocal images of an I/R CS stained with ethidium homodimer (golden), and with antibodies against CD31 for endothelial cells (blue), cTNT for cardiomyocytes (red) and vimentim for fibroblasts (green), optimised under Imaris software. (A) and (B) shows the frontal overview of (C) and (D) highlighting all the dead cardiomyocytes. Images (E) and (F) are highlighting dead endothelial cells and fibroblasts, respectively. (G) and (H) shows the arrows point at nuclei of dead cardiomyocytes, and arrowheads to nuclei of dead endothelial cells and fibroblasts.

and renin 1 structural (Ren1) were upregulated in both *in vivo* and *in vitro* compared to control (table 1).

Ace, Mmp13 and Ren1 were similarly upregulated following DOX-mediated damaged. They all were upregulated in both mCSs and hCSs compared to control and were consistent with our I/R injury model and previous DOX mediated cardiac damage studies (table 2) [30, 39, 40].

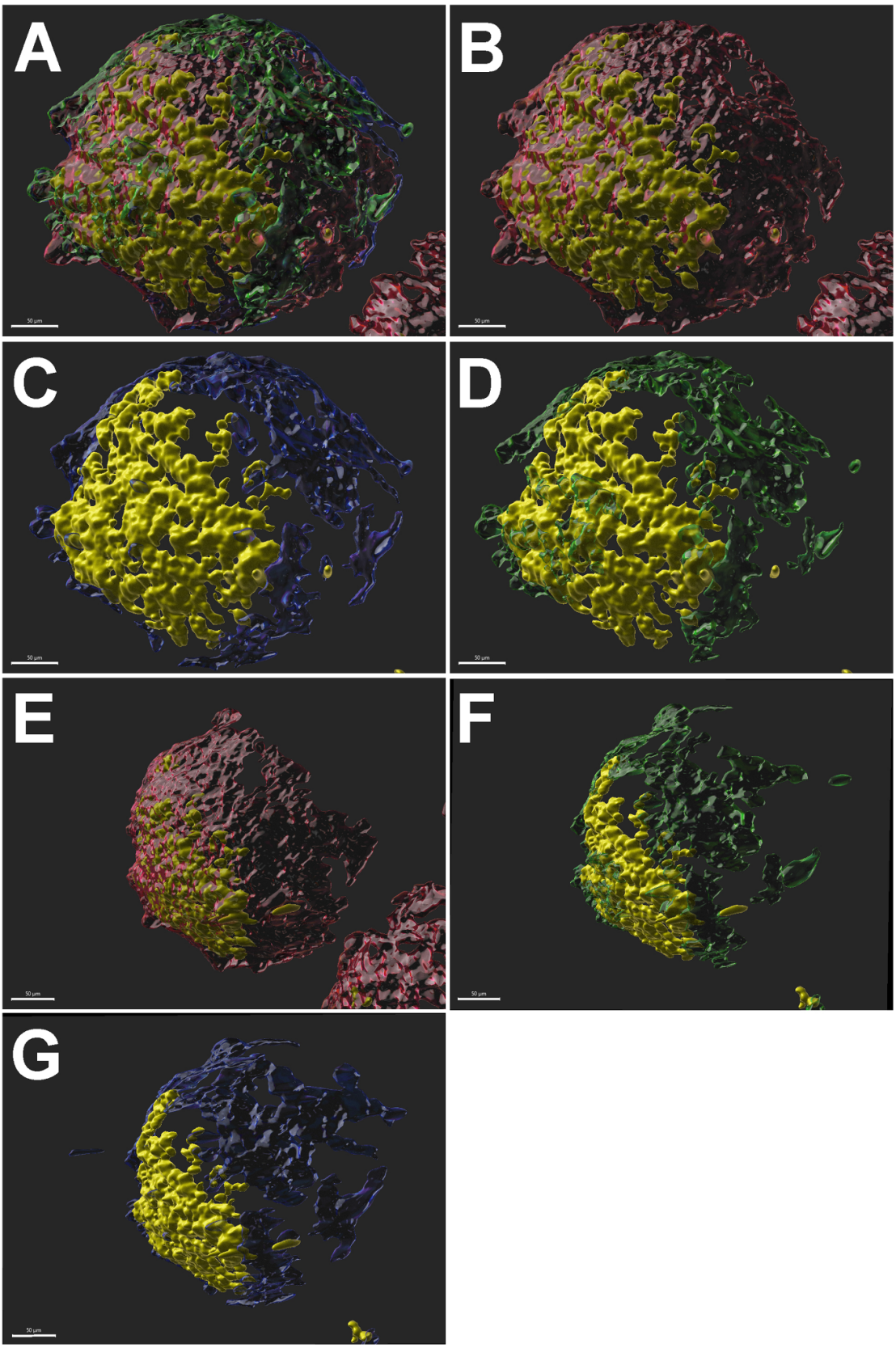

Figure 6. 3D cell death analyses of confocal images of a DOX CS using Imaris software. Confocal images of a DOX CS stained with ethidium homodimer (golden), and with antibodies against CD31 for endothelial cells (blue), cTNT for cardiomyocytes (red) and vimentim for fibroblasts (green), optimised under Imaris software. Image (A) is the overlay of (B), (C) and (D) which showed the frontal view highlighting all the dead cardiomyocytes, endothelial cells, and fibroblasts, respectively. (E), (F) and (G) images showed sideview of CS showing dead cardiomyocytes, fibroblasts, and endothelial cells respectively.

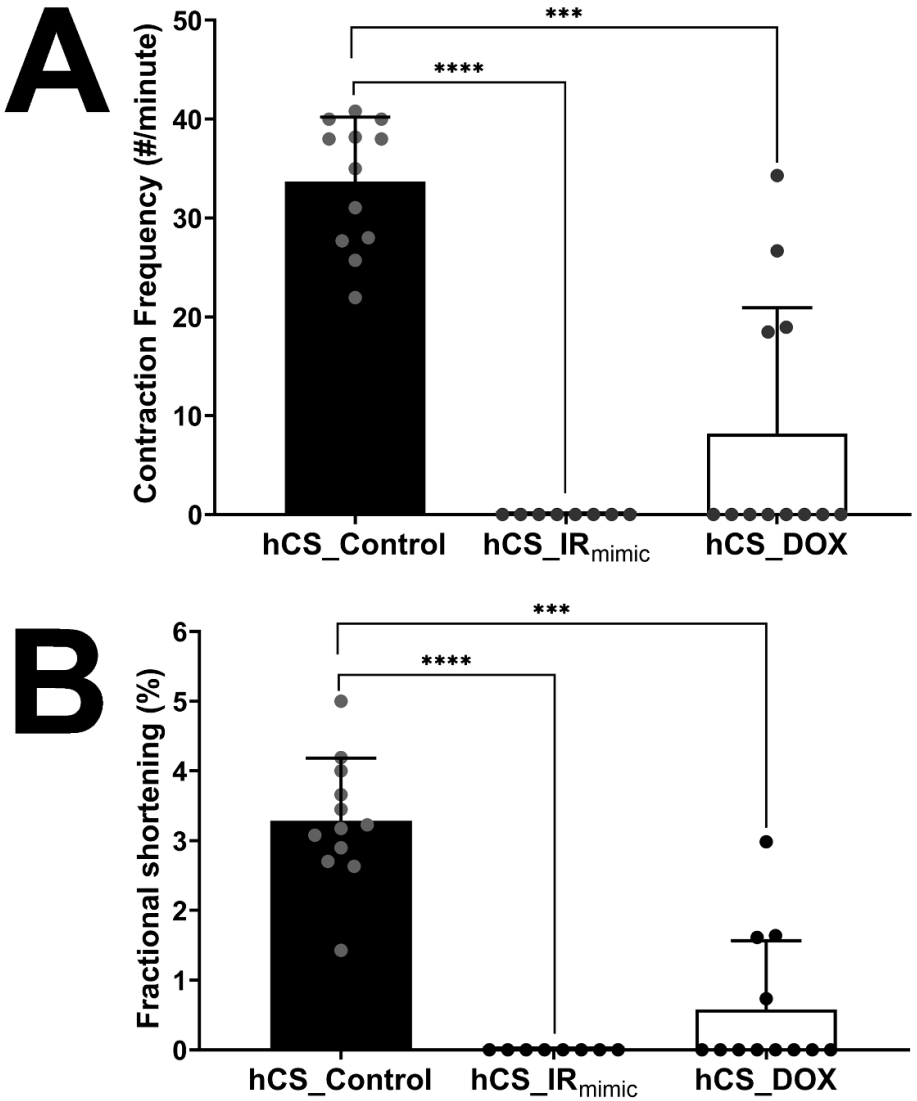

Figure 7. Decrease in contraction frequency and fractional shortening of CSs. Statistical analysis of contractile frequency (A) and fractional shortening (B) of hCSs optimized under Olympus microscope. One-way ANOVA with Tukey post-hoc test was used for comparison of all groups, $p > 0.05$ = ns, $p < 0.05$ = *, $p < 0.01$ = **, $p < 0.001$ = *** and $p < 0.0001$ = ****. Error bars represent the mean ± SD ($n > 8$).

3.5.5. Apoptosis regulating genes were differentially regulated in I/R and DOX CSs

As cell death follows an MI event, several apoptotic genes change following I/R injury *in vivo* [41]. Our qPCR analysis showed a similar trend *in vitro* and *in vivo* models for annexin A4 (Anxa4), chemokine (C-C motif) ligand (Ccl2), monoamine oxidase A (Maoa), natriuretic peptide receptor 1 (Npr1), phosphodiesterase 3 A cGMP inhibited (Pde3a) and synuclein alpha (Snca). However, natriuretic peptide type A (Nppa) and natriuretic peptide type B (Nppb) were differentially regulated in *in vivo* and *in vitro* models. Nppa and Nppb were upregulated following myocardial I/R injury in *in vivo* and *in vitro* (table 1). The differential response of Nppa and Nppb seen in *in vivo* and *in vitro* models of our study could be linked to the fact that in *in vivo* there are several additional factors that influence the disease progression other than the confounding cell types we have in our *in vitro* CS models [36, 42]. Moreover the time difference is critical for genes to respond to a stimulus, and we have different time slots for *in vivo* and *in vitro* models. The difference in both types of CSs could be species specific as one is sourced from mouse and other from human cells [43].

In mCSs all apoptotic genes (such as, Anxa4, Ccl2, Maoa, Npr1, Nppa, Nppb, Pde3a and Snca) were significantly upregulated compared to controls. However, in hCSs, Anxa4, Ccl2, Maoa, Npr1, Pde3a and Snca were upregulated, whereas Nppa and Nppb downregulated compared to control (table 2). The differential expression of Nppa and Nppb in hCSs following DOX treatment could be related to the fact that increase in their expression could be observed after 4 weeks as suggested by Boucek *et al* in 1999 while studying persistent effect of DOX on expression of cardiac genes [30].

Table 1. Expression of cardiovascular genes following I/R injury. Relative expression of sacromeric genes, calcium transporting genes, cell cycles genes, apoptotic genes, fibrotic genes and signal transduction genes in *in vivo* and *in vitro* mCSs, and *in vitro* hCSs. The blue colour represents downregulated genes and red represents the upregulated genes. Unpaired t-test, $p > 0.05$ = ns, $p<0.05$ = *, $p < 0.01$ = **, $p < 0.001$ = *** and $p < 0.0001$ = ****, ($n = 4$).

	QPCR analyses of cardiovascular genes for I/R injury evaluation					
		In vivo mouse		*In vitro* mCSs		*In vitro* hCSs	
Classification of genes	Genes	Fold change	*P*-value	Fold change	*P*-value	Fold change	*P*-value
Sarcomeric Genes	Actc1	0.137942	***	0.04	*	0.42	**
	Myh10	2.443794	***	2.08	**	5.3167	****
	Myh6	0.167832	**	0.04	**	0.44	ns
	Tnni3	0.248503	**	0.17	****	0.56	ns
	Tnnt2	0.041484	****	0.08	**	0.1	**
Calcium Transporting Genes	Atp2a2	0.168072	***	0.08	**	0.43	**
	Atp5a1	0.048586	***	0.22	****	0.5047	*
Cell Cycle Genes	Ccnd1	2.413644	***	3.37	*	3.52	***
	Rarres1	2.866099	**	16.44	****	1.46	ns
Cardiac Remodelling Genes	Ace	3.21338	****	4.43	***	1.16	ns
	Mmp13	2.571323	***	2.68	**	2.0766	*
	Ren1	2.863292	****	23.9	****	7.4	****
Apoptotic Genes	Anxa4	2.651639	****	5.54	****	1.6567	ns
	Ccl2	2.834338	**	1.97	**	1.848	*
	Maoa	2.52	***	22.14	****	1.93	ns
	Nppa	5.938162	****	0.07	ns	0.09	*
	Nppb	0.496905	ns	13.57	****	0.28	*
	Npr1	2.529959	***	21.83	****	2.753	***
	Pde3a	1.637685	ns	2.36	**	2.1	*
	Snca	2.863292	***	23.9	****	2.10443	*
Fibrotic Genes	Col11a1	3.240188	****	8.76	***	2	*
	Col1a1	6.175983	****	0.1	*	0.53	ns
	Col3a1	6.653946	****	0.07	*	0.13	****
	Ctgf	3.743725	****	0.46	ns	1.877	*
	Dcn	0.644718	ns	0.21	**	0.094	*
	F2r	2.613409	****	1.96	ns	2.055	ns
	Fn1	5.051019	****	1.08	ns	0.0782	*
Signal Transduction Genes	Adra1a	2.529959	***	23.9	****	1.497	ns
	Adra1b	2.529959	**	2.05	***	1.28612	ns
	Adra1d	2.529959	***	21.87	****	2.038	ns
	Adrb1	1.76	**	1.25	****	2.46	ns
	Adrb2	2.52	***	32.97	****	4.2363	****
	Mapk1	1.053645	ns	1.6	*	1.48	ns
	Mapk8	2.178454	**	5	****	1.2	ns
	Pde3b	2.539398	**	74.77	****	1.54	ns
	Pde5a	2.52	***	9.57	****	2.68	*
	Pde7a	2.571273	***	9.78	****	2.68	*

3.5.6. Fibrotic genes were differentially regulated in in vivo *and* in vitro *cardiac disease models*

Cardiac fibrosis post-I/R injury in the heart is dependent on cardiac fibroblasts activation *in vivo* [44]. Our analyses showed that changes in decorin (Dcn), collagen, type XI, alpha 1 (Col11a1) and coagulation factor II (thrombin) receptor (F2r) were similar *in vitro* and *in vivo* compared to the controls. All other genes were differently regulated *in vitro* and *in vivo*. In particular, collagen, type III, alpha 1 (Col3a1) and fibronectin 1 (Fn1) were upregulated *in vivo* and downregulated in both *in vitro* models. Collagen, type I, alpha 1 (Col1a1) and connective tissue growth factor (Ctgf) were upregulated *in vivo* and in hCSs but downregulated in mCSs (table 1). The difference in expression of fibrotic genes could be because it requires 3 d to fibrotic genes to fully express themselves following a hypoxic event in *in vivo*. Therefore I/R CSs may require additional time for the reoxygenation to induce the fibrotic response *in vitro* [19].

Our analyses of fibrotic genes after DOX treatment showed that the expression of Dcn and Col3a1 was downregulated in both hCSs and mCSs compared to their respective controls, whereas Col11a1, Ctgf and F2r were upregulated in both hCSs and mCSs in comparison to their controls. Unlike other fibrotic genes Col1a1 and Fn1 showed differential expression in mCSs and hCSs where both the genes were upregulated in mCSs and are downregulated in

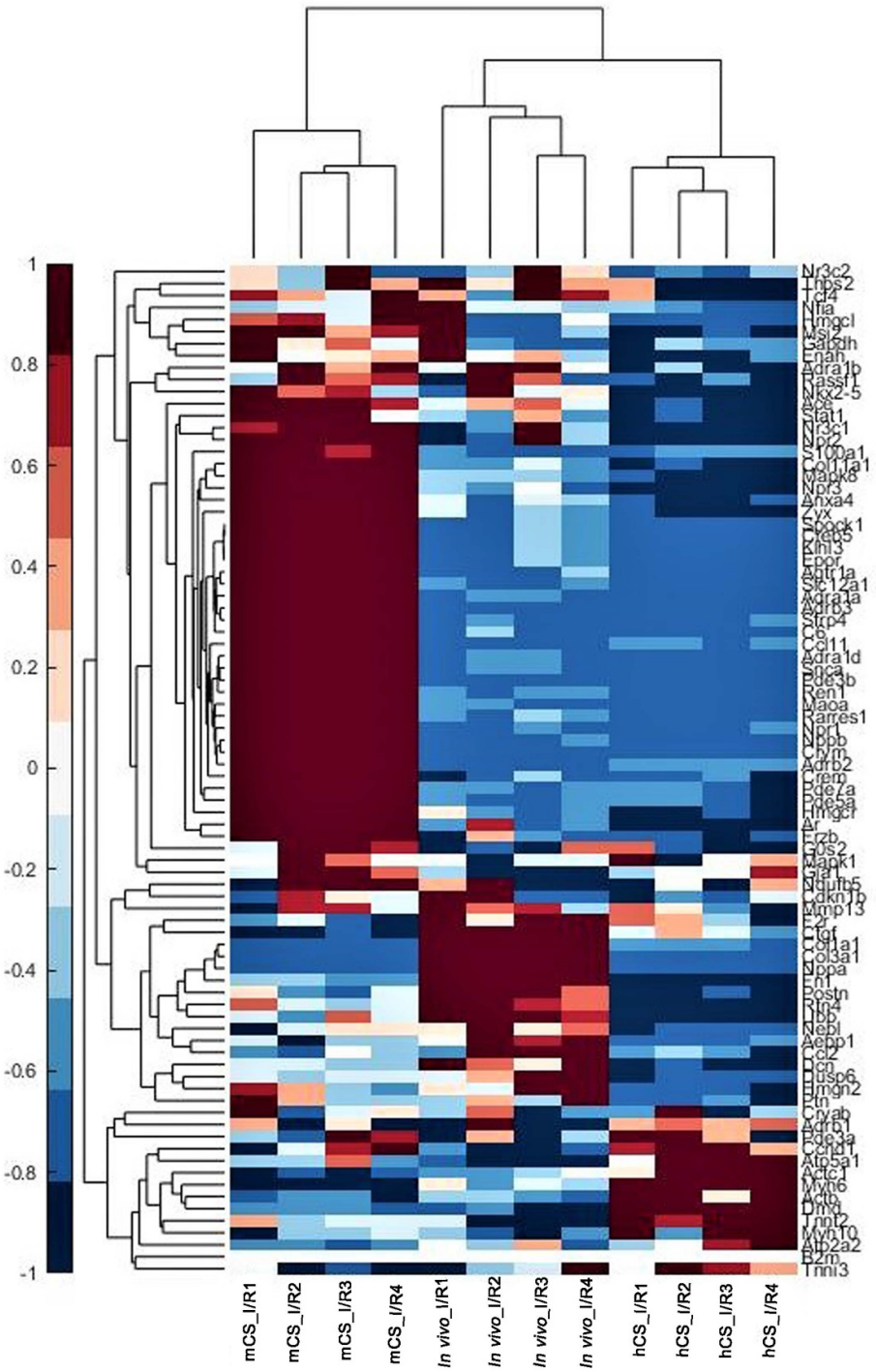

Figure 8. Difference in expression of cardiac genes in *in vivo* and *in vitro* models of myocardial I/R injury. Heat map of the differential expression of cluster of genes obtained after principal component analyses in mCSs, *in vivo* mouse and hCSs moving from right to left. The color bar on the right side indicates the intensity of expression.

hCSs compared to their respective controls (table 2). Fibrosis caused by DOX was also confirmed by a previous study where expression of osteopontin a cytokine that is involved in reconfiguration of the extracellular matrix and contributes to cardiomyocyte death in H9c2 rat heart derived embryonic myocytes and adult mice hearts was studied which is consistent with our study [45].

3.5.7. Signal transduction genes were consistently regulated in I/R and DOX CSs

Adrenergic receptors, mitogen-activated protein kinases and phosphodiesterases play a critical role in the regulation of signal transduction in the myocardium [42, 46, 47]. All of these genes were upregulated in both *in vitro* and *in vivo* following injury. These include: (a) adrenergic receptors, such as alpha 1a

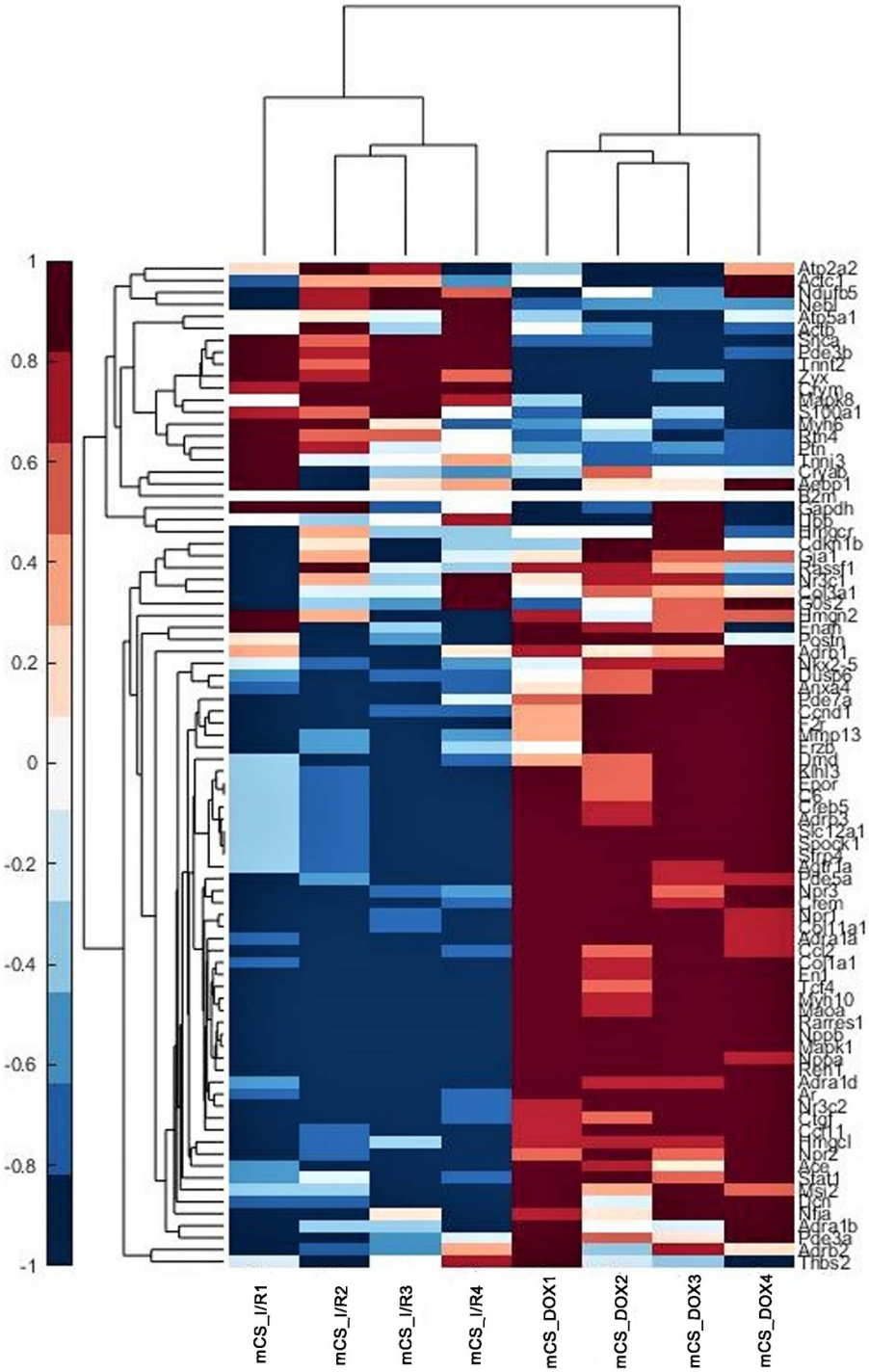

Figure 9. Difference in expression of cardiac genes in *in vitro* I/R and DOX mCSs. Heat map of the differential expression of cluster of genes obtained from principal component analyses in mCSs, comparing I/R and DOX-mediated response from right to left. The color bar on the right side indicates the intensity of expression.

(Adra1a), alpha 1b (Adra1b), alpha 1d (Adra1d), beta 2 (Adrb2) and beta3 (Adrb3); (b) mitogen-activated protein kinases, such as Mapk1 and Mapk8 and (c) phosphodiesterase enzymes, such as 3B cGMP-inhibited (Pde3b), 5 A cGMP-specific (Pde5a) and 7a (Pde7a) (table 1).

All the signal transduction genes analyzed in our study (such as, Adra1a, Adra1b, Adra1d, Adrb2, Adrb3, Mapk1, Mapk8, Pde3b, Pde5a and Pde7a) were upregulated in both mCSs and hCSs compared to controls (table 2). These results are consistent with others, suggesting that in response to the DOX-mediated cardiotoxicity the expression of signal transduction proteins such as adrenergic receptor proteins, Map kinases and phosphodiesterases is increased to induce a cardioprotective effect [48, 49].

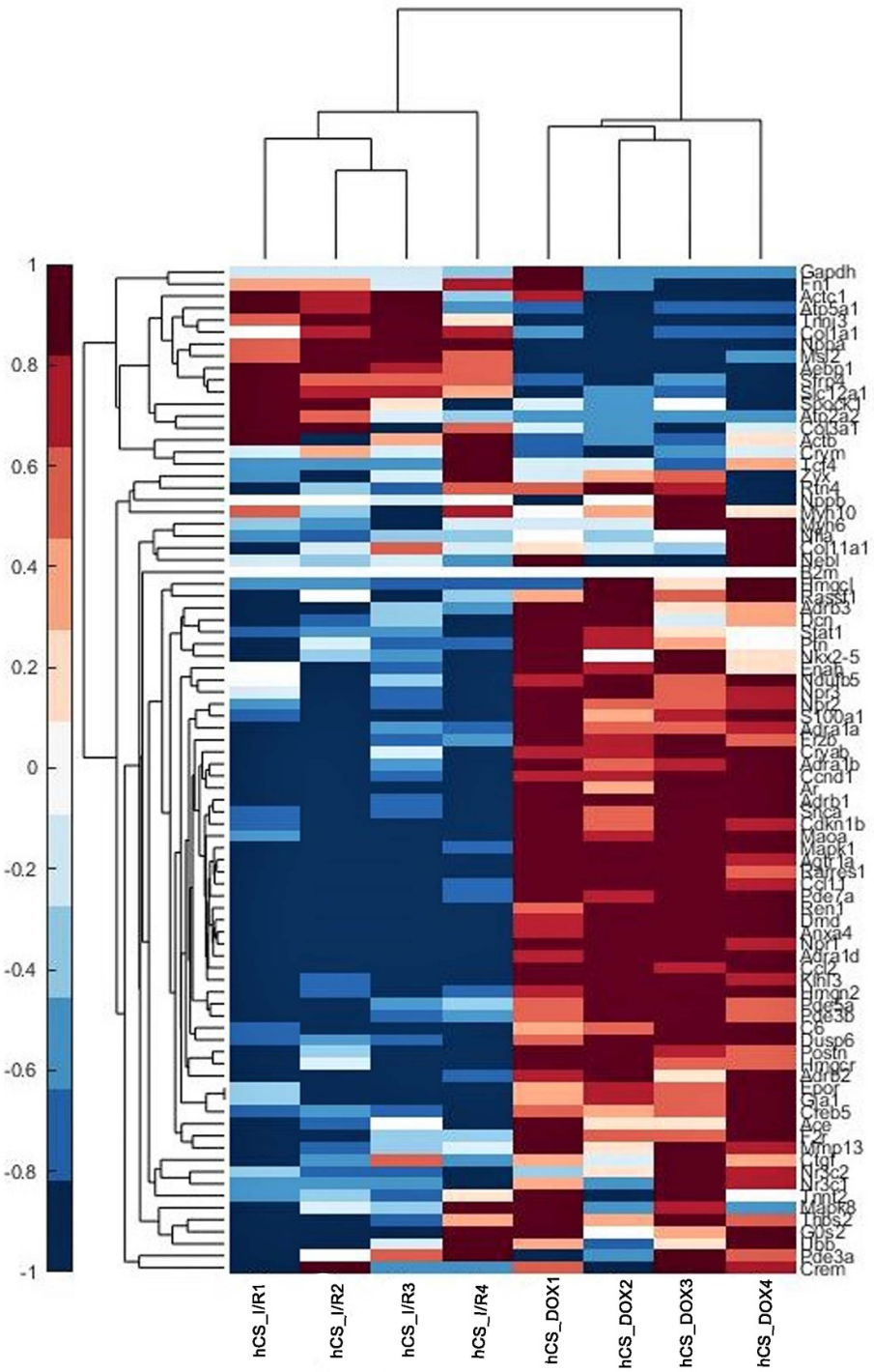

Figure 10. Difference in expression of cardiac genes in *in vitro* I/R and DOX hCSs. Heat map of the differential expression of cluster of genes obtained from principal component analyses in hCSs, comparing I/R and DOX-mediated response from right to left. The color bar on the right side indicates the intensity of expression.

4. Discussion

Myocardial I/R and drug-induced cardiac damages are the primary causes of all the deaths that occurred due to CVD across the globe [17, 18]. There is an urgent need for advanced *in vitro* human heart models that can closely recapitulate these complex scenarios. More specifically, clinically relevant approaches that can easily and directly translated into clinical trials are required to combat these major killers [17]. In this study, we showed that *in vitro* CSs from human cells can serve as a clinically relevant approach to model several aspects of myocardial I/R injury typical of an MI event and drug-induced cardiac damage in humans. These include changes in cell viability and death, contractile function and gene expression levels. In order to replicate *in vivo* conditions typical of an MI event in *in vitro* CSs, we exposed CSs to pathophysiological changes in O_2. Given the novelty of this approach, we developed our own model

Table 2. Expression of cardiovasular genes following DOX-treatment. Relative expression of sacromeric genes, calcium transporting genes, cell cycles genes, apoptotic genes, fibrotic genes and signal transduction genes in *in vitro* mCSs, and *in vitro* hCSs. The blue colour represents downregulated genes and red represents the upregulated genes. Unpaired t-test, $p > 0.05$ = ns, $p < 0.05$ = *, $p < 0.01$ = **, $p < 0.001$ = *** and $p < 0.0001$ = ****, ($n = 4$).

		QPCR analyses of cardiovascular genes to evaluate the DOX-induced cardiac damage			
		In vitro mCSs		*In vitro* hCSs	
Classification of genes	Genes	Fold change	*P*-value	Fold change	*P*-value
Sarcomeric Genes	Actc1	0.05	**	0.13	*
	Myh10	12.85	****	6.35	****
	Myh6	0.03	**	0.75	ns
	Tnni3	0.04	**	0.025	**
	Tnnt2	0.01	***	0.15	**
Calcium Transporting Genes	Atp2a2	0.04	****	0.07238	****
	Atp5a1	0.12	****	0.19	****
Cell Cycle Genes	Ccnd1	11.64	****	7.99	****
	Rarres1	75.14	****	9.63	****
Cardiac Remodelling Genes	Ace	8.19	****	2.56	*
	Mmp13	4.72	****	3.96	***
	Ren1	44.24	****	6.63	****
Apoptotic Genes	Anxa4	10.04	****	12.05	****
	Ccl2	4.32	****	6.88	****
	Maoa	36.59	****	5.26	****
	Nppa	2.614748	*	0.016	ns
	Nppb	79.05	****	0.33	ns
	Npr1	43.41	****	9.32	****
	Pde3a	4.37	****	2.56	***
	Snca	12.38333	****	7.56	****
Fibrotic Genes	Col11a1	14.77	****	2.43	**
	Col1a1	3.516667	****	0.13	ns
	Col3a1	0.06	*	0.11	*
	Ctgf	4	****	2.47	**
	Dcn	0.74	ns	0.11	***
	F2r	7.7966	****	4.33	***
	Fn1	9.5767	****	0.06	ns
Signal Transduction Genes	Adra1a	44.24	****	3.61	***
	Adra1b	3.79	****	3.76	****
	Adra1d	37.03	****	15.35	****
	Adrb1	2.31	****	4.302	****
	Adrb2	36.36	****	7.987	ns
	Mapk1	10.37	****	4.74	ns
	Mapk8	4.89	****	1.19	****
	Pde3b	32.38	****	3.77	****
	Pde5a	17.71	****	4.676	**
	Pde7a	15.15	****	9.43	****

of myocardial I/R injury by exposing CSs incubated with reversible hypoxic dye to normoxic conditions followed by hypoxic conditions followed by normoxic conditions (figure 2). The overtime reversible changes in fluorescence of the hypoxic dye showed that the CSs very well sense the pathophysiological alterations in O_2 concentration to mimic *in vivo* I/R. For the evaluation of drug-induced cardiac damage, CSs were incubated with DOX. Sebastio *et al* [15] in their recent study showed that post I/R injury in both *in vitro* and *in vivo* conditions, cardiomyocytes die and cannot form spheroid cultures. We observed a similar response following I/R conditions *in vitro* for cardiomyocytes, fibroblasts and endothelial cells, as demonstrated by our toxicity ratio and 3D rendering analyses of I/R CSs (figures 3 and 5, video 2). Our results of I/R mediated toxicity are also consistent with a previous study focusing on *in vitro* and *in vivo* necrosis caused by I/R, demonstrated by flouresecent staining for cell death and infarct size, respectively [50]. Similarly, Maillet *et al* [51] reported cell death in human iPSC-derived cardiomyocytes following DOX treatment, also consistent with our DOX-induced cell death results. Our toxicity ratio and 3D rendering analyses of DOX-treated CSs follow our previous studies focused on the response of cardiomyocytes, endothelial cells and fibroblasts in CSs (figures 4 and 6, video 3) [8]. We report that cell death in I/R and DOX CSs is also correlated with a reduction in fractional shortening and contraction frequency in DOX CSs, with the greatest inhibitory effects in I/R CSs (figure 7, videos 4, 5 and 6).

Our results showing that fractional shortening and contractile reductions in *in vitro* CSs could reflect the scenario observed in *in vivo* functional cardiomyopathies, as measured by ultrasound techniques as fractional shortening, contraction frequency and ejection fraction [52–55]. Our qPCR analyses demonstrated that changes in mRNA expression levels of cardiac damage-related genes measured *in vivo* were recapitulated for a variety of gene in I/R CSs (figure 8, table 1). For this study, *in vivo* I/R ventricular samples were isolated from adult male murine hearts that underwent a temporary LAD ligation, whereas control animals received a sham procedure only. These tissues were then used to compare the changes measured in *in vitro* models. Among the genes that presented a similar trend *in vivo* and *in vitro*, we report the downregulation in Actc1 mRNA expression levels following I/R injury (table 1), which is consistent with a previous study by Zimmermann *et al* [56], in a pig *in vivo* model. It was also reported that Actc1 was severely downregulated following oxidative stress in a mouse model of heart failure [24]. In our study we also measured a decrease in Myh6 in I/R CSs compared to control cultures, which is consistent with another study reporting a similar trend in both non ischaemic and ischaemic cardiomyopathy of a non-failing adult human heart [25]. Myh6 was also shown to be downregulated following the establishment of heart failure and left ventricular pressure overload in rabbits [26]. The upregulation of Myh10 we measured in CSs was consistent with what reported in rats post MI injury [27]. In another study, Wang *et al* [23] showed that Tnni3 is downregulated in mice two days post MI, which is consistent with our findings. The downregulation in Tnni3 and Tnnt2 was also linked to necrosis [22] and metabolic inhibition [57, 58]. In terms of calcium transporters Atp2a2 [33] and Atp5a1 [32, 59], they were both downregulated in I/R CSs compared to control cultures, consistent with another study conducted in mice [23]. Regarding changes in cell cycle related genes, Chen *et al* [60], showed that the Ccnd1 levels were increased in both neonatal mice and their cell cultures post MI, supporting our results. Similarly, Ccnd1 expression levels increased in adult T-box20 double transgenic mice following MI compared to α-Myosin Heavy Chain MerCreMer single transgenic mice as controls [61]. Another gene regulating cell cycle is Rarres1, a retinoic acid receptor, which was reported to be upregulated in unstable carotid endarterectomy plaque, consistent with our findings [62]. Among the several signal transduction genes we measured, phosphodiesterases, Map kinases and adrenergic receptors were previously reported to be upregulated post injury *in vivo*, which is again consistent with our study [63]. Among the apoptotic genes considered, Anxa4 was previously reported to be upregulated following hypoxic conditions *in vitro*, similar to what we reported in this study [64]. Similarly, another study by Korkmaz-Icöz *et al* [41] reported similar changes in apoptotic and fibrotic genes with our results.

When we analyzed changes in gene expression of DOX CSs, these showed a similar response as of I/R CSs. In particular, sarcomeric genes, such as Actc1, Tnni3, Tnnt2 and Myh6 were downregulated and Myh10 was upregulated compared to their respective controls (table 2). This is consistent with previously reported DOX-induced cardiac damage studies [28–30]. Our analyses of calcium transporting genes was also consistent with studies reporting reduced expression of Atp2a2 and Atp5a1 following DOX treatment [34]. We reported an upregulation of Ccnd1 and Rarres1 following DOX treatment, consistent with previous studies [36, 37]. Genes correlated with cardiac remodeling, such as Ace, Mmp13 and Ren1 were overexpressed in response to DOX treatment, typical of DOX- mediated myocardial damage [30, 39, 40]. We also observed that most of the apoptosis regulating genes are upregulated following DOX treatment compared to controls in both mCSs and hCSs, consistent with previous studies [30]. Signal transduction related genes were all upregulated in both mCSs and hCSs compared to controls suggesting consistency of our *in vitro* model with previous studies (table 2) [48, 49].

Previous studies using 3D *in vitro* cardiac models have been reported to study I/R and drug-induced damage on the heart [2, 65]. However, the majority of these studies lack a thorough recapitulation of features typical of the human heart in terms of cell composition and pathophysiological O_2 concentrations. More importantly, these studies only recapitulated the hypoxic event, without any analysis of the reoxygenation effects. To our knowledge, our study using *in vitro* CSs is the only one that deeply looked into these features by overcoming previous limitations. In this study, we have generated our CS models by using the three major cell types (cardiac myocytes, endothelial cells and fibroblasts), which were then used to recapitulate more clinically relevant aspects of an MI event. In particular, in our I/R injury we have used pathophysiological concentrations of O_2 (0% and 5%) to mimic *in vivo* I/R. However, it is important to highlight that our model may still lack important features of the *in vivo* MI event and the factors that elucidate pharmacokinetic and pharmacodynamic effects of a drug. The difference in behaviour of some of the genes in *in vivo* and *in vitro* could be linked to the fact that in *in vivo* there are several additional factors that influence the disease progression other than the confounding cell types we have in our *in vitro* CS models [1, 66]. In particular, in order to fully recapitulate the increase in expression levels of fibrotic genes measured *in vivo* (3 d following the hypoxic event), I/R CSs may require additional time for the reoxygenation to induce the fibrotic response observed *in vitro* and it may be used to discern between early and late effects of an MI event, given

the right conditions. Moreover, differences in gene expression levels between mCSs and hCSs could be species-specific [9, 67]. It is critical to acknowledge the limitations of our models and the fact that not all genes were upregulated and downregulated similarly *in vitro* and *in vivo*. One of these limitations is the absence of blood, blood derived cells and their effects on the myocardium, such as platelets, macrophages and other blood cells, all critical for the release of vasoconstrictive and proinflammatory agents typical of the myocardial I/R injury and DOX-induced cardiac damage *in vivo* [68]. Another important consideration is the fact we did not measure nor change the pH and calcium concentration to pathophysiological levels in I/R CSs [1]. This is due to the intrinsic static nature of our model, and future studies integrating I/R and DOX CSs in dynamic conditions may develop new approaches integrating the use of platelets and changes in pH and calcium concentrations *in vitro*. For instance, state-of-the-art microfluidics devices and bioprinting technology could be explored for the generation of high-throughput assays using I/R and DOX CSs and dynamic culture conditions mimicking blood flow.

5. Conclusion

Our study has presented for the first time a direct comparison between *in vivo* myocardial I/R injury and *in vitro* biofabricated CSs models that mimic features typical of MI. The cardiac damage observed in *in vivo* and *in vitro* demonstrated by our gene expression analyses of I/R CSs makes them suitable models to study myocardial damage following I/R injury and advanced alternatives to using animals for studies focusing on MI damage by using human cells in 3D *in vitro* cultures. Moreover, cardiac damage induced by DOX showed that our CS model is a multifaceted model that can be also used to test drug induced cardiac effects, including safety of drugs for patients. To our knowledge, this is the only *in vitro* 3D model able to mimic so many features typical of a damaged heart tissue following I/R injury, allowing the study of pathophysiological conditions, including the use of drugs in patients. This study has the potential to advance the field of cardiac tissue engineering for the biofabrication of novel *in vitro* cardiac models by better recapitulating the complex pathophysiology typical of a heart attack compared to other existing models.

Data availability statement

The data that support the findings of this study are available upon reasonable request from the authors.

Acknowledgments

Poonam Sharma was supported by University of Newcastle with UNIPRS and UNRS Central & Faculty School (UNRSC5050) scholarships. Laura A Bienvenu is supported by a National Heart Foundation (NHF) of Australia Postdoctoral Fellowship; Xiaowei Wang is supported by an NHF Future Leader Fellowship and a Baker Fellowship. Carmine Gentile was supported by a UTS Seed Funding, Catholic Archdiocese of Sydney Grant for Adult Stem Cell Research and a University of Sydney/Sydney Medical School Foundation Cardiothoracic Surgery Research Grant. A special thanks to Prof Louise Cole (UTS, Sydney) and to Dr Imala Alwis (Heart Research Institute, Sydney) for their assistance with confocal microscopy imaging.

Ethical statement

In vitro mCSs were generated under our approved protocol number RESP_17/55 from the Animal Ethics Committee at the Northern Sydney Local Health District St Leonards, NSW, Australia. *In vivo* animal procedures were performed under the approved protocol number E/1950/2019/B from Molecular Imaging and Theranostics Laboratory, Baker Heart and Diabetes Institute, Melbourne, Australia.

Conflicts of interest

The authors declare no conflict of interest.

ORCID iD

Carmine Gentile https://orcid.org/0000-0002-3689-4275

References

[1] Sharma P *et al* 2021 *Small* **17** 2003765
[2] Richards D J *et al* 2020 *Nat. Biomed. Eng.* **4** 446–62
[3] Ojha N *et al* 2020 *Myocardial Infarction, in StatPearls* (Treasure Island, FL: StatPearls Publishing)
[4] Kunecki M *et al* 2017 *Postepy Hig. Med. Dosw.* **71** 20–31
[5] Neri M *et al* 2017 *Mediators Inflammation* **2017** 7018393
[6] Ferlay J *et al* 2021 *Int. J. Cancer* **149** 778–89
[7] Soares R O S *et al* 2019 *Int. J. Mol. Sci.* **20** 5034
[8] Polonchuk L *et al* 2017 *Sci. Rep.* **7** 7005
[9] Chen T *et al* 2018 *Regen. Eng. Transl. Med.* **4** 142–53
[10] Kofron C M *et al* 2017 *J. Physiol.* **595** 3891–905
[11] Gentile C 2016 *Curr. Stem Cell Res. Ther.* **11** 652–65
[12] Zuppinger C 2019 *Front. Cardiovasc. Med.* **6** 87
[13] Veldhuizen J *et al* 2019 *J. Biol. Eng.* **13** 29
[14] Mills R *et al* 2020 *Nat. Biomed. Eng.* **4** 366–7
[15] Sebastiao M J *et al* 2020 *Transl. Res.* **215** 57–74
[16] Keeley T P *et al* 2019 *Physiol. Rev.* **99** 161–234
[17] Polonchuk L *et al* 2021 *Biofabrication* **13** 045009
[18] Sharma P *et al* 2021 *J. Vis. Exp.* **167** e61962
[19] Figtree G A *et al* 2017 *Cells Tissues Organs* **204** 191–8
[20] Bienvenu L A *et al* 2020 *Circ. Res.* **127** 1211–3
[21] Ziegler M *et al* 2018 *Eur. Heart J.* **39** 111–6
[22] Park K C *et al* 2017 *Cardiovasc. Res.* **113** 1708–18
[23] Wang Y *et al* 2018 *Acta Cardiol. Sin.* **34** 175–88
[24] Angelini A *et al* 2020 *FASEB J.* **34** 2987–3005
[25] Kittleson M M *et al* 2005 *Physiol. Genomics* **21** 299–307
[26] James J *et al* 2010 *J. Mol. Cell. Cardiol.* **48** 999–1006
[27] Wan W *et al* 2014 *Appl. Physiol. Nutr. Metab.* **39** 226–32
[28] Lenčová-Popelová O *et al* 2014 *PLoS One* **9** e96055

[29] Adamcova M *et al* 2019 *Int. J. Mol. Sci.* **20** 2638
[30] Boucek R J Jr *et al* 1999 *J. Mol. Cell. Cardiol.* **31** 1435–46
[31] Inesi G *et al* 2008 *Biochem. Biophys. Res. Commun.* **369** 182–7
[32] Ni R *et al* 2016 *Diabetes* **65** 255–68
[33] Lipskaia L *et al* 2014 *Biochim. Biophys. Acta* **1843** 2705–18
[34] Zhang Y *et al* 2014 *Cell Biochem. Biophys.* **70** 1791–8
[35] Lafontant P J *et al* 2006 *Heart Failure: Molecules, Mechanisms and Therapeutic Targets: Novartis Foundation Symposium* (Hoboken, NJ: Wiley Online Library) vol 274 pp 196–207 discussion 208–13, 272–6
[36] Haybar H *et al* 2021 *Jundishapur J. Chronic Dis. Care* **10** e112413
[37] Ma X *et al* 2020 *Sci. Adv.* **6** eaay2939
[38] Evans S *et al* 2020 *Sci. Rep.* **10** 14129
[39] Sobczuk P *et al* 2020 *Heart Fail. Rev.* **27** 295–319
[40] Sun X *et al* 2021 *Evidence-Based Complementary Altern. Med.* **2021** 6659676
[41] Korkmaz-Icöz S *et al* 2015 *J. Diabetes Res.* **2015** 396414
[42] Rose B A *et al* 2010 *Physiol. Rev.* **90** 1507–46
[43] Sergeeva I A *et al* 2013 *Biochim. Biophys. Acta* **1832** 2403–13
[44] Fu X *et al* 2020 *Front. Physiol.* **11** 416
[45] Schunke K J *et al* 2013 *J. Cell. Physiol.* **228** 2006–14
[46] Lohse M J *et al* 2003 *Circ. Res.* **93** 896–906
[47] Zhao C Y *et al* 2016 *J. Mol. Cell. Cardiol.* **91** 215–27
[48] Fajardo G *et al* 2006 *J. Mol. Cell. Cardiol.* **40** 375–83
[49] Prysyazhna O *et al* 2016 *J. Biol. Chem.* **291** 17427–36
[50] Hwang I-C *et al* 2018 *Hypertension* **71** 1143–55
[51] Maillet A *et al* 2016 *Sci. Rep.* **6** 25333
[52] Smiseth O A *et al* 2016 *Eur. Heart J.* **37** 1196–207
[53] Gnyawali S C *et al* 2010 *J. Vis. Exp.* **41** e1781
[54] Al-Biltagi M *et al* 2012 *ISRN Pediatr.* **2012** 870549
[55] Mitry M A *et al* 2016 *Int. J. Cardiol. Heart Vasc.* **10** 17–24
[56] Zimmermann M *et al* 2017 *Oncotarget* **8** 60809–25
[57] Hessel M H *et al* 2008 *Exp. Mol. Pathol.* **85** 90–95
[58] Rains M G *et al* 2014 *Clin Intervention Aging* **9** 1081–90
[59] Sommakia S *et al* 2017 *J. Mol. Cell. Cardiol.* **113** 22–32
[60] Chen Z *et al* 2017 *Cardiovasc. Res.* **113** 620–32
[61] Xiang F L *et al* 2016 *Circulation* **133** 1081–92
[62] van der Pouw Kraan T C *et al* 2010 *BMC Genomics* **11** 388
[63] López-Neblina F *et al* 2006 *J. Surg. Res.* **134** 292–9
[64] Vicic N *Exp. Cell. Res.* **340** 283–94
[65] Shen S *et al* 2021 *Biomed. Pharmacother.* **133** 110990
[66] Lindsey M L *et al* 2018 *Am. J. Physiol. Heart Circ. Physiol.* **314** H812–38
[67] van der Velden J *et al* 2019 *Physiol. Rev.* **99** 381–426
[68] Ziegler M *et al* 2019 *Cardiovasc. Res.* **115** 1178–88

2.3 Cardiovascular Damage Model using Patient-derived Plasma

Summary:

This chapter comprises a manuscript currently under review and was submitted on the 20 of January 2024 to the AHA Hypertension Journal. This paper introduces a groundbreaking 3D *in vitro* model for studying CVD post-HDP. We have unveiled previously unexplored effects of GH and PE patients' plasma five years postpartum on cardiac health, which is potentially implicated in escalating the risk of long-term CVD. The results showed distinct signaling pathways between GH and PE activation, which could lead to CVD. While GH leads to a decrease in cell viability, PE significantly decreases contractile function. We also found a distinction between HDP plasma groups, GH-activated mechanisms related to homeostasis and cell death signaling. In contrast, PE led to dysfunctional inflammatory pathways and exhibited heightened protein expression of markers associated with endothelial dysfunction and malfunction in cardiomyocyte contractility.

For the overall thesis, this chapter contributes to the application of CS model as a tool for early detection of cardiac function alterations post-HDP. Future work will involve using the patient-specific model to test the protective role of ACh and personalize ACh treatment for patients.

3D in vitro Modelling of Post-Partum Cardiovascular Health reveals Unique Characteristics and Signatures following Hypertensive Disorders in Pregnancy

Clara Liu Chung Ming[1#], Dillan Pienaar[2#], Sahar Ghorbanpour[2], Hao Chen[2], Lynne Margaret Roberts[3,4], Louise Cole[5], Kristine C McGrath[2], Matthew Padula[2], Amanda Henry[3,4,6], Carmine Gentile[1*], Lana McClements[2*].

1. School of Biomedical Engineering, Faculty of Engineering and Information Technology, University of Technology Sydney, Sydney, NSW, Australia
2. School of Life Sciences, Faculty of Science, University of Technology Sydney, Sydney, NSW, Australia
3. Department of Women's and Children's Health, St. George Hospital, Sydney, NSW, Australia.
4. St George and Sutherland Clinical Campus, School of Clinical Medicine, University of New South Wales Medicine and Health, Sydney, NSW, Australia.
5. Australian Institute of Microbiology and Infection, Faculty of Science, University of Technology Sydney, Sydney, NSW, Australia.
6. Discipline of Women's Health, School of Clinical Medicine, University of New South Wales Medicine and Health, Sydney, NSW, Australia.

***Corresponding authors:** Associate Professor Lana McClements, School of Life Science, Faculty of Science, University of Technology Sydney, Ultimo, NSW; email: lana.mcclements@uts.edu.au

Dr Carmine Gentile, School of Biomedical Engineering, Faculty of Engineering and IT, University of Technology Sydney, Ultimo, NSW; email: carmine.gentile@uts.edu.au

Funding: This study was supported by the Cardiac and Vascular Health Clinical Academic Group, Maridula Budyari Guman, the Sydney Partnership of Health, Education, Research and Enterprise (SPHERE), and Future Leader Fellowship Level 1 from the National Heart Foundation of Australia (L.M., 106628).

Running title: Modelling and deciphering early cardiovascular damage post-partum

Keywords: pregnancy, hypertensive disorders of pregnancy, cardiovascular disease, post-partum, biomarkers, proteomics

Abstract

Background: Hypertensive disorders of pregnancy (HDP) affect 2-8% of pregnancies and are associated postpartum with ongoing, increased cardiovascular disease (CVD) risk. In this study, we aimed to model HDP-induced CVD and decipher systemic mechanisms, using an innovative 3D *in vitro* cardiac spheroid model.

Methods: Human iPSC-derived cardiomyocytes, cardiac fibroblasts and coronary artery endothelial cells were tri-cultured to form cardiac spheroids (CS) in collagen type-1 hydrogels containing 10% patient plasma collected five years postpartum (n=5 per group: normotensive control, gestational hypertension (GH) and preeclampsia (PE). Plasma-treated CS were assessed for cell viability, contractile function and markers of cardiac damage using immunofluorescence staining and imaging. An untargeted, label-free quantitative proteomic analysis of plasma samples was conducted (controls n=21; GH n=5; PE n=12).

Results: Contraction frequency (CF) was increased in PE-treated CS (CF:45.5±3.4 contractions/minute, $p<0.001$) and GH-treated CS (CF:45.7±4.0 contractions/minute, $p<0.001$), compared to controls (CF=21.8±2.6 contractions/minute). Only PE-treated CS presented statistically significant increased fractional shortening (FS) % (9.95±1.8%, $p<0.05$), compared to controls (3.7±1.1%). GH-treated CSs showed a reduction in cell viability by ~20% ($p<0.05$), and an increase in α-SMA expression ($p<0.05$). Proteomics analysis identified twenty differentially abundant proteins, with hemoglobin A2 being the only protein perturbed in both GH and PE, versus control ($p<0.05$).

Conclusions: Novel biomarkers and therapeutic targets were identified linked to cell death signaling and cardiac remodeling in GH-induced CVD and vascular/endothelial cell dysfunction in PE-induced CVD. Patient-relevant CS platform can be used to assess early cardiac changes and as a precision medicine tool for improved post-HDP CVD clinical management.

Introduction

Hypertensive disorders of pregnancy (HDP) affect 2-8% of all pregnancies and are a leading cause of mortality and morbidity in pregnancy [1, 2]. HDP are characterized by pregnancy hypertension (defined as blood pressure ≥140/90 mmHg) including chronic hypertension (already present pre-pregnancy), gestational hypertension (GH) (new-onset at ≥20 weeks of gestation), and preeclampsia (PE), which may occur *de-novo* or superimposed on chronic hypertension and is characterized by evidence of maternal organ involvement and/or utero-placental dysfunction [1]. Pathophysiological mechanisms of HDP remain incompletely elucidated; however, maladaptation of the maternal cardiovascular system appears to play a central role in GH, whereas poor placentation is a dominant link in PE [2, 3]. Moreover, individuals affected by HDP have increased risk of developing cardiovascular disease (CVD), up to 7-fold higher than those who had normotensive pregnancies, within 5-10 years of affected

pregnancy and continuing lifelong [4]. Even though the epidemiological link between HDP and future CVD is well-established, the mechanisms driving this association are poorly understood. This has impeded the development and implementation of effective monitoring and treatment strategies for women post-HDP, which are needed to ameliorate their CVD risk.

Heightened inflammation has been identified as one of the key mechanisms in HDP. Galectin-3 (Gal-3) has emerged as important due to its key role in cardiac remodeling and heart failure [5], and more recently in PE [6]. Another important marker of cardiac remodeling is alpha smooth muscle actin (αSMA), highly expressed in activated cardiac myofibroblasts regulating cardiac fibrosis and subsequent heart failure [7]. Endothelial dysfunction is also important in pathogenesis of both HDP and CVD, and can lead to high blood pressure, reduced vascular endothelial-cadherin (VE-cadherin) and angiogenesis [8, 9]. FK506-binding protein like (FKBPL) is a critical molecule of developmental, physiological and pathological angiogenesis, a key determinant of CVD, and a predictive and diagnostic biomarker of PE [10-12]. All these molecules play a direct role on cardiac tissue hypertrophy and fibrosis, and may be potential targets for HDP-induced CVD [13, 14].

Nevertheless, the causes of HDP-induced cardiac dysfunction post-partum are still not well understood as current *in vivo* and *in vitro* models fail to recapitulate this complex disease [15]. In this study, we modelled, for the first time, HDP-induced CVD by using our clinically-amenable *in vitro* cardiac spheroids (CS), capable of mimicking the molecular, cellular and extracellular features of the human heart microenvironment. CS have been shown to be an optimal tool for studying angiogenesis, contractile function and cell signalling regulating cardiovascular health [16-18]. They are generated by tri-culturing human induced-pluripotent stem cells-derived cardiomyocytes (iCMs), human coronary artery endothelial cells (HCAECs) and human cardiac fibroblasts (HCFs) at ratios approximating the ones found in the human heart [16, 19]. In a recent study, we demonstrated that spheroids generated from HCFs and HCAECs and treated with plasma from women with early-onset preeclampsia (EOPE; diagnosed before 34 weeks of gestation) or late-onset preeclampsia (LOPE; diagnosed from 34 weeks of gestation) can be used to study changes in angiogenesis, such as the increase in an anti-angiogenic protein, FKBPL, in the context of LOPE [20].

Here, we demonstrate, for the first time, that patient-relevant 3D CS platform is an effective platform to model HDP-induced CVD post-partum, facilitating identification of early cardiovascular changes. We show distinct cellular and molecular changes five-year post GH or PE, compared to healthy pregnancy, despite no differences in cardiovascular and metabolic clinical characteristics. Both GH and PE led to aberrant cardiac function as measure by the CS contractility assay. Interestingly, GH-relevant CS show early signs of cardiac cell death and fibrosis due to increased α-SMA expression whereas PE-relevant CS were characterised by heightened inflammation due to higher Gal-3 expression. Finally, to better understand the mechanism within the secretome driving these cellular and molecular changes with CS, we conducted comprehensive unbiased and untargeted proteomics analysis and identified twenty differentially abundant proteins between these three groups that could be viable therapeutic targets or biomarkers. The vast majority of proteins identified show difference between PE and GH, representative of unique proteome profiles five-year post-GH or PE, which were characterised by disrupted cell death signalling and cardiac remodelling or vascular and endothelial dysfunction, respectively.

Methodology

Reagents

Fibronectin bovine plasma was purchased from Sigma-Aldrich (Missouri, USA). Cardiomyocytes iCell Plating Medium and iCell Maintenance Culture Medium were purchased from Cellular Dynamics (Wisconsin, USA). L-glutamine solution, penicillin-streptomycin and TrypLE were purchased from Thermo Fisher Scientific (Massachusetts, USA).

Plasma isolation from patients

Peripheral blood was collected from 43 patients as part of the P4 study presenting five-years after PE (n=12), GH (n=5) and normotensive pregnancy (n=21) [21]. Blood was collected in Lithium Heparin Plasma tubes and centrifuged at 3000g x 10 min to collect plasma. The plasma from each participant was aliquoted and stored at -80°C. The study was conducted in accordance with the Declaration of Helsinki and approved by both South Eastern Sydney Local Health District and University of Technology Sydney, human ethics committees.

Cell cultures

HCAECs were cultured in MesoEndo Media (Sigma-Aldrich, Missouri, USA), whereas HCFs were cultured in Cardiac Fibroblast Growth Media (Sigma-Aldrich, Missouri, USA) both supplemented with 1% penicillin streptomycin and 1% L-glutamine. Media was changed every 2-3 days and cells cultured until 70-90% confluency before being passaged using TrypLE. A cryovial of iCMs (5 x10^6 cells) was thawed and transferred to a fibronectin-precoated T-75 tissue flask and incubated for 20 hrs with iCell Plating Media at 37ºC and 5% CO_2, following the manufacturer's guidelines. After 20hrs, media was replaced with iCell Maintenance Media and after 72 hours, iCMs were detached with TryplE for CS formation.

Cardiac spheroid (CS) formation

Prior to CS formation, agarose powder (Sigma-Aldrich, Missouri, USA) and 3D micromoulds (Sigma-Aldrich, Missouri, USA) were sterilised. Agarose powder (1%) was reconstituted in phosphate buffered saline (PBS) solution, then heated for a few seconds to allow proper dissolution of the powder, and finally pipetted into 3D micromoulds to set and form moulds for spheroids. Solidified moulds were submerged in culture media and incubated at 37ºC and 5% CO_2, following manufacturer's guidelines.

HCAECs, HCFs and iCMs were detached from their respective flasks with TrypLE, counted and mixed in a ratio of 2:1:1 (iCMs: HCAEC: HCF). Cell pellets were resuspended in CS culture media (iCMs: HCAECs:HCF Media at a ratio of 2:1:1, respectively). Cell suspension (190µl) was added to the inner cavity of the agarose moulds and incubated at 37ºC and 5% CO_2 with daily media changes. Following 48 hours, CS were collected and carefully transferred to a 96-well plate (a minimum of five CS per well). Media was replaced with a solution containing 1:1 collagen 1 rat tail (Merck, Massachusetts, USA) and the whole plate was moved to an incubator at 37ºC and 5% CO_2 overnight.

Plasma treatment of cardiac spheroids

Patient-derived plasma samples were added onto wells containing CS in collagen hydrogels for 96 hours and incubated at 37ºC and 5% CO_2. Plasma samples from age and BMI-matched PE, GH and normotensive control groups (n=5 per group) were added as 10% of the total volume. A media change occurred at 48 hours to ensure cells remained viable.

Live and dead assay

CS embedded in collagen were washed twice with Dulbecco′s Phosphate Buffered Saline. Live/Dead® Viability/Cytotoxicity Kit for mammalian cells and NucBlue® Live ReadyProbes® Reagent (Hoechst 33342) (Invitrogen, Massachusetts, USA) were used according to the manufacturer's instructions. The cell viability was determined by quantifying percentage live cells using an EVOS M7000 Imaging System (Invitrogen, Massachusetts, USA).

Contractile activity assay

The contractile activity of CS was analysed using videos acquired with a Nikon Eclipse TiE2-widefield fluorescence microscope, which were used to measure fractional shortening percentage (FS%, % of difference between contracted and relaxed CS diameter) and frequency of contractions (number of contractions per minute).

Immunolabeling and confocal imaging

Media were removed from each well and CS were fixed with 10% formalin (Sigma-Aldrich, Missouri, USA) for one hour at room temperature. Post incubation, cells were washed three times with phosphate buffer saline containing 1% sodium azide (PBSA), permeabilised with 0.2% Triton X-100 for 30 minutes and then blocked in 3% bovine serum albumin (BSA)/PBSA overnight at 4˚C on a rocking plate. CS were then probed with Galectin-3 (1:100, Abcam, Cambridge, UK), FKBPL (1:100, Proteintech, Rosemont, USA), CD31 (1:10, BD Biosciences, Franklin Lakes, USA), VE-cadherin (1:100, Abcam, Cambridge, UK), αSMA (1:100, Abcam, Cambridge, UK) primary antibodies and incubated at 4 °C overnight. Following washing, goat anti-rabbit IgG H&L (Alexa Fluor® 488, Abcam, Cambridge, UK) and goat anti-mouse IgG H&L (Alexa Fluor® 594, Abcam, Cambridge, UK), and Cy5-Donkey anti-mouse (1:142, Jackson immunoresearch, Pennsylvania, USA) secondary antibodies were added and incubated at 4 °C overnight. CS were then incubated with Vimentin (1:250, Abcam, Cambridge, UK) and Troponin C (1:10, Santa Cruz, California, USA) primary-conjugated antibodies and DAPI (10 µg/mL, Invitrogen, Massachusetts, USA) at 4 °C overnight. Finally, CSs were washed three times with PBSA and stored at 4 °C.

Confocal fluorescence images were acquired with Leica Stellaris confocal, employing a 20× objective with a numerical aperture (NA) of 1.45 and Nyquist sampling. Z stacks were obtained with 0.9 µm optical slices, utilizing 1 AU pinhole. Widefield fluorescence images were acquired using Nikon Ti2-E, with a 20× objective, NA 0.75 and a long working distance of 2300 µm. Widefield images were then clarified using NIS-Elements Clarify.ai [22]. The fluorescent signal intensity, an indicator of protein expression, was quantitatively analyzed using ImageJ software (NIH, USA, version 2.1.0) on maximum intensity projection images. Analysis involved ≥ 3 CS per condition, and the fluorescent intensity was subsequently normalized to the nuclear count.

Preparation of Plasma for Proteomics Analysis

Using an Acquity M-class nanoLC system (Waters, USA), 2 µL of the sample was loaded with MS Solvent A (0.1% Formic Acid) onto a HSS T3 column (Waters; 300µm x 150mm) heated to 50˚C at 5 µl/min. Peptides were eluted from the column and into the source of a Synapt XS mass spectrometer (Waters Instruments) using the following program: 1-40% MS solvent B (100% Acetonitrile) over 46 minutes, 40-85% MS solvent B over 1 minutes, 85% MS solvent B for 2 minutes, 85-1% for 1 min. The eluting peptides were ionised at 3000V at a fixed Cone Voltage of 20V. A UDMSE experiment was performed in positive mode with the Analyser Mode set to Resolution and Dynamic Range set to Extended. Peptide ions were first separated by Travelling Wave Ion Mobility Spectrometry (TWIMS) at a Transfer Wave Velocity of 155 m/s and applying a Charge State/Drift Time Stripping Rule file to remove 1+ ions during the Low CID Energy scan before being subjected to alternating low energy (6eV) and high energy Collision Induced Dissociation (CID) with an accumulation time of 0.4 seconds for each scan type. High Energy CID was performed in the Transfer cell using a Look Up Table adapted from Distler et al. [23]. TOF scans were performed over the mass range of 50-1500 m/z. Total run time per sample was 60 minutes. The MS/MS data files were searched using the Ion Accounting method in Progenesis QI for Proteomics against the UniProt Human Proteome database (downloaded 01/03/2021) as previously described [5, 24].

Statistical Analysis

Images were analyzed with ImageJ for cell viability, contraction frequency, fractional shortening, and protein expression measurements in CS. CS protein expressions were calculated as the Corrected Total Cell Fluorescence (CTCF) and represented as a fold change

compared to the control group. Statistical analysis was performed using GraphPad Prism 9 software. Normality testing was performed using Shapiro-Wilks test before parametric or non-parametric tests were employed based on the normal distribution of the data. If normally distributed, the data was analysed using a two-tailed unpaired t-test or one-way ANOVA with post-hoc multiple comparison tests. For non-normally distributed data, Mann-Whitney or Kruskal-Wallis were used where appropriate. P-value <0.05 was considered statistically significant.

Results

GH-derived plasma reduces cells' viability in CS.

To assess effects of normotensive, GH and PE plasma on CS viability, the percentage of live cells was quantified by counting dead cells stained with ethidium homodimer and by normalising against total cells stained with Hoechst (**Figure 1)**. There was a significant decrease of 19.1 ± 8.0%, (p <0.05) live cells for GH-treated CS compared to control, whereas the reduction in cell viability for PE-treated CS of 6.5 ±7.5% was not statistically significant.

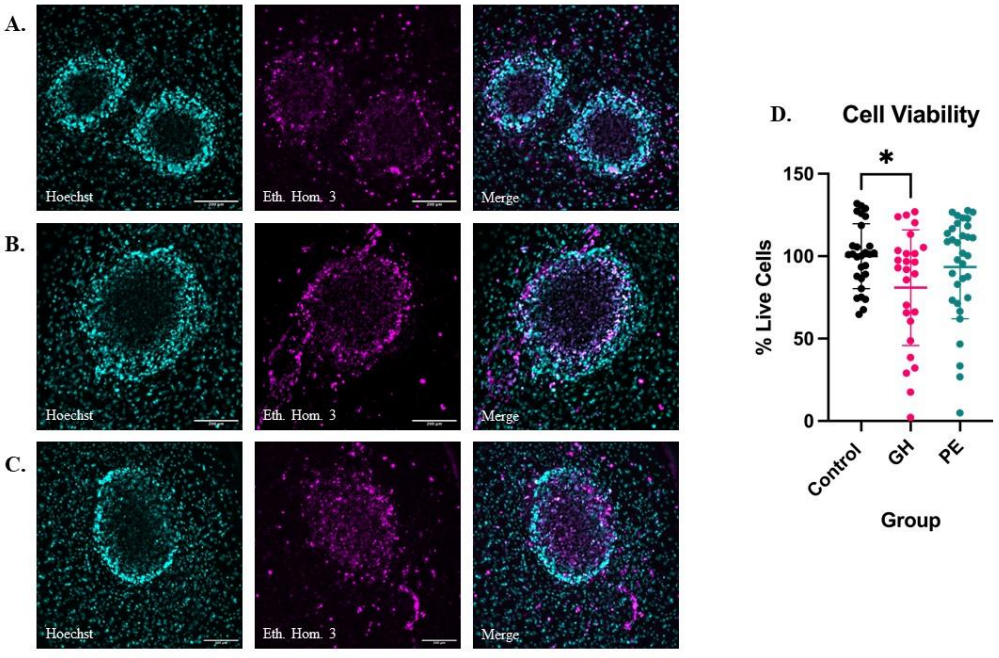

Figure 1. Plasma derived from women with HDP reduce viability of CS. (A-C) Representative collapsed Z-stacks images of all and dead cells within CS. The percentage of live cells remaining following exposure to human plasma from women with HDP was quantified for A) Control (normotensive plasma). B) GH plasma. C) PE plasma. 10% of normotensive, GH or preeclampsia plasma are added to CS plated in collagen hydrogel, respectively. After 96 hours, CS were stained with Hoechst for nuclei stain, and ethidium

homodimer for dead cells. Scale bar equals 100µM. D) Statistical analysis of percentage of live cells comparing all three sample groups: controls, GH and PE. Data represented as Mean ± SEM; n = 5 patients per group; n >26; P-value was calculated using one-way ANOVA post-hoc analysis comparison test; * p<0.05.

Both contraction frequency and fractional shortening % are increased in GH- or PE-plasma treated CS.

To evaluate the effects of normotensive, GH and PE plasma on CS functionality, we measured the fractional shortening % (FS%) and contraction frequency of CS following exposure to plasma for 96 hours. This was done by recording the time frame of each CS for 30sec using Nikon Ti2 microscope. As shown in **Figure 2**, contraction frequency was significantly increased in PE-treated CS (CF:45.5±3.4 contractions/minute, p<0.001) and GH-treated CS (CF:45.7±4.0 contractions/minute, p<0.001), compared to controls (CF:21.7±2.6). Whilst HDP plasma increased the fractional shortening %, this was statistically significant for PE-relevant CS only (9.95±1.8%, P<0.03). Altogether, our results showed that HDP-derived plasma impair both cell viability (Figure 1) and contractile function (Figure 2) in CS.

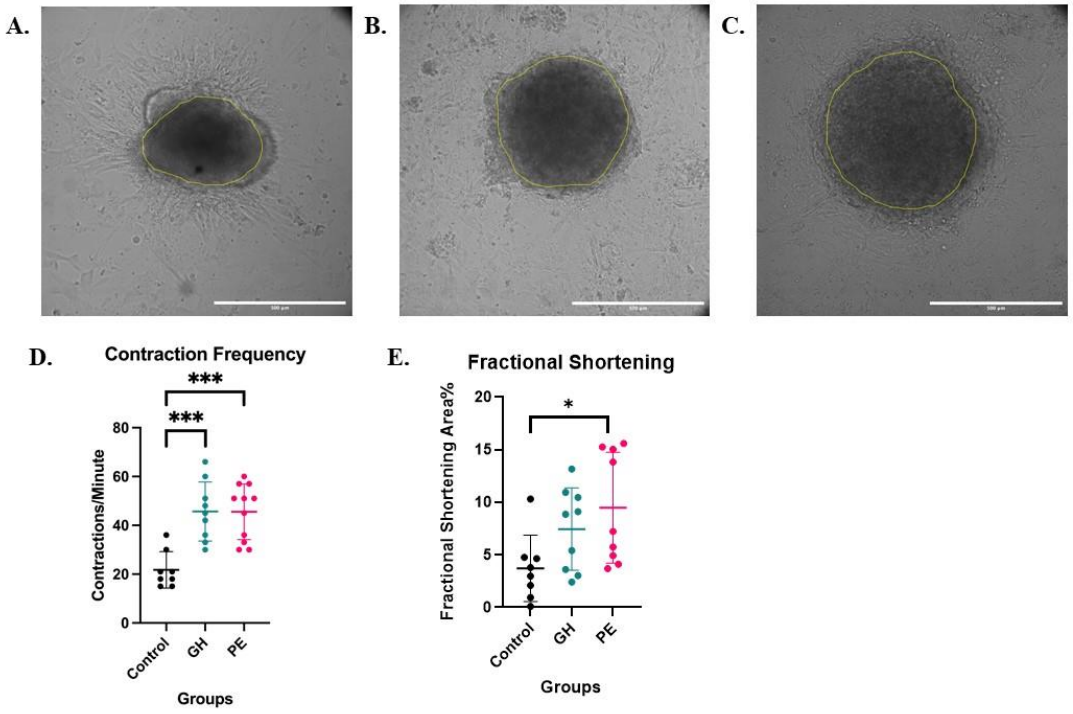

Figure 2. HDP-derived plasma impairs contractile function in CS. (A-C) representative images from videos of contracting control- (A), GH- (B) and PE- (C) treated CS, where yellow outlines the area of the cardiac spheroid during the phase of contraction in each spheroid. (D-E) Statistical analyses of contraction frequency (D) and fractional shortening % (E) in CS. Data

represented as Mean ± SEM; n ≥8 CSs per group from 1-3 patients per group; P-value was calculated using one-way ANOVA post-hoc analysis. Data represented as Mean ± SEM; n = 1-3 patients per group; n ≥8; P-value was determined using one-way post-hoc analysis; * $p<0.05$, *** $p<0.001$.

Key cardiac cell populations do not change following treatment with HDP-derived plasma.

To evaluate if HDP-derived plasma altered the overall cardiac cell population within CS, we performed immunofluorescence staining to semi-quantitatively determine the expression of specific cell markers identifying three key cardiac cell types between the three groups (**Figure 3).** CS were stained with antibodies against cardiac troponin (cTNT) for iCMs, CD31 for HCAECs and vimentin for HCF. The analyses showed that the addition of HDP-derived plasma did not affect any of the cell types across normotensive, GH and PE groups. This suggests that the secretome present within plasma from women five years post GH or PE does not specifically affect a particular cardiac cell type.

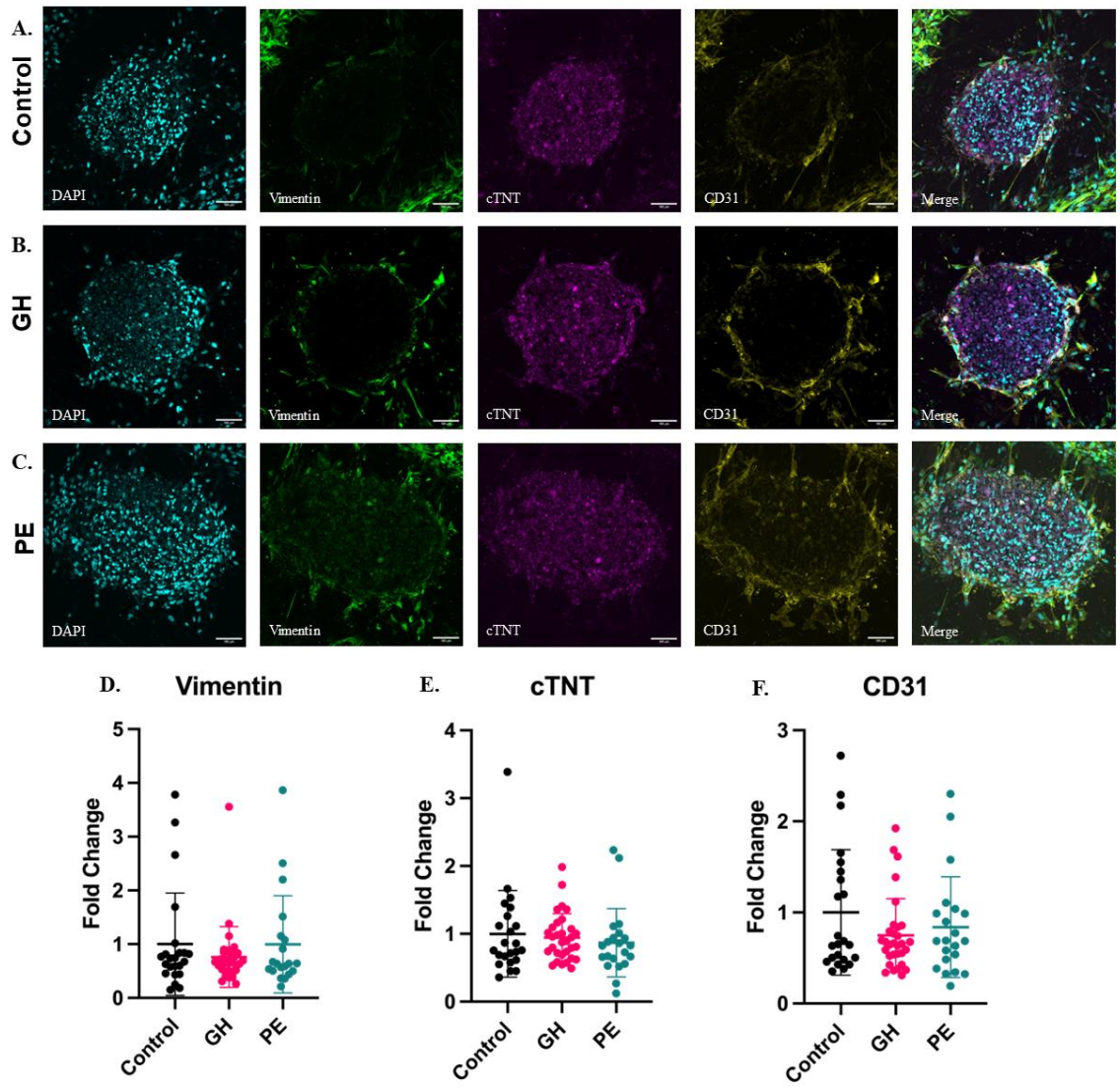

Figure 3. Cardiomyocytes, cardiac endothelial cells and cardiac fibroblasts do not change in numbers following treatment with HDP plasma. (A-C) Representative collapsed Z-stacks of confocal images of CS stained for the three cell markers. CS were exposed to 10% plasma A) normotensive (control), B) GH, and C) PE, for 96 hours, fixed and stained with antibodies against cardiomyocytes (cTNT, magenta), endothelial cells (CD31, yellow) and fibroblasts (vimentin, green). Nuclei are stained with DAPI stain (cyan). (D-F) Statistical analysis of the fold change in protein expression of vimentin (D), cTNT (E) and CD31 (F) for normotensive, GH and PE CS, normalised to control. Data represented as Mean ± SEM; n = 5 patients per group; n > 20 CSs per group; one-way ANOVA test Dunn's multiple comparison test.

Pro-fibrotic α-SMA is increased in the presence of GH plasma, Gal-3 is increased in PE-treated CS.

To evaluate if HDP plasma played any role on angiogenesis and fibrosis in CS, we measured the changes in FKBPL and α-SMA protein expression, respectively (**Figure 4)**. Our statistical analysis of protein abundance in **Figure 4D** showed no significant changes in FKBPL protein abundance in GH and PE groups compared to controls. Furthermore, we measured α-SMA protein abundance given its important role in cardiac remodelling and fibrosis [25]. Addition of GH plasma induced a significant increase in α-SMA protein abundance compared to control (p=0.01), whereas this was not statistically significant for the PE group (**Figure 4E**).

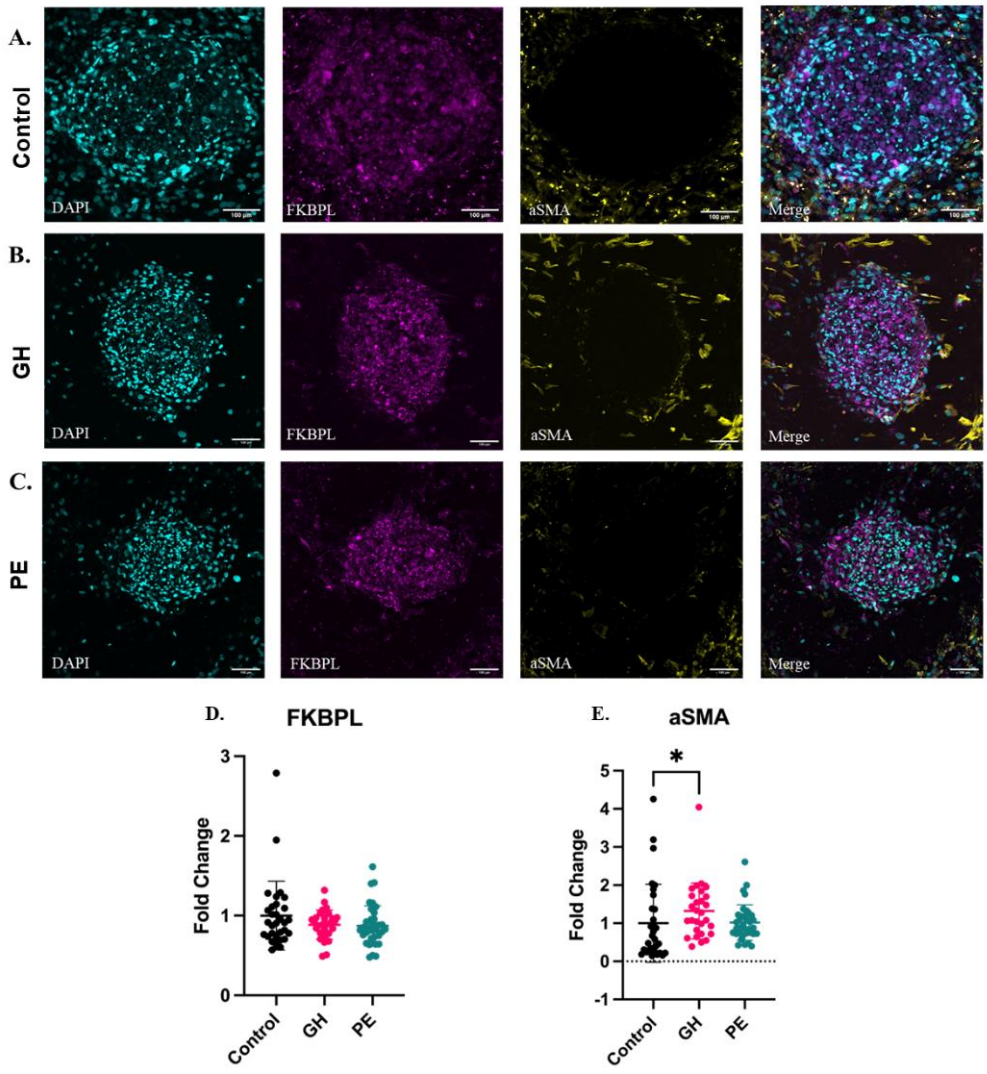

Figure 4. α-SMA is increased following HDP plasma treatment in CSs. (A-C) Collapsed Z-stacks of CS exposed to normotensive (control) (A), GH (B) and PE (C) plasma for 96 hours. Samples were stained with DAPI (cyan) for nuclei stain, as well as antibodies against FKBPL (magenta) and α-SMA (yellow). (D) Statistical analysis of the fold change of protein expression of FKBPL for control, GH and preeclampsia groups, normalised to control. Data represented as Mean ± SEM; n = 5 patients per group; n > 29; P-value was determined using one-way ANOVA test with Dunn's multiple comparison test; protein expression is not significant. (E) Statistical analysis of the fold change of protein expression of α-SMA for control, GH and preeclampsia groups. Data represented as Mean ± SEM; n = 5 patients per group; n > 29; P-

value was determined using one-way ANOVA test with Dunn's multiple comparison test; *p<0.05

Moreover, we examined the abundance of inflammatory and vascular stability markers, Gal-3 and VE-Cadherin, respectively, after HDP plasma treatment in CS. Gal-3 protein abundance was increased (p=0.04) in the PE-treated CS group compared to the GH CS but not to the control group (**Figure 5D**). We did not detect any changes in VE-cadherin protein abundance across the three groups (**Figure 5E**). Altogether, our results from the markers studied support an enhanced inflammatory response in PE plasma compared to GH (**Figures 4-5**).

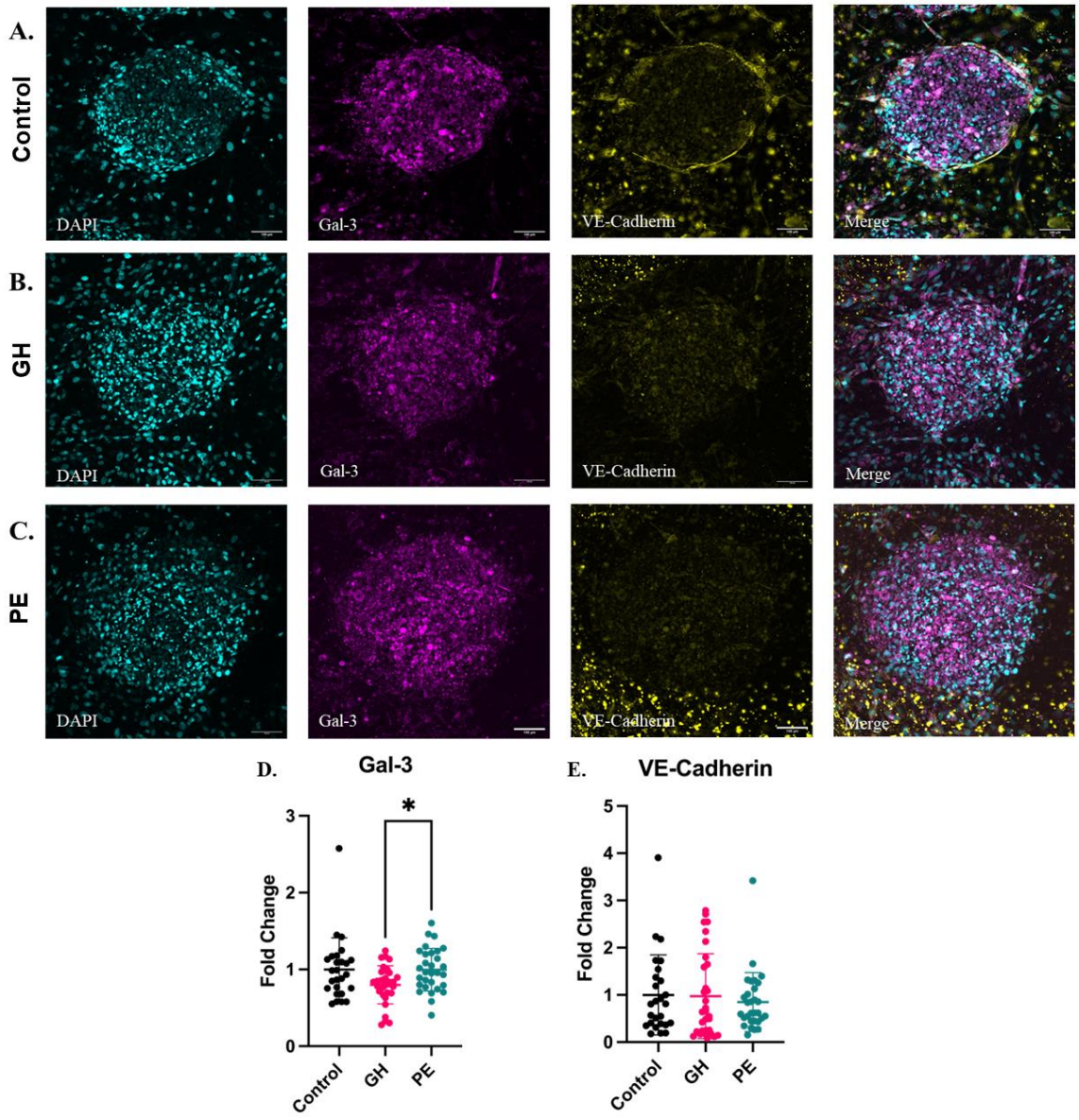

Figure 5. Gal-3 is increased in PE CS, and no changes in VE-Cadherin among groups. (A-C) Collapsed Z-stacks of CS exposed to normotensive (control) (A), GH (B) and PE (C)

plasma for 96 hours. Samples were stained with DAPI (cyan) for nuclei stain, as well as antibodies against Gal-3 (magenta) and VE-Cadherin (yellow). **(**D) Statistical analysis of the fold change of protein expression of Gal-3 for control, GH and PE groups. Data represented as Mean ± SEM; n = 5 patients per group; n > 26; P-value was determined using one-way ANOVA test with Dunn's multiple comparison test; * $p<0.05$. (E) Statistical analysis of the fold change of protein expression of VE-Cadherin for control, GH and PE groups. Data represented as Mean ± SEM; n = 5 patients per group; n > 26 CS per group; P-value was calculated using one-way ANOVA test Dunn's multiple comparison test; P-value is not significant.

Plasma proteomics analysis.

In order to identify the mechanisms driving some of the changes observed in CS functional and inflammatory and fibrotic measurements, differences in the secretome proteome profile across the different HDP groups and normotensive controls were performed using untargeted proteomics analyses with all available P4 substudy samples [21]. In terms of cardiovascular and metabolic clinical characteristics, there were no significant differences between the three groups in the most relevant parameters, including age, body mass index (BMI), systolic blood pressure (SBP), diastolic blood pressure (DBP), blood glucose levels, insulin, HOMA-IR, HbA1c, eGFR, cholesterol, triglycerides, HDL, LDL and smoking status (**Table 1**).

Table 1. Clinical characteristics of P4 participants subgroups.

Characteristics	Control (n = 21)	GH (n = 5)	PE (n = 12)	p-value
Age (Years)	39.6 ± 4.3	38.3 ± 5.0	36.9 ± 4.2	0.16
Time post-pregnancy (months)	61.6 ± 1.3	61.6 ± 1.4	61.8 ± 1.6	0.9
BMI (kg/m^2)	26.4 ± 6.0	32.2 ± 8.9	26.9 ± 5.0	0.17
Average SBP (mmHg)	109.4 ± 9.8	118.7 ± 13.1	113.1 ± 8.1	0.14
Average DBP (mmHg)	71.7 ± 9.1	76.3 ± 9.8	74.9 ± 7.9	0.41
Glucose (mmol/L)	4.7 ± 0.6	4.6 ± 0.4	4.5 ± 0.4	0.58
Insulin (mU/L)	8.7 ± 5.8	13.1 ± 10.2	12.7 ± 11.0	0.33
HOMA-IR	1.8 ± 1.2	2.7 ± 2.1	2.7 ± 2.5	0.35
HbA1c (%)	5.2 ± 0.3	5.3 ± 0.2	5.2 ± 0.3	0.8
eGFR (mL/min)	98.7 ± 4.4	98.0 ± 4.5	96.8 ± 6.0	0.6
Cholesterol (mmol/L)	4.7 ± 0.7	4.9 ± 0.5	4.6 ± 0.9	0.67
Triglycerides (mmol/L)	1.0 ± 0.7	1.1 ± 0.3	1.0 ± 0.6	0.94
HDL (mmol/L)	1.5 ± 0.3	1.4 ± 0.3	1.6 ± 0.4	0.74

LDL (mmol/L)	2.8 ± 0.6			3.0 ± 0.6			2.6 ± 0.7			0.42
Smoking %	Yes (0%)	No (76%)	Ex (23%)	Yes (0%)	No (80%)	Ex (20%)	Yes (0%)	No (67%)	Ex (33%)	0.8

Data presented as mean ± SD; Ordinary one-way ANOVA.
SBP – systolic blood pressure
DBP – diastolic blood pressure

Our quantitative label-free proteomic analysis of non-depleted pooled plasma samples was conducted by measuring the relative abundance of tryptic peptides using DDA mass spectrometry [5, 24]. This detected 573 proteins across the grouped samples with minimal percentage of missing values. Heterogeneity of grouped plasma samples was demonstrated through the hierarchical clustering of sample triplicates in the multigroup heat map and principal component analysis (PCA) plot (**Figure 6A**).

Subsequently, differential abundance (DE) analysis was performed by three individual comparisons, PE versus control, GH versus control group and PE versus GH. Post DE analysis, 20 unique proteins were identified in at least one of the group comparisons with some proteins being significant in multiple comparisons. Across groups, 8 proteins were differentially abundant in PE versus control group, 6 proteins in GH versus control group and 15 proteins in PE versus GH (Table 2).

Table 2. Multiple group comparison for differential expression of plasma proteins.

Protein	Adj. p-value	Ratio
Preeclampsia versus control		
BRIP1 (BRCA1 interacting helicase 1)	0.046	2.64
CUL2 (Cullin-2)	5.11E-08	2.21
HbA2 (Hemoglobin A2)	0.039	1.28
MYCBPAP (MYCBP Associated Protein)	8.95E-11	-3.23
IGKV1D-33 (Immunoglobulin kappa variable 1D-33)	0.00258	-0.934
PPIP5K2 (Diphosphoinositol Pentakisphosphate Kinase 2)	0.003	1.66
PZP (Pregnancy zone protein)	3.87E-06	1.31
VIRMA (Vir Like M6A Methyltransferase Associated)	0.0001	-1.16
Gestational hypertension versus control		
ABR (ABR Activator Of RhoGEF And GTPase)	0.042	-2.52
DNMT1_fragment (DNA-methyltransferase 1)	0.004	-1.01
HbA2 (Hemoglobin A2)	0.002	1.49

IGKV3-7 (Immunoglobulin Kappa Variable 3-7 (Non-Functional))	0.007	1.06
IGLV1-36 (Immunoglobulin Lambda Variable 1-36)	0.0498	2.05
PIK3CA (phosphatidylinositol-4,5-bisphosphate 3-kinase catalytic subunit alpha)	0.0069	-0.871
Preeclampsia versus gestational hypertension		
BMP10 (Bone morphogenetic protein 10)	0.001	-2.44
CNOT3 (CCR4-NOT Transcription Complex Subunit 3)	3.07E-06	1.08
CUL2 (Cullin-2)	2.81E-14	2.66
CYBA (Cytochrome B-245 Alpha Chain)	0.047	-1.26
DNMT1_fragment (DNA-methyltransferase 1)	0.004	0.961
ERCC3 (ERCC excision repair 3, TFIIH core complex helicase subunit)	0.009	-1.54
HADH (Hydroxyacyl-CoA Dehydrogenase)	0.020	-1.09
IGKV1D-33 (Immunoglobulin Kappa Variable 1D-33)	3.40E-07	-1.22
IKZF1 (IKAROS Family Zinc Finger 1)	0.004	-1.85
KLK4 (Kallikrein Related Peptidase 4)	0.0001	-1.34
MYCBPAP (MYCBP Associated Protein)	2.81E-14	-3.3
PIK3CA (phosphatidylinositol-4,5-bisphosphate 3-kinase catalytic subunit alpha)	8.22E-05	1.1
PPIP5K2 (Diphosphoinositol Pentakisphosphate Kinase 2)	0.008	1.29
PZP (Pregnancy zone protein)	2.81E-14	1.94
VIRMA (Vir Like M6A Methyltransferase Associated)	1.15E-05	-1.13

DE analysis accentuated the distinct proteomes profiles of both PE or GH versus control (**Figure 6B**). There was only 1 overlapping DE protein, haemoglobin A2 (HBA2), which was increased in both PE (p=0.039, ratio = 1.28) and GH (p =0.0023, ratio = 1.49), compared to control plasma.

BRCA1 interacting helicase 1 (BRIP1) (p=0.046, ratio=2.64) and diphosphoinositol pentakisphosphate kinase 2 (PPIP5K2) (p=0.003, ratio=1.66) were increased in PE compared to control plasma, suggesting a reduction in cellular ability to maintain genetic integrity and cellular homeostasis [26, 27]. An increase in pregnancy zone protein (PZP) (p=3.87E-06, ratio=1.31), an immune cell placenta-specific protein critical for successful pregnancy [28], was also observed in PE compared to control group (**Figure 6C**).

ABR (ABR activator of RhoGEF and GTPase) was decreased in GH compared to control plasma (p=0.043, ratio=-2.52), supporting increased regulated cell death signalling. Phosphatidylinositol-4,5-bisphosphate 3-kinase catalytic subunit alpha (PIK3CA) (p=0.007,

ratio=-0.871) and DNA-methyltransferase 1 (DNMT1) fragments (p = 0.004, ratio =-1.01) were both decreased in GH compared to control group (**Figure 6D**).

The distinction between PE and GH proteomic profiles included 15 DE proteins (**Figure 6E**). Cytochrome B-245 alpha chain (CYBA) (p=0.047, ratio=-1.26), immunoglobulin kappa variable 1 D-33 (IGKV1D-33) (p=3.40E-07, ratio=-1.22) and IKAROS family zinc finger 1 (IKZF1) (p = 0.004, ratio =-1.85) abundance was decreased in PE versus GH plasma, supporting a lower immune response [29]. Conversely, homeostatic proteins were increased in PE plasma, specifically phosphatidylinositol-4,5-bisphosphate 3-kinase catalytic subunit alpha (PIK3CA) (p=8.22E-05, ratio=1.1) and diphosphoinositol pentakisphosphate kinase 2 (PPIP5K2) (p=0.00823, ratio=1.29), compared to GH. Another pronounced variation concerning PE versus GH was the abundance of proteins associated with the maintenance of cellular genetic material. PE plasma presented increases CCR4-NOT transcription complex subunit 3 (CNOT3) (p=3.07E-06, ratio=1.08) and DNA-methyltransferase 1 (DNMT1 fragment) (p=0.00387, ratio=0.961).

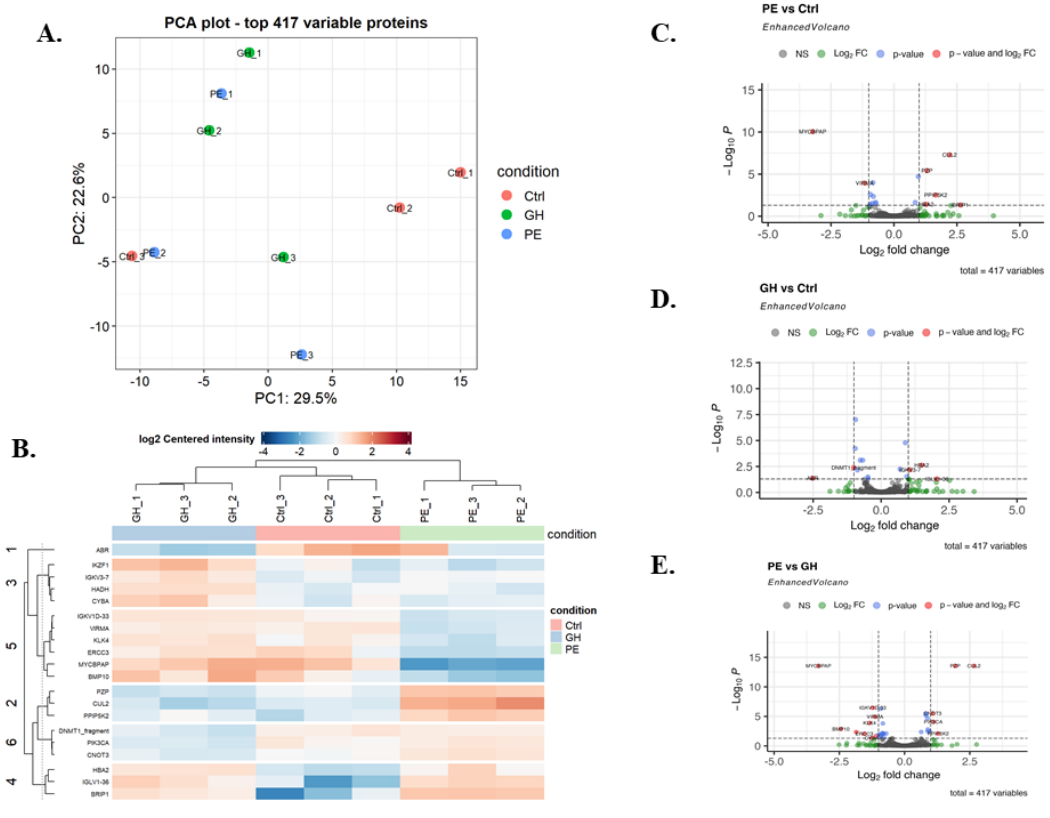

pp

Figure 6. Differential expression analysis of grouped patient plasma for untargeted proteomics analysis. Grouped samples were measures in triplicates to account for anomalies. A) Principal component analysis (PCA) plot of grouped proteomic data for control, GH and

PE. B) Multigroup heatmap with hierarchical clustering dendrogram of proteomic data levels across control, gestational hypertension and preeclampsia groups. Volcano plots of proteomic data for C) PE vs normotensive D) GH versus normotensive E) PE vs GH. Significant proteins were defined as Benjamini–Hochberg adjusted p-value < 0.05.

Discussion

HDP, including GH and PE, are the leading causes of mortality and morbidity in pregnancy and are associated with increased risk of developing CVD post-partum [30]. The mechanisms of this association remain unclear, leading to the lack of effective monitoring and treatment strategies for women post-HDP. In this study, we developed and characterised 3D *in vitro* GH- and PE-relevant cardiac platform to study, for the first time, cellular and molecular mechanisms of HDP, five years post-partum, and identify early cardiac changes. We also performed a comprehensive proteomic analysis to identify potential biomarkers or therapeutic targets in the secretome that could be responsible for these early signs of cardiovascular dysfunction.

Although there were no observable clinical differences in cardiovascular and metabolic profile between the three groups as demonstrated in Table 1, our findings revealed that after four days of treatment with GH plasma, there was a decrease in the overall proportion of live cells, whereas PE did not impact cell viability. This aligned with our plasma proteome profile, indicating decreased abundance of ABR, a regulator of cell death signalling [29], in GH plasma. Consequently, ABR might have implications in the advancement of CVD in GH, akin to the findings in hypertensive patients, increasing the risk of stroke and heart failure [29, 31]. Additionally, the proteomic analysis of GH revealed a notable decrease in PIK3CA abundance, a crucial component of AKT-mediated cell survival, and DNMT1, regulating cardiomyocyte gene expression, morphology, and function. The decrease in protein abundance of both PIK3CA and DNMT1 are closely linked to cell death and survival, cell morphology, and cardiac function. A reduction in abundance of these proteins could be potentially responsible for contractile dysfunction and arrhythmia [32, 33]. Overexpression of α-SMA protein is commonly observed in early stages of cardiac fibrosis, highly expressed in myofibroblasts, leading to increased collagen deposition and reduction of contractility of the heart, through attenuated fibroblast proliferative activity [34]. Our results align with this, as we measured an increased abundance of α-SMA in CS treated with GH-derived plasma, supporting early indications of cardiac remodelling and fibrosis in individuals five year post-GH [35]. This new insight into the mechanisms of early cardiac dysfunction post-partum associated with GH

identified potential therapeutic targets that could attenuate early adverse cardiac remodelling and increased cell death signalling, potentially preventing or delaying the onset of future heart failure.

Furthermore, we demonstrated an increase in HbA2 in both GH and PE patient's plasma. This correlates with a significant rise in contraction frequency in GH and PE CS and fractional shortening in PE CS. Previous work has shown that HbA2 is positively associated with blood pressure, and although there was no difference in blood pressure between HDP groups and healthy controls, this could indicate likely early cardiac alterations five years post-partum that could lead to hypertension in the future [36]. In contrast to normotensive patients, PE plasma presented an increase in BRIP1 expression, which is linked to genetic instability and commonly observed in women with cervical or breast cancer and postmenopausal CVD. PPIP5K2 was also increased, which could disrupt cardiac cell growth and proliferation [37]. Moreover, our analyses support an increased risk of arterial stiffness post-PE, as indicated by abnormal PZP expression, an emerging biomarker for cardiovascular risk as identified in chronic kidney disease patients [38]. This suggests that individuals five years post-PE may exhibit vascular and endothelial dysfunction indicative of early stages of CVD. The distinction between HDP plasma groups lies in dysregulated immune response observed in preeclampsia, as supported by the measured increase in Gal-3 abundance in PE CS, and a reduction in CYBA, IGKV1D-33, and IKZF1 in plasma samples. Increase in pro-inflammatory Gal-3 is linked to cardiac fibrosis and impaired angiogenesis, contributing to cardiac remodelling [39]. In our study, there are no changes in FKBPL, this could be due to the nature of the plasma, which was isolated five years after the PE-affected pregnancy, and in individuals without clinically diagnosed CVD. It is also possible that no obvious changes were evident in angiogenesis in these individuals five-years post-HDP, given no differences were demonstrated in the expression of endothelial cell marker, CD31, or vascular dysfunction marker, VE-cadherin.

The findings of this study offer a novel tissue engineering platform to better understand the mechanisms of early cardiac changes regulating HDP-associated CVD post-partum, with the potential to be used to screen for novel biomarkers and therapeutic targets, and develop personalised treatment and monitoring options for those individuals at high-risk of CVD including post-HDP. Future studies could include longer term treatment of CS to identify kinetics of disease progression, as well the use of agonists and antagonists of the proteins identified as potential therapeutic targets such as αSMA and Gal-3 for the development of

better treatments to prevent CVD as a consequence of HDP. Post-partum care following HDP is poorly understood and adequate clinical management is lacking thus this is a high-priority area where further research is needed to fill in the knowledge gaps and address unmet clinical need that will improve clinical management in this high-risk population. Our findings provide a number of promising candidates as biomarkers or therapeutic targets that should be explored further and facilitate the development of proactive monitoring and intervention strategies for women post-HDP. Another strategy may include longitudinal studies tracking women who experienced HDP over extended periods (beyond five years). By pursuing these research directions, we could significantly improve the prevention, early detection, and management of CVD in women post-HDP.

Conclusions

This study established an innovative 3D *in vitro* model of CVD post-HDP to unveiled novel mechanistic insights into the impact of HDP secretome five years after childbirth on the heart, which is implicated in escalating the risk of long-term CVD. Our platform was able to detect early signs of cardiac dysfunction at the cellular and molecular levels despite the fact that clinically cardiovascular and metabolic profile of these individuals appeared healthy. We showed that GH and PE trigger distinct mechanistic pathways that can lead to cardiac damage and CVD. GH activates mechanisms related to homeostasis, cell death signaling, and malfunction of cardiomyocyte contractility. In contrast, PE leads to dysfunctional inflammatory pathways and exhibits heightened protein expression of markers associated with endothelial dysfunction. Understanding the underlying cellular and molecular processes could provide valuable insights into targeted therapeutic approaches for each condition and potentially pave the way for implementation of personalized treatments for preventing and treating early-stage CVD following HDP.

Acknowledgements: We thank the participants and staff of the P4 study for donating their blood and helping us with the recruitment, respectively. We also thank Dr Amy Bottomley from the Microbial Imaging Facility for their help with imaging and image analyses.

References

[1] M.A. Brown, L.A. Magee, L.C. Kenny, S.A. Karumanchi, F.P. McCarthy, S. Saito, D.R. Hall, C.E. Warren, G. Adoyi, S. Ishaku, Hypertensive disorders of pregnancy: ISSHP classification, diagnosis, and management recommendations for international practice, Hypertension 72(1) (2018) 24-43.
[2] L.C. Chappell, C.A. Cluver, S. Tong, Pre-eclampsia, The Lancet 398(10297) (2021) 341-354.
[3] B. Buddeberg, R. Sharma, J. O'Driscoll, A.K. Agten, A. Khalil, B. Thilaganathan, Cardiac maladaptation in term pregnancies with preeclampsia, Pregnancy hypertension 13 (2018) 198-203.
[4] C. Arnott, M. Nelson, M.A. Ramirez, J. Hyett, M. Gale, A. Henry, D.S. Celermajer, L. Taylor, M. Woodward, Maternal cardiovascular risk after hypertensive disorder of pregnancy, Heart 106(24) (2020) 1927-1933.
[5] H. Chen, M. Chhor, B.S. Rayner, K. McGrath, L. McClements, Evaluation of the diagnostic accuracy of current biomarkers in heart failure with preserved ejection fraction: A systematic review and meta-analysis, Archives of Cardiovascular Diseases 114(12) (2021) 793-804.
[6] S.M. Ghorbanpour, C. Richards, D. Pienaar, K. Sesperez, H. Aboulkheyr Es, V.N. Nikolic, N. Karadzov Orlic, Z. Mikovic, M. Stefanovic, Z. Cakic, A. Alqudah, L. Cole, C. Gorrie, K. McGrath, M.M. Kavurma, M. Ebrahimi Warkiani, L. McClements, A placenta-on-a-chip model to determine the regulation of FKBPL and galectin-3 in preeclampsia, Cellular and Molecular Life Sciences 80(2) (2023) 44.
[7] L. Li, Q. Zhao, W. Kong, Extracellular matrix remodeling and cardiac fibrosis, Matrix biology 68 (2018) 490-506.
[8] J. Ding, Z. Li, L. Li, Y. Ding, D. Wang, S. Meng, Q. Zhou, S. Gui, W. Wei, H. Zhu, Myosin light chain kinase inhibitor ML7 improves vascular endothelial dysfunction and permeability via the mitogen-activated protein kinase pathway in a rabbit model of atherosclerosis, Biomedicine & Pharmacotherapy 128 (2020) 110258.
[9] Y.H. Chan, H.H. Harith, D.A. Israf, C.L. Tham, Differential regulation of LPS-mediated VE-cadherin disruption in human endothelial cells and the underlying signaling pathways: a mini review, Frontiers in cell and developmental biology 7 (2020) 280.
[10] S. Masoumeh Ghorbanpour, S. Wen, T.u.J. Kaitu'u-Lino, N.J. Hannan, D. Jin, L. McClements, Quantitative Point of Care Tests for Timely Diagnosis of Early-Onset Preeclampsia with High Sensitivity and Specificity, Angewandte Chemie International Edition 62(26) (2023) e202301193.
[11] N. Todd, R. McNally, A. Alqudah, D. Jerotic, S. Suvakov, D. Obradovic, D. Hoch, J.R. Hombrebueno, G.L. Campos, C.J. Watson, M. Gojnic-Dugalic, T.P. Simic, A. Krasnodembskaya, G. Desoye, K.-A. Eastwood, A.J. Hunter, V.A. Holmes, D.R. McCance, I.S. Young, D.J. Grieve, L.C. Kenny, V.D. Garovic, T. Robson, L. McClements, Role of A Novel Angiogenesis FKBPL-CD44 Pathway in Preeclampsia Risk Stratification and Mesenchymal Stem Cell Treatment, The Journal of Clinical Endocrinology & Metabolism 106(1) (2020) 26-41.
[12] A.S. Januszewski, C.J. Watson, V. O'Neill, K. McDonald, M. Ledwidge, T. Robson, A.J. Jenkins, A.C. Keech, L. McClements, FKBPL is associated with metabolic parameters and is a novel determinant of cardiovascular disease, Sci Rep 10(1) (2020) 21655.
[13] R. de Oliveira Camargo, B. Abual'anaz, S.G. Rattan, K.L. Filomeno, I.M. Dixon, Novel factors that activate and deactivate cardiac fibroblasts: A new perspective for treatment of cardiac fibrosis, Wound Repair and Regeneration 29(4) (2021) 667-677.
[14] L. Zeng, C. Liao, Multivariate logistic regression analysis of preeclampsia in patients with pregnancy induced hypertension and the risk predictive value of monitoring platelet, coagulation function and thyroid hormone in pregnant women, American Journal of Translational Research 14(9) (2022) 6805.
[15] C. Liu Chung Ming, K. Sesperez, E. Ben-Sefer, D. Arpon, K. McGrath, L. McClements, C. Gentile, Considerations to Model Heart Disease in Women with Preeclampsia and Cardiovascular Disease, Cells 10(4) (2021) 899.
[16] L. Polonchuk, M. Chabria, L. Badi, J.-C. Hoflack, G. Figtree, M.J. Davies, C. Gentile, Cardiac spheroids as promising in vitro models to study the human heart microenvironment, Scientific reports 7(1) (2017) 1-12.

[17] G.A. Figtree, K.J. Bubb, O. Tang, E. Kizana, C. Gentile, Vascularized cardiac spheroids as novel 3D in vitro models to study cardiac fibrosis, Cells Tissues Organs 204(3-4) (2017) 191-198.
[18] P. Sharma, X. Wang, C.L.C. Ming, L. Vettori, G. Figtree, A. Boyle, C. Gentile, Considerations for the Bioengineering of Advanced Cardiac In Vitro Models of Myocardial Infarction, Small 17(15) (2021) 2003765.
[19] P. Sharma, C.L.C. Ming, X. Wang, L.A. Bienvenu, D. Beck, G.A. Figtree, A. Boyle, C. Gentile, Biofabrication of advanced in vitro 3D models to study ischaemic and doxorubicin-induced myocardial damage, Biofabrication (2022).
[20] C. Richards, K. Sesperez, M. Chhor, S. Ghorbanpour, C. Rennie, C.L.C. Ming, C. Evenhuis, V. Nikolic, N.K. Orlic, Z. Mikovic, M. Stefanovic, Z. Cakic, K. McGrath, C. Gentile, K. Bubb, L. McClements, Characterisation of cardiac health in the reduced uterine perfusion pressure model and a 3D cardiac spheroid model, of preeclampsia, Biol Sex Differ 12(1) (2021) 31.
[21] G.K. Davis, L. Roberts, G. Mangos, A. Henry, F. Pettit, A. O'Sullivan, C.S.E. Homer, M. Craig, S.B. Harvey, M.A. Brown, Postpartum physiology, psychology and paediatric follow up study (P4 Study) – Study protocol, Pregnancy Hypertension: An International Journal of Women's Cardiovascular Health 6(4) (2016) 374-379.
[22] NIS-Elements, Nikon introduces Clarify.ai for NIS-Elements, an artificial intelligence algorithm for removing blur from widefield microscope images, in: N.N.I. In (Ed.) NIS-Elements, 2023.
[23] U. Distler, J. Kuharev, P. Navarro, S. Tenzer, Label-free quantification in ion mobility-enhanced data-independent acquisition proteomics, Nat Protoc 11(4) (2016) 795-812.
[24] H. Chen, I. Aneman, V. Nikolic, N. Karadzov Orlic, Z. Mikovic, M. Stefanovic, Z. Cakic, H. Jovanovic, S.E.L. Town, M.P. Padula, L. McClements, Maternal plasma proteome profiling of biomarkers and pathogenic mechanisms of early-onset and late-onset preeclampsia, Scientific Reports 12(1) (2022) 19099.
[25] O.M. Andrejic, R.M. Vucic, M. Pavlovic, L. McClements, D. Stokanovic, T. Jevtovic–Stoimenov, V.N. Nikolic, Association between Galectin-3 levels within central and peripheral venous blood, and adverse left ventricular remodelling after first acute myocardial infarction, Scientific Reports 9(1) (2019) 13145.
[26] X.D. Ma, G.Q. Cai, W. Zou, Y.H. Huang, J.R. Zhang, D.T. Wang, B.L. Chen, First evidence for the contribution of the genetic variations of BRCA1-interacting protein 1 (BRIP1) to the genetic susceptibility of cervical cancer, Gene 524(2) (2013) 208-213.
[27] P. Denorme, M.-A. Morren, S. Hollants, M. Spaepen, K. Suaer, N. Zutterman, V. Labarque, E. Legius, H. Brems, Phosphatidylinositol-4,5-bisphosphate 3-kinase catalytic subunit alpha (PIK3CA)-related overgrowth spectrum: A brief report, Pediatric Dermatology 35(3) (2018) e186-e188.
[28] J.H. Cater, J.R. Kumita, R. Zeineddine Abdallah, G. Zhao, A. Bernardo-Gancedo, A. Henry, W. Winata, M. Chi, B.S. Grenyer, M.L. Townsend, Human pregnancy zone protein stabilizes misfolded proteins including preeclampsia-and Alzheimer's-associated amyloid beta peptide, Proceedings of the National Academy of Sciences 116(13) (2019) 6101-6110.
[29] R.A. Dee, K.D. Mangum, X. Bai, C.P. Mack, J.M. Taylor, Druggable targets in the Rho pathway and their promise for therapeutic control of blood pressure, Pharmacology & therapeutics 193 (2019) 121-134.
[30] T.K.J. Groenhof, B.B. van Rijn, A. Franx, J.E. Roeters van Lennep, M.L. Bots, A.T. Lely, Preventing cardiovascular disease after hypertensive disorders of pregnancy: Searching for the how and when, European Journal of Preventive Cardiology 24(16) (2017) 1735-1745.
[31] C. Cario-Toumaniantz, D. Ferland-McCollough, G. Chadeuf, G. Toumaniantz, M. Rodriguez, J.-P. Galizzi, B. Lockhart, A. Bril, E. Scalbert, G. Loirand, RhoA guanine exchange factor expression profile in arteries: evidence for a Rho kinase-dependent negative feedback in angiotensin II-dependent hypertension, American Journal of Physiology-Cell Physiology 302(9) (2012) C1394-C1404.
[32] X. Fang, R. Poulsen, L. Zhao, J. Wang, S.A. Rivkees, C.C. Wendler, Knockdown of DNA methyltransferase 1 reduces DNA methylation and alters expression patterns of cardiac genes in embryonic cardiomyocytes, FEBS Open Bio 11(8) (2021) 2364-2382.

[33] A. Ghigo, M. Laffargue, M. Li, E. Hirsch, PI3K and Calcium Signaling in Cardiovascular Disease, Circulation Research 121(3) (2017) 282-292.
[34] A.V. Shinde, C. Humeres, N.G. Frangogiannis, The role of α-smooth muscle actin in fibroblast-mediated matrix contraction and remodeling, Biochim Biophys Acta Mol Basis Dis 1863(1) (2017) 298-309.
[35] J. Wang, W. Huang, R. Xu, Y. Nie, X. Cao, J. Meng, X. Xu, S. Hu, Z. Zheng, MicroRNA-24 regulates cardiac fibrosis after myocardial infarction, Journal of Cellular and Molecular Medicine 16(9) (2012) 2150-2160.
[36] A. Nguweneza, C. Oosterwyk, K. Banda, V. Nembaware, G. Mazandu, A.P. Kengne, A. Wonkam, Factors associated with blood pressure variation in sickle cell disease patients: a systematic review and meta-analyses, Expert Review of Hematology 15(4) (2022) 359-368.
[37] Y. Wang, W. Xie, M. Hou, J. Tian, X. Zhang, Q. Ren, Y. Huang, J. Chen, Calycosin stimulates the proliferation of endothelial cells, but not breast cancer cells, via a feedback loop involving RP11-65M17.3, BRIP1 and ERα, Aging (Albany NY) 13(8) (2021) 11026-11042.
[38] W.L. Chen, W.T. Liao, C.N. Hsu, Y.L. Tain, Pregnancy Zone Protein as an Emerging Biomarker for Cardiovascular Risk in Pediatric Chronic Kidney Disease, J Clin Med 12(18) (2023).
[39] V. Blanda, U.M. Bracale, M.D. Di Taranto, G. Fortunato, Galectin-3 in Cardiovascular Diseases, International Journal of Molecular Sciences 21(23) (2020) 9232.

2.4 Closing Remarks for Part 2

The objective of Part 2 was to establish our *in vitro* CSs as a CVD model that could replicate human heart myocardial damage. We have demonstrated that our bioengineered CSs could be used as a disease model, a toxicity model, and a patient-tailored model.

As existing models are limited to fully recapitulate the complex scenario of human heart pathophysiology. In **Chapter 2.2**, we established I/R and DOX-induced myocardial damage using CSs and our findings are consistent to previous *in vivo* and *ex vivo* studies. Our findings demonstrated that our I/R *in vitro* models recapitulated features typical of the human heart in terms of cell composition and pathophysiological O_2 concentrations. Foremost, our results indicated that contractile dysfunction occurred through a reduction of contraction frequency and fractional shortening in human cardiomyocytes. Similar to previous studies, we also demonstrated that I/R and DOX-induced models have similar gene expression as *in vivo* models, such as an increase in cell death, including apoptosis and necrosis, contractile dysfunction and changes of sarcomeric and cardiac remodeling genes. Furthermore, our models recapitulated more clinically relevant aspects of those cardiac dysfunction events.

The innovation of this study lies in its development of an advanced 3D *in vitro* bioengineered CS model, which could simulate human heart pathophysiologies. However, the limitation of this study is that our model has an intrinsic static nature and, hence, may not fully capture the complexity of whole-organ responses compared to *in vivo* models. Moreover, our models still lack important features to study inflammation and platelet clotting and to elucidate pharmacokinetic and pharmacodynamic effects, which could further bridge the gap between *in vitro* and *in vivo* models. Future directions for this study involve the use of microfluidic devices and the addition of other cells present in the heart.

We also demonstrated in **Chapter 2.3** that *in vitro* bioengineered CSs could mimic the early stages of human cardiac pathophysiology using patients-derived plasma. It unveils a previously uncharted link between HDP and CVD, a connection unexplored due to the absence of suitable model systems. Our findings demonstrated that CS could be used as a platform to detect early changes and mechanisms of CVD-derived five years post-partum. We also demonstrated that GH and PE trigger distinct mechanistic pathways that can lead to cardiac damage and CVD. GH led to a decrease in cell viability and activated mechanisms related to homeostasis, and cell death signaling. While PE led to dysfunctional inflammatory pathways and exhibited heightened protein expression of markers associated with endothelial dysfunction and

malfunction in cardiomyocyte contractility. Future work should investigate the long-term effects of GH and PE on cardiac health and explore potential therapeutic interventions.

The innovation of this study lies in the use of an advanced 3D *in vitro* bioengineered CS model as a patient-specific model. However, there are limitations to consider, such as the need for more extensive validation in diverse patient populations and the complexity of translating findings from the CS model to clinical practice. Future directions for this research include refining the CS model to further enhance its predictive accuracy and expanding its application to a broader range of cardiac conditions.

Overall, **Chapter 2** provides an overview of the applications of bioengineered heart CSs using advanced *in vitro* models.

CHAPTER 3 – ACETYLCHOLINE PROTECTIVE ROLE AGAINST MYOCARDIAL DAMAGE

3.1 Introduction and Relevance

ACh has crucial cardioprotective roles against myocardial damage; however, it has been poorly translated to clinical studies due to delivery challenges and the complexity of ACh in the human body. My goal in this thesis is to evaluate the protective role of ACh using our advanced *in vitro* I/R and DOX-induced myocardial damage CS models (**Chapter 2.2**). This chapter aims to evaluate our hypothesis that ACh protects against myocardial damage, **Chapter 3.2** solves Aim 2 and **Chapter 3.3** solves Aim 3:

Specific-Aim 2: To evaluate the effects of ACh on I/R-induced myocardial damage CSs, and MI in a murine model.

Sub aims

2.1: To evaluate the protective effect of ACh against I/R-induced CSs.

2.2: To evaluate the protective effect of cholinergic nerve cells (CNs) producing ACh against I/R-induced CSs.

2.3: To evaluate the protective effect of ACh-loaded nanoparticles (ACh-NPs) against I/R-induced CSs.

2.4: To evaluate the protective effect of ACh-NPs on a MI murine model.

Specific-Aim 3: To evaluate the effects of ACh on DOX-induced CSs and *ex vivo* human heart biopsies.

Sub aims

3.1: To evaluate the protective effect of ACh against DOX-induced CSs.

3.2: To evaluate the protective effect of ACh-derived CNs against DOX-induced CSs.

3.3: To evaluate the protective effect of ACh-NPs against DOX-induced CSs.

3.4: To evaluate the protective effect of ACh on *ex vivo* human heart biopsies.

This chapter looked at three ACh delivery techniques, which are 1) the addition of free-dissolved ACh to CSs and 2) co-culturing of ACh-producing CNs with CSs. Given that ACh hydrolyses rapidly and the limitations of current approaches to increasing ACh levels (Kröger et al., 2015, Zafeiropoulos et al., 2023). Our multidisciplinary team developed a

novel ACh-NPs using Poly-butylcyanoacrylate (PBCA), a biodegradable and biocompatible homopolymer, to deliver ACh at low doses in the injured heart. The third method is by 3) delivering ACh-NPs to CSs. The analyses performed were:

- Toxicity assay
- Looking at cell death among the cell types
- Contractile function
- qPCR to evaluate the mRNA level changes of cardiac damage-related genes
- Spatial transcriptomics (Stereoseq)

Our findings showed that the three ACh delivery techniques attenuate I/R and DOX-induced cell death, prevent the reduction of CS contractility and prevent cardiac remodeling. For **Chapter 3.2**, we further validated the effect of ACh-NPs on a MI murine model through ultrasound imaging for up to 28 days, histology, RNA sequencing and stereoseq analyses. To reinforce our understanding of the protective role of ACh, we compared our *in vitro* I/R model to ischemic heart disease tissue samples through stereoseq analysis. Additionally, for **Chapter 3.3**, we compared our *in vitro* DOX-induced cardiotoxicity CS model to *ex vivo* DOX cardiomyopathy heart tissue sample by evaluating nitric oxide synthase level and through stereoseq analysis. However, due to delays in analyzing the stereoseq data, the chapters won't cover the stereoseq analyses, which we will publish separately when the data are finalized.

These pioneering studies add further evidence of ACh's beneficial effects in the infarcted heart and also propose innovative strategies for preventing and treating heart tissue damage following MI and exposure to cardiotoxic agents. This research heralds a new era of offering fresh perspectives on therapeutic interventions for CVD patients. For the overall thesis, **Chapter 3** aims to solve the hypothesis that ACh has a protective role against myocardial damage.

3.2 Cardioprotective Role of ACh against I/R and MI Myocardial Damage

Summary:

The manuscript is currently under review and was submitted on 19 June 2024 to the Advanced Functional Materials journal. This chapter sets the foundation for the protective role of ACh against I/R-induced CS models, optimized in **Chapter 2.2**, and against MI *in vivo* mice models. The study aimed to evaluate Aim 2, that ACh has protective effects against I/R and MI myocardial damage. Due to the variability of existing approaches, the protective effects of ACh remain unexplored in CVD patients. Hence, it is imperative to find a new therapeutic approach to increase the ACh level at a dose that targets only the infarcted area. Firstly, we evaluated the effect of ACh against I/R myocardial damage using three ACh delivery methods which are 1) the addition of free-dissolved 100μM ACh to CSs, 2) co-culturing of ACh-producing CNs with CSs and 3) delivering ACh-NPs to CSs. The results showed that the three ACh delivery methods attenuated I/R-induced cell death and restored contractile function, which was consistent with previous studies.

We also provided new insights on the administration of ACh before inducing I/R injury in CS, which reduced I/R-induced fibrosis production and attenuated contractile dysfunction. While the addition of a low dose of free-dissolved ACh has cardioprotective in I/R-induced cardiac cells, untargeted administration of ACh in patients may not be safe and raises concerns. Our second method was to co-culture healthy ACh-derived CNs in CSs and then induce I/R injury. Given the strong effects exerted by CNs against I/R injury, we further confirm the importance of the optimal delivery method for ACh.

Our multidisciplinary team developed a novel ACh-NPs, which we successfully demonstrated has protective effects against acute I/R injury in CSs and chronic MI in a murine model. While most nanotechnology research focuses on the efficacy and durability of the drug-nanoparticles. We showed for the first time that our nanoparticles (NPs) successfully delivered the drugs *in vitro* and *in vivo* by comparing them to the PBCA-NPs (without ACh). Our findings indicated that PBCA-NPs have no protective effect against myocardial damage as well as have no toxicity effects in our models.

More importantly, our *in vitro* findings showed that ACh-NPs protected against I/R-induced cell death for endothelial cells and fibroblasts, as well as prevented contractile dysfunction. Our *in vivo* findings demonstrated that ACh-NPs prevented the reduction in left ventricle ejection fraction and the increase in collagen deposition post-MI. Moreover, our RNA sequencing findings showed that ACh-NPs reduce the abundance of ROS, inhibit apoptosis

pathways and increase cell cycle and proliferation post-MI. These striking findings suggest that delivering the drug at a low dose in the myocardium may have significant protective effects against myocardial damage.

Overall, this paper identified the protective effect of ACh against acute and chronic myocardial damage, supporting the hypothesis and adding a significant advancement in our understanding of the protective role of ACh against myocardial damage. We also provided insights into why ACh-NPs have protective effects post-MI and I/R injury, which could be a promising therapeutic approach in treating CVD patients. However, additional preclinical studies are needed to evaluate the proper dosage of ACh-NPs delivery and to translate our findings from the bench to the bedside.

WILEY-VCH

Acetylcholine-loaded nanoparticles protect against myocardial injury in *in vitro* cardiac spheroids and in an *in vivo* myocardial infarction murine model

Clara Liu Chung Ming[1,2], *Runali Patil*[3,4], *Laura Vettori*[1,2], *Timothy A. Couttas*[5], *Dominik Beck*[1], *Xiaowei Wang*[3,6,7,*], *Carmine Gentile*[1,2,*].

1. School of Biomedical Engineering, Faculty of Engineering and Information Technology, University of Technology Sydney, Sydney, NSW, Australia.
2. Cardiovascular Regeneration Group, Heart Research Institute, Newtown, NSW 2042, Australia.
3. Molecular Imaging and Theranostics Laboratory, Baker Heart and Diabetes Institute, Melbourne, VIC 3004, Australia.
4. IIT-Bombay Monash Research Academy, IIT Bombay, Powai, Mumbai, Maharashtra 400076, India
5. Brain and Mind Centre, Faculty of Medicine and Health, University of Sydney, Sydney, NSW, Australia.
6. Department of Medicine, Monash University, Melbourne, VIC 3800, Australia.
7. Department of Cardiometabolic Health, University of Melbourne, Melbourne, VIC 3010, Australia.

*** Equally Contributing Corresponding authors:**

A/Prof Xiaowei Wang, email: xiaowei.wang@unimelb.edu.au

Dr Carmine Gentile, email: carmine.gentile@uts.edu.au

Keywords: Myocardial infarction; nanoparticles; acetylcholine; cardiac spheroids; *in vitro* disease modeling.

Abstract

Acetylcholine (ACh) is cardioprotective and attenuates the damage following myocardial infarction (MI) and ischemic-reperfusion (I/R) injury. However, side effects associated with its broad activity prevent the development of new therapeutic strategies to prevent myocardial damage. This study delves into evaluating the cardioprotective effects of ACh in *in vitro* I/R cardiac spheroids (CSs) and an *in vivo* MI mouse model. Three different delivery methods to deliver ACh are explored: *i*) freely-dissolved 100μM ACh; *ii*) ACh-producing cholinergic nerves (CNs); and *iii*) ACh-loaded nanoparticles (ACh-NPs). Our analyses of cell viability and death, contractile function, and gene expression profiles through qPCR in *in vitro* I/R CSs show that increasing ACh levels improve fractional shortening % (FS%) and protect against cell death, toxicity, and gene changes associated with I/R-like conditions. Furthermore, our ultrasound imaging, histology and bulk RNAseq analyses show that ACh-NPs improve the ejection fraction % (EF%) by 20.24 +/- 2.925, prevent cardiac remodeling and improve cell survival and proliferation in MI animals. Altogether, our *in vitro* and *in vivo* results support the cardioprotective role of ACh, underscoring the potential of ACh-NPs as a therapeutic approach to target deliver ACh and prevent myocardial injury with limited broad activity.

1. Introduction

Cardiovascular disease (CVD), including myocardial infarction (MI) and its subsequent ischemia-reperfusion (I/R) injury, is the leading cause of mortality and morbidity worldwide, accounting for approximately 17.9 million fatalities annually, according to the World Health Organization. [1] MI occurs when one or more coronary arteries are obstructed, resulting in a reduced supply of oxygen and nutrients to the myocardium. [2, 3] Therapeutic interventions such as percutaneous coronary intervention (PCI) mitigate ischemic injury by reinstating perfusion; however, this reperfusion is associated with the generation of reactive oxygen species (ROS) at the occlusion site, further exacerbating cell death. [4] Given the limited regenerative capacity of the adult human heart, I/R injuries are mainly irreversible, with existing pharmacotherapies primarily slowing the progression of ischemic heart failure (HF), rather than offering a curative solution. [5, 6]

During the early phases of CVD, dysregulation of the cardiac cholinergic system leads to an autonomic imbalance, resulting in decreased acetylcholine (ACh) levels in the heart. [7, 8] Reduction in ACh impairs cardiac functionality due to its pivotal role in modulating heart rate, myocardial contractility and cardiac homeostasis. [9-11] Increasing ACh levels through vagus nerve stimulation (VNS) or cholinesterase inhibitors, including donepezil and pyridostigmine, has cardioprotective effects against MI, I/R and HF *in vitro* and *in vivo* mouse, rat, swine, rabbit and canine models. [12-17] Multiple studies showed that VNS preserved ventricular function by reducing ventricular tachycardia and fibrillation, improving left ventricular ejection fraction (LVEF) and preventing cardiomyocyte apoptosis and remodeling post-MI. [18-20] Moreover, ACh has a central role in the cholinergic anti-inflammatory pathway by inhibiting the production of inflammatory cytokines, such as tumor necrosis factor (TNF-α), interleukin (IL)-6, IL-1β and IL-18. [8, 14, 21] ACh also maintains cardiac homeostasis and decreases arrhythmia score, oxidative stress, infarct size and apoptosis. [22-25]

However, the use of VNS is notably invasive and potentially unsafe for patients and clinical trials have shown mixed results. [26] Notably, the INOVATE-HF clinical trial, which assessed the effects of VNS in 390 HF patients, found 46 complications in 37 patients within 90 days and no significant improvement in reversing remodeling or enhancing LVEF% and reducing HF-related events after 16 months. [27] Moreover, cholinesterase inhibitors are widely used for Alzheimer's disease [28] and dementia [29, 30], but their benefit-to-harm ratio also remains a concern due to significant adverse effects, including neuropsychiatric, gastrointestinal, and cardiovascular disorders. [31] Finally, high-dosage ACh injections of high dosages ranging from

20 to100µg, are also used as a diagnostic tool for inducing coronary artery spasms in coronary artery disease assessment, though some patients may experience transient adverse effects, such as bradycardia. [32] Hence, it is imperative to find a new therapeutic approach to increase ACh level at a safe dose, which targets only the infarcted area.

Nanoparticles (NPs) demonstrated a great potential for targeted drug delivery by enhancing therapeutic effects while minimizing side effects associated with systemic delivery. [33, 34] Recent studies have developed novel ACh-loaded NPs (ACh-NPs), that might improve both spatial learning and memory capability through a reduction of oxidative damage in Alzheimer's disease murine models and by decreasing cytotoxicity in cancer cells. [35, 36] In this study, we generated ACh-NPs using poly-butylcyanoacrylate (PBCA), a biodegradable and biocompatible homopolymer, which allows us to deliver ACh at low doses in the injured heart. The monomer is commonly used as a tissue adhesive due to the fast polymerization mechanism. [37, 38] PBCA-NPs have attracted considerable attention as they are easy to fabricate, have high entrapment efficiency of poorly soluble substances and are low-toxic drug carriers. [39, 40] PBCA-NPs have been adopted as a drug delivery system for cancer chemotherapy [41, 42] and through the brain-blood barrier. [43, 44] Numerous studies have demonstrated that PBCA-NPs are safe, non-toxic, stable and have the potential to treat atherosclerosis. [33, 45]

Given the broad activity of ACh following its delivery to the heart and the potential side effects associated with existing approaches, we explored for the first time whether targeted delivery of ACh using NPs could be used to safely protect against myocardial damage. In this study, we hypothesized that ACh-NPs protect against MI and I/R-induced cardiac injury in *in vitro* cardiac spheroids (CSs) and an *in vivo* murine MI model.

In vitro modeling of I/R injury in CSs (I/R CSs) offers a comparative analysis of the pathophysiology typical of *in vivo* I/R models in mice. [46] CSs are generated by co-culturing human coronary artery endothelial cells (HCAEC), human cardiac fibroblasts (HCF), and induced-pluripotent stem cell-derived cardiomyocytes (iCMs) embedded in hydrogels to mimic extracellular matrix support. [47, 48] *In vivo* modeling of MI injury following permanent ligation of the left anterior descending artery in mice recapitulates the chronic myocardial damage typical of heart failure in humans. [49, 50]

To compare results from different strategies for ACh delivery, we explored three distinct administration methodologies in *in vitro* CSs. In the first method, we used freely-suspended 100 µM ACh. The second method involved co-culturing ACh-producing IPSC-derived cholinergic nerve cells (CNs) with CSs. The third delivery method consisted of ACh-NPs. In

all delivery methods, we evaluated any changes in cell viability and death, contractile function and gene expression levels. To translate the applicability of our ACh-NPs *in vitro* findings to the *in vivo* scenario, we evaluated the cardioprotective effects of ACh-NPs in our MI mouse model over 28 days, employing ultrasound imaging, and histological and RNA-sequencing analyses.

2. Results

2.1 ACh addition protects against I/R-induced myocardial injury in CSs

To study the protective effects of ACh against I/R injury, we used our previously established *in vitro* model of I/R injury in human CSs. [51] Briefly, CSs were exposed to changes in normoxia (5% O_2), hypoxia (0% O_2) and normoxia (5% O_2) to model I/R-like conditions. Pre-treatment of I/R CSs with 100 μM ACh reduced the toxicity ratio (cell death/viability), while the addition of atropine (an ACh competitive antagonist) significantly counteracted ACh protective effects (**Figure 1A-B**). After we colocalized ethidium homodimer (cell death marker) with antibodies against markers for the three cell types in I/R CSs, 100 μM ACh significantly reduced I/R-induced death only in cardiac fibroblasts (**Figure 1E)**, while a non-statistically significant effect was also measured in cardiomyocytes (**Figure 1C)** and endothelial cells (**Figure 1D)**. The addition of atropine further increased the I/R-induced cell death in cardiomyocytes, suggesting that ACh signaling may play additional roles in cardiomyocyte survival (**Figure 1C)**.

To evaluate any protective role played by ACh on contractile function in I/R CSs, we measured any changes in contraction frequency (**Figure 1G**) and fractional shortening % (FS%) (**Figure 1H**) in CSs. Our findings showed that 100 μM ACh protected against I/R-induced reduction in FS%, which was inhibited by the addition of atropine.

To assess the molecular changes following I/R injury in CSs, we performed qPCR analyses of genes regulating cardiovascular damage (**Table 1**). The addition of 100 μM ACh significantly reduced the upregulation of myosin heavy chain 10 non-muscle (MYH10) mRNA levels in I/R CSs. Additionally, 100 μM ACh significantly increased cardiac troponin T2 (TNNT2) and ATPase sarcoplasmic/endoplasmic reticulum Ca^{2+} transporting 2 (ATP2A2) mRNA levels, which control contractile activity in cardiomyocytes. This is consistent with our results showing that 100 μM ACh improved FS % (**Figure 1H**). 100 μM ACh also attenuated I/R-induced overexpression of the retinoic acid receptor responder (RARRES1) gene, which is associated with metabolism-associated pathological changes. Moreover, 100 μM ACh significantly upregulated synuclein alpha (SNCA), a gene regulating apoptosis and impairing the autonomic

system. Our qPCR results also showed that 100 µM ACh treatment significantly decreased the expression of fibrotic genes, such as collagen type III, alpha 1 (COL3A1). Finally, 100 µM ACh increased the expression levels of adrenergic receptor alpha 1A (ADRA1A), while reducing the expression of 5A cGMP-specific phosphodiesterase (PDE5A), a HF marker.

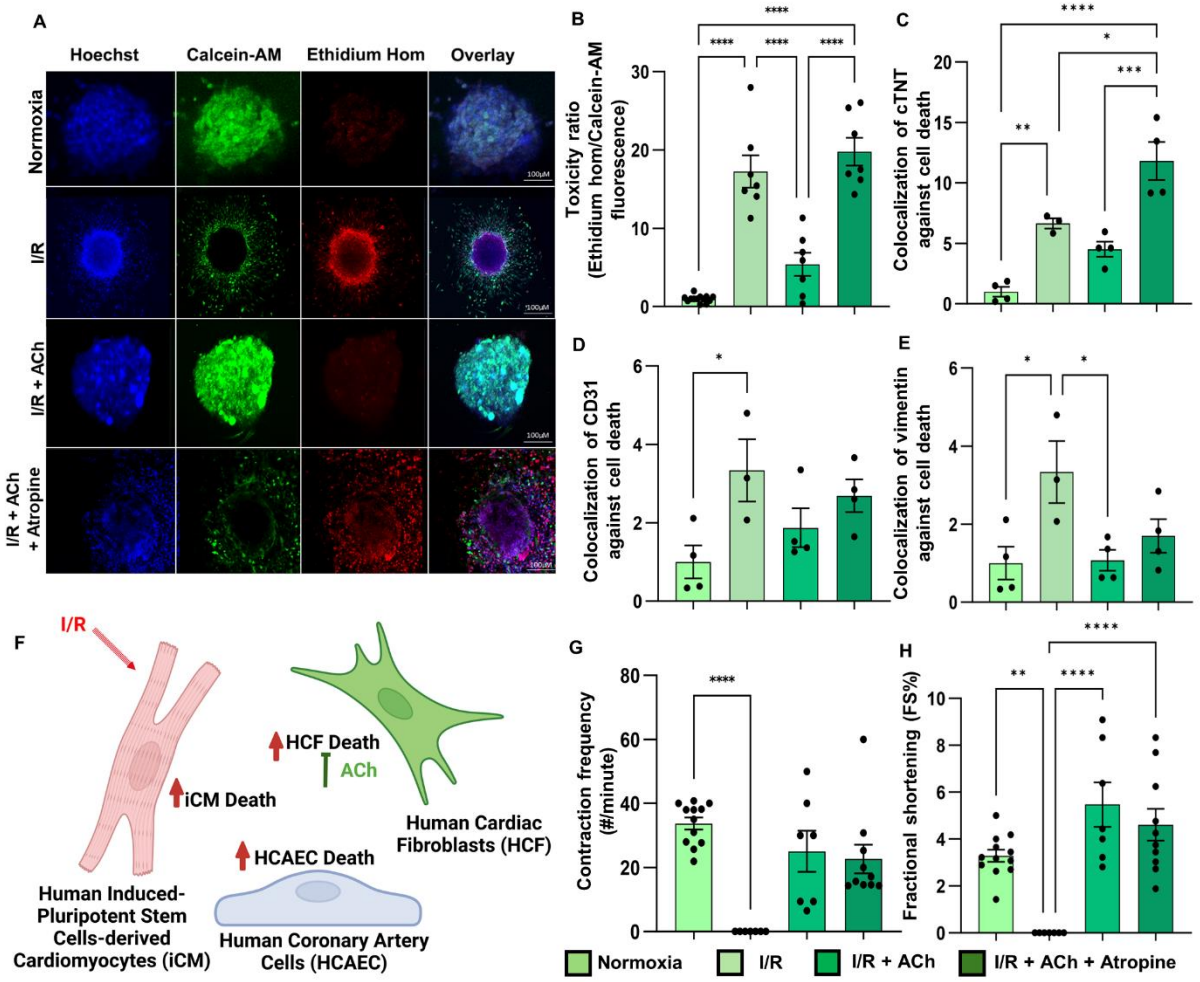

Figure 1. ACh's protective effects against I/R injury in CSs. A) Confocal microscopy stack images of CSs stained for total nuclei (blue, Hoechst), live cells (green, calcein-AM), and dead cells (red, ethidium homodimer). CSs were cultured: *i*) with normoxia (control); *ii*) in I/R conditions; *iii*) in I/R conditions plus 100µM ACh; *iv*) and in I/R conditions plus 100µM ACh and 50µM atropine. Magnification bars equal 100µm. B) Toxicity ratios (dead cells divided by live cells, normalized against media-only control CSs) (N≥7). C) Colocalization of cTNT (iCMs) and ethidium homodimer (cell death) in CSs. Individual data points and mean values are shown with error bars (normalized against media-only control CSs); N≥3. D) Colocalization of CD31 (HCAECs) against cell death (ethidium homodimer); N≥3. E) Colocalization of vimentin (HCFs) against cell death (ethidium homodimer); N≥3. F) Schematic illustration summarizing the protective role of ACh administration against I/R-induced cell death for the

three cell types (iCMs, HCAECs and HCFs). G) Fractional shortening (FS %) analyses of CSs treated as in (A) (N≥7). H) Contraction frequency analyses of CSs treated as in (A) (N≥7). B-E and G-H) Results are presented as individual points and mean ± SEM, with error bars indicating the standard error of the mean. Statistical significance is denoted as P< 0.05 = *, p<0.01 = **, p<0.001 = *** and p<0.0001 = ****, analyzed using one-way ANOVA followed by Tukey's multiple comparisons tests [normalized against control CSs, except for (G) and (H)].

Table 1. Statistically significant changes in the relative expression of genes regulating contractility, cardiac remodeling, apoptosis and signal transduction in CSs. Downregulated genes are labeled in blue, and upregulated genes are labeled in red. P-values were calculated using two-way ANOVA test with Tukey's multiple comparisons test, p<0.05 = ∗ and p < 0.0001 = ∗∗∗∗, (n = 3).

Classification of genes	Symbol	Comparing to Control		Comparing to Control	
		I/R		I/R + ACh	
		Fold Change	P-Value	Fold Change	P-Value
Contractility Genes	MYH10	6.82	<0.0336 (*)	0.57	>0.9935
	TNNT2	0.83	>0.9999	28.43	0.0041 (**)
Calcium Transporting Genes	ATP2A2	5.27	0.6669	22.59	0.0017 (**)
Cell Cycle Genes	RARRES1	703.14	<0.00001 (****)	0.42	>0.9996
Apoptotic Genes	SNCA	4.14	0.9474	180.68	<0.00001 (****)
Fibrotic Genes	COL3A1	18.62	0.0061 (**)	0.14	0.9952
Signal Transduction Genes	ADRA1A	3.30	0.9682	22.55	0.0129 (*)
	MAPK1	147.78	<0.00001 (****)	0.57	0.9995

2.2 CNs attenuate I/R-induced cell death, reduction in contraction function and signal transduction genes

To study the protective effects of ACh-derived cholinergic nerves against I/R injury, we co-cultured CNs with CSs (CN-CSs). After inducing I/R in CNs-CSs (**Figure 2A**), no change in cell viability and toxicity compared to the control group was observed (normoxic CNs-CSs), whereas the addition of atropine led to a significant increase in cell death. Our statistical analyses confirmed that there were no changes in toxicity levels between I/R and control, while atropine significantly increased the toxicity in I/R-induced CNs-CSs (**Figure 2B)**. In colocalizing ethidium homodimer with cell-specific markers in CNs-CSs, cell death was prevented in cardiomyocytes (**Figure 2C**), endothelial cells (**Figure 2D**), cardiac fibroblasts (**Figure 2E**) and CNs (**Figure 2F**), suggesting that optimal delivery of ACh from CNs is critical to prevent cell death in all cell types in the myocardium.

We also assessed the impact of CNs on contractile function following I/R injury. Consistently with our findings on cell viability, we observed no changes in contraction frequency (**Figure 2G**) and FS% (**Figure 2H**) in CNs-CSs post-I/R injury, whereas atropine significantly reduced both FS% and contraction frequency.

Our qPCR analyses in CNs-CSs (**Table 2**) showed a significant increase in the expression of natriuretic peptide type A (NPPA), which prevents cardiac remodeling, and phosphodiesterase 3A cGMP inhibited (PDE3A), which plays a critical role in regulating the cardiac sympathetic nervous system. Additionally, we measured a significant upregulation in adrenoceptor beta 1 (ADRB1), regulating signal transduction, and mitogen-activated protein kinase 1 (MAPK1), involved in cardiomyocyte growth, while the expression of mitogen-activated protein kinase 8 (MAPK8) was significantly decreased.

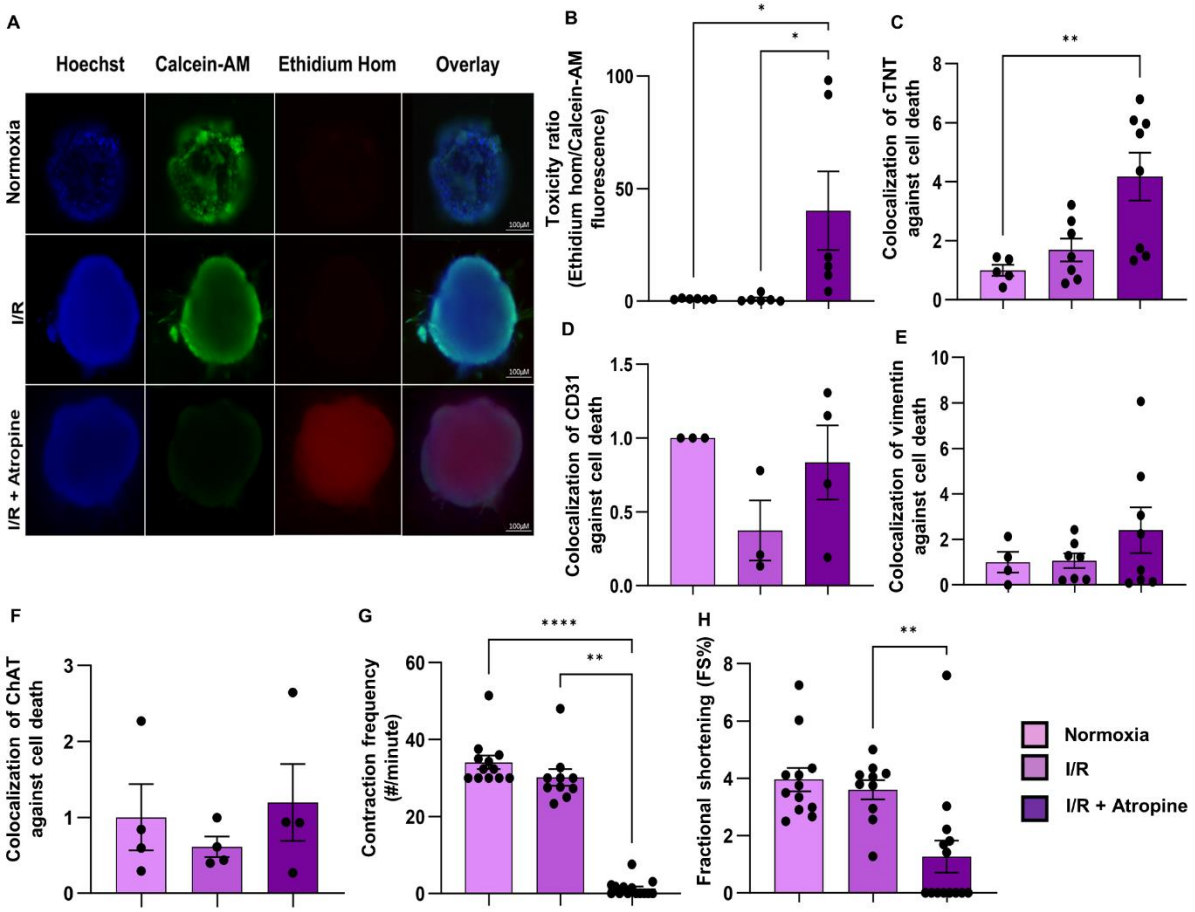

Figure 2. Protective roles of ACh-producing CNs against I/R in CNs_CSs. A) Epifluorescence Stack images of CNs_CSs normoxia (control), I/R, I/R + atropine depicting the total number of nuclei stained with Hoechst, live cell using Calcein-am and dead cells with ethidium homodimer. The magnification bar is 100µm. B) Toxicity ratio (dead cells/ live cells, normalized against control); N≥6. C) Colocalization of cTNT expression (iCMs) against cell death (ethidium homodimer); N≥6. D) Colocalization of CD31 expression (HCAEC) against cell death (ethidium homodimer); N=3. E) Colocalization of vimentin expression (HCF) against cell death (ethidium homodimer); N≥4. F) Colocalization of ChAT expression in CNs against cell death (ethidium homodimer); N=4. G) Fractional shortening analysis; N≥10. H) Contraction Frequency analysis; N≥10. B-H) Data are presented as individual points and mean ± SEM, with error bars indicating the standard error of the mean. Statistical significance is denoted as P< 0.05 = *, p<0.01 = **, p<0.001 = *** and p<0.0001 = ****, analyzed using One-way ANOVA followed by Tukey's multiple comparisons test (Normalized against control except G and H).

Table 2. Relative expression of statistically significant changes for cardiovascular genes and signal transduction genes by qPCR analyses. The I/R sample was compared to control, CNs-CSs, showing its fold change values and P-value. For the Fold change columns, red color is used for upregulated genes, and blue for downregulated genes. P-values were calculated using a one-way ANOVA test with Tukey's multiple comparisons test, $p < 0.0001$ = ****, (n = 3).

Classification of genes	Symbol	Comparing to Control	
		I/R	
		Fold Change	P-Value
Cardiovascular Genes	NPPA	36.86	<0.0017 (**)
	PDE3A	17.50	<0.0066 (**)
Signal Transduction Genes	ADRB1	17.89	<0.0061 (**)
	MAPK1	352.38	<0.0001 (***)
	MAPK8	0.86	<0.0036 (**)

2.3 ACh-NPs protect against I/R-induced cell death and reduction in contractile function in CSs

To evaluate the potential use of NPs to stably deliver ACh to cardiac cells and to protect against I/R injury, we used ACh-NPs in I/R CSs. First, we generated ACh-NPs by loading ACh in PBCA-NPs (loading efficiency equal 17.50%, **Supplementary Figure S1, Supplementary Table S1**). Subsequently, we evaluated any effects of ACh-NPs on cell viability and function in IR CSs. Our results showed that ACh-NPs significantly protected against I/R-induced cell death and increased the number of live cells (**Figure 3A-B**). Control PBCA-NPs that did not contain any ACh exerted no protective effects against I/R-induced toxicity (**Figure 3A-B**). After we co-stained I/R CSs with ethidium homodimer (cell death) and antibodies against the three cell types, we found that ACh-NPs significantly attenuated I/R-induced death in endothelial cells (**Figure 3D**) and fibroblasts (**Figure 3E**), while this effect was not statistically significant in cardiomyocytes (**Figure 3C**). Moreover, ACh-NPs significantly improved contraction frequency (**Figure 3F**) and fractional shortening % (**Figure 3G**) in I/R CSs.

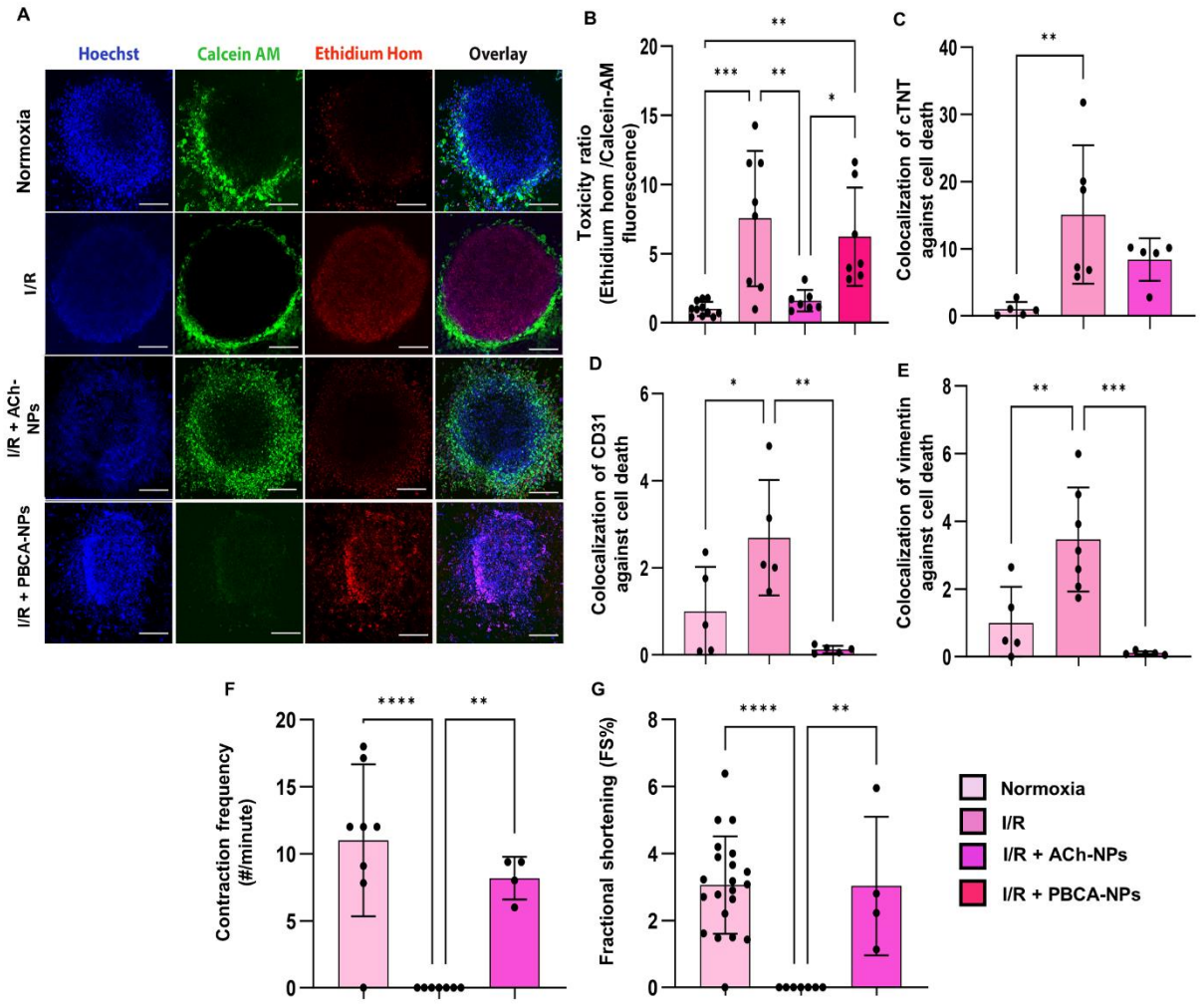

Figure 3. Protective roles of ACh-NPs against I/R-induced myocardial damage. A) Confocal stack images of normoxia (control), I/R, I/R + ACh-NPs and I/R + PBCA-NPs showing the total number of nuclei stained with Hoechst, live cells using Calcein-am and dead cells with ethidium homodimer. The magnification bar is 100µm. B) Toxicity ratio (dead cells/ live cells, normalized against control); N≥7. C) Colocalization of cTNT expression (iCMs) against cell death (ethidium homodimer); N≥5. D) Colocalization of CD31 expression in HCAEC against cell death (ethidium homodimer); N≥5. E) Colocalization of vimentin expression (HCF) against cell death (ethidium homodimer); N≥5. F) Fractional shortening analysis; N≥4. G) Contraction Frequency analysis; N≥4. B-G) Data are presented as individual points and mean ± SEM, with error bars indicating the standard error of the mean. Statistical significance is denoted as P< 0.05 = *, p<0.01 = **, p<0.001 = *** and p<0.0001 = ****, analyzed using One-way ANOVA followed by Tukey's multiple comparisons test (Normalized against control except F and G).

2.4 ACh-NPs are cardioprotective post-MI *in vivo*

To extend our *in vitro* findings to *in vivo* models, we tested the efficacy of ACh-NPs in mitigating MI-induced reduction in cardiac function, as well as any effects on fibrosis in a murine model of permanent LAD ligation. [49, 50] Mice were divided as follows: *i*) SHAM (healthy controls); *ii*) MI; *iii*) MI + ACh-NPs; and *iv*) MI + PBCA-NPs. Cardiac imaging using ultrasound was performed at baseline (before the procedure, **Figure 4A.I**), midpoint (day 14, **Figure 4A.II**) and endpoint (day 28, **Figure 4A.II**), and the ejection fraction % (EF%) were measured in the left ventricle using B-mode. Our results showed that ACh-NPs significantly protected against MI-induced reduction in EF% at 14 and 28 days, while control PBCA-NPs had no protective effects against MI.

Our histological using Hematoxylin and Eosin (H&E), Masson's Trichrome, and Picrosirius Red staining (**Figure 4B**) showed that ACh-NPs protected against MI-induced fibrosis. Our quantitative analysis of the collagen content using Masson's Trichrome staining (**Figure 4C**) and Picrosirius Red staining (**Figure 4D**) indicated that ACh-NPs significantly reduced MI-induced collagen deposition, while PBCA-NPs had no protective effects.

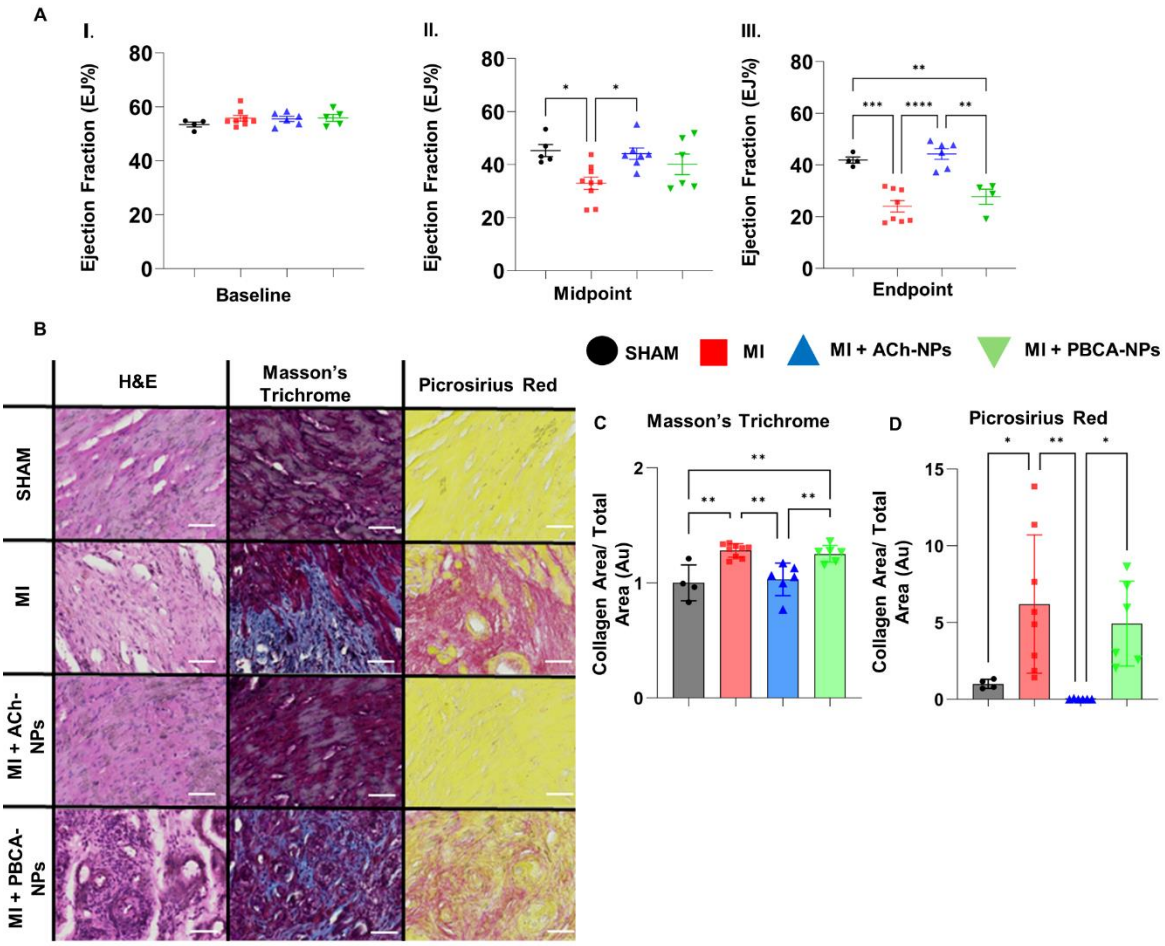

Figure 4. Protective role of ACh-NPs against myocardial injury in an MI murine model. A) Ejection Fraction % (EF%) analyses for SHAM, MI, ACh nanoparticles and PBCA nanoparticles; N≥4. I) EF% of baseline; N≥4. II) EF% of Midpoint (14 days); N≥4. III) EF% of Endpoint (28 days); N≥4. B) Brightfield images of SHAM, MI, ACh-NPs and PBCA-NPs stained with H&E, Masson's Trichome and PicroSirius Red. The magnification bar is 10μm. C) Analysis of collagen production over total area using Masson's Trichome images; N≥4. D) Analysis of collagen production over the total area using PicroSirius Red images; N≥4. A, C, D) Data are presented as individual points and mean ± SEM, with error bars indicating the standard error of the mean. Statistical significance is denoted as $P< 0.05$ = *, $p<0.01$ = **, $p<0.001$ = *** and $p<0.0001$ = ****, analyzed using One-way ANOVA followed by Tukey's multiple comparisons test (Normalized by control for C and D).

To identify the molecular drivers utilized by ACh-NPs to protect against MI we first isolated the apex from MI mice treated *in vivo* with (*i*) PBCA-NPs, (ii) Ach-NPs, and (iii) untreated controls and performed RNA-Seq. Principal component analysis (PCA) of the genome-wide expression profiles showed that samples from these groups indeed formed distinct clusters (**Figure 5A**). Differential expression analysis across the three sample groups identified 144 differentially expressed genes (fold-change ≥ 1.5, p-value < 0.05) and hierarchical cluster analysis further showed a clearly diverged pattern of up- and down-regulated genes in the MI compared to the MI + ACh-NPs samples (**Figure 5B**). Ingenuity pathway analyses (IPA) of MI + ACh-NPs over MI samples identified enrichment in canonical pathways, including the upregulations of genes regulating detoxification of ROS (genes: CYBA, TXN), interleukin (IL)-7 (gene: IL7R) and IL-12 (gene: IL27) signaling pathways, which are associated with regulating T cells and macrophages, and neutrophil degranulation (genes: CD300A, CYBA, LGALS3) (**Figure 5C, Supplementary Table S2**). Conversely, we also measured a downregulation in IL-13 signaling pathway (genes: ALOX15, ANO1), which play crucial roles in the development of HF (**Figure 5C, Supplementary Table S2**). Our results also showed significant downregulation of thrombin signaling pathways through proteinase-activated receptors (PARs) (gene: GNA12) and apoptotic execution phase (gene: DSG2) (**Figure 5C, Supplementary Table S2**). Moreover, ACh-NPs increased the expression of genes regulating cell-mediated immune response, and cardiovascular system development and function, including connective tissue, nervous system, vascular and muscular system **(Supplementary Table S3**).

Our IPA of MI plus ACh-NPs over MI samples also identified an enrichment in molecular functions, including the upregulation of genes associated with cell cycle regulation and proliferation (**Figure 5D, Table 3**). Specifically, ACh-NPs upregulated BCL2A1, CCL19, CD300A, TXN, IL7R, GLI1, IL27, and UNC119, and it downregulated ALOX15 and ANO1, which control cell cycle, survival and proliferation (**Figure 5D, Table 3**).

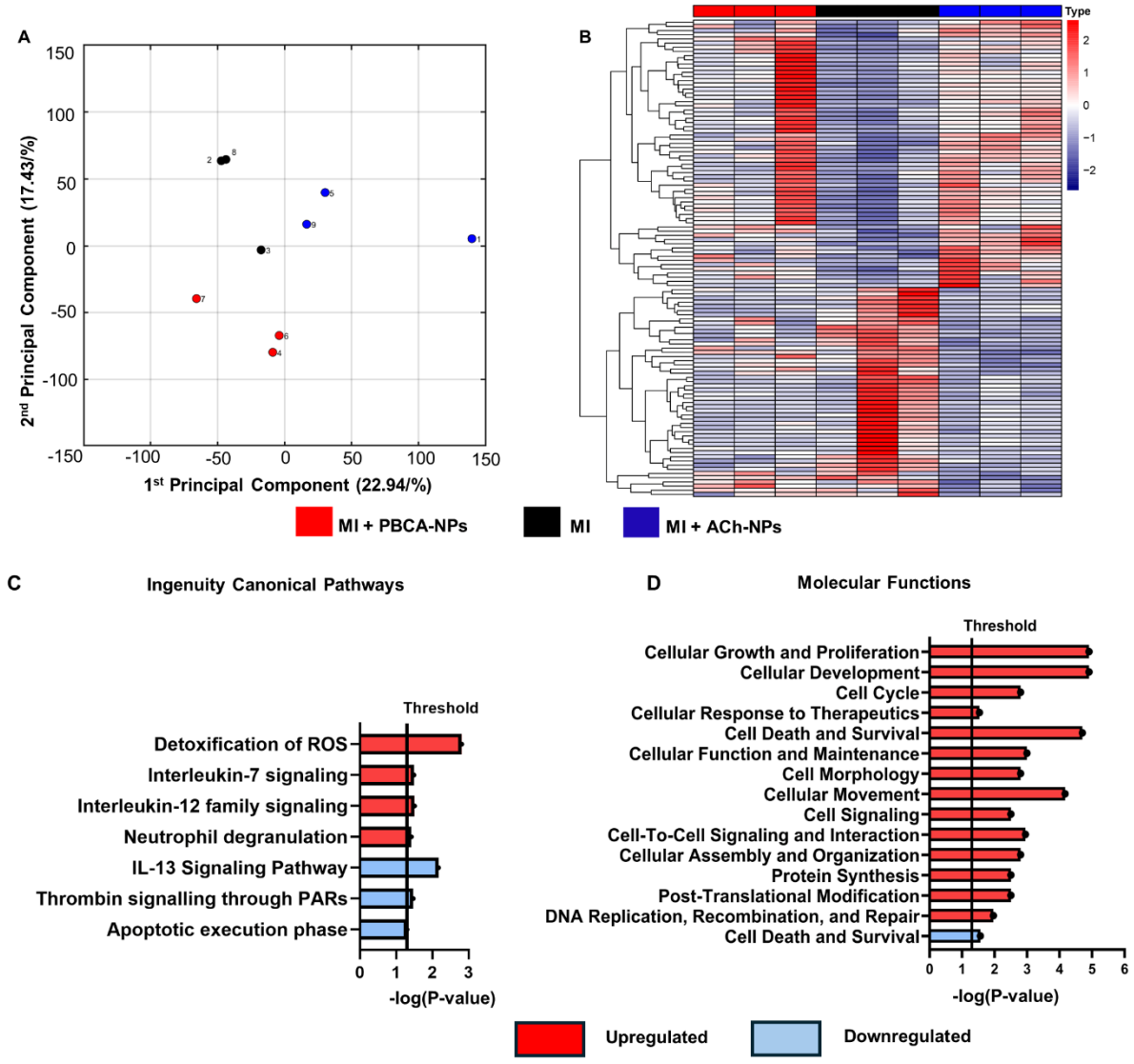

Figure 5. The transcriptomic profile of ACh-NPs against MI mice model. A) Principal component analysis of whole transcriptome expression levels. B) Heatmap of gene expression for all transcripts differential gene expressed between ACh-NPs and MI. C) Ingenuity canonical pathways analysis for genes differentially expressed between ACh-NPs and MI (Red- upregulated genes and Blue- downregulated genes). D) Molecular functions for genes differentially expressed between ACh-NPs and MI (Red- upregulated genes and Blue- downregulated genes). N=3.

Table 3. Ingenuity Pathway Analysis (IPA) on RNAseq identified molecular functions in MI treated with ACh-NPs (A cutoff of $p < 0.05$ and logFC >1.5 or <1.5 was applied).

Category	p-value	-log(p-value)	Molecules
Cellular Development	1.24E-05	4.906578315	BCL2A1,CCL19,CD300A,CLEC4A,CYBA,ELL3, GLI1,IL27,IL7R,KRR1,LGALS3,SLAMF7,SNORD22, TXN,UNC119,UNC13A
Cellular Growth and Proliferation	1.24E-05	4.906578315	BCL2A1,CCL19,CD300A,CLEC4A,CYBA, ELL3,GLI1,IL27,IL7R,LGALS3,SLAMF7, SNORD22,TXN,UNC119,UNC13A
Cell Death and Survival	1.98E-05	4.70333481	BCL2A1,CCL19,CD300A,CENPO,CYBA,GLI1, IL27,IL7R,LGALS3,Mt3,PTGR1,SLAMF7, SNORD22,TMEM132A,TXN,UNC119
Cellular Movement	6.72E-05	4.172630727	ARHGAP25,CCL19,CD300A,CENPO,CYBA, GLI1,IL27,IL7R,LGALS3,TXN,UNC119
Cellular Function and Maintenance	1.01E-05	2.995678626	BCL2A1,CCL19,CD300A,CYBA,GLI1,IL27,IL7R, KRR1,LGALS3,Mt3,SLAMF7,TXN,UNC119,UNC13 A
Cell-To-Cell Signaling and Interaction	1.12E-05	2.950781977	CCL19,CD300A,CLEC4A,GLI1,IL27,IL7R, LGALS3,SLAMF7,TXN,UNC119,UNC13A
Cell Cycle	1.57E-03	2.804100348	CENPO,GLI1,IL7R,LGALS3,TXN
Cell Morphology	1.57E-03	2.804100348	CCL19,CYBA,GLI1,IL27,IL7R,LGALS3, Mt3,TXN,UNC13A
Cellular Assembly and Organization	1.57E-03	2.804100348	BCL2A1,CCL19,LGALS3,TXN,UNC13A
Cell Signalling	3.13E-03	2.504455662	CCL19,CD300A,CYBA,LGALS3,TXN

Post-translational Modification	3.13E-03	2.504455662	CYBA,TXN
Protein Synthesis	3.13E-03	2.504455662	CCL19,CLEC4A,CYBA,IL7R,KRR1,TXN
DNA Replication, Recombination, and Repair	1.09E-02	1.962573502	ELL3,GINS2,GLI1,LGALS3,TXN
Cellular Response to Therapeutics	2.93E-02	1.53313238	IL7R

3. Discussion

In this study, we examined the potential use of NPs to target and deliver ACh to the myocardium using a combination of *in vitro* and *in vivo* models of myocardial injury. We demonstrated the protective effects of ACh through three delivery methods in human CSs. Importantly, we demonstrate the benefits of novel ACh-NPs against myocardial damage in an *in vivo* MI murine model. First, ACh protected against I/R-induced cell death, reduction in contractile function and gene expression changes in I/R CSs (**Figures 1-3, Tables 1-2**). Subsequently, we showed that ACh-NPs prevent the reduction in LVEF% and the increase in fibrosis post-MI in mice (**Figure 4**). Finally, our transcriptomics analyses identified the mechanisms responsible for the ACh-NP-mediated cardioprotection against myocardial I/R injury, primarily through: *i*) the detoxification of ROS; *ii*) the attenuation of apoptotic signaling pathways; and *iii*) the activation of cell cycle and proliferation pathways post-MI (**Figure 5, Table 3**). Altogether, our findings support that ACh-NPs might be a suitable therapeutic approach to protect against myocardial injury following I/R and MI.

Despite the well-documented cardioprotective effects of increasing ACh levels in MI and I/R injury in pre-clinical models, the limited translation of these findings from the bench to the bedside could be due to the variability of the approaches used, as well as the broad activity of ACh. [13, 27] Our findings are consistent with previous reports, supporting the need to further

explore the therapeutic potential of ACh in cardioprotection. Recently, Intachai et al. [16] demonstrated that administering ACh in H9c2 cells before or during I/R prevented mitochondria dysfunction, reduced ROS production and protected against I/R-induced apoptosis and autophagy. Roy et al. [52] showed that deficiency in ACh production *via* the inhibition of the vesicular ACh transporter (VAChT) and choline acetyltransferase (ChAT) gene expression in cardiomyocytes, led to a decrease in FS% and EJ%, leading to ventricular dysfunction in mice models. In this study, we found that increasing ACh levels in CSs attenuated I/R-induced toxicity, *via* necrosis, and prevented cell death (**Figure 1**). Additionally, our study demonstrated that ACh treatment improves the FS% in I/R CSs concurrent with a significant increase in TNNT2 and Ca^{2+} transporting gene levels (**Figure 1** and **Table 1**). Hence, our findings add support toward increasing ACh levels in cardiac cells to protect against cell death and improve contractile activity. [53-55] Moreover, our results demonstrated that ACh pretreatment reduces I/R-induced fibrosis production through the COL1A1 gene (**Table 1**), which is associated with cardiac remodeling and HF progression. [56] We also measured a significant upregulation of ADRA1A expression (**Table 1**). This is consistent with previous studies showing that ADRA1A is cytoprotective by enhancing contractility [57] and activating glucose intake [58] in cardiomyocytes.

While our study provides new insights into the protective effects of increasing ACh levels in cardiac cells, the untargeted administration of ACh at a relatively low dose (100µM) in patients may raise concerns regarding its safety and efficacy. ACh hydrolyses rapidly *in vivo*, and the inhibition of ACh degradation through cholinesterase inhibitors leads to ACh side effects, including lacrimation, salivation, tremors, loss of motor activity, hypothermia and tonic convulsions. [59] When VNS is used to elevate myocardial ACh levels, mixed results in previous clinical trials have limited translation to the clinic, mostly due to the broad effects achieved. [13, 27] Previous studies showed that CNs-derived ACh can restore the autonomic balance and prevent autonomic dysfunction. [7, 8, 11] Therefore, we sought to explore the effects of CNs instead of freely suspended ACh in I/R CSs. Our results showed that CNs significantly reduced toxicity in all the cell types following I/R injury in CSs (**Figure 2**). Moreover, CNs protected against I/R-induced contractile dysfunction, which is consistent with previous *in vivo* studies. [13, 60, 61] Our qPCR analyses of genes regulating cardiovascular damage indicated that CNs significantly upregulated NPPA gene expression against I/R injury (**Table 2**), which has been previously shown to inhibit cardiac hypertrophy, fibrosis, remodeling and dysfunction. [62, 63] Additionally, CNs also upregulated PDE3A and ADRB1 genes, which regulate the sympathetic system post-I/R (**Table 2**). Given the strong effects exerted by CNs on I/R CSs, we think further

considerations regarding the delivery of ACh might be important and a more complex machinery might be required for optimal results that prevent its degradation.

Over the years, NPs have been explored to encompass a wide array of clinical applications and enhance therapeutic outcomes.[64] Therefore, we used NPs to improve the stability and solubility of ACh and prolong its durability to enhance efficacy and safety. In our study, we developed novel ACh-NPs and investigated the effects of the direct delivery of low doses of ACh in I/R-induced CSs. Our findings showed that ACh-NPs protected against I/R-induced toxicity and prevented the necrotic death of cardiac cells. Also, ACh-NPs protected against contractile dysfunction in I/R CSs (**Figure 3**).

To exclude any effects of PBCA-NPs alone (no ACh) in CSs, these were used as our negative controls. Our results are consistent with previous studies that demonstrated that PBCA-NPs did not induce any cytotoxic or inflammatory effects in rats. [65] Furthermore, our *in vivo* findings demonstrated that administrating ACh-NPs before inducing MI injury in a murine model protected against the reduction in EF% measured in MI animals, to measurements that were comparable to SHAM and baseline animals (**Figure 4**). Additionally, ACh-NPs decreased collagen deposition and fibrosis post-MI injury (**Figure 4**). Through our transcriptomics analyses, we identified that ACh-NPs downregulated 15-lipoxygenase (ALOX15) and anoctamin-1 (ANO1) post-MI, leading to an attenuation of cell death signaling and IL-13 signaling pathway. These observations are consistent with previous studies where high expression of ALOX15 was measured in hypoxic human cardiomyocytes and cardiac endothelial cells, promoting thrombosis and cardiomyocytes cell death. [66, 67] Additionally, upregulation of ANO1 was previously measured following MI which led to cardiac fibrosis in the infarcted area. [68]

Our findings are important as, for the first time, we show an increase in EF% *in vivo* by using ACh in MI animals. Previously, Durand et al. [69] demonstrated that pyridostigmine, a cholinesterase inhibitor that increases ACh levels, reduces collagen deposition and improves LV diastolic function post-MI, but did not improve cardiac function in a murine model. From a molecular perspective, our *in vivo* transcriptomics results showed that ACh-NPs improved the expression of genes regulating the development and functions of the cardiovascular system and downregulated genes responsible for apoptosis and thrombin signaling post-MI (**Figure 5**). Our findings are also consistent with previous ones showing that ACh inhibits ROS generation. [11, 61, 70] Additionally, ACh-NPs have a positive effect on cell survival, cell cycle and proliferation (as we measured an increase in IL-27 [71] and IL-7R [72] signaling pathways), as well as on

apoptosis (as we measured an increase in the anti-apoptotic gene BCL2A1 [73]), proinflammatory cytokines (chemokines CCL19 [74]), anti-fibrosis (GLI1 [75]) and anti-ROS (TXN [76]).

Altogether, we showed for the first time that ACh-NPs could act as an alternative therapeutic approach to improve the cardiovascular system post-MI, by preventing the reduction of LVEF% and ventricular remodeling. We also demonstrated that ACh-NPs maintain ventricular function and activate cell proliferation signaling post-MI. However, further studies are required to optimize ACh-NP delivery to the myocardium, including analyses of ACh-NPs stability, targeting efficiency and controlled release properties.

Limitations of this study should be considered. Firstly, we tested the effects of increasing ACh-NPs in *in vitro* I/R CS model and then tested their role in MI *in vivo* models. Nevertheless, we used the I/R CSs model to look at the acute effects on myocardial protection, whereas the permanent LAD ligation was used to look at the chronic effects of MI-leading to HF. Furthermore, we injected ACh-NPs in the myocardial muscle before performing the LAD ligation, while they will be delivered after the MI event to prevent further damage leading to HF in patients. Assessing the efficacy of the timing for the delivery of ACh-NPs (how long after the MI event) in patients will be critical. We also injected ACh-NPs right before the MI event to assess its maximal potential cardioprotective effect, as well as reopening of the chest wall in mice is challenging following the MI procedure. Additionally, we did not evaluate other delivery methods for ACh-NPs other than directly to the myocardium, such as intravenously or orally. We excluded these to prevent any systemic delivery of ACh-NPs and associated side effects. Lastly, while our *in vitro* and *in vivo* models have demonstrated promising results, there is a significant gap in translating these findings to clinical settings. The complexity of human CVD may not be fully replicated in animal models, and there may be species-specific and sex-specific differences in response to ACh treatments. Future work should involve further *in vivo* experimentation in large animals, potentially using pig models that have largely comparable cardiac functions to humans. [77]

In addressing these limitations and pursuing these future directions for ACh-NPs, we hope to provide an effective cardioprotective strategy against MI and associated myocardial damage, ultimately benefiting patients with CVD.

4. Conclusion

In conclusion, our findings support the protective role played by ACh against myocardial damage-induced toxicity, necrosis, reduction in contractile function and progression to HF.

This study also showed for the first time that ACh-NPs could be employed as a promising novel treatment against MI injury, as they reduced MI-induced apoptosis and necrosis, LV remodeling, and prevented reduction in LVEF%. ACh-NPs also increased cell survival, cell cycle and proliferation, as well as attenuated ROS levels post-MI. Additional preclinical studies are needed to evaluate the proper dosage of ACh-NPs delivery and to translate our findings from the bench to the bedside.

5. Methods and Materials

The Animal Care and Ethics Committee from the University of Technology Sydney in Australia approved the use of MI murine models. The project number is UTS Animal Ethics Committee REF NO. ETH19-4338.

5.1 Drugs and reagents

Cell culture: L-glutamine solution (catalogue number: G8540), penicillin-streptomycin (catalogue number: P4458), and fibronectin derived from bovine plasma (catalogue number: 10838039001) were acquired from Sigma-Aldrich. Cardiomyocytes iCells plating and maintenance media were sourced from Fujifilm Cellular Dynamics (catalogue number R1017). Laminin of natural mouse origin was obtained from Thermo Fisher Scientific (catalogue number 23017015), while the maintenance medium iN1(AP) was procured from Elixirgen Scientific (catalogue number CH-MM). For cell passaging, trypsin-EDTA and TrypLE Express were used, purchased from Sigma-Aldrich and Thermo Fisher Scientific (catalogue numbers T4049 and 12604021, respectively).

Drugs: Acetylcholine chloride (catalogue number: A2661) and atropine (catalogue number: PHR3846) were purchased from Sigma-Aldrich.

Antibodies: Primary antibody purified mouse anti-human CD31 and purified rat anti-mouse CD31 (BD Bioscience, catalogue number: 550389 and 557355, respectively) were used to immunolabelled HCAEC in human and mouse tissues. Secondary antibody alexa fluor® 647 AffiniPure™ goat anti-mouse IgG (H+L) or Alexa fluor® 790 affinipure™ Goat Anti-Mouse IgG (H+L) (catalog number: 115-655-146) and alexa fluor® 647 AffiniPure™ goat anti-rat IgG (H+L) were utilized as secondary antibodies (Jackson ImmunoResearch, catalog number: 115-605-003, 115-655-146 and112-605-003). Alexa Fluor® 488 Mouse monoclonal (Vimentin - Cytoskeleton Marker) was purchased from Abcam (catalogue number: AB195877) and Troponin T-C (CT3) Alexa Fluor® 546 was purchased from Santa Cruz

(catalogue number: sc-20025). Anti-Choline Acetyltransferase (ChAT) Antibody was sourced from Sigma-Aldrich (catalogue number: SAB5701171).

5.2 Generation of human cardiac spheroids (CSs) and CS with cholinergic nerve cells (CNs)

Following the provider's protocols, human cardiac fibroblasts (HCF) (Cell Applications, Inc; catalogue number: 306-05A) were cultured using cardiac fibroblast growth medium (Cell Applications, Inc.; catalogue number: 316-500) and human coronary artery endothelial cells (HCAEC) (Cell Applications, Inc.; catalogue number: 300-05A) were maintained human mesoendothelial cell growth medium (Cell Applications, Inc.; catalogue number 212-500). 1% solution of L-glutamine–penicillin–streptomycin was added to both media to enhance nutrient content. Human induced pluripotent stem cell-derived cardiomyocytes (iCMs, Passage 0) (Cellular Dynamics; catalogue number: R1017) were cultivated in iCell plating and maintenance media within fibronectin-coated flasks for 3 days, adhering to Cellular Dynamics' instructions. F following the supplier's instructions, quick-Neuron Cholinergic-Human iPSC-derived Neurons from a 74-year-old donor (Elixirgen Scientific, catalogue number: CHSeV-CW50065-S, Passage 0) were cultured in Maintenance Medium iN1(AP) for three days, with the culture surface pre-coated with laminin. Prior to CSs and CNs formation, 3D Petri dishes were prepared using a micro-mold from Sigma-Aldrich (catalogue number: Z764027), following the provided guidelines with 2% agarose (Sigma-Aldrich, catalogue number: A4718) in PBS (Sigma-Aldrich, catalogue number: D8537). To precondition the 3D dishes, they were incubated in a culture medium at 37°C with 5% O2 and 5% CO2 overnight.

Cells were then passaged using trypsin-EDTA for HCAECs and HCF (Passage <6) and TrypLE for iCMs and ACh-producing IPSC-derived cholinergic nerve cells (CNs). CSs were created using our established procedures.[78] Briefly, the passaged cells were quantified using trypan blue solution (Thermo Fisher Scientific; catalogue number: 15250061) and were mixed in a predetermined ratio of 2:1:1 (iCMs: HCF: HCAEC), each CS comprised of 30,000 cells (**Figure 6.I**). The cells were centrifuged at 300g for 5 minutes and resuspended in a volume of 190µl of CS media (a mixture of iCM, HCF, and HCAEC media in the same ratio) and were seeded into agarose-based 3D Petri dishes with 81 wells and left in the incubator at 37°C with 5% O2 and 5% CO2 (media changed every two days). For CNs-CSs (comprising of ACh-producing CNs), the co-culture ratio, based on the literature, was 1:1 for neuronal cells to cardiomyocytes.[79-81] The overall culture consisted of a ratio of 2 iCMs: 2 CNs: 1 HCF: 1 HCAEC, with the medium composition adjusted accordingly and put in the incubator similar to CSs.

After three days, CSs and CNs-CSs had matured (**Figure 6.II**) and were relocated to Falcon® 96-well Clear Microplates, embedded within a 100µl matrix of type 1 collagen rat tail biopolymer gel (Merck, catalogue number: 08-115), mixed equally and with additional media to normalize the pH to 7(**Figure 6.III**).

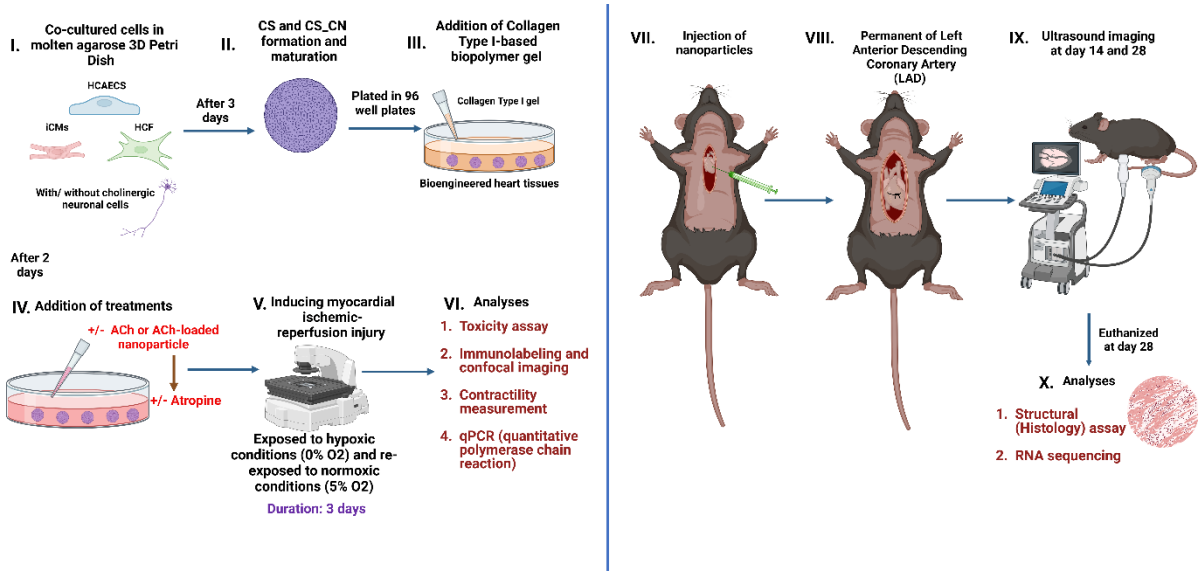

Figure 6. Schematic illustration of I/R *in vitro* and MI *in vivo* modeling. I) Co-culture of human IPSC-derived cardiomyocytes (iCMs), HCAEC, HCF with or without ACh-producing cholinergic nerve cells (CNs) in a 3D Petri dish. II) After three days, CSs are formed and matured. III) CSs are plated in collagen type I-biopolymer gel, which was diluted with CS media in a 96-well plate. IV) After two days, acetylcholine (ACh) or NPs were added in some samples, as well as atropine, which is the antagonist of ACh. V) After two hours, I/R was then induced through changes in oxygen level in the incubator of EVOS M7000 microscope, and after 3 days, samples underwent analyses. VI) The analyses are toxicity assay, immunolabeling and confocal imaging, and qPCR. VII) Injection of ACh-loaded nanoparticle intramyocardially. VIII) Induced permanent LAD in mice. IX) Monitor mice for 28 days and do ultrasound imaging at baseline, day 14 and day 28. X) After euthanizing mice, analyses performed were histology assay and bulk RNA sequencing analysis.

5.2.1 ACh and atropine treatment:

Two days post-culture, CSs were treated with 100µM ACh, a dosage informed by prior research [52, 82, 83], as depicted in **Figure 6. IV.** Following a 2-hour interval after ACh administration, 50µM atropine was introduced to both the CSs treated with ACh and the CSs co-cultured with

CNs that had been encapsulated in hydrogel for two days. Atropine, a known ACh antagonist, was used to explore the inhibitory effects on ACh-mediated responses.

5.3 Fabrication of ACh-loaded and PBCA-NPs

To synthesize ACh-loaded nanoparticles, 10 mg of Polyvinylpyrrolidone (PVP) (Sigma-Aldrich, catalog number: PVP40T) was dissolved in a 1% Tween-20 solution to create a 1% w/v PVP solution. Subsequently, 10 mg of Acetylcholine chloride was incorporated. Following this, 1% v/v Poly-butylcyanoacrylate (PBCA) (BRAUN, catalog number: 15054-BU) was added to the mixture in a 1:100 ratio, as per the procedure outlined by Mehta et al. [33]. The mixture was then filtered through a 1µm PTFE syringe filter and centrifuged at 13,860g for 40 minutes. After centrifugation, 1 ml of phosphate-buffered saline (PBS) at pH 7.4 was introduced, and the solution was lyophilized using a SpeedVac (SpeedVac™ SPD121P) on an automated setting overnight for 12 hours. The lyophilization parameters were set as follows: a run temperature of 45°C, heat time of 2.00 hours, run time of 2.00 hours, and a vacuum level of 14 Torr. For the control group involving PBCA-NPs, the same procedure was employed excluding the addition of Acetylcholine chloride. The prepared nanoparticles were stored at 4°C for a duration of up to one month.

5.3.1 Calculation of entrapment efficiency:

Before transferring the nanoparticles and spinning the solution, the weight of the empty tube (We) was noted. After the lyophilization step, the weight of respective tubes containing lyophilized nanoparticles (Ws) was taken. The weight of NPs (Wn) is (Ws-We).

The PBCA-NPs are referred to as Wnc and ACh-NPs as Wns, the formula for loading efficiency is as follows:

Loading efficiency= (Wns -Wnc)/Wnc×100

The result for loading efficiency is 17.50 % as shown **in supplementary figure S1**.

5.3.2 Preparation of ACh-loaded and PBCA-NPs for *in vitro* and *in vivo* experiments

For *in vitro* experiment, CS media was added to 1.70 mg/ml for either ACh-loaded or PBCA-NPs and were sonicated for 12 minutes. Then further diluted with media, 0.17 mg/ml of nanoparticles was added to the well (**Figure 6.IV**).

For *in vivo* experiment, saline solution was added to 1.70 mg/ml for both ACh-loaded and PBCA-NPs and were sonicated for 12 minutes to ensure uniform dispersion. The prepared

solution was then administered intramyocardially at a concentration of 0.17 mg/ml directly into the myocardial tissue of mice (**Figure 6.VII**).

5.4 Myocardial I/R *in vitro* and MI *in vivo*

5.4.1 Establishment of I/R-induced myocardial damage in CSs

I/R myocardial damage was performed by exposing CSs and CNs-CSs to hypoxia/reoxygenation conditions (**Figure 6.V**). They were placed in the EVOS M7000 microscope (Thermo Fisher Scientific) in the incubated chamber (5% O_2, 5% CO_2, 21% N at 37°C). For the first 24 hours, the chamber was in normoxia condition (5% O_2). For the next 24 hours, a hypoxia condition (0% O_2, 5% CO_2, 21% N at 37°C) was induced for oxygen deprivation. Reperfusion was initiated by re-exposing the plate to the normoxia condition for 24hrs.[46, 78] Therefore, the experiment was conducted over a period of three days, following which assays to assess the impact of ACh against I/R-induced toxicity were carried out, including toxicity, contractile assays, immunolabelled cell types against cell death and qPCR analyses (**Figure 6.VI**).

5.4.2 Establishment of MI-induced myocardial damage in mice model

Male RAG1 mice were procured from Australian Bioresources and were used from 7-10 weeks old. Mice were randomly divided into four groups: 1) SHAM, 2) MI, 3) MI + ACh-loaded nanoparticles, and 4) MI + PBCA nanoparticles. All mice were kept in the same room in a light-controlled environment at the ERNST facility at the University of Technology Sydney with a 12:12-h light-dark cycle and with free access to standard food and water.

The MI procedure was performed as previously described, by one experienced researcher (CG).[84] Briefly, the mice were first anesthetized by injection of ketamine 40 mg/kg, xylazine 5 mg/kg and atropine 0.15 mg/kg by the intraperitoneal route and after 10 minutes, were intubated through PhysioSuite and were continuously anesthetized with 2-3% isoflurane inhalation and O_2 level was kept between 0.4-0.6% till the end of the operation. Prior to the permanent left coronary artery (LAD) for groups 3 and 4, ACh-loaded and PBCA-NPs were injected intramyocardially directly into the myocardial tissue of mice (**Figure 6.VII**). A slipknot was tied around the descending branch of the LAD, a 3mm long 3-0 silk suture with a 7-0 silk suture piece passed in between the LAD and knot to prevent any bleeding (**Figure 6.VIII**). For the SHAM group, the LAD artery was threaded but not ligated, and the remaining operations followed the same procedures as the forementioned groups. After suturing the mice's chest, isoflurane is turned off, and the O2 level is at 2%. For post-surgical analgesia and care, 2 mg/mL solution of bupivacaine in 0.9% saline was applied topically to the surgical site.

Subsequently, buprenorphine (Temvet) was administered subcutaneously at a dosage of 0.08 mg/kg in 0.1 mL of 0.9% saline. Additional medications included atipamezole (Antisedan) at 1 mg/kg, furosemide (Lasix) at 8 mg/kg, and 600 µL of 0.9% saline solution for recovery support. The mice were observed for 28 days post-operation, after which they were humanely euthanized. Transverse (axial) heart tissue slices of 1mm thickness from the left ventricle, below the site of the left anterior descending (LAD) artery ligation, were excised for further analysis. These tissue samples were then processed for RNA sequencing and histological analysis (**Figure 6.IX**).

5.5 Analyses *in vitro*

5.5.1 Toxicity assay

The Live/Dead® Viability/Cytotoxicity Kit for mammalian cells (Invitrogen, catalogue number: L32250) was utilized as per the provided guidelines to assess cell viability by determining the ratio of dead stained with Ethidium homodimer to live cells stained with Calcein-AM. Additionally, NucBlue® Live ReadyProbes® Reagent (Hoechst 33342, Invitrogen, catalogue number: R37605) was applied in accordance with the manufacturer's protocol (2 drops per ml) to quantify the overall cell count.

Four hours post-application, the specimens were examined under a Leica Stellaris 8 confocal microscope (Leica Microsystems). For each specimen, images were captured using three distinct fluorescent filters to ascertain counts of live, dead, and total cells. Subsequent image analysis was performed with ImageJ software (Fiji), focusing on the fluorescence intensity of live cells relative to the total area and dead cells relative to the total area. The viability assessment was quantified by the ratio of dead to live cells using Excel version 2401 (Microsoft 365) for initial calculations, followed by further analysis with GraphPad Prism.

5.5.2 Immunolabelling and confocal imaging

To assess cell mortality across all cell types within both CSs and CNs-CSs, the specimens underwent staining with Ethidium Homodimer for a minimum of two hours before being fixed in 10% neutral-buffered, 4% (w/v) formaldehyde solution (Sigma-Aldrich, catalogue number: HT5012) for a day. Subsequently, they were rinsed thrice in phosphate-buffered saline containing 0.01% (w/v) sodium azide (PBSA) for 30 minutes each time, followed by permeabilization in a 0.02% (v/v) Triton X-100 solution for 30 minutes. The samples were then incubated in a 3% (v/v) bovine serum albumin (BSA) in PBSA solution overnight to block non-specific binding sites. Primary antibodies, specifically mouse monoclonal anti-human CD31 (1:10) to identify HCAEC and/or Anti-Choline Acetyltransferase (ChAT) Antibody (1:100) for ACh-producing cholinergic nerve cells, were diluted in 3% BSA/PBSA and added to the

samples overnight at 4ºC. Afterwards, the specimens were washed three times with 0.001% (v/v) PBSA before the addition of secondary antibodies: Alexa Fluor 647 goat anti-mouse (1:142) for CS, and/or Alexa Fluor 647 Goat Anti-Rabbit (1:142) and Alexa Fluor 790 Goat Anti-mouse (1:142) for CNs and incubated overnight at 4ºC. Post-secondary antibody incubation, the samples were washed thrice with 0.001% (v/v) PBSA. NucBlue® Live ReadyProbes® Reagent (Hoechst 33342; 2 drops per ml) was diluted in 3% BSA/PBSA alongside cTNT (1:10) for staining iCMs and Alexa Fluor® 488 vimentin (1:250) for HCF identification, and the mixture was left on the samples overnight at 4ºC. Finally, the samples were washed with 0.001% (v/v) PBSA and stored at 4ºC. The samples were imaged using the Leica Stellaris 8 confocal microscope (Leica Microsystems). Optical sectioning along the Z-axis was performed, and the images collapsed into a single focal plane using the manufacturer's software, which is Microscope Software Platform LAS X Life Science (Leica Microsystems). The Z-stacks were processed using IMARIS software (Oxford Instruments plc, RRID:SCR_007370).

5.5.3 Fractional shortening and contractile frequency measurements

The contractile function of CSs and CN-CSs are measured by taking timeframe videos of 30 seconds using Nikon Eclipse Ti2-E Inverted microscope. The fractional shortening percentage and the frequency of contractions are measured. This was done by measuring the total number of contractions for each sample and by measuring the total length of each CS when contracted or relaxed.

5.5.4 mRNA isolation and quantitative polymerase chain reaction (qPCR) analysis

mRNAs were extracted from the samples and analyzed through real-time polymerase chain reaction (qPCR) to measure changes in cardiovascular disease markers (angiogenesis, fibrosis, inflammation, cytoskeletal proteins, cell cycle-related proteins, apoptosis).

RNA was isolated according to the guanidine-isothiocyanate lysis method using the RNeasy Mini Kit (Qiagen, catalog number: 74104). The samples were first lysed and homogenized in absolute ethanol (100% v/v) for ideal binding conditions, then loaded onto the RNeasy silica membrane. Total RNA was quantified by A260/280 ratios (measured in 10 mM Tris¬·Cl, pH 7.5). The total RNA of each sample was reverse transcribed to cDNA using RT² First Strand Kit (Qiagen, catalog number: 330411) and diluted for use with RT² SYBR Green qPCR (Qiagen, catalog number: 330503).

qPCR is performed by using Quantstudio 12K Flex Real-Time PCR System (Thermo Fisher Scientific). RT^2 Profiler PCR Arrays (Qiagen, catalog number: 330231) are specific to human

cardiovascular diseases mRNA. The data are then analyzed using Qiagen web-based software (Qiagen) using the fold-change (ΔΔCt) method (N=3).

5.6 Analyses *in vivo*

5.6.1. Cardiac imaging (Echocardiography)

The mice were all imaged using a Vevo 3100 Preclinical Imaging System (FUJIFILM VisualSonics) at baseline, midpoint (day 14) and endpoint (day 28) under isoflurane via a nose cone (4 ml/min induction followed by 1.5 ml/min maintenance). Mice echocardiography was performed by a trained researcher (CL). Mice were placed supine on a warming platform and B and M mode echo data were obtained for parasternal long axis and short axis views. Long-axis data were analyzed manually using the Vevo LAB software (FUJIFILM VisualSonics).

5.6.2. Histology analysis

Formalin-fixed, paraffin-embedded heart sections (10µm) were deparaffinized and rehydrated. After being washed in distilled water, some sections were stained using Harris Hematoxylin Nuclear Stains (Leica Biosystems, catalog number: 3801560). Other sections were stained with either Masson Trichrome Stain kit (Abcam, catalogue number: ab150686) or Picro Sirius Red Stain Kit (Connective Tissue Stain) (Abcam, catalogue number: ab150681). Images of sections were acquired using the ZEISS Axioscan 7 microscope. For the sections stained using Masson Trichrome, the mean percentage of the collagen area over the total area was measured using Deconvolution and calculated using ImageJ software. The sections stained using Picro Sirius Red were analyzed using PSR_quantify macro, and the mean percentage of the fibrotic area over the total area was measured and calculated using ImageJ software.[85]

5.6.3. RNAseq analysis

The cryosections of the cardiac apex for each sample were processed for mRNA transcriptomic analysis according to the protocol of the commercially available RNeasy Fibrous Tissue Mini Kit (Qiagen, Catalog number: 74704). Total RNA from the sections were isolated using 14.3 M β-mercaptoethanol (β-ME) (Sigma-Aldrich, Catalog number: 444203) and purified according to the manufacturer's instructions. RNA quality assessment, library preparation, and sequencing were performed by BGI Genomics (Hong Kong, China) using DNBSEQ Eukaryotic Strand-specific mRNA libraries sequencing technology. Similar to previous studies [50], the raw sequencing reads were processed to remove adapters – (i.e. if > 25% of bases matching an adapter sequence) and reads matching the following five quality criteria were removed (1) reads shorter than 150 bps, (2) reads with more than 0.1% N's, (3) reads with more than 50 bps of polyX's (A,T,G,C), (4) reads with more than 40% of bases having a base quality < 20. The resultant high-quality reads were aligned to the mouse genome (mm10) using the software STAR (Spliced Transcripts Alignment to a Reference). [86] We mapped an average of

23,714,108 reads per sample achieving an average alignment rate was 98.48%. The gene expression levels were quantified using the tool featureCounts [87] and we removed genes that had less than 100 reads across the nine samples, reducing the gene count from 26214 to 13058. The resulting expression levels were normalized using the DeSeq2 package [88] in the R statistical analysis software. [89] Genome-wide expression profiles were analyzed through principal component analysis (PCA) in commercially available software MATLAB. Furthermore, we identified 115 genes that were differentially expressed across the sample groups Arch, Nano and MI (logFC >1.5 or <1.5 and a p-value 0.05), and we performed hierarchical clustering, with complete linkage and the Euclidean distance, in the tool pheatmap in the R statistical analysis software.

5.7 Statistical analysis

Data were analyzed using GraphPad Prism software to calculate mean ± SEM, and a one-way ANOVA test (Turkey multiple comparisons) was used for comparisons of every sample. Significance was set to $p<0.05$. For gene expression for the qPCR analysis, fold changes were calculated as 2^(-Avg.ΔΔCt) and analyzed based on Qiagen web-based software.

6. Supplementary data

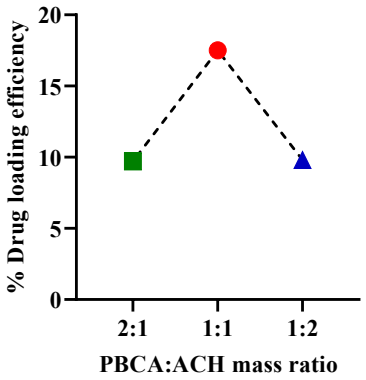

Supplementary Figure S1: Loading efficiency of ACH in PBCA-NPs. The mass ratio of PBCA to ACH taken was 2:1, 1:1 and 1:2 (n=1)

Supplementary Table S1. Loading efficiency of ACH in PBCA-NPs (n=1)

Amount of PBCA added (mg)	Amount of ACH Added (mg)	PBCA:ACH mass ratio	Loading of ACH (mg)	% Loading efficiency (LE)
20	10	2:1	0.87	8.70
10	10	1:1	1.75	17.50
10	20	1:2	0.98	9.80

Supplementary Tables S2 and S3 are found in Excel sheets.

7. Data availability

Data are available in the main article and Supplementary Information. Source data are provided in this paper.

8. Acknowledgements

We thank Associate Professor Louise Cole and Dr Amy Bottomley (Microbial Imaging Facility, UTS) for microscopy assistance. CG was supported by a UTS Seed Funding and Catholic Archdiocese of Sydney Grant for Adult Stem Cell Research, a Heart Research Institute Fellowship, Heart Research Australia, a Perpetual IMPACT Grant and the Ian Potter Foundation. XW was supported by the National Heart Foundation Future Leader Fellowship and Baker Fellowship. CLCM was supported by a NSW Waratah Scholarship.

Received: ((will be filled in by the editorial staff))
Revised: ((will be filled in by the editorial staff))
Published online: ((will be filled in by the editorial staff))

9. Biography

Miss Clara Liu Chung Ming (First Author)

Miss Clara Liu Chung Ming is a 3rd year PhD candidate in the School of Biomedical Engineering at the University of Technology Sydney. Her research focuses on the bioengineering of advanced 3D *in vitro* models of the human heart pathophysiology, including "the heart attack-in-a-Petri-dish" and heart failure using patient-derived stem cells. Clara has also developed patient-specific models using iPSCs and organoid technologies, which could translate the gap between animal models and human species. Clara's multidisciplinary project is carried out in collaboration with the University of Sydney/Charles Perkins Centre/Sydney Heart Bank, Royal Prince Alfred Hospital and Baker Heart and Diabetes Institute/Monash University.

A/Prof Xiaowei Wang (Equally Contributed Senior authors)

Associate Professor Xiaowei Wang heads the Molecular Imaging and Theranostics laboratory at the Baker Heart and Diabetes Institute and co-chairs the Atherothrombosis Program. Her work has a strong focus on translational cardiovascular research, spanning across several scientific fields, including physics, chemistry, biology and biotechnology, and uniquely combines both basic research and translational development of future diagnostic tools to be used in patients. Her research focuses on preclinical molecular imaging across a range of technologies and her other research interests are targeted drug therapy and the use of micro/nanoparticles for targeted delivery of drugs and mRNA.

Dr Carmine Gentile (Equally Contributed Senior authors)

Dr Carmine Gentile, PharmD/PhD, FAHA, leads the Cardiovascular Regeneration Group working on 3D bioprinting, organoid and stem cell technologies at the Heart Research Institute and the University of Technology Sydney. He is a Senior Lecturer (Faculty) within the School of Biomedical Engineering (Faculty of Engineering and IT) at UTS. He is an internationally recognized expert in the field of 3D bioprinting and stem cell technologies and his more recent studies focus on novel molecular and cellular approaches to treat cardiovascular disease, including myocardial infarction and heart failure. These studies are based on the use of "mini-hearts" he developed as "bioink" for human heart tissues.

10. References

[1] Cardiovascular Diseases (CVDs), 2021. https://www.who.int/news-room/fact-sheets/detail/cardiovascular-diseases-(cvds). (Accessed 3 January 2022).
[2] F. Sanchis-Gomar, C. Perez-Quilis, R. Leischik, A. Lucia, Epidemiology of coronary heart disease and acute coronary syndrome, Ann Transl Med 4(13) (2016) 256-256.

[3] B. Bhandari, B.S.Q. Rodriguez, W. Masood, Ischemic Cardiomyopathy, StatPearls [Internet] (2020).
[4] M.J. Sebastião, M. Serra, R. Pereira, I. Palacios, P. Gomes-Alves, P.M. Alves, Human cardiac progenitor cell activation and regeneration mechanisms: exploring a novel myocardial ischemia/reperfusion in vitro model, Stem Cell Research & Therapy 10(1) (2019) 77.
[5] K.O. Lui, L. Zangi, K.R. Chien, Cardiovascular regenerative therapeutics via synthetic paracrine factor modified mRNA, Stem cell research 13(3) (2014) 693-704.
[6] E.B. Brandt, S.J. Bashar, A.I. Mahmoud, Stimulating ideas for heart regeneration: the future of nerve-directed heart therapy, Bioelectronic Medicine 5(1) (2019) 8.
[7] A.I. Mahmoud, C.C. O'Meara, M. Gemberling, L. Zhao, D.M. Bryant, R. Zheng, J.B. Gannon, L. Cai, W.-Y. Choi, G.F. Egnaczyk, C.E. Burns, C.G. Burns, C.A. MacRae, K.D. Poss, R.T. Lee, Nerves Regulate Cardiomyocyte Proliferation and Heart Regeneration, Developmental cell 34(4) (2015) 387-399.
[8] K. Intachai, S. C. Chattipakorn, N. Chattipakorn, K. Shinlapawittayatorn, Revisiting the Cardioprotective Effects of Acetylcholine Receptor Activation against Myocardial Ischemia/Reperfusion Injury, International Journal of Molecular Sciences 19(9) (2018) 2466.
[9] Y. Kakinuma, M. Ando, M. Kuwabara, R.G. Katare, K. Okudela, M. Kobayashi, T. Sato, Acetylcholine from vagal stimulation protects cardiomyocytes against ischemia and hypoxia involving additive non-hypoxic induction of HIF-1α, FEBS Letters 579(10) (2005) 2111-2118.
[10] C. Rocha-Resende, A. Roy, R. Resende, M.S. Ladeira, A. Lara, E.R. de Morais Gomes, V.F. Prado, R. Gros, C. Guatimosim, M.A.M. Prado, S. Guatimosim, Non-neuronal cholinergic machinery present in cardiomyocytes offsets hypertrophic signals, Journal of Molecular and Cellular Cardiology 53(2) (2012) 206-216.
[11] C. Rocha-Resende, A.M.d. Silva, M.A.M. Prado, S. Guatimosim, Protective and anti-inflammatory effects of acetylcholine in the heart, American Journal of Physiology-Cell Physiology 320(2) (2021) C155-C161.
[12] Y.-x. Lv, S. Zhong, H. Tang, B. Luo, S.-J. Chen, L. Chen, F. Zheng, L. Zhang, L. Wang, X.-y. Li, VEGF-A and VEGF-B coordinate the arteriogenesis to repair the Infarcted Heart with vagus nerve stimulation, Cellular Physiology and Biochemistry 48(2) (2018) 433-449.
[13] B. Buchholz, M. Donato, V. Perez, A.C.R. Deutsch, C. Höcht, J.S. Del Mauro, M. Rodríguez, R.J. Gelpi, Changes in the loading conditions induced by vagal stimulation modify the myocardial infarct size through sympathetic-parasympathetic interactions, Pflügers Archiv - European Journal of Physiology 467(7) (2015) 1509-1522.
[14] L. Calvillo, E. Vanoli, E. Andreoli, A. Besana, E. Omodeo, M. Gnecchi, P. Zerbi, G. Vago, G. Busca, P.J. Schwartz, Vagal stimulation, through its nicotinic action, limits infarct size and the inflammatory response to myocardial ischemia and reperfusion, J Cardiovasc Pharmacol 58(5) (2011) 500-7.
[15] D. McAreavey, J. Neilson, D. Ewing, D. Russell, Cardiac parasympathetic activity during the early hours of acute myocardial infarction, Heart 62(3) (1989) 165-170.
[16] K. Intachai, S.C. Chattipakorn, N. Chattipakorn, K. Shinlapawittayatorn, Acetylcholine exerts cytoprotection against hypoxia/reoxygenation-induced apoptosis, autophagy and mitochondrial impairment through both muscarinic and nicotinic receptors, Apoptosis 27(3) (2022) 233-245.
[17] Z. Wang, G. Zhao, A.I. Zibrila, Y. Li, J. Liu, W. Feng, Acetylcholine ameliorated hypoxia-induced oxidative stress and apoptosis in trophoblast cells via p38 MAPK/NF-κB pathway, Molecular Human Reproduction 27(8) (2021).
[18] E. Beaumont, E.M. Southerland, J.C. Hardwick, G.L. Wright, S. Ryan, Y. Li, B.H. KenKnight, J.A. Armour, J.L. Ardell, Vagus nerve stimulation mitigates intrinsic cardiac neuronal and adverse myocyte remodeling postmyocardial infarction, American Journal of Physiology-Heart and Circulatory Physiology 309(7) (2015) H1198-H1206.
[19] B.g. Nasi-Er, Z. Wenhui, S. HuaXin, Z. Xianhui, L. Yaodong, L. Yanmei, W. Hongli, Z.l. TuEr-Hong, Z. Qina, T. BaoPeng, Vagus nerve stimulation reduces ventricular arrhythmias and increases ventricular electrical stability, Pacing and Clinical Electrophysiology 42(2) (2019) 247-256.

[20] V. Dusi, F. Angelini, G.M. De Ferrari, Vagus Nerve Stimulation for Myocardial Ischemia: The Sooner the Better, JACC Basic Transl Sci 8(9) (2023) 1119-1122.
[21] R. Zhang, N. Wugeti, J. Sun, H. Yan, Y. Guo, L. Zhang, M. Ma, X. Guo, C. Jiao, W. Xu, Effects of vagus nerve stimulation via cholinergic anti-inflammatory pathway activation on myocardial ischemia/reperfusion injury in canine, Int J Clin Exp Med 7(9) (2014) 2615.
[22] O. Islam, P. Patil, S.K. Goswami, R. Razdan, M.N. Inamdar, M. Rizwan, J. Mathew, B. Inceoglu, K.S. Stephen Lee, S.H. Hwang, B.D. Hammock, Inhibitors of soluble epoxide hydrolase minimize ischemia-reperfusion-induced cardiac damage in normal, hypertensive, and diabetic rats, Cardiovascular Therapeutics 35(3) (2017) e12259.
[23] L.V. Borovikova, S. Ivanova, M. Zhang, H. Yang, G.I. Botchkina, L.R. Watkins, H. Wang, N. Abumrad, J.W. Eaton, K.J. Tracey, Vagus nerve stimulation attenuates the systemic inflammatory response to endotoxin, Nature 405(6785) (2000) 458-62.
[24] T. Kawada, T. Yamazaki, T. Akiyama, M. Li, H. Ariumi, H. Mori, K. Sunagawa, M. Sugimachi, Vagal stimulation suppresses ischemia-induced myocardial interstitial norepinephrine release, Life sciences 78(8) (2006) 882-887.
[25] J. Sun, Y. Lu, Y. Huang, N. Wugeti, Unilateral vagus nerve stimulation improves ventricular autonomic nerve distribution and functional imbalance in a canine heart failure model, Int J Clin Exp Med 8(6) (2015) 9334-9340.
[26] S. Zafeiropoulos, U. Ahmed, A. Bikou, I.T. Mughrabi, S. Stavrakis, S. Zanos, Vagus nerve stimulation for cardiovascular diseases: Is there light at the end of the tunnel?, Trends Cardiovasc Med (2023).
[27] M.R. Gold, D.J.V. Veldhuisen, P.J. Hauptman, M. Borggrefe, S.H. Kubo, R.A. Lieberman, G. Milasinovic, B.J. Berman, S. Djordjevic, S. Neelagaru, P.J. Schwartz, R.C. Starling, D.L. Mann, Vagus Nerve Stimulation for the Treatment of Heart Failure, Journal of the American College of Cardiology 68(2) (2016) 149-158.
[28] J.S. Birks, R.J. Harvey, Donepezil for dementia due to Alzheimer's disease, Cochrane Database Syst Rev 6(6) (2018) Cd001190.
[29] C.E. Battle, A.H. Abdul-Rahim, S.D. Shenkin, J. Hewitt, T.J. Quinn, Cholinesterase inhibitors for vascular dementia and other vascular cognitive impairments: a network meta-analysis, Cochrane Database of Systematic Reviews (2) (2021).
[30] W.-x. Jian, Z. Zhang, J.-h. Zhan, S.-f. Chu, Y. Peng, M. Zhao, Q. Wang, N.-h. Chen, Donepezil attenuates vascular dementia in rats through increasing BDNF induced by reducing HDAC6 nuclear translocation, Acta Pharmacologica Sinica 41(5) (2020) 588-598.
[31] E. Kröger, M. Mouls, M. Wilchesky, M. Berkers, P.-H. Carmichael, R. van Marum, P. Souverein, T. Egberts, M.-L. Laroche, Adverse Drug Reactions Reported With Cholinesterase Inhibitors:An Analysis of 16 Years of Individual Case Safety Reports From VigiBase, Annals of Pharmacotherapy 49(11) (2015) 1197-1206.
[32] T. Isogai, H. Yasunaga, H. Matsui, H. Tanaka, T. Ueda, H. Horiguchi, K. Fushimi, Serious cardiac complications in coronary spasm provocation tests using acetylcholine or ergonovine: analysis of 21 512 patients from the diagnosis procedure combination database in Japan, Clin Cardiol 38(3) (2015) 171-7.
[33] S. Mehta, V. Bongcaron, T.K. Nguyen, Y. Jirwanka, A. Maluenda, A.P. Walsh, J. Palasubramaniam, M.D. Hulett, R. Srivastava, A. Bobik, An Ultrasound-Responsive Theranostic Cyclodextrin-Loaded Nanoparticle for Multimodal Imaging and Therapy for Atherosclerosis, Small 18(31) (2022) 2200967.
[34] A. Refaat, B. del Rosal, V. Bongcaron, A.P.G. Walsh, G. Pietersz, K. Peter, S.E. Moulton, X. Wang, Activated Platelet-Targeted IR780 Immunoliposomes for Photothermal Thrombolysis, Advanced Functional Materials 33(4) (2023) 2209019.
[35] M. Sankar, R. Karthikeyan, S. Vigneshkumar, Synthesis and Characterization of Chitosan Acetylcholine Nanoparticles for Neural Disorders Associated with Cancer Treatment, Journal of Inorganic and Organometallic Polymers and Materials 33(8) (2023) 2465-2484.
[36] L. Fan, J. Wang, F. Meng, Y. Luo, X. Sui, B. Zhao, W. Li, D. Quan, J. Yang, Y. Wang, Delivering the acetylcholine neurotransmitter by nanodrugs as an effective treatment for Alzheimer's disease, Journal of Biomedical Nanotechnology 14(12) (2018) 2066-2076.

[37] S. Gao, Y. Xu, S. Asghar, M. Chen, L. Zou, S. Eltayeb, M. Huo, Q. Ping, Y. Xiao, Polybutylcyanoacrylate nanocarriers as promising targeted drug delivery systems, Journal of Drug Targeting 23(6) (2015) 481-496.
[38] B.-L. Keller, C.A. Lohmann, S.O. Kyerematen, G. Fricker, Synthesis and Characterization of Biodegradable Poly(butyl cyanoacrylate) for Drug Delivery Applications, Polymers 14(5) (2022) 998.
[39] P. Thammasit, C.S. Tharinjaroen, Y. Tragoolpua, V. Rickerts, R. Georgieva, H. Bäumler, K. Tragoolpua, Targeted Propolis-Loaded Poly (Butyl) Cyanoacrylate Nanoparticles: An Alternative Drug Delivery Tool for the Treatment of Cryptococcal Meningitis, Frontiers in Pharmacology 12 (2021).
[40] A. Graf, A. McDowell, T. Rades, Poly (alkycyanoacrylate) nanoparticles for enhanced delivery of therapeutics–is there real potential?, Expert Opinion on Drug Delivery 6(4) (2009) 371-387.
[41] A. Evangelatov, R. Skrobanska, N. Mladenov, M. Petkova, G. Yordanov, R. Pankov, Epirubicin loading in poly (butyl cyanoacrylate) nanoparticles manifests via altered intracellular localization and cellular response in cervical carcinoma (HeLa) cells, Drug delivery 23(7) (2016) 2235-2244.
[42] E. Sulheim, H. Baghirov, E. von Haartman, A. Bøe, A.K. Åslund, Y. Mørch, C.d.L. Davies, Cellular uptake and intracellular degradation of poly (alkyl cyanoacrylate) nanoparticles, Journal of nanobiotechnology 14 (2016) 1-14.
[43] R. Rempe, S. Cramer, S. Hüwel, H.-J. Galla, Transport of Poly(n-butylcyano-acrylate) nanoparticles across the blood–brain barrier in vitro and their influence on barrier integrity, Biochemical and Biophysical Research Communications 406(1) (2011) 64-69.
[44] V. Reukov, V. Maximov, A. Vertegel, Proteins conjugated to poly(butyl cyanoacrylate) nanoparticles as potential neuroprotective agents, Biotechnol Bioeng 108(2) (2011) 243-52.
[45] C. Wang, H. Jiang, J. Zhu, Y. Jin, A new agent for contrast-enhanced intravascular ultrasound imaging in vitro: polybutylcyanoacrylate nanoparticles with drug-carrying capacity, Artificial Cells, Nanomedicine, and Biotechnology 52(1) (2024) 218-228.
[46] P. Sharma, C.L.C. Ming, X. Wang, L.A. Bienvenu, D. Beck, G.A. Figtree, A. Boyle, C. Gentile, Biofabrication of advanced in vitro 3D models to study ischaemic and doxorubicin-induced myocardial damage, Biofabrication (2022).
[47] L. Polonchuk, M. Chabria, L. Badi, J.-C. Hoflack, G. Figtree, M.J. Davies, C. Gentile, Cardiac spheroids as promising in vitro models to study the human heart microenvironment, Scientific reports 7(1) (2017) 1-12.
[48] L. Polonchuk, L. Surija, M.H. Lee, P. Sharma, C. Liu Chung Ming, F. Richter, E. Ben-Sefer, M.A. Rad, H. Mahmodi Sheikh Sarmast, W.A. Shamery, H.A. Tran, L. Vettori, F. Haeusermann, E.C. Filipe, J. Rnjak-Kovacina, T. Cox, J. Tipper, I. Kabakova, C. Gentile, Towards engineering heart tissues from bioprinted cardiac spheroids, Biofabrication 13(4) (2021) 045009.
[49] C.D. Roche, C. Gentile, Transplantation of a 3D bioprinted patch in a murine model of myocardial infarction, JoVE (Journal of Visualized Experiments) (163) (2020) e61675.
[50] C.D. Roche, H. Lin, Y. Huang, C.E. de Bock, D. Beck, M. Xue, C. Gentile, 3D bioprinted alginate-gelatin hydrogel patches containing cardiac spheroids recover heart function in a mouse model of myocardial infarction, Bioprinting 30 (2023) e00263.
[51] P. Sharma, C.L.C. Ming, X. Wang, L.A. Bienvenu, D. Beck, G. Figtree, A. Boyle, C. Gentile, Biofabrication of advanced in vitro 3D models to study ischaemic and doxorubicin-induced myocardial damage, Biofabrication 14(2) (2022) 025003.
[52] A. Roy, M. Dakroub, G.C. Tezini, Y. Liu, S. Guatimosim, Q. Feng, H.C. Salgado, V.F. Prado, M.A. Prado, R. Gros, Cardiac acetylcholine inhibits ventricular remodeling and dysfunction under pathologic conditions, The FASEB Journal 30(2) (2016) 688-701.
[53] F. Braczko, S.R. Fischl, J. Reinders, H.R. Lieder, P. Kleinbongard, Activation of the non-neuronal cholinergic cardiac system by hypoxic preconditioning protects isolated adult cardiomyocytes from hypoxia/reoxygenation injury, American Journal of Physiology-Heart and Circulatory Physiology (2024).

[54] F. Braczko, J. Reinders, H. Lieder, G. Heusch, P. Kleinbongard, The Non-Neuronal Cholinergic System is Causal for Cardioprotection by Hypoxic Preconditioning in Isolated Adult Rat Cardiomyocytes, The FASEB Journal 35(S1) (2021).
[55] Y. Kakinuma, T. Akiyama, K. Okazaki, M. Arikawa, T. Noguchi, T. Sato, A non-neuronal cardiac cholinergic system plays a protective role in myocardium salvage during ischemic insults, PLoS One 7(11) (2012).
[56] X. Hua, Y.Y. Wang, P. Jia, Q. Xiong, Y. Hu, Y. Chang, S. Lai, Y. Xu, Z. Zhao, J. Song, Multi-level transcriptome sequencing identifies COL1A1 as a candidate marker in human heart failure progression, BMC Med 18(1) (2020) 2.
[57] M.C. Mohl, S.E. Iismaa, X.-H. Xiao, O. Friedrich, S. Wagner, V. Nikolova-Krstevski, J. Wu, Z.-Y. Yu, M. Feneley, D. Fatkin, D.G. Allen, R.M. Graham, Regulation of murine cardiac contractility by activation of α1A-adrenergic receptor-operated Ca2+ entry, Cardiovascular Research 91(2) (2011) 310-319.
[58] M. Sato, B.A. Evans, A.L. Sandström, L.Y. Chia, S. Mukaida, B.S. Thai, A. Nguyen, L. Lim, C.Y.R. Tan, J.-A. Baltos, P.J. White, L.T. May, D.S. Hutchinson, R.J. Summers, T. Bengtsson, α1A-Adrenoceptors activate mTOR signalling and glucose uptake in cardiomyocytes, Biochemical Pharmacology 148 (2018) 27-40.
[59] C.A. Broomfield, D. Maxwell, R. Solana, C. Castro, A. Finger, D. Lenz, Protection by butyrylcholinesterase against organophosphorus poisoning in nonhuman primates, Journal of Pharmacology and Experimental Therapeutics 259(2) (1991) 633-638.
[60] M. Zhao, X. He, X.Y. Bi, X.J. Yu, W. Gil Wier, W.J. Zang, Vagal stimulation triggers peripheral vascular protection through the cholinergic anti-inflammatory pathway in a rat model of myocardial ischemia/reperfusion, Basic Res Cardiol 108(3) (2013) 345.
[61] W. Nuntaphum, W. Pongkan, S. Wongjaikam, S. Thummasorn, P. Tanajak, J. Khamseekaew, K. Intachai, S.C. Chattipakorn, N. Chattipakorn, K. Shinlapawittayatorn, Vagus nerve stimulation exerts cardioprotection against myocardial ischemia/reperfusion injury predominantly through its efferent vagal fibers, Basic Res Cardiol 113(4) (2018) 22.
[62] M. Forte, S. Marchitti, F. Di Nonno, R. Stanzione, L. Schirone, M. Cotugno, F. Bianchi, S. Schiavon, S. Raffa, D. Ranieri, S. Fioriniello, F. Della Ragione, M.R. Torrisi, R. Carnevale, V. Valenti, F. Versaci, G. Frati, C. Vecchione, M. Volpe, S. Rubattu, S. Sciarretta, NPPA/atrial natriuretic peptide is an extracellular modulator of autophagy in the heart, Autophagy 19(4) (2023) 1087-1099.
[63] V. Franco, Y.-F. Chen, S. Oparil, J.A. Feng, D. Wang, F. Hage, G. Perry, Atrial Natriuretic Peptide Dose-Dependently Inhibits Pressure Overload-Induced Cardiac Remodeling, Hypertension 44(5) (2004) 746-750.
[64] E. Blanco, H. Shen, M. Ferrari, Principles of nanoparticle design for overcoming biological barriers to drug delivery, Nature biotechnology 33(9) (2015) 941-951.
[65] M. Kolter, M. Ott, C. Hauer, I. Reimold, G. Fricker, Nanotoxicity of poly(n-butylcyano-acrylate) nanoparticles at the blood–brain barrier, in human whole blood and in vivo, Journal of Controlled Release 197 (2015) 165-179.
[66] A. Lundqvist, M. Sandstedt, J. Sandstedt, R. Wickelgren, G.I. Hansson, A. Jeppsson, L.M. Hultén, The Arachidonate 15-Lipoxygenase Enzyme Product 15-HETE Is Present in Heart Tissue from Patients with Ischemic Heart Disease and Enhances Clot Formation, PLoS One 11(8) (2016) e0161629.
[67] W. Cai, L. Liu, X. Shi, Y. Liu, J. Wang, X. Fang, Z. Chen, D. Ai, Y. Zhu, X. Zhang, Alox15/15-HpETE Aggravates Myocardial Ischemia-Reperfusion Injury by Promoting Cardiomyocyte Ferroptosis, Circulation 147(19) (2023) 1444-1460.
[68] X. Tian, C. Sun, X. Wang, K. Ma, Y. Chang, Z. Guo, J. Si, ANO1 regulates cardiac fibrosis via ATI-mediated MAPK pathway, Cell Calcium 92 (2020) 102306.
[69] M.T. Durand, C. Becari, M. de Oliveira, J.M. do Carmo, C.A. Silva, C.M. Prado, R. Fazan, Jr., H.C. Salgado, Pyridostigmine restores cardiac autonomic balance after small myocardial infarction in mice, PLoS One 9(8) (2014) e104476.
[70] D.-J. Li, H. Fu, J. Tong, Y.-H. Li, L.-F. Qu, P. Wang, F.-M. Shen, Cholinergic anti-inflammatory pathway inhibits neointimal hyperplasia by suppressing inflammation and oxidative stress, Redox Biology 15 (2018) 22-33.

[71] X.-M. Qiu, Z.-Z. Lai, S.-Y. Ha, H.-L. Yang, L.-B. Liu, Y. Wang, J.-W. Shi, L.-Y. Ruan, J.-F. Ye, J.-N. Wu, IL-2 and IL-27 synergistically promote growth and invasion of endometriotic stromal cells by maintaining the balance of IFN-γ and IL-10 in endometriosis, Reproduction 159(3) (2020) 251-260.
[72] D. Chen, T.-X. Tang, H. Deng, X.-P. Yang, Z.-H. Tang, Interleukin-7 biology and its effects on immune cells: mediator of generation, differentiation, survival, and homeostasis, Frontiers in immunology 12 (2021) 747324.
[73] M. Vogler, BCL2A1: the underdog in the BCL2 family, Cell Death Differ 19(1) (2012) 67-74.
[74] M. Akhavanpoor, C.A. Gleissner, S. Gorbatsch, A.O. Doesch, H. Akhavanpoor, S. Wangler, F. Jahn, F. Lasitschka, H.A. Katus, C. Erbel, CCL19 and CCL21 modulate the inflammatory milieu in atherosclerotic lesions, Drug Des Devel Ther 8 (2014) 2359-71.
[75] C. Wang, B. Shang, C. Yang, Y. Liu, X. Li, S. Wang, MicroRNA-325 alleviates myocardial fibrosis after myocardial infarction via downregulating GLI1, European Review for Medical & Pharmacological Sciences 22(16) (2018).
[76] M.G. Roman, L.C. Flores, G.M. Cunningham, C. Cheng, S. Dube, C. Allen, H. Van Remmen, Y. Bai, G.B. Hubbard, T.L. Saunders, Y. Ikeno, Thioredoxin overexpression in mitochondria showed minimum effects on aging and age-related diseases in male C57BL/6 mice, Aging Pathobiol Ther 2(1) (2020) 20-31.
[77] I. Hunter, D. Terzic, N.E. Zois, L.H. Olsen, J.P. Goetze, Pig models for the human heart failure syndrome, Cardiovascular Endocrinology & Metabolism 3(1) (2014) 15-18.
[78] P. Sharma, C. Liu Chung Ming, C. Gentile, In vitro modeling of myocardial ischemia/reperfusion injury with murine or human 3D cardiac spheroids, STAR Protoc 3 (2022) 101751.
[79] Y. Takayama, Y.S. Kida, In Vitro Reconstruction of Neuronal Networks Derived from Human iPS Cells Using Microfabricated Devices, PLoS One 11(2) (2016) e0148559.
[80] Y. Mukae, M. Itoh, R. Noguchi, K. Furukawa, K.-i. Arai, J.-i. Oyama, S. Toda, K. Nakayama, K. Node, S. Morita, The addition of human iPS cell-derived neural progenitors changes the contraction of human iPS cell-derived cardiac spheroids, Tissue and Cell 53 (2018) 61-67.
[81] K. Sakai, K. Shimba, K. Ishizuka, Z. Yang, K. Oiwa, A. Takeuchi, K. Kotani, Y. Jimbo, Functional innervation of human induced pluripotent stem cell-derived cardiomyocytes by co-culture with sympathetic neurons developed using a microtunnel technique, Biochemical and Biophysical Research Communications 494(1) (2017) 138-143.
[82] T. Krieg, Q. Qin, S. Philipp, M.F. Alexeyev, M.V. Cohen, J.M. Downey, Acetylcholine and bradykinin trigger preconditioning in the heart through a pathway that includes Akt and NOS, American Journal of Physiology-Heart and Circulatory Physiology 287(6) (2004) H2606-H2611.
[83] O.R. Rana, P. Schauerte, R. Kluttig, J.W. Schröder, R.R. Koenen, C. Weber, K.W. Nolte, J. Weis, R. Hoffmann, N. Marx, E. Saygili, Acetylcholine as an age-dependent non-neuronal source in the heart, Autonomic Neuroscience 156(1) (2010) 82-89.
[84] C.D. Roche, C. Gentile, Transplantation of a 3D Bioprinted Patch in a Murine Model of Myocardial Infarction, J Vis Exp (163) (2020).
[85] J. Hildyard, PSR_quantify macro, figshare, 2022.
[86] A. Dobin, C.A. Davis, F. Schlesinger, J. Drenkow, C. Zaleski, S. Jha, P. Batut, M. Chaisson, T.R. Gingeras, STAR: ultrafast universal RNA-seq aligner, Bioinformatics 29(1) (2013) 15-21.
[87] Y. Liao, G.K. Smyth, W. Shi, featureCounts: an efficient general purpose program for assigning sequence reads to genomic features, Bioinformatics 30(7) (2014) 923-930.
[88] M.I. Love, W. Huber, S. Anders, Moderated estimation of fold change and dispersion for RNA-seq data with DESeq2, Genome biology 15 (2014) 1-21.
[89] R.C. Team, R: A language and environment for statistical computing. R Foundation for Statistical Computing, Vienna, Austria, http://www. R-project. org/ (2016).

Contents

Supplementary Figure 1

Supplementary table S2

Click here to access/download

Supporting Information

Supplementary table S2.xlsx

Supplementary table S3

Click here to access/download

Supporting Information

Supplementary table S3.xlsx

3.3 Cardioprotective Role of ACh Against DOX-induced Myocardial Damage

Summary:

The research paper is currently under review and was submitted on 21 June 2024 to the Advanced Functional Materials journal. In this chapter, a similar concept as **Chapter 3.2**, we evaluated the role of ACh against DOX-induced cardiotoxicity (DIC) in the bioengineered CS model. The DOX-induced CS model was optimized in **Chapter 2.2**. The study aimed to evaluate Aim 3, that ACh would exert cardioprotection on DOX myocardial damage in CS, using three ACh delivery methods which are 1) the addition of free-dissolved 100μM ACh to CSs, 2) co-culturing of ACh-producing CNs with CSs and 3) delivering ACh-NPs to CSs. We showed that the addition of ACh and ACh-derived from CNs attenuated DOX-induced cell death for all cell types and restored contractile function against DIC. Moreover, our results in CSs on DOX-dependent eNOS signaling in endothelial cells are consistent with the ones in *ex vivo* DOX-treated biopsies. It is only with the use of *in vitro* CSs that we were then able to show that ACh reduced eNOS activation in endothelial cells following DOX treatment, which was associated with improved viability and contractile function. Pretreatment of ACh also countered the DOX-related downregulation of genes involved in signal transduction, ATPase function, cell cycle progression, and survival. While addition of ACh is not safe for CVD patients as injection of ACh at high doses (20μg-100μg) detects coronary artery spasms, and excess ACh in the body could lead to lacrimation, salivation, tremors, loss of motor activity, hypothermia, and tonic convulsions. In this study, we also tested our novel ACh-NPs against DIC in the CS model. Our findings demonstrated that ACh-NPs attenuated DOX-induced toxicity in endothelial cells and fibroblasts, as well as maintained the contractile function of CS. ACh-NPs could be a promising therapeutic approach against DIC. However, future work should revolve around the efficacy and delivery of ACh-NPs including improving their stability, targeting efficiency, and controlled release properties, which is necessary.

For the overall thesis, this paper supports Aim 3 and provides further evidence of the protective role of ACh.

WILEY-VCH

Acetylcholine-loaded nanoparticles protect against doxorubicin-induced toxicity in *in vitro* cardiac spheroids

Clara Liu Chung Ming[1,2], *Runali Patil*[3,4], *Sean Lal*[5], *Xiaowei Wang*[4,6,7], *Carmine Gentile*[1,2*]

1. School of Biomedical Engineering, Faculty of Engineering and Information Technology, University of Technology Sydney, Sydney, NSW, Australia.
2. Cardiovascular Regeneration Group, Heart Research Institute, Newtown, NSW 2042, Australia.
3. IIT-Bombay Monash Research Academy, IIT Bombay, Powai, Mumbai, Maharashtra 400076, India
4. Department of Medicine, Monash University, Melbourne, VIC 3800, Australia.
5. Molecular Imaging and Theranostics Laboratory, Baker Heart and Diabetes Institute, Melbourne, VIC 3004, Australia.
6. School of Medical Sciences, Faculty of Medicine and Health, University of Sydney, Camperdown, NSW 2050, Australia.
7. Department of Cardiometabolic Health, University of Melbourne, Melbourne, VIC 3010, Australia.

***Corresponding authors:** Dr Carmine Gentile, School of Biomedical Engineering, Faculty of Engineering and IT, University of Technology Sydney, Ultimo, NSW; email: carmine.gentile@uts.edu.au

Keywords: Doxorubicin, 3D *in vitro* modeling, cardiac spheroids, acetylcholine, nanoparticles

Abstract

Doxorubicin (DOX) is widely used in chemotherapy, yet it significantly contributes to heart failure-associated death. Acetylcholine (ACh) is cardioprotective by enhancing heart rate variability and reducing mitochondrial dysfunction and inflammation. Nonetheless, the protective role of ACh in countering DOX-induced cardiotoxicity (DIC) remains underexplored as current approaches to increasing ACh levels are invasive and unsafe for patients. In this study, we explore the protective effects of ACh against DIC through three distinct ACh administration strategies: *i*) freely-suspended 100μM Ach; ii) ACh-producing cholinergic neurons (CNs); or *iii*) ACh-loaded nanoparticles (ACh-NPs). These are tested in *in vitro* cardiac spheroids (CSs), which have previously been shown to approximate the complex DIC. We assess ACh's protective effects by measuring the toxicity ratio (cell death/viability), contractile activity, gene expression changes *via* qPCR and nitric oxide (NO) signaling. Our findings show that ACh effectively attenuates DOX-induced cell death and contractile dysfunction. ACh also counteracts the DOX-induced downregulation of genes controlling myocardial fibrosis, endothelial and cardiomyocyte dysfunction, and autonomic dysregulation. ACh cardioprotection against DOX is dependent on NO signaling in endothelial cells, but not in cardiomyocytes or fibroblasts. Altogether, this study shows for the first time that elevating ACh levels represents a promising therapeutic approach for preventing DIC.

1. Introduction

Doxorubicin (DOX) is an antineoplastic agent extensively employed in treating various types of cancer, such as leukemia, lymphoma, and others. [1, 2] Despite its clinical utility in oncology, DOX is notoriously associated with chronic cardiotoxicity, and it is estimated that up to 65% of oncology patients may experience DOX-induced cardiotoxicity (DIC). This leads to adverse cardiac outcomes, including reduced left ventricular ejection fraction, ventricular wall thickening, arrhythmias, and congestive heart failure (HF). [2, 3] The mechanisms involved in DIC include inhibition of autophagy, DNA/RNA damage, nitric oxide (NO) release, endothelial dysfunction, increase of inflammatory mediators, and cell death. [4] While NO produced at a standard dose in the heart maintains cardiac function and exerts anti-apoptotic effects, excess NO in endothelial cells can be detrimental, leading to cardiac dysfunction associated with increased cardiomyocyte death and endothelial dysfunction. [5] Previous studies utilizing cardiac spheroids (CS) models have elucidated that DIC is mechanistically linked to NO synthesis, through the activation of endothelial nitric oxide synthase (eNOS) *via* its phosphorylation, facilitating superoxide generation. [6] DOX-mediated redox activation of eNOS has been implicated in cardiac apoptosis and eNOS-dependent reactive oxygen species (ROS) generation, significantly contributing to myocardial dysfunction. [7] Additionally, we previously showed that DOX increased necrotic death of cardiac cells and reduced contractility function in CS via NOS signaling in cardiac endothelial cells and fibroblasts. [8]

Previous studies have demonstrated the critical role played by the neurotransmitter acetylcholine (ACh) in regulating cardiovascular health for maintaining cardiac homeostasis. [9-11] Unbalance in ACh levels is characterized by sympathetic overactivation and parasympathetic deterioration, exacerbating cardiac mortality and impeding myocardial regeneration. [12-14] Kalay et al. [15] demonstrated that carvedilol, a nonselective β-adrenoceptor antagonist, attenuated DOX-induced side effects and significantly improved the left ventricular function in patients. Additionally, Prathumsap et al. [3] reported that activation of ACh receptors protected against DOX-induced myocardial inflammation and cardiomyocyte cell death and reduced ROS levels by preventing mitochondrial dysfunction. ACh has been shown to protect against myocardial infarction [16, 17], ischemic-reperfusion injury [18-21], diabetes [22] and heart failure. [23, 24] These cardioprotective effects are associated with the restoration of autonomic balance, reduction of heart rate variability, mitigation of mitochondrial dysfunction, and attenuation of inflammatory responses. [18, 25, 26] Notably, recent studies have demonstrated ACh's efficacy in ameliorating DIC in rat models through the inhibition of NO synthase activity, diminution of DOX-induced apoptosis, and alleviation of mitochondrial dysfunction. [27-29]

However, the long-term impact of DIC and the inadequacies of current *in vitro* and *in vivo* models of the human heart fail to capture the intricate pathophysiological landscape and fully underscore the necessity for advanced modeling techniques. [30]

This study employs cardiac spheroids (CSs), 3D *in vitro* models of the human heart, which are composed of human-induced pluripotent stem cell-derived cardiomyocytes (iCMs), human coronary artery endothelial cells (HCAEC), and human cardiac fibroblasts (HCF). Following our previous research showing the feasibility of testing DOX-induced toxicity in CSs, we, therefore, use them in this study to evaluate the protective effects of ACh against DIC. We hypothesize that ACh has protective effects against DOX-induced toxicity in CSs. ACh cardioprotection was tested using approaches: *i*) either by adding freely-suspended ACh against DOX-treated CSs; *ii*) or by adding ACh-producing iPSC-derived cholinergic neurons (CNs) to CSs (CN-CSs). To prevent ACh hydrolyses and its multitarget effects in the human body [31, 32], we developed novel ACh-loaded nanoparticles (ACh-NPs) made of poly-butylcyanoacrylate (PBCA) to deliver ACh in small doses and to target the injured area. PBCA-NPs have been thoroughly developed as a drug delivery system for cancer chemotherapy [33-35] and to pass through the brain-blood barrier [36, 37]. Wang et al. [38] demonstrated that PBCA-NPs are safe, non-toxic, stable and can release the encapsulated drug in primary rat aortic endothelial cells to treat atherosclerosis. Given their unique properties, our third (*iii*) approach to delivering ACh was based on the addition of ACh-NPs to DOX-treated CS.

Our analytical approach to assess ACh cardioprotection included toxicity ratio (dead/live cells), colocalization of a cell death marker in the three cell types, contractile activity, and gene expression analysis *via* qPCR. Furthermore, we aimed to juxtapose our DOX-treated CSs model with human heart tissue specimens, including healthy cardiac tissue, DOX cardiomyopathy, ischemic heart disease (IHD), and dilated cardiomyopathy (DCM), focusing on NOS signaling. This comprehensive study aims to elucidate the cardioprotective potential of ACh and to develop a novel and efficient therapeutic approach using ACh-NPs at the early stage of DIC.

2. Results

2.1 Addition of ACh protects against DOX-induced toxicity and reduction in contractile activity

To evaluate the cardioprotective effects of ACh against DOX-induced toxicity, we added freely-suspended 100 μM ACh to DOX-treated for 24 hours. We measured the toxicity ratio (dead/live cells) in CSs by staining dead cells with ethidium homodimer and live cells with calcein-AM. As shown in **Figure 1A-B**, the addition of ACh significantly reduced cell death

and increased cell viability in DOX-treated CSs, while atropine (an ACh antagonist) counteracted ACh's protective effects.

Subsequently, we colocalized ethidium homodimer as a marker of cell death with cell-specific markers to identify cell-specific responses to ACh cardioprotection using IMARIS 3D rendering software. Our findings showed that ACh significantly attenuated DOX-induced death of cardiomyocytes (**Figure 1C**), endothelial cells (**Figure 1D**) and cardiac fibroblast (**Figure 1E**). The addition of atropine counteracted ACh's effect, resulting in a significant increase in cardiomyocyte cell death in DOX-treated CSs, with no significant changes in cardiac endothelial cells and fibroblasts.

To evaluate any effects of ACh on DOX-induced reduction in CS contractile activity, we measured their contraction frequency and fractional shortening % (FS%) [8]. Our results showed that ACh protected against DOX-induced reduction in FS% while the addition of atropine counteracted ACh's protective effects (**Figure 1H**). ACh did not significantly improve contraction frequency in DOX-treated CSs (**Figure 1G**). To identify the mechanisms regulating ACh cardioprotection, we performed qPCR analyses of genes regulating cardiovascular pathophysiology (**Table 1**). ACh significantly reversed DIC-induced upregulation of cardiac remodeling genes, such as matrix metallopeptidase 13 (MMP13) and renin (REN), indicative of extracellular matrix (ECM) protein degradation. Additionally, ACh reduced the DOX-induced increase of SNCA (alpha-synuclein) mRNA levels, which regulates apoptosis. The addition of ACh to DOX-treated CSs also increased phosphodiesterase 5A (PDE5A), which controls the β-adrenergic system.

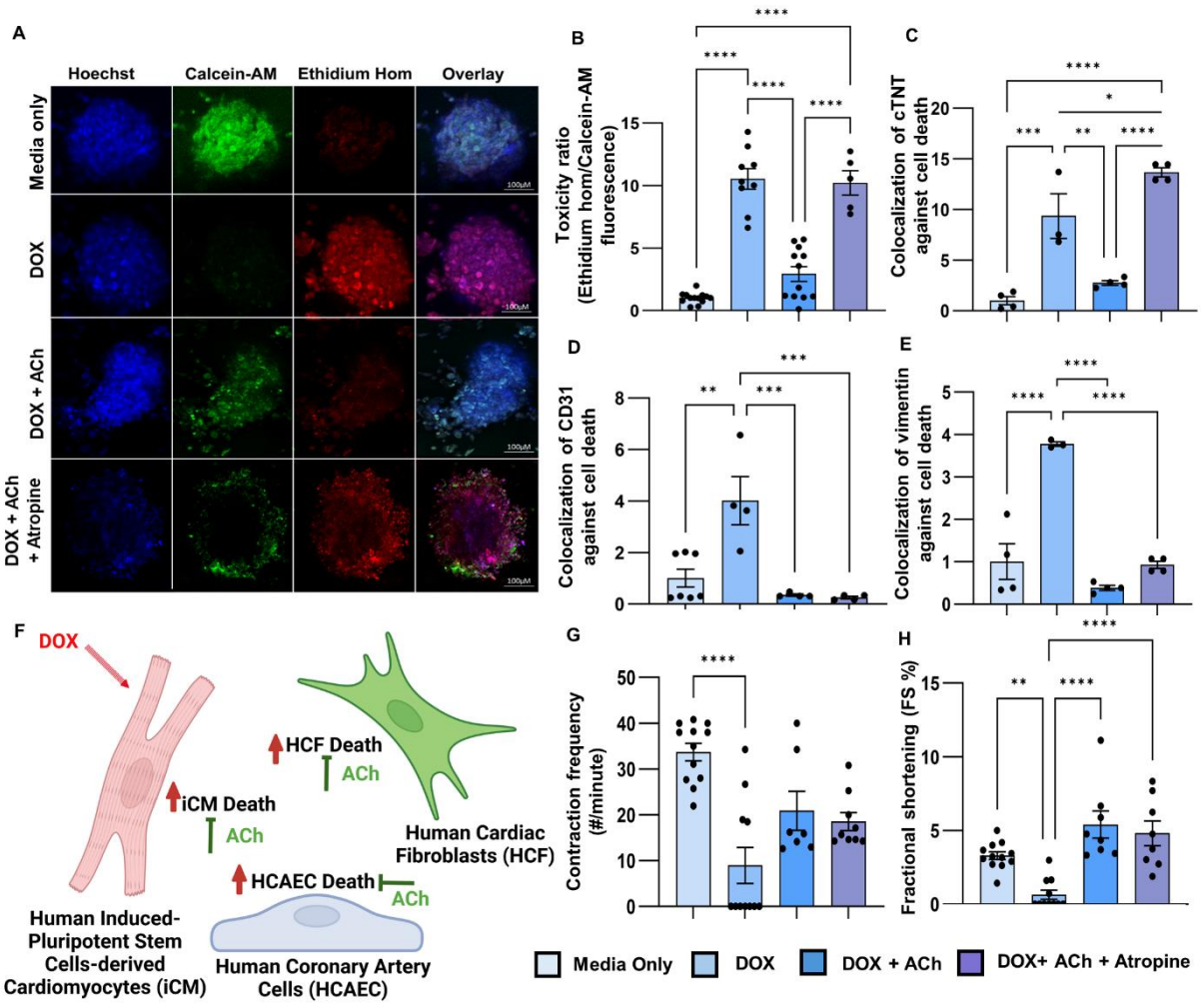

Figure 1. Protective role of addition of 100 µM ACh against DOX CS. A) Confocal stack images of CSs treated as follows: *i*) media only (control); *ii*) 10µM DOX; *iii*) 10µM DOX + 100µM ACh; and *iv*) 10µM DOX + 100µM ACh + 50µM atropine. CSs were stained with Hoechst (blue, nuclei), calcein-AM (green, live cells) and ethidium homodimer (red, dead cells). The magnification bars equal 100µm. B) Toxicity ratio (dead cells/ live cells, normalized against control); N≥5. C) Colocalization of cTNT-positive cells (iCMs) and cell death (ethidium homodimer) in CSs; N≥3. D) Colocalization of CD31-positive cells (HCAECs) and cell death (ethidium homodimer) in CSs; N≥3. E) Colocalization of vimentin-positive cells (HCFs) and cell death (ethidium homodimer) in CSs; N≥3. F) Schematic illustration of the protective effects of ACh against DOX based on the colocalization measurements in (C-E). G) Fractional shortening % (FS%) in CSs; N>7. H) Contraction frequency of CS; N>7. B-E and G-H) Data are presented as individual points and mean ± SEM, with error bars indicating the standard error of the mean. Statistical significance is denoted as P< 0.05 = *, p<0.01 = **, p<0.001 = *** and p<0.0001 = ****, analyzed using One-way ANOVA followed by Tukey's multiple comparisons tests (normalized against control except for G and H).

Table 1. qPCR relative expression of statistically significant changes for cardiac remodeling, apoptotic, and signal transduction genes of addition of ACh in DOX-induced CS. Fold change values and p-values for gene expression changes for DOX and DOX + ACh when compared to the control group (media only). Downregulated genes are indicated in blue, whereas upregulated genes are indicated in red. P-values were calculated using two-way ANOVA test with Tukey's multiple comparisons test, $p<0.05$ = ∗ and $p < 0.0001$ = ∗∗∗∗, (n = 3).

Classification of genes	Symbol	Comparing to Control		Comparing to Control	
		DOX		DOX + ACh	
		Fold Change	P-Value	Fold Change	P-Value
Cardiac Remodelling Genes	MMP13	13.74	<0.0102 (*)	0.18	0.9916
	REN	134.16	<0.0001 (****)	0.18	0.999
Apoptotic Genes	SNCA	125.37	<0.0001 (****)	0.18	0.998
Signal Transduction Genes	PDE5A	1.15	>0.9999	13.74	<0.0001 (****)

2.2 Cholinergic neurons (CNs) protect against DOX-induced toxicity and reduction in contractile activity

We next sought to elucidate the cardioprotective role of ACh-derived from cholinergic nerves against DOX by co-culturing CNs with CSs (CN-CSs). As illustrated in **Figure 2A**, viable cells stained with calcein-AM and dead cells stained with ethidium homodimer either in the presence or absence of DOX when CNs were added to CSs. These observations were confirmed by our statistical analysis of the toxicity ratios (**Figure 2B**). Atropine significantly increased the toxicity ratios in DOX-treated CSs (**Figures 2A-B**), supporting an ACh-dependent protective effect. After the colocalization of ethidium homodimer (cell death marker) with cell-specific markers in CN-CSs, we measured no significant changes in cell death for cardiomyocytes (**Figure 2C**), endothelial cells (**Figure 2D**), fibroblasts (**Figure 2E**), and CNs (**Figure 2F**) following DOX treatment. On the contrary, atropine increased DOX-induced toxicity in CN-CSs specifically in endothelial cells (**Figure 2D**).

The addition of CNs to DOX-treated CSs also prevented any changes in contraction frequency (**Figure 2G**) and FS% (**Figure 2H**), while atropine significantly reduced contractile activity in CN-CSs (**Figures 2G-H**).

When we measured changes in gene expression levels, monoamine oxidase-A (MAOA) was significantly increased in DOX-treated CN-CSs compared to CN-CSs (**Table 2**). MAO controls the breakdown of other neurotransmitters, such as serotonin, epinephrine, norepinephrine, and dopamine. Following the addition of DOX to CN-CSs, we also measured an upregulation in adrenergic receptors ADRA1A and ADRA1D, which regulate catecholamines, norepinephrine and epinephrine signaling. DOX also upregulated phosphodiesterase 3B (PDE3B), which regulates lipolysis, energy homeostasis and insulin secretion, in CN-CSs.

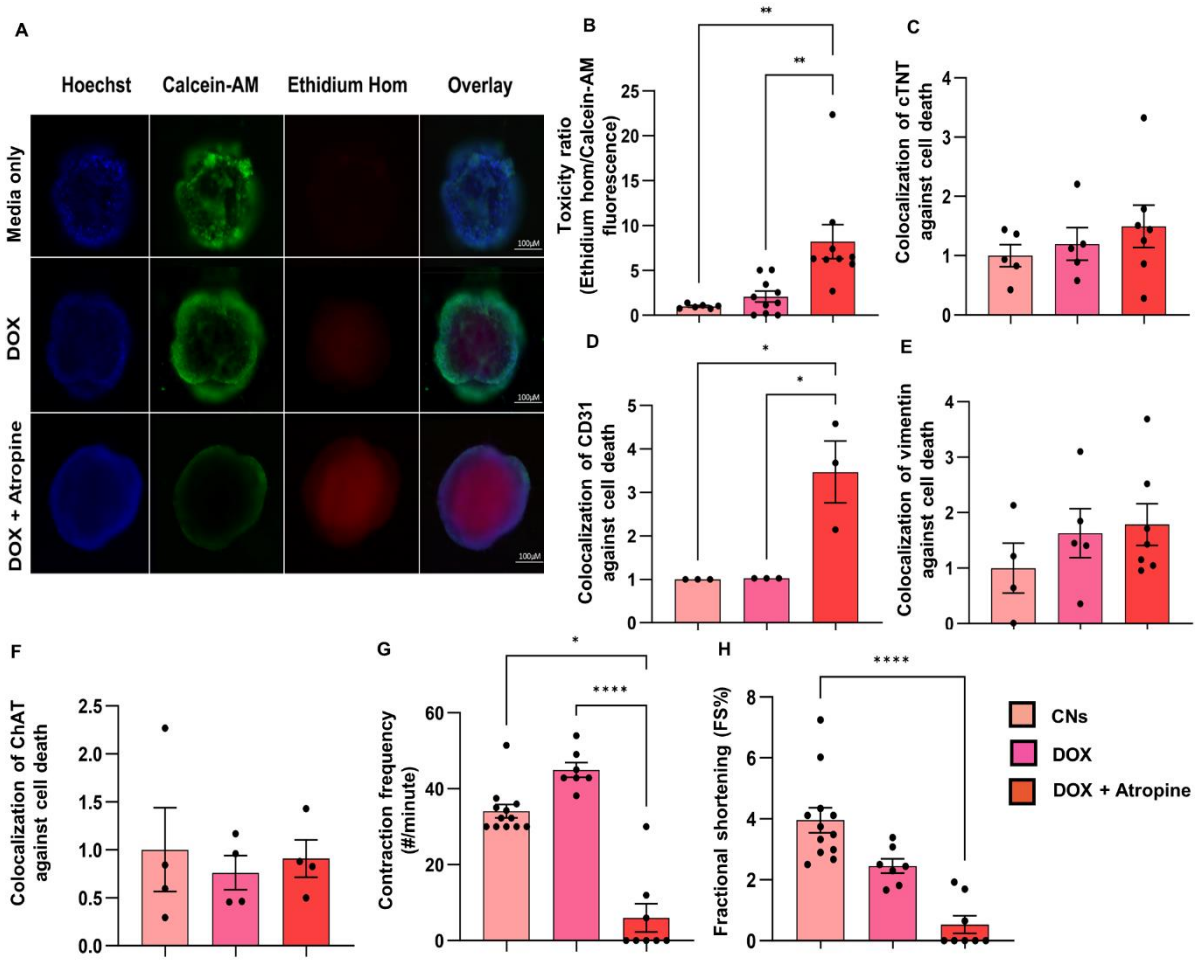

Figure 2. Protective role of ACh-producing CNs against DIC in CN-CSs. A) Epifluorescence stack images of CN-CSs treated as follows; *i*) media only (control); *ii*) 10µM DOX; *iii*) 10µM DOX + 50µM atropine. CN-CSs were stained with Hoechst (blue, nuclei), calcein-AM (green, live cells) and ethidium homodimer (red, dead cells). The magnification bars equal 100µm. B) Toxicity ratio (dead cells/ live cells, normalized against control); N≥6.

C) Colocalization of cTNT-positive cells (iCMs) and cell death (ethidium homodimer) in CN-CSs; N≥4. D) Colocalization of CD31-positive cells (HCAECs) and cell death (ethidium homodimer) in CN-CSs; N=3. E) Colocalization of vimentin-positive cells (HCFs) and cell death (ethidium homodimer) in CN-CSs; N≥4. F) Colocalization of ChAT expression in CNs and cell death (ethidium homodimer) in CN-CSs; N=4. G) Contraction Frequency of CN-CSs; N≥7. H) FS% analysis of CN-CSs; N≥7. B-H) Data are presented as individual points and mean ± SEM, with error bars indicating the standard error of the mean. Statistical significance is denoted as P< 0.05 = *, p<0.01 = **, p<0.001 = *** and p<0.0001 = ****, analyzed using One-way ANOVA followed by Tukey's multiple comparisons tests (normalized against control except for G and H).

Table 2 illustrates qPCR relative expression of significant changes for cardiovascular genes and signal transduction genes of DOX-induced in CN-CSs. Fold change values and p-values for gene expression changes for DOX when compared to the control group (media only). Upregulated genes are indicated in red. P-value was found using one-way ANOVA test with Tukey's multiple comparisons test, p < 0.0001 = ****, (n = 3).

Classification of genes	Symbol	Comparing to Control	
		CNs + DOX	
		Fold Change	P-Value
Cardiovascular Genes	MAOA	121.08	<0.0001 (****)
Signal Transduction Genes	ADRA1A	134.24	<0.0001 (****)
	ADRA1D	237.35	<0.0001 (****)
	PDE3B	88.30	<0.0001 (****)

2.3 ACh-NPs protect against DOX-induced cell death and reduction in contraction function

Given the fact that ACh hydrolyses rapidly and higher doses might be used to achieve the desired biological response, there is a high chance that systemic ACh administration could lead to undesired side effects, including lacrimation, salivation, tremors, loss of motor activity, hypothermia, and tonic convulsions. [39] To deliver ACh in a targeted manner and prevent its

potential side effects in other tissues and organs, while also reducing its dose, we generated a novel therapeutic approach for ACh delivery in combination with PBCA-NPs. ACh-NPs were created by loading ACh in PBCA-NPs, with a loading efficacy of 17.50% (**Supplementary Figure S1 and Supplementary Table S1**). As indicated in **Figures 3A-B**, ACh-NPs significantly mitigated DOX-induced toxicity in CSs, while control PBCA-NPs (which did not contain any ACh) had no significant protective effects. After our colocalization of DOX-treated CSs with ethidium homodimer (cell death) and antibodies against the three cell types, we found that ACh-NPs significantly attenuated cell death in endothelial cells (**Figure 3D**) and fibroblasts (**Figure 3E**), while this effect was not statistically significant in cardiomyocytes (**Figure 3C**). The protection provided by ACh-NPs against cell death was supported by similar effects on contractile frequency and FS% (**Figures 3F and 3G**).

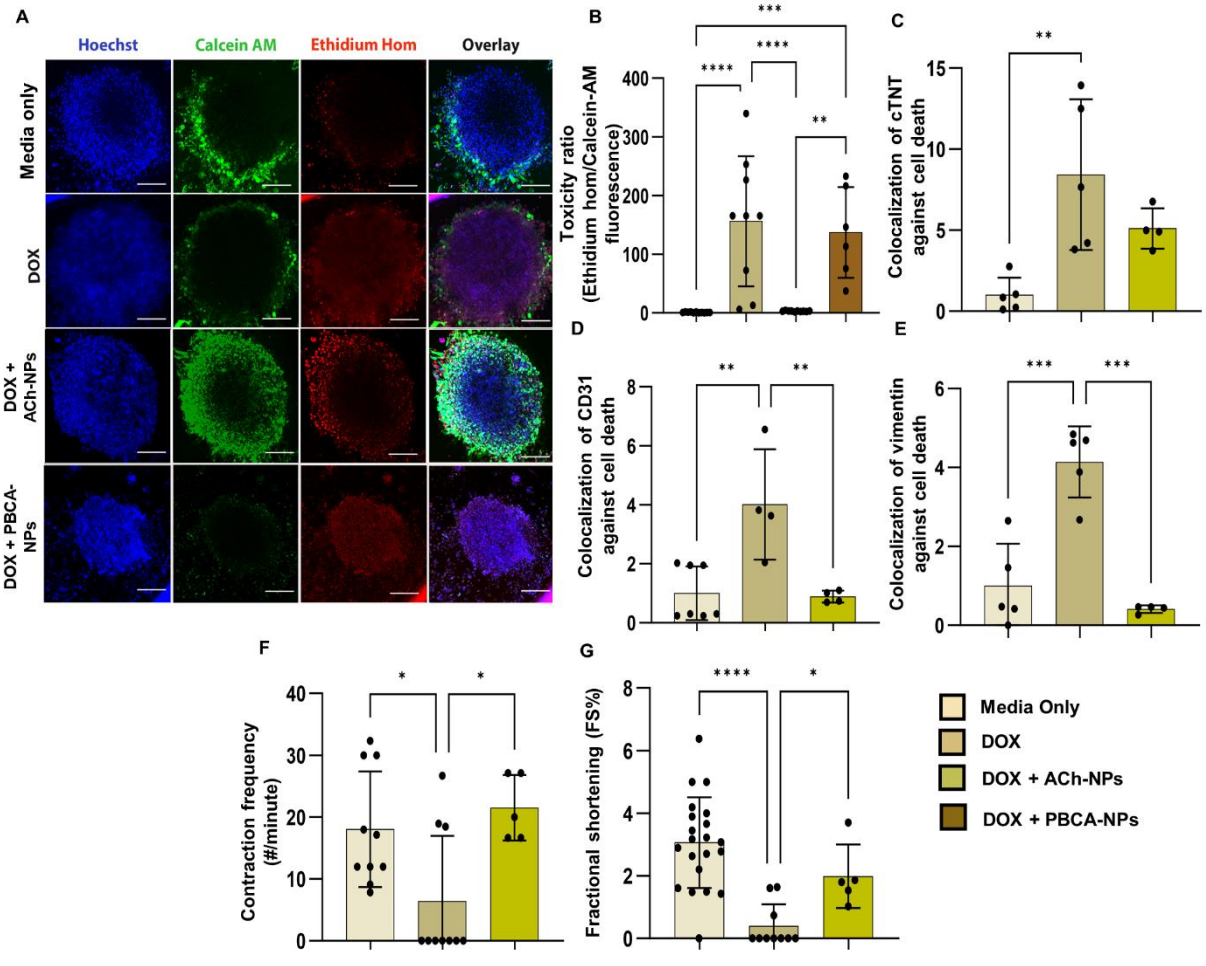

Figure 3. Protective role of ACh-NPs against DOX CS. A) Confocal stack images of CSs treated as follows: *i*) media only (control); *ii*) 10µM DOX; *iii*) 10µM DOX + ACh-NPs; and *iv*) 10µM DOX + PBCA-NPs. CSs were stained with Hoechst (blue, nuclei), calcein-AM (green, live cells) and ethidium homodimer (red, dead cells). The magnification bars equal 100µm. B)

Toxicity ratio (dead cells/ live cells, normalized against control); N≥7. C) Colocalization of cTNT-positive cells (iCMs) and cell death (ethidium homodimer) in CSs; N≥4. D) Colocalization of CD31-positive cells (HCAECs) and cell death (ethidium homodimer) in CSs; N≥4. E) Colocalization of vimentin-positive cells (HCFs) and cell death (ethidium homodimer) in CSs; N≥4. F) FS% in CSs; N≥5. G) Contraction Frequency in CSs; N≥5. B-G) Data are presented as individual points and mean ± SEM, with error bars indicating the standard error of the mean. Statistical significance is denoted as P< 0.05 = *, p<0.01 = **, p<0.001 = *** and p<0.0001 = ****, analyzed using One-way ANOVA followed by Tukey's multiple comparisons tests (normalized against control except for F and G).

2.4 ACh inhibits phosphor-eNOS expression in endothelial cells of DOX-treated CSs

We previously identified NO through the activation of eNOS signaling as a major regulator of DOX-induced toxicity in endothelial cells and fibroblasts in CSs. [6] Therefore, we investigated whether ACh could inhibit NO signaling following DOX treatment in CS (**Figure 4A**). We, therefore, measured any changes in intracellular NO production using DAF-FM, which becomes fluorescent in the presence of NO within cells. ACh did not significantly decrease the overall NO in CSs (**Supplementary Figure S2**). However, after colocalizing antibodies against activated eNOS (phospho-eNOS) and antibodies staining cell-specific markers, ACh significantly inhibited eNOS activation in endothelial cells (**Figure 4B-E**), suggesting that ACh protection against DOX toxicity in CSs is dependent on NO signaling within endothelial cells. This is consistent with previous findings highlighting a dual role of NO in being both cardioprotective at homeostasis and cardiotoxic when exacerbated to high levels, especially in the generation of peroxynitrite. [6]

To potentially translate our *in vitro* findings to human heart samples, we stained human heart biopsies from the Sydney Heart Biobank with antibodies against phospho-eNOS and antibodies against the markers of the three cell types in CSs (**Supplementary Figure S3**). Consistent with our *in vitro* results in CSs, DOX significantly increased phospho-eNOS expression in endothelial cells in human heart tissues (**Supplementary Figure S3C**). Altogether, our *in vitro* and *ex vivo* findings support that ACh is cardioprotective against DOX by inhibiting eNOS signaling in endothelial cells.

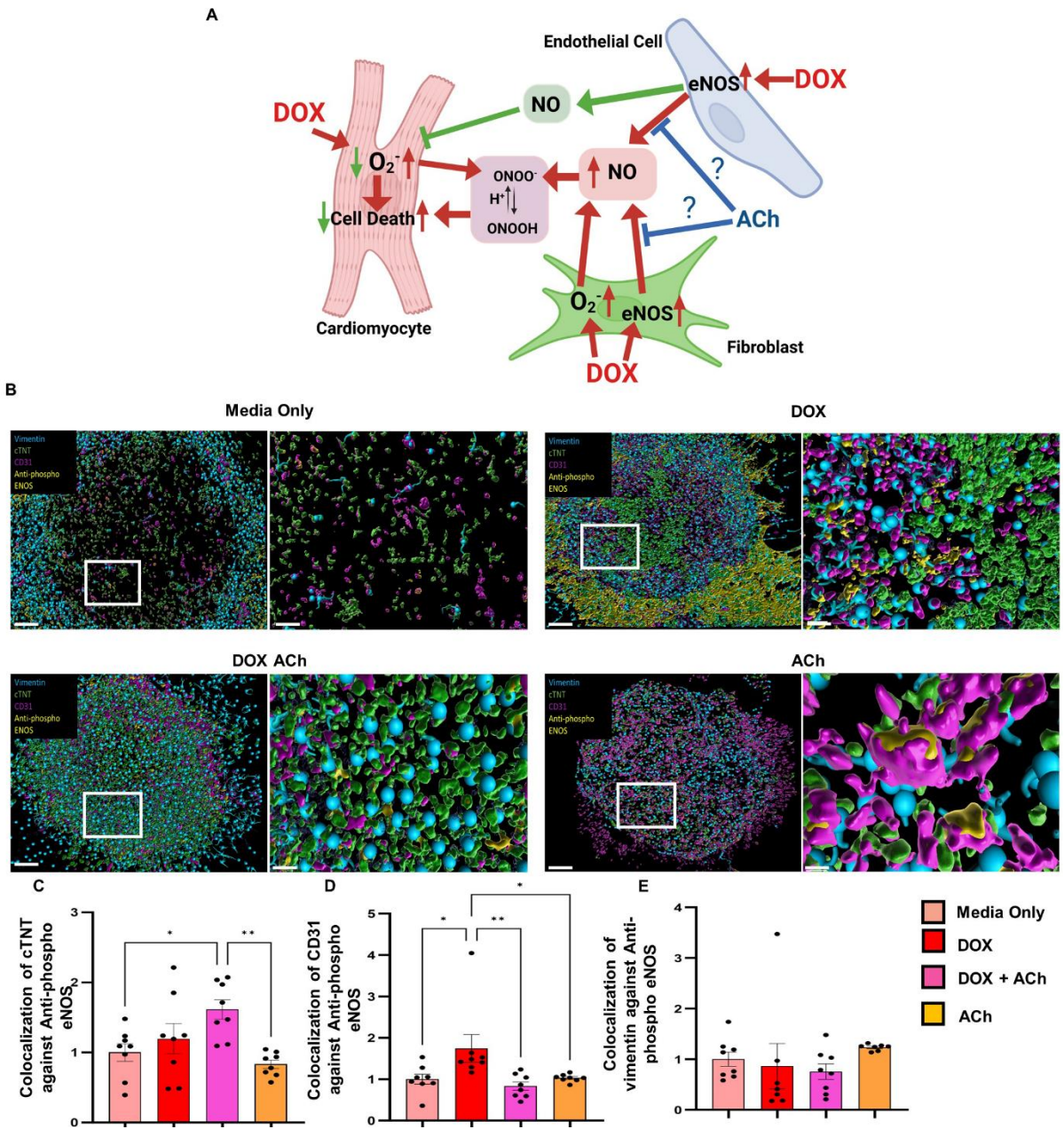

Figure 4. Effect of ACh on nitric oxide synthase through eNOS pathway. A) Schematic illustration of DOX-induced cell death in CSs dependent on eNOS signaling and potential ACh-mediated protection in endothelial cells and fibroblasts *via* eNOS inhibition. B) 3D rendering images of the three cell types of CS against ENOS. Samples are as follows: *i*) media only (control); *ii*) 10μM DOX; *iii*) 10μM DOX + 100μM ACh; and *iv*) 100μM ACh. CSs were stained with vimentin (cyan, HCF), cTNT (green, iCMs), CD31 (magenta, HCAECs), and anti-phospho eNOS (yellow, eNOS) in CS. Magnification bars are 100μm and 20μm. C) Colocalization of cTNT against anti-phospho ENOS in CS; N≥9. D) Colocalization of CD31 against anti-phospho ENOS in CS; N≥7. E) Colocalization of vimentin against anti-phospho ENOS in CS; N≥6. C-E) Data are presented as individual points and mean ± SEM, with error

bars indicating the standard error of the mean. Statistical significance is denoted as P< 0.05 = *, p<0.01 = **, p<0.001 = *** and p<0.0001 = ****, analyzed using One-way ANOVA followed by Tukey's multiple comparisons test (normalized against control).

3. Discussion

Previous studies showed that ACh is protective against cardiovascular disease [18, 22, 24, 40], Alzheimer's disease [41-43] and dementia. [44, 45] Increasing ACh levels through vagus nerve stimulation (VNS) and cholinesterase inhibitors, such as donepezil, are cardioprotective against DIC by improving mitochondrial function, reducing cardiomyocyte apoptosis and improving left ventricles function in rat models. [3, 27-29] However, VNS is an invasive surgical procedure [46], and cholinesterase inhibitors lead to adverse drug reactions, including tiredness, panic, sweating, diarrhea, vomiting, muscle tension, speech difficulty, and involuntary tremors. [47] VNS protects against endothelial dysfunction [48] and prevents contractile dysfunction in DOX-induced rat models. [40, 49] However, clinical trials using ACh and VNS have shown mixed results, mostly due to the lack of a systematic approach in the experimental plan. [32] We have previously shown that CSs can be used to study DOX-induced toxicity and potentially prevent its toxic effects by inhibiting downstream signaling pathways by using either pharmacological or genetic inhibition. [6] In this study, we demonstrated that the addition of ACh through the three delivery methods reduced total cell death (**Figures 1-3**). However, ACh-NPs predominantly reduced cell death in endothelial cells and fibroblasts (**Figure 3**), which is consistent with our previous findings in CSs [6], where eNOS signaling inhibition reduced DOX-induced toxicity from both cell types. Additionally, ACh-NPs also protected against the reduction in contraction frequency and FS% (Figure 3).

Our results in CSs on DOX-dependent eNOS signaling in endothelial cells are consistent with the ones in *ex vivo* DOX-treated biopsies (**Figure 4 and Supplementary Figure S3**). It is only with the use of *in vitro* CSs that we were then able to show that ACh reduced eNOS activation in endothelial cells following DOX treatment [6], which was associated with improved viability and contractile function (**Figure 1**). Our findings are consistent with previous studies. At physiological concentrations, NO plays a protective role in the heart when synthesized by eNOS in both cardiomyocytes and endothelial cells. [50] NO release from vascular eNOS regulates myocyte relaxation, diastolic function and vascular function. [51-53] It also plays a crucial role in cardiomyocyte functions, such as ion channel regulation, contractility, Ca^{2+} homeostasis, cell growth and survival. [54] Nevertheless, excessive eNOS activation in endothelial cells can trigger DOX-induced toxicity in cardiomyocytes. [6] Kalivendi et al. [55] demonstrated that inhibiting

eNOS in endothelial cells attenuated DOX-induced ROS production and apoptosis. Kuwabara et al. [56] reported that increasing ACh in cardiomyocytes during hypoxia led to an increase in NO production, which activated the production of vascular endothelial growth factor (VEGF) and accelerated angiogenesis. [56] Oikawa et al. [5] showed that knocking down a heart-specific choline acetyltransferase (ChAT) leads to a significant decrease in NO production in cardiomyocytes and cardiac dysfunction in mice.

Our results also suggested that ACh protected CSs against DIC by inhibiting ECM protein degradation, myocardial fibrosis and cardiac remodeling through MMP-13 (**Table 1**). DOX upregulates MMP-13 expression, which is also a typical feature of vascular disease, myocardial fibrosis and cardiac remodeling. [57-60] Furthermore, the administration of ACh reduced the overexpression of the SNCA (**Table 1**), which is a common biomarker for Parkinson's disease and is highly expressed in patients with stroke or atrial fibrillation, impairing the autonomic system by increasing norepinephrine levels and inhibiting ACh-induced relaxation. [61] Studies have also shown that DIC causes a shift in the autonomic balance toward sympathetic predominance [27, 62] and has an atropine-like inhibitory effect on cardiac ACh receptor signaling, drastically reducing cardiac contractility and heart rate. [3, 63] Our results demonstrated that increasing ACh in DOX-treated CSs led to the upregulation of PDE5A expression (**Table 1**), which activates β-adrenergic receptors and is responsible for pressure overload in the heart. [64, 65] We also measured an upregulation of MAOA and adrenergic receptors, including ADRA1A and ADRA1B, in ACh-derived CNs exposed to DIC (**Table 2**). These genes are associated with the sympathetic nervous pathway, and the elevation of catecholamines, epinephrine, and norepinephrine are hallmarks of many cardiovascular disorders. [66] Moreover, emerging evidence suggests that ADRA1A could provide cytoprotective effects by enhancing contractility [67] and activating glucose intake [68] in cardiomyocytes.

In this study, we demonstrated for the first time a novel therapeutic approach using ACh-NPs that has shown to be promising in improving contractile function and reducing necrotic death in endothelial cells and fibroblasts against DOX-induced CSs (**Figure 3A**). To ensure specificity to ACh in any effects of ACh-NPs in CSs and not to the PBCA-NPs themselves, we also tested the effects of PBCA-NPs (without any ACh), as a negative control. [69] Our findings indicated that PBCA-NPs had no effects (**Figure 3A**). However, further studies are required to explore the protective role of ACh-NPs specifically in cardiomyocytes and their long-term effects. Future work should also revolve around the efficacy and delivery of ACh-NPs including improving their stability, targeting efficiency, and controlled release properties, which is necessary.

One of the limitations of our study is the potential variability in the response of CS models compared to *in vivo* conditions. While CSs effectively mimic human heart tissue pathophysiology, they still lack features that are dependent on blood flow multi-organ responses. For instance, future studies using CSs to study DOX-induced toxicity could include other cell types, such as inflammatory, immune and sympathetic neuron cells, and dynamic conditions, such as blood flow and paracrine effects, for a more comprehensive understanding of mechanisms regulating DOX-induced toxicity. Future studies evaluating DOX-induced toxicity on both heart and cancer tissues could facilitate the optimal dosage of DOX to be delivered to patients in conjunction with the cardioprotective activity of ACh-NPs. Other limitations include administering ACh-NPs before inducing DOX myocardial damage in CSs, while DOX can take years in developing heart failure in cancer patients. [70] Hence, assessing the optimal efficacy of the timing for the delivery of ACh-NPs in cancer patients will be critical. Furthermore, it will be critical to test the optimal delivery method for ACh-NPs, whether this will be intravenously or directly in the myocardium. Lastly, while our *in vitro* models have demonstrated promising results, there is a significant gap in translating these findings to clinical settings. The complexity of human CVD may not be fully replicated in *in vitro* CSs, and there may be species-specific and sex-specific differences in response to ACh treatments. Future work could include *in vivo* experimentation in small and large animals to evaluate any protective effects of ACh-NPs on cardiac functions. [77]

4. Conclusions

In conclusion, our study highlights the potential of increasing ACh levels as a therapeutic strategy against DIC and underscores the utility of the CS model in advancing our understanding of cardiac protection mechanisms. Our findings support the protective role played by ACh against DOX-induced toxicity, reduction in contractile function and progression to HF. We also showed for the first time that ACh-NPs could be a promising therapeutic approach to attenuate DOX-induced cell death in endothelial cells and fibroblasts and prevent contractile dysfunction. However, future studies are required to identify the optimal dosage and delivery method of ACh-NPs to translate our *in vitro* findings from the bench tot he bedside.

5. Methods and Materials

The Human Ethics Committee of the University of Technology Sydney and Sydney Human Heart Biobank, University of Sydney (HREC 2021/122), approved the use of human left

ventricle myocardial tissue samples (UTS HREC REF NO. ETH21-5968, approved till 27/05/26). Human heart samples were from donor hearts that were not used for heart transplantation because of primarily logistical reasons. Anatomical pathology confirmed these tissues were normal. Heart failure samples were from patients with end-stage heart failure undergoing heart transplantation. Donor and heart failure samples were flash-frozen within 15 minutes of procurement.

5.1 Drugs and reagents

Cell culture: L-glutamine solution, penicillin-streptomycin and fibronectin bovine plasma were purchased from Sigma-Aldrich (catalogue number: G8540, P4458 and 10838039001, respectively). Cardiomyocytes iCell plating medium and iCell maintenance culture medium were purchased from Fujifilm Cellular Dynamics (catalog number: R1017). Laminin (Natural Mouse) was purchased from Thermo Fisher Scientific (catalog number: 23017015), and maintenance medium iN1(AP) was purchased from Elixirgen Scientific (catalog number: CH-MM)

Drugs: Acetylcholine chloride was used at 100µM (catalog number: A266), Doxorubicin hydrochloride was used at a concentration of 10µM (catalog number: D1515), and Atropine was used at 50µM (catalog number: PHR3846) were purchased from Sigma-Aldrich.

Antibodies: Primary antibody purified mouse anti-human CD31 (BD Bioscience, catalog number: 550389) were used to immunolabelled HCAEC. Secondary antibody Alexa fluor® 647 affinipure™ goat anti-mouse IgG (H+L) (catalog number: 115-605-003), Alexa fluor® 790 affinipure™ Goat Anti-Mouse IgG (H+L) (catalog number: 115-655-146) and Alexa fluor® 647 affinipure™ Goat Anti-Rabbit IgG (H+L) (catalog number: 111-605-003) were purchased from Jackson ImmunoResearch. Alexa fluor® 488 mouse monoclonal (vimentin - cytoskeleton marker) was purchased from Abcam (catalog number: AB195877), and Troponin T-C (CT3) Alexa fluor® 546 was purchased from Santa Cruz (catalog number: sc-20025). Anti-choline acetyltransferase (ChAT) rabbit anti-human primary antibody from Sigma-Aldrich (catalog number: SAB5701171).

5.2 Generation of human cardiac spheroids (CSs) and CSs with cholinergic neuronal cells (CNs)

Human induced pluripotent stem cell-derived cardiomyocytes (iCMs) were obtained from Cellular Dynamics (catalog number: R1017). Human cardiac fibroblasts (HCF) and human coronary artery endothelial cells (HCAEC) were purchased from Cell Applications, Inc. (catalog numbers: 306-05A and 300-05A, respectively). Cells were plated and cultured according to the supplier's instructions. Briefly, HCFs were cultured in cardiac fibroblast

growth medium, and HCAECs were cultured in human MesoEndo Cell Growth Medium (Cell Applications, Inc, catalog number 316-500 and 212-500, respectively). L-glutamine–penicillin–streptomycin solution (1%) was added to both media for nutrient enrichment. According to the manufacturer's guidelines, iCMs were cultured in iCell plating medium and iCell maintenance culture medium in fibronectin pre-coated culture flasks (Cellular Dynamics, catalog number: R1017).

Human CSs were generated using the methodologies previously outlined. [71, 72] In summary, the monolayer cell cultures were passaged with trypsin-EDTA (Sigma-Aldrich; catalog number: T4049) and TrypLE™ Express Enzyme (Thermofisher Scientific; catalog number: 12604021) for iCMs and then counted with trypan blue solution (Thermofisher Scientific; catalog number: 15250061). The cells were then mixed accordingly based on the chosen cellular ratio of 2:1:1 (iCMs:HCF: HCAEC), which has proven effective in mimicking the human heart's microenvironment and were centrifuged at 300g for 5 minutes. The cell pellet was resuspended in 190µl of CS media, which is made up of iCMs media: HCF media: HCAEC media (2:1:1, respectively) and was plated in molten agarose 3D Petri dishes (81 wells) (**Figure 5.I**). Prior to that, the 3D Petri dishes were cast using micro-mold 3D Petri Dish® Microtissues® (Sigma-Aldrich, catalog number: Z764027), following the manufacturer's guidelines using 2% agarose (Sigma-Aldrich, catalog number: A4718) and diluted in PBS (Sigma-Aldrich, catalog number: D8537). To equilibrate the 3D Petri dishes, they were submerged in cell culture medium and left in the incubator (37°C, 5%O_2, 5%CO_2) overnight before use. Each CS contained 30,000 cells and was generated by co-culturing 15,000 iCMs (three days post-thaw) with 7500 HCF and 7500 HCAEC, the co-culture medium, a blend tailored to the cellular components, facilitated spheroid formation within three days, with media replacements every two days (**Figure 5.II**).

To evaluate the impact of ACh-producing CNs, iCMs, HCAEC and HCF were co-cultured with Quick-Neuron Cholinergic-Human iPSC-derived Neurons (F, 74yr donor) (Elixirgen Scientific, catalog number: CHSeV-CW50065-S) to form CNs. According to the manufacturer protocol, CNs were plated in Maintenance Medium iN1(AP) for 3 days. Before thawing the cell line, the plate was coated overnight with laminin. According to previous studies, the ratio of the co-culture of neuronal cells to cardiomyocytes is 1:1. [73-75] Overall, the ratio of 2 iCMs: 2 CNs: 1 HCF: 1 HCAEC for the culture, with the medium composition reflecting this ratio.

Upon reaching maturity after 3 days, both CS and CNs (**Figure 5.III**) were harvested and transferred to Falcon® 96-well Clear Microplates. These were embedded in a 100µl collagen

rat tail type 1 biopolymer gel (Merck, catalog number: 08-115) and mixed at a 1:1 ratio with additional media to adjust the gel's pH to 7.

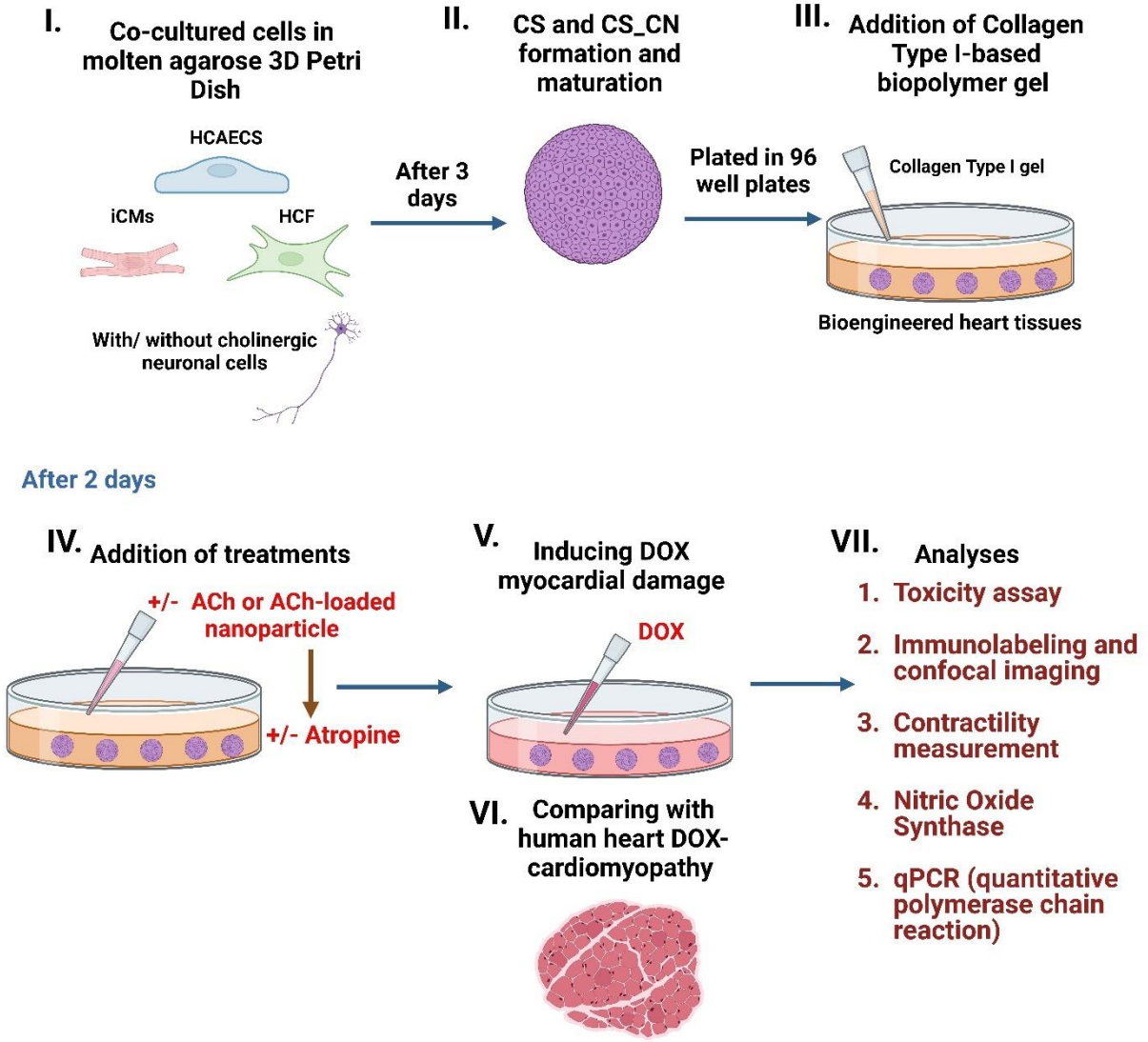

Figure 5. Schematic illustration of *in vitro* DOX-induced CS modeling. I) Co-culture of human IPSC-derived cardiomyocytes (iCMs), human coronary artery endothelial cells (HCAEC), and human cardiac fibroblast (HCF) with or without CNs in a 3D petri dish. II) Cardiac spheroids (CS) were formed and matured after three days. III) CS are plated in collagen type I-biopolymer gel diluted with CS media in a 96-well plate. IV) Acetylcholine (ACh) was added in some samples, as well as atropine, the antagonist of ACh. V) Doxorubicin (DOX) was added to the samples and, after 24 hours, underwent analyses. VI) Human heart tissue cryosection was also used to compare with our DOX CS. VII) The analyses are toxicity assay, immunolabeling and confocal imaging, contractile measurement and qPCR for *in vitro*, and nitric oxide synthase analysis for both *in vitro* and *ex vivo*.

5.3 ACh and atropine treatment

After 2 days, 100μM ACh was added to CS (**Figure 5.IV**), with a concentration based on previous studies. [76-78] 50μM atropine was added after 2hrs of administrating ACh as well as atropine was added to CNs after 2 days of being embedded in hydrogel. Atropine is an antagonist of ACh to understand the counter-effects of ACh.

5.4 Fabrication of ACh-NPs and PBCA-NPs

10 mg of Polyvinylpyrrolidone (PVP) (Sigma-Aldrich, catalog number: PVP40T) is added to 1% Tween-20 solution (1% w/v Polyvinylpyrrolidone), followed by the addition of 10mg of Acetylcholine chloride. 1% v/v Poly-butylcyanoacrylate (PBCA) (BRAUN, catalog number: 15054-BU) was added to the solution at a ratio of 1:100 [79]. The ACh-loaded nanoparticle solution was passed through pass nanoparticles (NPs) through a 1μm PTFE syringe filter and was centrifuged at 13860g for 40 minutes. Then, 1ml of PBS at pH 7.4 was added and lyophilized using SpeedVac (SpeedVac™ SPD121P) in auto-run mode overnight (12 hours). The auto mode parameters are as follows: run temperature: 45°C; heat time: 2.00; run time: 2.00; vacuum level: 14 Torr. For the PBCA-NPs, the same protocol was followed as the aforementioned group without the addition of ACh. The nanoparticles were then stored at 4ºC for up to 1 month.

5.4.1 Calculation of entrapment efficiency:

Before transferring the nanoparticles and spinning the solution, the weight of the empty tube (We) was noted. After the lyophilization step, the weight of respective tubes (Ws) was retaken (i.e., tube with lyophilized nanoparticles). The weight of NPs (Wn) is (Ws-We).

The PBCA-NPs are referred to as Wnc, and ACh-NPs as Wns. The formula for entrapment efficiency is as follows:

Entrapment efficiency= (Wns -Wnc)/Wnc×100

5.4.2 Preparation of ACh-NPs and PBCA-NPs

CS media was added to 1.70 mg/ml for either ACh-NPs or PBCA-NPs and was sonicated for 12 minutes. Then, further diluted with media, 0.17 mg/ml of nanoparticles was added to the wells (**Figure 5.IV**).

5.5 Addition of DOX

After 2 hours of adding either ACh alone or together with atropine or ACh-NPs, 10μm of DOX was added to the samples for 24 hours (**Figure 5.V**). After that, the samples were analyzed

through toxicity assay, immunolabelled cell types against cell death or eNOS, contractility assay, qPCR and stereo-seq analysis (**Figure 5.VII**).

5.6 Toxicity assay

The Live/Dead® Viability/Cytotoxicity Kit for mammalian cells (Invitrogen, catalog number: L32250) was employed following the instructions to evaluate cell viability, explicitly calculating the proportion of cells dead (stained with Ethidium Homodimer) relative to those alive (marked by Calcein-AM staining). In addition, NucBlue® Live ReadyProbes® Reagent (Hoechst 33342, Invitrogen, catalog number: R37605) was used as directed to determine the total cell population. 4hrs after application; observations were made using a Leica Stellaris 8 confocal microscope (Leica Microsystems). Images were captured across three different fluorescent channels for each sample to determine the live, dead, and total cell counts. These images were analyzed using ImageJ software (Fiji), quantifying the fluorescence intensity of live versus dead cells, each compared to the total area. The viability metrics, calculated as the ratio of the dead-to-live cell, were initially compiled in Excel version 2401 (Microsoft 365) and subsequently analyzed using GraphPad Prism for detailed evaluation.

5.7 Tissue and CS immunolabelling and confocal imaging

To determine cell death for all cell types in CSs and CNs-CSs, the samples were stained with Ethidium Homodimer for at least 2hrs then fixed with 10% neutral buffered, 4% (w/v) formaldehyde (Sigma-Aldrich, catalog number: HT5012) for 24hrs. Afterward, the samples were washed in phosphate buffered saline/0.01% (w/v) sodium azide (0.01% (v/v) PBSA) three times for a period of 30min and were permeabilized in 0.02% (v/v) Triton-X-100 (30 min). The samples were then blocked with 3% (v/v) bovine serum albumin (BSA)/PBSA solution (overnight). First antibody mouse monoclonal anti-human CD31 (1:10, diluted in 3% BSA/PBSA) was added to stain HCAEC and/or Anti-Choline Acetyltransferase (ChAT) (1:100, diluted in 3% BSA/PBSA) antibody to stain CNs overnight at 4ºC. The samples were then washed with 0.001% (v/v) PBSA three times and secondary antibody was added, Alexa fluor 647 goat anti-mouse (1:142, diluted in 3% BSA/PBSA) for CS and/or Alexa Fluor 647 Goat Anti-Rabbit (1:142, diluted in 3% BSA/PBSA) and Alexa Fluor 790 Goat Anti-mouse (1:142, diluted in 3% BSA/PBSA) for CNs (overnight at 4ºC). The solution was removed, and the samples were washed three times with 0.001% (v/v) PBSA. NucBlue® Live ReadyProbes® Reagent (Hoechst 33342) was added for nuclei labeling in 3% BSA/PBSA with cTNT (1:10) to stain iCMs and Alexa Fluor® 488 vimentin (1:250) to stain HCF and the solution was left overnight at 4ºC. The samples were then washed with 0.001% (v/v) PBSA and stored at 4ºC.

To determine the concentration of eNOS level in human heart tissue samples (healthy, IHD, DOX cardiomyopathy and DCM) (**Figure 5.VI**), the frozen samples were cut at 50µM at -20ºC using the NX70 cryostat (Leica Biosystems). We also evaluated the level of eNOS production in CS (media only, DOX and DOX ACh). All samples were fixed following the procedure above and stained with anti-phospho-eNOS/NOS III (Ser 114) antibody (15µg/ml, rabbit immunoaffinity purified antibody) (Sigma-Aldrich; catalog number: 07-357) and Mouse Monoclonal anti-human CD31 overnight. After the three washes with 0.001% (v/v) PBSA, secondary antibodies were added following the conjugated antibodies and Hoechst.

All samples were visualized using the Leica Stellaris 8 confocal microscope (Leica Microsystems). Optical sectioning along the Z-axis was performed, and the images collapsed into a single focal plane using the manufacturer's software, Microscope Software Platform LAS X Life Science (Leica Microsystems). The Z-stacks were processed using IMARIS software (Oxford Instruments plc, RRID:SCR_007370).

5.8 Fractional shortening and contractile frequency measurements

The contractile function of CS and CNs were analyzed using a Nikon Eclipse Ti2-E inverted microscope, and the contractility of each CS was recorded using the time frame option on NIS-Elements software. The fractional shortening percentage and the frequency of contractions are measured using Image J. This was done by measuring each sample's total number of contractions and the total length of each CS when contracted or relaxed.

5.9 mRNA isolation and quantitative polymerase chain reaction (qPCR) analysis

mRNA was extracted from the collected samples and analyzed through real-time polymerase chain reaction (qPCR) to measure changes in cardiovascular disease markers (angiogenesis, fibrosis, inflammation, cytoskeletal proteins, cell cycle-related proteins, apoptosis).

RNA isolation was carried out utilizing the guanidine-isothiocyanate lysis technique with the aid of the RNeasy Mini Kit (Qiagen, catalog number: 74104). Initially, samples underwent lysis and homogenization in the presence of absolute ethanol (100% v/v) to ensure optimal conditions for RNA binding. Subsequently, the lysates were applied to a RNeasy silica membrane for purification. The concentration and purity of the isolated total RNA were determined based on the absorbance ratio at 260 nm to 280 nm (A260/280), measured in a 10 mM Tris-Cl solution, pH 7.5. After quantification, each sample's total RNA was reverse transcribed into complementary DNA (cDNA) using the RT² First Strand Kit (Qiagen, catalog number: 330411). The resultant cDNA was then diluted appropriately for subsequent analyses using the RT² SYBR Green qPCR Master Mix (Qiagen, catalog number: 330503).

The qPCR assays were conducted on the Quantstudio 12K Flex Real-Time PCR System (Thermo Fisher Scientific), employing the RT2 Profiler PCR Arrays (Qiagen, catalog number: 330231), which are designed to target mRNAs associated with human cardiovascular diseases specifically. Data analysis was performed using Qiagen's web-based software, applying the fold-change (ΔΔCt) method for quantitative assessment (N=3).

5.10 Nitric oxide (NO) synthesis

Intracellular NO was detected using 1μM DAF-FM diacetate solution (Sigma-Aldrich; catalog number: D2321) as previously described. [6] Briefly, CS were treated with or without L-NIO (100μM, Sigma-Aldrich; catalog number: 400600) for 60 minutes after two days of being plated in collagen gel. Then DOX, ACh and DOX + ACh were added and left in for two hours. The samples were rinsed twice with PBS, and 1 μM DAF-FM DA solution was freshly prepared in DMEM media with no phenol red (Thermo Fisher Scientific; catalog number: 21063029). After two hours, DAF-FM diacetate solution was removed, and the samples were rinsed twice with PBS, and fresh media was added. The samples were imaged using Leica Stellaris 8 confocal microscope (Leica Microsystems). Optical sectioning along the Z-axis was performed, and the images were collapsed into a single focal plane using Image J software (maximum intensity). NO synthesis was calculated by normalizing measurements against a total number of cells and then against all samples with Image J and analyzed using GraphPad Prism™ (La Jolla, CA).

5.11 Statistical analysis

Data were analyzed using GraphPad Prism software to calculate mean ± SEM, and a one-way ANOVA test (Turkey multiple comparisons) was used to compare every sample. Significance was set to $p<0.05$. For gene expression for the qPCR analysis, fold changes were calculated as 2^(-Avg.ΔΔCt) and analyzed based on Qiagen web-based software.

6. Supplementary figures

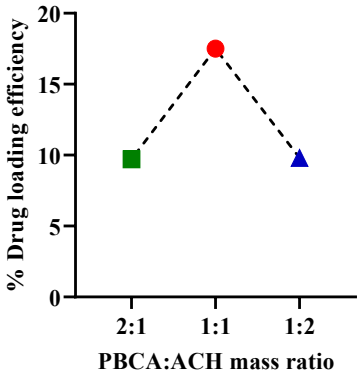

Supplementary Figure S1: Loading efficiency of ACH in PBCA nanoparticles. The mass ratio of PBCA to ACH taken was 2:1, 1:1 and 1:2 (n=1)

Supplementary Table S1. Loading efficiency of ACH in PBCA nanoparticles (n=1).

Amount of PBCA added (mg)	Amount of ACH Added (mg)	PBCA:ACH mass ratio	Loading of ACH (mg)	% Loading efficiency (LE)
20	10	2:1	0.87	8.70
10	10	1:1	1.75	17.50
10	20	1:2	0.98	9.80

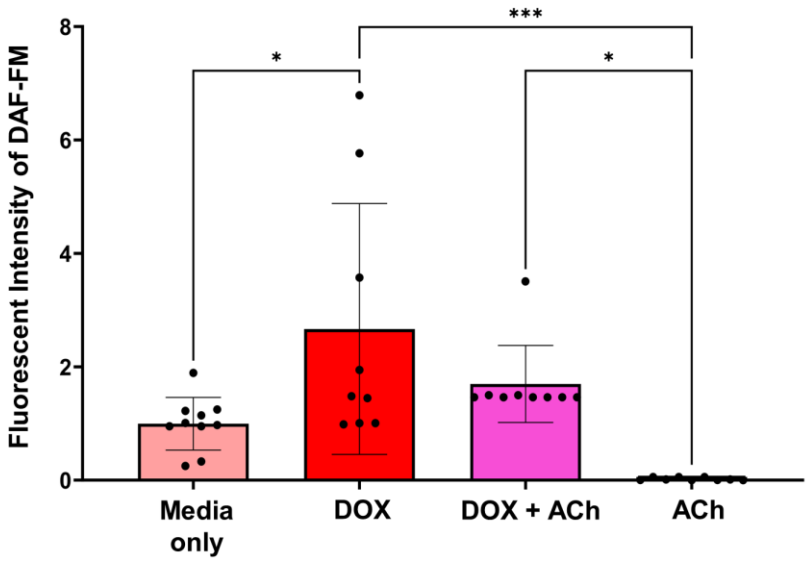

Supplementary Figure S2. Confocal image analyses of fluorescent intensity of DAF-FM to look at nitric oxide production. Samples are as follows: *i*) media only (control); *ii*) 10µM DOX; *iii*) 10µM DOX + 100µM ACh; and *iv*) 100µM ACh. Individual data points and mean values are shown with error bars: Mean ± SEM. P< 0.05 = *, p<0.01 = **, p<0.001 = *** and p<0.0001 = ****, N≥9, (One way ANOVA with Tukey's multiple comparisons test, normalized against media only).

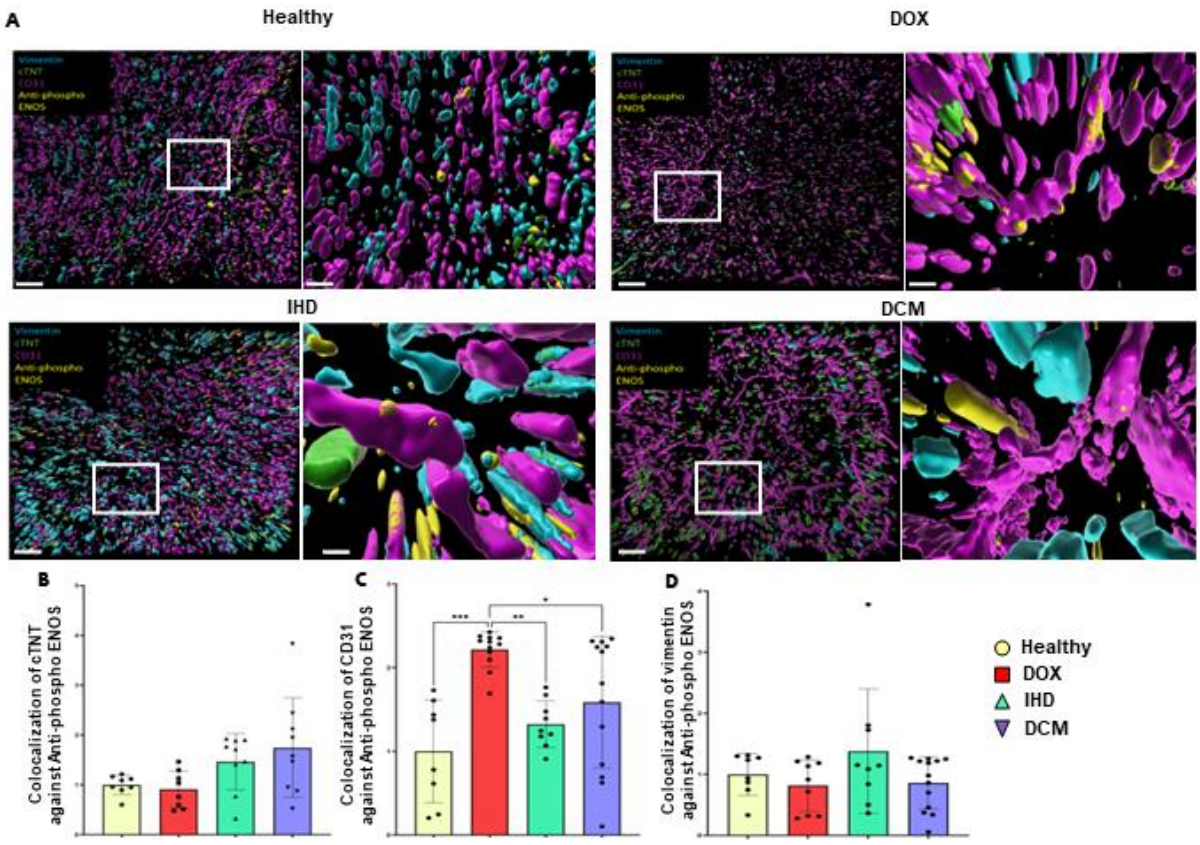

Supplementary Figure S3. eNOS pathway in human heart tissue *ex vivo*. A) 3D rendering images of human heart tissue to look at the eNOS pathway for cardiomyocytes, fibroblast and endothelial cells. Human heart tissues were stained with vimentin (cyan, HCF), cTNT (green, iCMs) and CD31 (magenta, HCAECs), and anti-phospho eNOS (yellow, eNOS) in CS. Magnification bars are 50µm and 5µm. Samples are as follows: *i)* healthy (control), *ii)* DOX, *iii)* IHD and *iv)* DCM human tissue samples. B) Colocalization of cTNT against anti-phospho ENOS; N>7. C) Colocalization of CD31 against anti-phospho ENOS; N>9. D) Colocalization of vimentin against anti-phospho ENOS; N>9. B-D) Data are presented as individual points and mean ± SEM, with error bars indicating the standard error of the mean. Statistical significance is denoted as P< 0.05 = *, p<0.01 = **, p<0.001 = *** and p<0.0001 = ****, analyzed using One-way ANOVA followed by Tukey's multiple comparisons test (normalized against control).

Data availability

Data are available in the main article and Supplementary Information. Source data are provided in this paper.

7. Acknowledgements

We thank Associate Professor Louise Cole and Dr Amy Bottomley (Microbial Imaging Facility, UTS) for microscopy assistance. We thank the staff and patients of St. Vincent's Hospital Sydney and the Australian Red Cross Blood Service. CG was supported by a UTS Seed Funding and Catholic Archdiocese of Sydney Grant for Adult Stem Cell Research, a Heart Research Institute Fellowship, Heart Research Australia, a Perpetual IMPACT Grant and the Ian Potter Foundation. XW was supported by the National Heart Foundation Future Leader Fellowship and Baker Fellowship. CLCM was supported by NSW Waratah Scholarship. SL was supported by the RT Hall Trust and the Baird Institute.

Received: ((will be filled in by the editorial staff))

Revised: ((will be filled in by the editorial staff))

Published online: ((will be filled in by the editorial staff))

8. Biography

Miss Clara Liu Chung Ming (First Author)

Miss Clara Liu Chung Ming is a 3rd year PhD candidate in the School of Biomedical Engineering at the University of Technology Sydney. Her research focuses on the bioengineering of advanced 3D *in vitro* models of the human heart pathophysiology, including "the heart attack-in-a-Petri-dish" and heart failure using patient-derived stem cells. Clara has also developed patient-specific models using iPSCs and organoid technologies, which could translate the gap between animal models and human species. Clara's multidisciplinary project is carried out in collaboration with the University of Sydney/Charles Perkins Centre/Sydney Heart Bank, Royal Prince Alfred Hospital and Baker Heart and Diabetes Institute/Monash University.

Dr Carmine Gentile

Dr Carmine Gentile, PharmD/PhD, FAHA, leads the Cardiovascular Regeneration Group working on 3D bioprinting, organoid and stem cell technologies at the Heart Research Institute and the University of Technology Sydney. He is a Senior Lecturer (Faculty) within the School of Biomedical Engineering (Faculty of Engineering and IT) at UTS. He is an internationally recognized expert in the field of 3D bioprinting and stem cell technologies and his more recent studies focus on novel molecular and cellular approaches to treat cardiovascular disease, including myocardial infarction and heart failure. These studies are based on the use of "mini-hearts" he developed as "bioink" for human heart tissues.

9. References

[1] M. Volkova, R. Russell, Anthracycline cardiotoxicity: prevalence, pathogenesis and treatment, Current cardiology reviews 7(4) (2011) 214-220.

[2] E. Christidi, L.R. Brunham, Regulated cell death pathways in doxorubicin-induced cardiotoxicity, Cell Death & Disease 12(4) (2021) 339.

[3] N. Prathumsap, B. Ongnok, T. Khuanjing, A. Arinno, C. Maneechote, N. Apaijai, T. Chunchai, B. Arunsak, K. Shinlapawittayatorn, S.C. Chattipakorn, N. Chattipakorn, Acetylcholine receptor agonists provide cardioprotection in doxorubicin-induced cardiotoxicity via modulating muscarinic M2 and α7 nicotinic receptor expression, Translational Research 243 (2022) 33-51.

[4] M.M. Abdel-Daim, O.E. kilany, H.A. Khalifa, A.A.M. Ahmed, Allicin ameliorates doxorubicin-induced cardiotoxicity in rats via suppression of oxidative stress, inflammation and apoptosis, Cancer Chemotherapy and Pharmacology 80(4) (2017) 745-753.

[5] S. Oikawa, Y. Kai, A. Mano, H. Ohata, A. Kurabayashi, M. Tsuda, Y. Kakinuma, Non-neuronal cardiac acetylcholine system playing indispensable roles in cardiac homeostasis confers resiliency to the heart, The Journal of Physiological Sciences 71(1) (2021) 2.

[6] L. Polonchuk, M. Chabria, L. Badi, J.-C. Hoflack, G. Figtree, M.J. Davies, C. Gentile, Cardiac spheroids as promising in vitro models to study the human heart microenvironment, Scientific reports 7(1) (2017) 1-12.

[7] Y. Octavia, C.G. Tocchetti, K.L. Gabrielson, S. Janssens, H.J. Crijns, A.L. Moens, Doxorubicin-induced cardiomyopathy: From molecular mechanisms to therapeutic strategies, Journal of Molecular and Cellular Cardiology 52(6) (2012) 1213-1225.

[8] P. Sharma, C.L.C. Ming, X. Wang, L.A. Bienvenu, D. Beck, G.A. Figtree, A. Boyle, C. Gentile, Biofabrication of advanced in vitro 3D models to study ischaemic and doxorubicin-induced myocardial damage, Biofabrication (2022).

[9] G.L. Cavalcante, F. Brognara, L.V.d.C. Oliveira, R.M. Lataro, M.d.T. Durand, A.P. de Oliveira, A.C.L. da Nóbrega, H.C. Salgado, J.P.J. Sabino, Benefits of pharmacological and electrical cholinergic stimulation in hypertension and heart failure, Acta Physiologica 232(3) (2021) e13663.

[10] A.B.A. Elamin, K. Forsat, S.S. Senok, N. Goswami, Vagus Nerve Stimulation and Its Cardioprotective Abilities: A Systematic Review, J Clin Med 12(5) (2023).

[11] J. Hadaya, J.L. Ardell, Autonomic modulation for cardiovascular disease, Frontiers in physiology 11 (2020) 617459.

[12] C. Rocha-Resende, A.M.d. Silva, M.A.M. Prado, S. Guatimosim, Protective and anti-inflammatory effects of acetylcholine in the heart, American Journal of Physiology-Cell Physiology 320(2) (2021) C155-C161.

[13] A.I. Mahmoud, C.C. O'Meara, M. Gemberling, L. Zhao, D.M. Bryant, R. Zheng, J.B. Gannon, L. Cai, W.-Y. Choi, G.F. Egnaczyk, C.E. Burns, C.G. Burns, C.A. MacRae, K.D. Poss, R.T. Lee, Nerves Regulate Cardiomyocyte Proliferation and Heart Regeneration, Developmental cell 34(4) (2015) 387-399.

[14] K. Intachai, S. C. Chattipakorn, N. Chattipakorn, K. Shinlapawittayatorn, Revisiting the Cardioprotective Effects of Acetylcholine Receptor Activation against Myocardial Ischemia/Reperfusion Injury, International Journal of Molecular Sciences 19(9) (2018) 2466.

[15] N. Kalay, E. Basar, I. Ozdogru, O. Er, Y. Cetinkaya, A. Dogan, A. Oguzhan, N.K. Eryol, R. Topsakal, A. Ergin, Protective effects of carvedilol against anthracycline-induced cardiomyopathy, Journal of the American College of Cardiology 48(11) (2006) 2258-2262.

[16] O.C. Bezerra, C.M. França, J.A. Rocha, G.A. Neves, P.R.M. Souza, M. Teixeira Gomes, C. Malfitano, T.C.A. Loleiro, P.M. Dourado, S. Llesuy, K. de Angelis, M.C.C. Irigoyen, L. Ulloa, F.M. Consolim-Colombo, Cholinergic Stimulation Improves Oxidative Stress and Inflammation in Experimental Myocardial Infarction, Scientific Reports 7(1) (2017) 13687.

[17] B. Buchholz, M. Donato, V. Perez, F.C. Ivalde, C. Höcht, E. Buitrago, M. Rodríguez, R.J. Gelpi, Preischemic efferent vagal stimulation increases the size of myocardial infarction in rabbits. Role of the sympathetic nervous system, International journal of cardiology 155(3) (2012) 490-491.

[18] K. Intachai, S.C. Chattipakorn, N. Chattipakorn, K. Shinlapawittayatorn, Acetylcholine exerts cytoprotection against hypoxia/reoxygenation-induced apoptosis, autophagy and mitochondrial impairment through both muscarinic and nicotinic receptors, Apoptosis 27(3) (2022) 233-245.

[19] Y. Kakinuma, T. Akiyama, K. Okazaki, M. Arikawa, T. Noguchi, T. Sato, A non-neuronal cardiac cholinergic system plays a protective role in myocardium salvage during ischemic insults, PLoS One 7(11) (2012) e50761.

[20] Y. Kakinuma, M. Tsuda, K. Okazaki, T. Akiyama, M. Arikawa, T. Noguchi, T. Sato, Heart-specific overexpression of choline acetyltransferase gene protects murine heart against ischemia through hypoxia-inducible factor-1α-related defense mechanisms, J Am Heart Assoc 2(1) (2013) e004887.

[21] R.G. Katare, M. Ando, Y. Kakinuma, M. Arikawa, T. Handa, F. Yamasaki, T. Sato, Vagal nerve stimulation prevents reperfusion injury through inhibition of opening of mitochondrial permeability transition pore independent of the bradycardiac effect, The Journal of Thoracic and Cardiovascular Surgery 137(1) (2009) 223-231.

[22] P.E. Munasinghe, E.L. Saw, M. Reily-Bell, D. Tonkin, Y. Kakinuma, M. Fronius, R. Katare, Non-neuronal cholinergic system delays cardiac remodelling in type 1 diabetes, Heliyon 9(6) (2023) e17434.

[23] G.M. De Ferrari, H.J.G.M. Crijns, M. Borggrefe, G. Milasinovic, J. Smid, M. Zabel, A. Gavazzi, A. Sanzo, R. Dennert, J. Kuschyk, S. Raspopovic, H. Klein, K. Swedberg, P.J. Schwartz, f.t.C.M.T. Investigators, Chronic vagus nerve stimulation: a new and promising therapeutic approach for chronic heart failure, European Heart Journal 32(7) (2010) 847-855.

[24] M.R. Gold, D.J.V. Veldhuisen, P.J. Hauptman, M. Borggrefe, S.H. Kubo, R.A. Lieberman, G. Milasinovic, B.J. Berman, S. Djordjevic, S. Neelagaru, P.J. Schwartz, R.C.

Starling, D.L. Mann, Vagus Nerve Stimulation for the Treatment of Heart Failure, Journal of the American College of Cardiology 68(2) (2016) 149-158.

[25] L.V. Borovikova, S. Ivanova, M. Zhang, H. Yang, G.I. Botchkina, L.R. Watkins, H. Wang, N. Abumrad, J.W. Eaton, K.J. Tracey, Vagus nerve stimulation attenuates the systemic inflammatory response to endotoxin, Nature 405(6785) (2000) 458-62.

[26] L. Calvillo, E. Vanoli, E. Andreoli, A. Besana, E. Omodeo, M. Gnecchi, P. Zerbi, G. Vago, G. Busca, P.J. Schwartz, Vagal stimulation, through its nicotinic action, limits infarct size and the inflammatory response to myocardial ischemia and reperfusion, J Cardiovasc Pharmacol 58(5) (2011) 500-7.

[27] F. Guo, Y. Wang, J. Wang, Z. Liu, Y. Lai, Z. Zhou, Z. Liu, Y. Zhou, X. Xu, Z. Li, M. Wang, F. Yu, R. Hu, L. Zhou, H. Jiang, Choline Protects the Heart from Doxorubicin-Induced Cardiotoxicity through Vagal Activation and Nrf2/HO-1 Pathway, Oxidative Medicine and Cellular Longevity 2022 (2022) 4740931.

[28] C. Siripakkaphant, B. Ongnok, N. Prathumsap, T. Khuanjing, T. Chunchai, B. Arunsak, P. Pantiya, N. Chattipakorn, S.C. Chattipakorn, Vagus Nerve Stimulation Provides Neuroprotection Against Doxorubicin-induced Chemobrain Via Activations of Both Muscarinic and Nicotinic Acetylcholine Receptors, Alzheimer's & Dementia 19(S13) (2023) e073548.

[29] T. Khuanjing, B. Ongnok, C. Maneechote, N. Siri-Angkul, N. Prathumsap, A. Arinno, T. Chunchai, B. Arunsak, S.C. Chattipakorn, N. Chattipakorn, Acetylcholinesterase inhibitor ameliorates doxorubicin-induced cardiotoxicity through reducing RIP1-mediated necroptosis, Pharmacological Research 173 (2021) 105882.

[30] C. Liu Chung Ming, K. Sesperez, E. Ben-Sefer, D. Arpon, K. McGrath, L. McClements, C. Gentile, Considerations to Model Heart Disease in Women with Preeclampsia and Cardiovascular Disease, Cells 10(4) (2021) 899.

[31] E. Kröger, M. Mouls, M. Wilchesky, M. Berkers, P.-H. Carmichael, R. van Marum, P. Souverein, T. Egberts, M.-L. Laroche, Adverse Drug Reactions Reported With Cholinesterase Inhibitors:An Analysis of 16 Years of Individual Case Safety Reports From VigiBase, Annals of Pharmacotherapy 49(11) (2015) 1197-1206.

[32] S. Zafeiropoulos, U. Ahmed, A. Bikou, I.T. Mughrabi, S. Stavrakis, S. Zanos, Vagus nerve stimulation for cardiovascular diseases: Is there light at the end of the tunnel?, Trends Cardiovasc Med (2023).

[33] A. Evangelatov, R. Skrobanska, N. Mladenov, M. Petkova, G. Yordanov, R. Pankov, Epirubicin loading in poly (butyl cyanoacrylate) nanoparticles manifests via altered intracellular localization and cellular response in cervical carcinoma (HeLa) cells, Drug delivery 23(7) (2016) 2235-2244.

[34] E. Sulheim, H. Baghirov, E. von Haartman, A. Bøe, A.K. Åslund, Y. Mørch, C.d.L. Davies, Cellular uptake and intracellular degradation of poly (alkyl cyanoacrylate) nanoparticles, Journal of nanobiotechnology 14 (2016) 1-14.

[35] A. Refaat, B. del Rosal, V. Bongcaron, A.P.G. Walsh, G. Pietersz, K. Peter, S.E. Moulton, X. Wang, Activated Platelet-Targeted IR780 Immunoliposomes for Photothermal Thrombolysis, Advanced Functional Materials 33(4) (2023) 2209019.

[36] R. Rempe, S. Cramer, S. Hüwel, H.-J. Galla, Transport of Poly(n-butylcyano-acrylate) nanoparticles across the blood–brain barrier in vitro and their influence on barrier integrity, Biochemical and Biophysical Research Communications 406(1) (2011) 64-69.

[37] V. Reukov, V. Maximov, A. Vertegel, Proteins conjugated to poly(butyl cyanoacrylate) nanoparticles as potential neuroprotective agents, Biotechnol Bioeng 108(2) (2011) 243-52.

[38] C. Wang, H. Jiang, J. Zhu, Y. Jin, A new agent for contrast-enhanced intravascular ultrasound imaging in vitro: polybutylcyanoacrylate nanoparticles with drug-carrying capacity, Artificial Cells, Nanomedicine, and Biotechnology 52(1) (2024) 218-228.

[39] C.A. Broomfield, D. Maxwell, R. Solana, C. Castro, A. Finger, D. Lenz, Protection by butyrylcholinesterase against organophosphorus poisoning in nonhuman primates, Journal of Pharmacology and Experimental Therapeutics 259(2) (1991) 633-638.

[40] W. Nuntaphum, W. Pongkan, S. Wongjaikam, S. Thummasorn, P. Tanajak, J. Khamseekaew, K. Intachai, S.C. Chattipakorn, N. Chattipakorn, K. Shinlapawittayatorn, Vagus nerve stimulation exerts cardioprotection against myocardial ischemia/reperfusion injury predominantly through its efferent vagal fibers, Basic Res Cardiol 113(4) (2018) 22.

[41] P. Bordier, S. Garrigue, S. Lanusse, J. Margaine, F. Robert, L. Gencel, A. Lafitte, Cardiovascular effects and risk of syncope related to donepezil in patients with Alzheimer's disease, CNS drugs 20 (2006) 411-417.

[42] B. Ongnok, T. Khuanjing, T. Chunchai, S. Kerdphoo, T. Jaiwongkam, N. Chattipakorn, S.C. Chattipakorn, Donepezil provides neuroprotective effects against brain injury and Alzheimer's pathology under conditions of cardiac ischemia/reperfusion injury, Biochimica et Biophysica Acta (BBA) - Molecular Basis of Disease 1867(1) (2021) 165975.

[43] Z. Pu, W. Xu, Y. Lin, J. Shen, Y. Sun, Donepezil decreases heart rate in elderly patients with Alzheimer's disease, International Journal of Clinical Pharmacology and Therapeutics 57(2) (2019) 94.

[44] C.E. Battle, A.H. Abdul-Rahim, S.D. Shenkin, J. Hewitt, T.J. Quinn, Cholinesterase inhibitors for vascular dementia and other vascular cognitive impairments: a network meta-analysis, Cochrane Database of Systematic Reviews (2) (2021).

[45] W.-x. Jian, Z. Zhang, J.-h. Zhan, S.-f. Chu, Y. Peng, M. Zhao, Q. Wang, N.-h. Chen, Donepezil attenuates vascular dementia in rats through increasing BDNF induced by reducing HDAC6 nuclear translocation, Acta Pharmacologica Sinica 41(5) (2020) 588-598.

[46] R.C. Choudhary, U. Ahmed, M. Shoaib, E. Alper, A. Rehman, J. Kim, K. Shinozaki, B.T. Volpe, S. Chavan, S. Zanos, K.J. Tracey, L.B. Becker, Threshold adjusted vagus nerve stimulation after asphyxial cardiac arrest results in neuroprotection and improved survival, Bioelectronic Medicine 8(1) (2022) 10.

[47] H.-C. Li, K.-X. Luo, J.-S. Wang, Q.-X. Wang, Extrapyramidal side effect of donepezil hydrochloride in an elderly patient: a case report, Medicine 99(11) (2020) e19443.

[48] M. Zhao, X. He, X.Y. Bi, X.J. Yu, W. Gil Wier, W.J. Zang, Vagal stimulation triggers peripheral vascular protection through the cholinergic anti-inflammatory pathway in a rat model of myocardial ischemia/reperfusion, Basic Res Cardiol 108(3) (2013) 345.

[49] R.-Q. Xue, L. Sun, X.-J. Yu, D.-L. Li, W.-J. Zang, Vagal nerve stimulation improves mitochondrial dynamics via an M3 receptor/CaMKKβ/AMPK pathway in isoproterenol-induced myocardial ischaemia, J Cell Mol Med 21(1) (2017) 58-71.

[50] F. Timolati, D. Ott, L. Pentassuglia, M.-N. Giraud, J.-C. Perriard, T.M. Suter, C. Zuppinger, Neuregulin-1 beta attenuates doxorubicin-induced alterations of excitation–contraction coupling and reduces oxidative stress in adult rat cardiomyocytes, Journal of molecular and cellular cardiology 41(5) (2006) 845-854.

[51] M. Seddon, A.M. Shah, B. Casadei, Cardiomyocytes as effectors of nitric oxide signalling, Cardiovascular Research 75(2) (2007) 315-326.

[52] S.R. Martin, K. Emanuel, C.E. Sears, Y.-H. Zhang, B. Casadei, Are myocardial eNOS and nNOS involved in the β-adrenergic and muscarinic regulation of inotropy? A systematic investigation, Cardiovascular research 70(1) (2006) 97-106.

[53] Y. Zhou, S. Varadharaj, X. Zhao, N. Parinandi, N.A. Flavahan, J.L. Zweier, Acetylcholine causes endothelium-dependent contraction of mouse arteries, American Journal of Physiology-Heart and Circulatory Physiology 289(3) (2005) H1027-H1032.

[54] H.E. Boycott, M.-N. Nguyen, B. Vrellaku, K. Gehmlich, P. Robinson, Nitric Oxide and Mechano-Electrical Transduction in Cardiomyocytes, Frontiers in Physiology 11 (2020).

[55] S.V. Kalivendi, S. Kotamraju, H. Zhao, J. Joseph, B. Kalyanaraman, Doxorubicin-induced apoptosis is associated with increased transcription of endothelial nitric-oxide synthase: effect of antiapoptotic antioxidants and calcium, Journal of Biological Chemistry 276(50) (2001) 47266-47276.

[56] M. Kuwabara, Y. Kakinuma, M. Ando, R.G. Katare, F. Yamasaki, Y. Doi, T. Sato, Nitric Oxide Stimulates Vascular Endothelial Growth Factor Production in Cardiomyocytes Involved in Angiogenesis, The Journal of Physiological Sciences 56(1) (2006) 95-101.

[57] B. Lavin, M. Gómez, O.M. Pello, B. Castejon, M.J. Piedras, M. Saura, C. Zaragoza, Nitric oxide prevents aortic neointimal hyperplasia by controlling macrophage polarization, Arterioscler Thromb Vasc Biol 34(8) (2014) 1739-1746.

[58] X. Sun, Y. Song, Y. Xie, J. Han, F. Chen, Y. Sun, B. Sui, D. Jiang, Shenlijia attenuates doxorubicin-induced chronic heart failure by inhibiting cardiac fibrosis, Evidence-Based Complementary and Alternative Medicine 2021 (2021).

[59] X. Sun, G. Chen, Y. Xie, D. Jiang, J. Han, F. Chen, Y. Song, Qiliqiangxin improves cardiac function and attenuates cardiac remodelling in doxorubicin-induced heart failure rats, Pharm Biol 58(1) (2020) 417-426.

[60] S. Thatcher, F. Yiannikouris, M. Gupte, L. Cassis, The adipose renin–angiotensin system: role in cardiovascular disease, Molecular and cellular endocrinology 302(2) (2009) 111-117.

[61] X. Wang, X. Meng, L. Meng, Y. Guo, Y. Li, C. Yang, Z. Pei, J. Li, F. Wang, Joint efficacy of the three biomarkers SNCA, GYPB and HBG1 for atrial fibrillation and stroke: Analysis via the support vector machine neural network, J Cell Mol Med 26(7) (2022) 2010-2022.

[62] A.E. El-Naggar, S.M. El-Gowilly, F.M. Sharabi, Possible ameliorative effect of ivabradine on the autonomic and left ventricular dysfunction induced by doxorubicin in male rats, Journal of Cardiovascular Pharmacology 72(1) (2018) 22-31.

[63] Y.-X. Wang, M. Korth, Effects of doxorubicin on excitation-contraction coupling in guinea pig ventricular myocardium, Circulation Research 76(4) (1995) 645-653.

[64] C.Y. Zhao, J.L. Greenstein, R.L. Winslow, Roles of phosphodiesterases in the regulation of the cardiac cyclic nucleotide cross-talk signaling network, Journal of Molecular and Cellular Cardiology 91 (2016) 215-227.

[65] G.E. Kim, D.A. Kass, Cardiac Phosphodiesterases and Their Modulation for Treating Heart Disease, Handb Exp Pharmacol 243 (2017) 249-269.

[66] J. Zhang, P.C. Simpson, B.C. Jensen, Cardiac α1A-adrenergic receptors: emerging protective roles in cardiovascular diseases, American Journal of Physiology-Heart and Circulatory Physiology 320(2) (2021) H725-H733.

[67] M.C. Mohl, S.E. Iismaa, X.-H. Xiao, O. Friedrich, S. Wagner, V. Nikolova-Krstevski, J. Wu, Z.-Y. Yu, M. Feneley, D. Fatkin, D.G. Allen, R.M. Graham, Regulation of murine cardiac contractility by activation of α1A-adrenergic receptor-operated Ca2+ entry, Cardiovascular Research 91(2) (2011) 310-319.

[68] M. Sato, B.A. Evans, A.L. Sandström, L.Y. Chia, S. Mukaida, B.S. Thai, A. Nguyen, L. Lim, C.Y.R. Tan, J.-A. Baltos, P.J. White, L.T. May, D.S. Hutchinson, R.J. Summers, T. Bengtsson, α1A-Adrenoceptors activate mTOR signalling and glucose uptake in cardiomyocytes, Biochemical Pharmacology 148 (2018) 27-40.

[69] M. Kolter, M. Ott, C. Hauer, I. Reimold, G. Fricker, Nanotoxicity of poly(n-butylcyano-acrylate) nanoparticles at the blood–brain barrier, in human whole blood and in vivo, Journal of Controlled Release 197 (2015) 165-179.

[70] S. Kumar, R. Marfatia, S. Tannenbaum, C. Yang, E. Avelar, Doxorubicin-induced cardiomyopathy 17 years after chemotherapy, Tex Heart Inst J 39(3) (2012) 424-7.

[71] G.A. Figtree, K.J. Bubb, O. Tang, E. Kizana, C. Gentile, Vascularized cardiac spheroids as novel 3D in vitro models to study cardiac fibrosis, Cells Tissues Organs 204(3-4) (2017) 191-198.

[72] P. Sharma, C. Liu Chung Ming, C. Gentile, In vitro modeling of myocardial ischemia/reperfusion injury with murine or human 3D cardiac spheroids, STAR Protocols 3(4) (2022) 101751.

[73] Y. Takayama, Y.S. Kida, In Vitro Reconstruction of Neuronal Networks Derived from Human iPS Cells Using Microfabricated Devices, PLoS One 11(2) (2016) e0148559.

[74] Y. Mukae, M. Itoh, R. Noguchi, K. Furukawa, K.-i. Arai, J.-i. Oyama, S. Toda, K. Nakayama, K. Node, S. Morita, The addition of human iPS cell-derived neural progenitors changes the contraction of human iPS cell-derived cardiac spheroids, Tissue and Cell 53 (2018) 61-67.

[75] K. Sakai, K. Shimba, K. Ishizuka, Z. Yang, K. Oiwa, A. Takeuchi, K. Kotani, Y. Jimbo, Functional innervation of human induced pluripotent stem cell-derived cardiomyocytes by co-culture with sympathetic neurons developed using a microtunnel technique, Biochemical and Biophysical Research Communications 494(1) (2017) 138-143.

[76] T. Krieg, Q. Qin, S. Philipp, M.F. Alexeyev, M.V. Cohen, J.M. Downey, Acetylcholine and bradykinin trigger preconditioning in the heart through a pathway that includes Akt and NOS, American Journal of Physiology-Heart and Circulatory Physiology 287(6) (2004) H2606-H2611.

[77] O.R. Rana, P. Schauerte, R. Kluttig, J.W. Schröder, R.R. Koenen, C. Weber, K.W. Nolte, J. Weis, R. Hoffmann, N. Marx, E. Saygili, Acetylcholine as an age-dependent non-neuronal source in the heart, Autonomic Neuroscience 156(1) (2010) 82-89.

[78] A. Roy, M. Dakroub, G.C. Tezini, Y. Liu, S. Guatimosim, Q. Feng, H.C. Salgado, V.F. Prado, M.A. Prado, R. Gros, Cardiac acetylcholine inhibits ventricular remodeling and dysfunction under pathologic conditions, The FASEB Journal 30(2) (2016) 688-701.

[79] S. Mehta, V. Bongcaron, T.K. Nguyen, Y. Jirwanka, A. Maluenda, A.P.G. Walsh, J. Palasubramaniam, M.D. Hulett, R. Srivastava, A. Bobik, X. Wang, K. Peter, An Ultrasound-Responsive Theranostic Cyclodextrin-Loaded Nanoparticle for Multimodal Imaging and Therapy for Atherosclerosis, Small 18(31) (2022) 2200967.

Table of Contents

3.4 Closing Remarks for Part 3

After establishing the models in **Chapter 2.2**, the two articles that makeup **Chapter 3** have successfully addressed Aim 2 (Evaluation of the effects of ACh on I/R-induced CSs and MI *in vivo*) and Aim 3 (Evaluation of the effects of ACh on DOX-induced CSs). Taken together, these chapters provide substantial information on the role of ACh against myocardial damage, which supports the overall hypothesis.

In **Chapter 3.2**, we identified the preventive role of increasing ACh levels in MI and subsequent I/R injury. In **Chapter 3.3**, we identified the preventive role of increasing ACh levels against DOX-induced myocardial damage. Both chapters provide new insights, and several questions for the field are answered, with perhaps the most being the use of NPs to deliver ACh. ACh-NPs have never been studied in the heart before, and only a few studies have used ACh-NPs as a treatment for Alzheimer's disease and cancer (Sankar et al., 2023, Abdelwahab et al., 2021). Regardless, our findings showed that ACh-NPs could be promising against MI and I/R injury by reducing cell death, improving contractile function, and left ventricle ejection fraction % (LVEF %) and promoting cell proliferation. We have also shown that ACh-NPs could attenuate DOX-induced cell death and restore the contractile function. The innovation of both studies lies in the development and application of ACh-NPs, representing a novel approach for delivering ACh to damaged cardiac tissue. This method shows potential in reducing both acute and chronic myocardial damage and improving cardiac function.

However, the limitations of both studies should be considered. Firstly, we tested the effects of ACh-NPs before inducing myocardial damage. This was done to assess its maximal potential cardioprotective effect and its prevention effects, whereas, for human patients, the treatment needed is after the myocardial damage event. Hence, assessing the efficacy of the timing for the delivery of ACh-NPs (how long after the myocardial damage event) in patients will be critical. Furthermore, we injected ACh-NPs directly into the myocardium of MI mice models to avoid any side effects associated with the systemic delivery of ACh-NPs. Hence, future work should also look at the other delivery methods for ACh-NPs, such as intravenously or orally.

While the therapeutic approach of ACh-NPs looks promising, it requires extensive validation in diverse patient populations to ensure its efficacy and safety. The complexity of translating these findings from *in vitro* models and animal studies to human clinical practice remains a significant challenge. Additionally, the long-term effects and potential side effects of ACh-NPs treatment need to be thoroughly investigated. Future directions for this research should include further refining the NPs delivery system to enhance its efficacy and safety and expanding its

application to a broader range of cardiac conditions.

In addressing these limitations and pursuing these future directions for ACh-NPs, we hope to provide an effective cardioprotective strategy against myocardial damage, ultimately benefiting patients with CVD.

CHAPTER 4 – DISCUSSION OF THESIS

4.1 Introduction and Relevance

Chapter 4 discusses the ways in which my PhD project has contributed to the field of myocardial regeneration with a focus on a unique combination of state-of-the-art technologies, such as organoids, nanoparticles, stem cells and advanced *in vitro* disease modeling.

My original hypothesis was defined in broad terms as:

Acetylcholine protects against myocardial damage.

The chapters/articles within my thesis have addressed this hypothesis via my specific aims. In **Chapter 2**, the articles sought to address Aim 1 and showed the versatile use of our 3D *in vitro* CS model to approximate the human heart tissue pathophysiology. In **Chapter 2.2**, we established I/R and DOX-induced myocardial damage in CSs. Next, we explored the protective role of ACh against I/R injury in *in vitro* model and MI in *in vivo* model for Aim 2 (**Chapter 3.2**) and the role of ACh against DOX-induced injury in *in vitro* CSs for Aim 3 (**Chapter 3.3**).

Chapter 4 provides a discussion (4.2), future directions (4.3) and conclusion (4.4) for the whole thesis, with a focus on the central hypothesis and the results from each aim. Whilst the hypothesis was defined in broad terms, the more specific contributions of the thesis will be highlighted in the discussion.

4.2 Thesis Discussion

The work embodied in this thesis supported its main hypothesis that ACh protects against myocardial damage and it introduces innovative contributions to the scientific field of cardiac regeneration with a multidisciplinary approach. The literature review part (**Chapters 1.2-1.4**) covers the previously studied cardioprotective role of ACh against myocardial damage in *in vitro* and *in vivo* models using different techniques to increase ACh levels. However, this thesis has heighted the limitations of those studies. For instance, therapeutic approaches to increase ACh levels are not safe for CVD patients given the broad activity of ACh, VNS is an invasive approach and requires further optimization (Choudhary et al., 2022). Moreover, cholinesterase inhibitors, which prevent the degradation of ACh, lead to excess ACh and overstimulation of ACh receptors. This results in ACh-induced side effects, including lacrimation, salivation, tremors, loss of motor activity, hypothermia, and tonic convulsions (Broomfield et al., 1991). Therefore, delivering ACh in small doses and targeting the infarcted area could minimize systemic side effects.

But before tackling this issue, we also identified limitations in the currently used model systems, which fail to fully replicate the complex scenario of human heart pathophysiology (Liu Chung Ming et al., 2021). There is also a translational gap in the physiology and pathology mechanisms between animal model species and humans (Mitchell et al., 2021). Furthermore, there are limited studies using meta-analysis and systemic review to solve the heterogeneity both in the biological underpinnings of diseases and amongst patients. Despite that, those studies do not fully address all the challenges and complexity of translational research and drug discovery (Sena et al., 2014). We therefore developed advanced myocardial injury models to fill the gaps in the translation of research and drug discovery using *in vitro* bioengineered CSs (**Chapter 2**).

First, the CS models have been shown to mimic similar features of I/R and DOX-induced myocardial damage (Sharma et al., 2022). Our findings (**Chapter 2.2**) are consistent with the ones observed in previous *in vivo* studies, including an increase in cell death, a decrease in contractile activity, and a reduction in cardiac remodelling and cardiac cell death. Altogether, these findings demonstrated the utility of CSs as models to understand cardiac pathophysiology and to test drug toxicity. In **Chapter 2.3**, we showed that the CS model has the potential to evaluate the correlation between HDP and CVD using patient-derived plasma. CSs treated with plasma from HDP patients showed early changes in cardiac function for GH and PE patients,

which represents an important breakthrough towards the prevention of CVD in these women. This novel and unexplored research led to the discovery that GH activates mechanisms related to homeostasis, cell death signaling, and malfunction in cardiomyocyte contractility, while PE leads to dysfunctional inflammatory pathways and exhibits heightened protein expression of markers associated with endothelial dysfunction. This is an unprecedented opportunity to investigate the correlation between HDP and CVD, marking a significant leap forward in the prevention of CVD in patients.

While there is the growing demand for more humane research practices but also offers a more reproducible and human-relevant model for studying heart disease (Liu Chung Ming et al., 2022). **Chapter 2** provides new insights to understanding, preventing, and treating heart diseases that could improve the outcomes in cardiovascular health. However, there are several limitations to consider with our *in vitro* bioengineered CSs. Although the CS model shows promise, it requires extensive validation across diverse patient populations to ensure its efficacy and accuracy. The complexity of translating findings from the CS model to clinical practice remains a significant challenge. Furthermore, while the CS model can replicate certain aspects of human cardiac pathophysiology, it may not fully capture the intricacies of human biology and disease progression. Finally, the development and application of the CS model are still in their early stages, and more studies are needed to understand its potential limitations and optimize its use for various research purposes.

While this project highlights the feasibility of CSs, further studies are also evaluating CSs' applications. For instance, we demonstrated the effect of SARS-CoV-2 in CSs. This study is currently under review, and I am an equally contributing first author. Our findings suggest that CSs offer a valuable tool for dissecting direct host-viral interactions and advancing our understanding of SARS-CoV-2-related cardiac injury. Our results showed that SARS-CoV-2 dysregulated gene expression of CVD markers leading to cardiac dysfunction which could increase HF risk. Moreover, another study that I have been working on, as a first author, was to differentiate blood cells from HDP post-partum patients to IPSC-derived cardiac cells such as cardiomyocytes and endothelial cells. To compare HDP to normotensive patients, I then co-cultured these cells to form CSs and then analyzed the cells' transcriptome profile through single-cell RNA sequencing (currently analyzing the data). While this project is still ongoing, our study could fill the gaps in the translation of research and drug discovery. Additionally, Roche et al. (2023) showed that 3D bioprinted CSs patches could improve cardiac function post-MI injury in mice models. This suggests that CSs could potentially be used as a cell

therapy to treat MI; however, future studies are needed to optimize the patches and translate the findings to large animal trials.

More importantly, we have also demonstrated the protective role of ACh against I/R and DOX-induced myocardial damage (**Chapter 3**). This is consistent with the hypothesis that ACh protects against myocardial damage. We tested the addition of free-dissolved ACh in CSs and ACh-producing CNs in CSs against I/R and DOX-induced myocardial damage. Our findings demonstrated that ACh has a protective role against cell death, prevents cardiac remodeling, and protects cardiac function against both myocardial damages. Furthermore, our results in CSs on DOX-dependent eNOS signaling in endothelial cells are consistent with the ones in *ex vivo* DOX-treated biopsies. It is only with the use of *in vitro* CSs that we were then able to show that ACh reduced eNOS activation in endothelial cells following DOX treatment, which was associated with improved viability and contractile function. While we have shown that increasing ACh levels in cardiac cells have cardioprotective effects against myocardial damage, the delivery of a low dose free-dissolved ACh in CVD patients may not be safe and may raise concerns.

Additionally, due to the variability of current approaches to increase ACh level and the complexity of this molecule (Broomfield et al., 1991, Capilupi et al., 2020, Zafeiropoulos et al., 2023). We, therefore, developed a novel delivery technique to deliver ACh using NPs. NPs have the potential for targeted drug delivery and enhancing therapeutic effects while minimizing systemic delivery side effects (Mehta et al., 2022, Refaat et al., 2023). Our results showed that ACh-NPs attenuate cell death and restore cardiac contractile function against I/R- and DOX-induced bioengineered CSs. To validate our *in vitro* findings, we tested the protective effect of ACh-NPs against MI in mice models. Our results showed that ACh-NPs protected against a decrease in LVEF% and attenuated the increase of collagen production in MI mice. As well, the novel therapeutic approach reduced ROS production and increased cell proliferation. This suggests that ACh-NPs have cardioprotective effects against myocardial damage; however, the limitations of the articles in **Chapter 3** should be considered.

The efficacy and delivery of ACh-NPs were not studied. Future work is necessary to improve their stability, targeting efficiency, and controlled release properties. While we administered ACh-NPs before inducing myocardial damage in the *in vitro* and *in vivo* models, we should also consider administering ACh-NPs after inducing the myocardial damage and evaluate the drug's protective effects. We should also consider how to deliver the ACh-NPs, while we injected the drug into the myocardium *in vivo* models, this method is not feasible for clinical

applications. Future work should involve further *in vivo* experimentation, potentially using pig models that have largely comparable cardiac functions to humans (Hunter et al., 2014). In addressing these limitations, we hope to provide an effective cardioprotective strategy against myocardial damage, ultimately benefiting patients with CVD.

I have also performed spatial transcriptomics to look at the effects of ACh-NPs in MI mice models, I/R and DOX-induced CSs and compare our findings to *ex vivo* human heart tissue (samples: healthy, DOX cardiomyopathy and ischemic heart disease). While the analyses of this experiment are still ongoing, those findings could provide further insights of the protective ability of ACh-NPs against myocardial damage.

To conclude, this thesis translated ACh protective effects from previous research to novel findings using groundbreaking techniques such as 3D *in vitro* modeling, stem cells and nanoparticles. **Chapter 3** provides substantial evidence that ACh protects against MI, I/R and DOX-induced myocardial damage and for the first time, we showed that ACh-NPs could be a therapeutic approach to deliver ACh safely.

4.3 Thesis Future Directions

This thesis supports its main hypothesis that ACh protects against myocardial damage and introduces groundbreaking contributions to the cardiovascular field that have not been previously addressed. Based on the findings and limitations discussed, several future directions are proposed to further advance this field. As our model is in a-static-nature, future directions for this research include further refining the CS model by exploring state-of-the-art microfluidics devices and bioprinting technology. This could generate high-throughput assays and dynamic culture conditions to mimic blood flow. Future work should also extend validation studies of the CS model across diverse patient populations to ensure its efficacy and accuracy in replicating human myocardial damage. We should also further develop patient-derived CS models to study individual variations in cardiac disease and responses to treatments. This will help in better understanding the translational potential of the CS model.

Another future direction for this project is to look at the effect of ACh against GH and PE. The synthesis, release and metabolism of ACh are dysregulated in HDP patients leading to early alterations in cardiac function (Wedn et al., 2021). Previous studies have found that ACh activates the cholinergic anti-inflammatory pathway, which plays an important regulatory role in maternal-fetal inflammation and placental remodeling in PE (Han et al., 2021, Xu et al., 2019, Machaalani et al., 2015) and protects against hypertension in pregnant women (Issotina Zibrila et al., 2021). Moreover, while GH leads to endothelial dysfunction; current studies have shown that ACh protects against endothelial dysfunction (Li et al., 2022, Li et al., 2020b). Therefore, studying the protective effect of ACh against HDP could lead to the prevention of CVD post-HDP.

While this thesis focused on the protective role of ACh against MI, I/R and DOX-induced cardiotoxicity. Previous studies have also shown that ACh has cardioprotective effects against atherosclerosis (Vieira-Alves et al., 2020), diabetes (Munasinghe et al., 2023, Saw et al., 2021) and hypertension (Cavalcante et al., 2021). ACh-NPs could also be tested to target and protect against damage in other organs, such as the brain or kidney. Other studies assessed the role of ACh as a treatment for Alzheimer's disease (Sankar et al., 2023), dementia (Battle et al., 2021, Birks and Harvey, 2018), renal dysfunction (Ahmad et al., 2018) and renal I/R injury (Malek and Nematbakhsh, 2015). Hence, future studies should also consider the effect of ACh-NPs against other diseases. However, it is primordial to first optimize ACh-NPs efficacy and delivery, to identify the optimal concentration of doses to be given to patients, the delivery

method of the drug and its long-term effect on patients.

To conclude, while my project has provided novel insights, further research is necessary to fully understand the protective role of ACh. Specifically, it is important to investigate the mechanisms of ACh-NPs, their efficacy in delivering the drug and their regenerative properties. The continued research will further elucidate the therapeutic potential of ACh-NPs and enhance our ability to treat a range of conditions.

4.4 Thesis Conclusion

This thesis has provided substantial evidence supporting the hypothesis that ACh plays a protective role against myocardial damage. We have advanced the understanding of ACh's cardioprotective effects within both 3D *in vitro* and *in vivo* model systems. Our *in vitro* findings support the protective role played by ACh against myocardial damage-induced toxicity, necrosis, reduction in contractile function and progression to HF. Furthermore, we showed for the first time that ACh-NPs could be employed as a promising novel treatment against MI injury, as they reduced MI-induced apoptosis and necrosis, LV remodeling, and prevented reduction in LVEF%. ACh-NPs also increased cell survival, cell cycle and proliferation, as well as attenuated ROS levels post-MI. While these findings are significant, additional preclinical studies are needed to evaluate the proper dosage of ACh-NPs delivery and to translate our findings from the bench to the bedside.

Bibliography

2021. *Cardiovascular Diseases (CVDs)* [Online]. World Health Organisation Available: https://www.who.int/news-room/fact-sheets/detail/cardiovascular-diseases-(cvds) [Accessed 3 January 2022].

ABDELWAHAB, G. M., MIRA, A., CHENG, Y. B., ABDELAZIZ, T. A., LAHLOUB, M. F. I. & KHALIL, A. T. 2021. Acetylcholine esterase inhibitory activity of green synthesized nanosilver by naphthopyrones isolated from marine-derived Aspergillus niger. *PLoS One,* 16**,** e0257071.

AHMAD, A., DEMPSEY, S. K., DANEVA, Z., AZAM, M., LI, N., LI, P.-L. & RITTER, J. K. 2018. Role of Nitric Oxide in the Cardiovascular and Renal Systems. *International Journal of Molecular Sciences,* 19**,** 2605.

ARNOTT, C., NELSON, M., RAMIREZ, M. A., HYETT, J., GALE, M., HENRY, A., CELERMAJER, D. S., TAYLOR, L. & WOODWARD, M. 2020. Maternal cardiovascular risk after hypertensive disorder of pregnancy. *Heart,* 106**,** 1927-1933.

BATTLE, C. E., ABDUL-RAHIM, A. H., SHENKIN, S. D., HEWITT, J. & QUINN, T. J. 2021. Cholinesterase inhibitors for vascular dementia and other vascular cognitive impairments: a network meta-analysis. *Cochrane Database of Systematic Reviews*.

BEZERRA, O. C., FRANÇA, C. M., ROCHA, J. A., NEVES, G. A., SOUZA, P. R. M., TEIXEIRA GOMES, M., MALFITANO, C., LOLEIRO, T. C. A., DOURADO, P. M., LLESUY, S., DE ANGELIS, K., IRIGOYEN, M. C. C., ULLOA, L. & CONSOLIM-COLOMBO, F. M. 2017. Cholinergic Stimulation Improves Oxidative Stress and Inflammation in Experimental Myocardial Infarction. *Scientific Reports,* 7**,** 13687.

BHANDARI, B., QUINTANILLA RODRIGUEZ, B. S. & MASOOD, W. 2021. Ischemic Cardiomyopathy. *StatPearls.* Treasure Island (FL): StatPearls Publishing

BIRKS, J. S. & HARVEY, R. J. 2018. Donepezil for dementia due to Alzheimer's disease. *Cochrane Database Syst Rev,* 6**,** Cd001190.

BOROVIKOVA, L. V., IVANOVA, S., ZHANG, M., YANG, H., BOTCHKINA, G. I., WATKINS, L. R., WANG, H., ABUMRAD, N., EATON, J. W. & TRACEY, K. J. 2000. Vagus nerve stimulation attenuates the systemic inflammatory response to endotoxin. *Nature,* 405**,** 458-62.

BRANDT, E. B., BASHAR, S. J. & MAHMOUD, A. I. 2019. Stimulating ideas for heart regeneration: the future of nerve-directed heart therapy. *Bioelectronic Medicine,* 5**,** 8.

BROOMFIELD, C. A., MAXWELL, D., SOLANA, R., CASTRO, C., FINGER, A. & LENZ, D. 1991. Protection by butyrylcholinesterase against organophosphorus poisoning in nonhuman primates. *Journal of Pharmacology and Experimental Therapeutics,* 259**,** 633-638.

BROWN, M. A., MAGEE, L. A., KENNY, L. C., KARUMANCHI, S. A., MCCARTHY, F. P., SAITO, S., HALL, D. R., WARREN, C. E., ADOYI, G. & ISHAKU, S. 2018. Hypertensive disorders of pregnancy: ISSHP classification, diagnosis, and management recommendations for international practice. *Hypertension,* 72**,** 24-43.

BUCHHOLZ, B., DONATO, M., PEREZ, V., IVALDE, F. C., HÖCHT, C., BUITRAGO, E., RODRÍGUEZ, M. & GELPI, R. J. 2012. Preischemic efferent vagal stimulation increases the size of myocardial infarction in rabbits. Role of the sympathetic nervous system. *International journal of cardiology,* 155**,** 490-491.

CALVILLO, L., VANOLI, E., ANDREOLI, E., BESANA, A., OMODEO, E., GNECCHI, M., ZERBI, P., VAGO, G., BUSCA, G. & SCHWARTZ, P. J. 2011. Vagal stimulation, through its nicotinic action, limits infarct size and the inflammatory response to myocardial ischemia and reperfusion. *J Cardiovasc Pharmacol,* 58**,** 500-

7.
CAPILUPI, M. J., KERATH, S. M. & BECKER, L. B. 2020. Vagus Nerve Stimulation and the Cardiovascular System. *Cold Spring Harb Perspect Med,* 10.
CAVALCANTE, G. L., BROGNARA, F., OLIVEIRA, L. V. D. C., LATARO, R. M., DURAND, M. D. T., DE OLIVEIRA, A. P., DA NÓBREGA, A. C. L., SALGADO, H. C. & SABINO, J. P. J. 2021. Benefits of pharmacological and electrical cholinergic stimulation in hypertension and heart failure. *Acta Physiologica,* 232**,** e13663.
CHAPPELL, L. C., CLUVER, C. A. & TONG, S. 2021. Pre-eclampsia. *The Lancet,* 398**,** 341-354.
CHEN, H., ANEMAN, I., NIKOLIC, V., KARADZOV ORLIC, N., MIKOVIC, Z., STEFANOVIC, M., CAKIC, Z., JOVANOVIC, H., TOWN, S. E. L., PADULA, M. P. & MCCLEMENTS, L. 2022. Maternal plasma proteome profiling of biomarkers and pathogenic mechanisms of early-onset and late-onset preeclampsia. *Scientific Reports,* 12**,** 19099.
CHOUDHARY, R. C., AHMED, U., SHOAIB, M., ALPER, E., REHMAN, A., KIM, J., SHINOZAKI, K., VOLPE, B. T., CHAVAN, S., ZANOS, S., TRACEY, K. J. & BECKER, L. B. 2022. Threshold adjusted vagus nerve stimulation after asphyxial cardiac arrest results in neuroprotection and improved survival. *Bioelectronic Medicine,* 8**,** 10.
CHRISTIDI, E. & BRUNHAM, L. R. 2021. Regulated cell death pathways in doxorubicin-induced cardiotoxicity. *Cell Death & Disease,* 12**,** 339.
DE FERRARI, G. M., CRIJNS, H. J. G. M., BORGGREFE, M., MILASINOVIC, G., SMID, J., ZABEL, M., GAVAZZI, A., SANZO, A., DENNERT, R., KUSCHYK, J., RASPOPOVIC, S., KLEIN, H., SWEDBERG, K., SCHWARTZ, P. J. & INVESTIGATORS, F. T. C. M. T. 2010. Chronic vagus nerve stimulation: a new and promising therapeutic approach for chronic heart failure. *European Heart Journal,* 32**,** 847-855.
EVANGELATOV, A., SKROBANSKA, R., MLADENOV, N., PETKOVA, M., YORDANOV, G. & PANKOV, R. 2016. Epirubicin loading in poly (butyl cyanoacrylate) nanoparticles manifests via altered intracellular localization and cellular response in cervical carcinoma (HeLa) cells. *Drug delivery,* 23**,** 2235-2244.
GERBIN, K. A. & MURRY, C. E. 2015. The winding road to regenerating the human heart. *Cardiovasc Pathol,* 24**,** 133-40.
GOLD, M. R., VELDHUISEN, D. J. V., HAUPTMAN, P. J., BORGGREFE, M., KUBO, S. H., LIEBERMAN, R. A., MILASINOVIC, G., BERMAN, B. J., DJORDJEVIC, S., NEELAGARU, S., SCHWARTZ, P. J., STARLING, R. C. & MANN, D. L. 2016. Vagus Nerve Stimulation for the Treatment of Heart Failure. *Journal of the American College of Cardiology,* 68**,** 149-158.
GUO, F., WANG, Y., WANG, J., LIU, Z., LAI, Y., ZHOU, Z., LIU, Z., ZHOU, Y., XU, X., LI, Z., WANG, M., YU, F., HU, R., ZHOU, L. & JIANG, H. 2022. Choline Protects the Heart from Doxorubicin-Induced Cardiotoxicity through Vagal Activation and Nrf2/HO-1 Pathway. *Oxidative Medicine and Cellular Longevity,* 2022**,** 4740931.
HAN, X., LI, W., LI, P., ZHENG, Z., LIN, B., ZHOU, B., GUO, K., HE, P. & YANG, J. 2021. Stimulation of α7 Nicotinic Acetylcholine Receptor by Nicotine Suppresses Decidual M1 Macrophage Polarization Against Inflammation in Lipopolysaccharide-Induced Preeclampsia-Like Mouse Model. *Front Immunol,* 12**,** 642071.
HUNTER, I., TERZIC, D., ZOIS, N. E., OLSEN, L. H. & GOETZE, J. P. 2014. Pig models for the human heart failure syndrome. *Cardiovascular Endocrinology & Metabolism,* 3**,** 15-18.

INTACHAI, K., CHATTIPAKORN, S. C., CHATTIPAKORN, N. & SHINLAPAWITTAYATORN, K. 2022. Acetylcholine exerts cytoprotection against hypoxia/reoxygenation-induced apoptosis, autophagy and mitochondrial impairment through both muscarinic and nicotinic receptors. *Apoptosis,* 27**,** 233-245.

ISSOTINA ZIBRILA, A., WANG, Z., ALI, M. A., OSEI, J. A., SUN, Y., ZAFAR, S., LIU, K., LI, C., KANG, Y. & LIU, J. 2021. Pyridostigmine ameliorates preeclamptic features in pregnant rats by inhibiting tumour necrosis factor-α synthetsis and antagonizing tumour necrosis factor-α-related effects. *Journal of Hypertension,* 39.

JARVIE, J. L., METZ, T. D., DAVIS, M. B., EHRIG, J. C. & KAO, D. P. 2018. Short-term risk of cardiovascular readmission following a hypertensive disorder of pregnancy. *Heart,* 104**,** 1187.

JIAN, W.-X., ZHANG, Z., ZHAN, J.-H., CHU, S.-F., PENG, Y., ZHAO, M., WANG, Q. & CHEN, N.-H. 2020. Donepezil attenuates vascular dementia in rats through increasing BDNF induced by reducing HDAC6 nuclear translocation. *Acta Pharmacologica Sinica,* 41**,** 588-598.

KAKINUMA, Y., AKIYAMA, T., OKAZAKI, K., ARIKAWA, M., NOGUCHI, T. & SATO, T. 2012. A non-neuronal cardiac cholinergic system plays a protective role in myocardium salvage during ischemic insults. *PLoS One,* 7**,** e50761.

KAKINUMA, Y., TSUDA, M., OKAZAKI, K., AKIYAMA, T., ARIKAWA, M., NOGUCHI, T. & SATO, T. 2013. Heart-specific overexpression of choline acetyltransferase gene protects murine heart against ischemia through hypoxia-inducible factor-1α-related defense mechanisms. *J Am Heart Assoc,* 2**,** e004887.

KATARE, R. G., ANDO, M., KAKINUMA, Y., ARIKAWA, M., HANDA, T., YAMASAKI, F. & SATO, T. 2009. Vagal nerve stimulation prevents reperfusion injury through inhibition of opening of mitochondrial permeability transition pore independent of the bradycardiac effect. *The Journal of Thoracic and Cardiovascular Surgery,* 137**,** 223-231.

KHUANJING, T., ONGNOK, B., MANEECHOTE, C., SIRI-ANGKUL, N., PRATHUMSAP, N., ARINNO, A., CHUNCHAI, T., ARUNSAK, B., CHATTIPAKORN, S. C. & CHATTIPAKORN, N. 2021. Acetylcholinesterase inhibitor ameliorates doxorubicin-induced cardiotoxicity through reducing RIP1-mediated necroptosis. *Pharmacological Research,* 173**,** 105882.

KHUANJING, T., PALEE, S., CHATTIPAKORN, S. C. & CHATTIPAKORN, N. 2020. The effects of acetylcholinesterase inhibitors on the heart in acute myocardial infarction and heart failure: From cells to patient reports. *Acta Physiologica,* 228**,** e13396.

KRÖGER, E., MOULS, M., WILCHESKY, M., BERKERS, M., CARMICHAEL, P.-H., VAN MARUM, R., SOUVEREIN, P., EGBERTS, T. & LAROCHE, M.-L. 2015. Adverse Drug Reactions Reported With Cholinesterase Inhibitors:An Analysis of 16 Years of Individual Case Safety Reports From VigiBase. *Annals of Pharmacotherapy,* 49**,** 1197-1206.

LI, H.-C., LUO, K.-X., WANG, J.-S. & WANG, Q.-X. 2020a. Extrapyramidal side effect of donepezil hydrochloride in an elderly patient: a case report. *Medicine,* 99**,** e19443.

LI, X., ZHU, X., LI, B., XIA, B., TANG, H., HU, J. & YING, R. 2022. Loss of α7nAChR enhances endothelial-to-mesenchymal transition after myocardial infarction via NF-κB activation. *Experimental Cell Research,* 419**,** 113300.

LI, Z., LI, X., ZHU, Y., CHEN, Q., LI, B. & ZHANG, F. 2020b. Protective effects of acetylcholine on hypoxia-induced endothelial-to-mesenchymal transition in human cardiac microvascular endothelial cells. *Molecular and Cellular Biochemistry,* 473**,** 101-110.

LIU CHUNG MING, C., BEN-SEFER, E. & GENTILE, C. 2022. Stem Cell-Based 3D Bioprinting for Cardiovascular Tissue Regeneration. *Advanced Technologies in Cardiovascular Bioengineering.* Springer.
LIU CHUNG MING, C., SESPEREZ, K., BEN-SEFER, E., ARPON, D., MCGRATH, K., MCCLEMENTS, L. & GENTILE, C. 2021. Considerations to Model Heart Disease in Women with Preeclampsia and Cardiovascular Disease. *Cells,* 10**,** 899.
LUI, K. O., ZANGI, L. & CHIEN, K. R. 2014. Cardiovascular regenerative therapeutics via synthetic paracrine factor modified mRNA. *Stem cell research,* 13**,** 693-704.
MACHAALANI, R., GHAZAVI, E., DAVID, R. V., HINTON, T., MAKRIS, A. & HENNESSY, A. 2015. Nicotinic acetylcholine receptors (nAChR) are increased in the pre-eclamptic placenta. *Hypertens Pregnancy,* 34**,** 227-40.
MALEK, M. & NEMATBAKHSH, M. 2015. Renal ischemia/reperfusion injury; from pathophysiology to treatment. *J Renal Inj Prev,* 4**,** 20-7.
MEHTA, S., BONGCARON, V., NGUYEN, T. K., JIRWANKA, Y., MALUENDA, A., WALSH, A. P., PALASUBRAMANIAM, J., HULETT, M. D., SRIVASTAVA, R. & BOBIK, A. 2022. An Ultrasound-Responsive Theranostic Cyclodextrin-Loaded Nanoparticle for Multimodal Imaging and Therapy for Atherosclerosis. *Small,* 18**,** 2200967.
MITCHELL, M. J., BILLINGSLEY, M. M., HALEY, R. M., WECHSLER, M. E., PEPPAS, N. A. & LANGER, R. 2021. Engineering precision nanoparticles for drug delivery. *Nature Reviews Drug Discovery,* 20**,** 101-124.
MITRY, M. A. & EDWARDS, J. G. 2016. Doxorubicin induced heart failure: Phenotype and molecular mechanisms. *IJC Heart & Vasculature,* 10**,** 17-24.
MUNASINGHE, P. E., SAW, E. L., REILY-BELL, M., TONKIN, D., KAKINUMA, Y., FRONIUS, M. & KATARE, R. 2023. Non-neuronal cholinergic system delays cardiac remodelling in type 1 diabetes. *Heliyon,* 9**,** e17434.
NORDSTRÖM, P., RELIGA, D., WIMO, A., WINBLAD, B. & ERIKSDOTTER, M. 2013. The use of cholinesterase inhibitors and the risk of myocardial infarction and death: a nationwide cohort study in subjects with Alzheimer's disease. *European Heart Journal,* 34**,** 2585-2591.
POLONCHUK, L., CHABRIA, M., BADI, L., HOFLACK, J.-C., FIGTREE, G., DAVIES, M. J. & GENTILE, C. 2017. Cardiac spheroids as promising in vitro models to study the human heart microenvironment. *Scientific reports,* 7**,** 1-12.
POLONCHUK, L., SURIJA, L., LEE, M. H., SHARMA, P., LIU CHUNG MING, C., RICHTER, F., BEN-SEFER, E., RAD, M. A., MAHMODI SHEIKH SARMAST, H., SHAMERY, W. A., TRAN, H. A., VETTORI, L., HAEUSERMANN, F., FILIPE, E. C., RNJAK-KOVACINA, J., COX, T., TIPPER, J., KABAKOVA, I. & GENTILE, C. 2021. Towards engineering heart tissues from bioprinted cardiac spheroids. *Biofabrication,* 13**,** 045009.
PRATHUMSAP, N., ONGNOK, B., KHUANJING, T., ARINNO, A., MANEECHOTE, C., APAIJAI, N., CHUNCHAI, T., ARUNSAK, B., SHINLAPAWITTAYATORN, K., CHATTIPAKORN, S. C. & CHATTIPAKORN, N. 2022. Acetylcholine receptor agonists provide cardioprotection in doxorubicin-induced cardiotoxicity via modulating muscarinic M2 and α7 nicotinic receptor expression. *Translational Research,* 243**,** 33-51.
REFAAT, A., DEL ROSAL, B., BONGCARON, V., WALSH, A. P. G., PIETERSZ, G., PETER, K., MOULTON, S. E. & WANG, X. 2023. Activated Platelet-Targeted IR780 Immunoliposomes for Photothermal Thrombolysis. *Advanced Functional Materials,* 33**,** 2209019.
REMPE, R., CRAMER, S., HÜWEL, S. & GALLA, H.-J. 2011. Transport of Poly(n-

butylcyano-acrylate) nanoparticles across the blood–brain barrier in vitro and their influence on barrier integrity. *Biochemical and Biophysical Research Communications,* 406**,** 64-69.
REUKOV, V., MAXIMOV, V. & VERTEGEL, A. 2011. Proteins conjugated to poly(butyl cyanoacrylate) nanoparticles as potential neuroprotective agents. *Biotechnol Bioeng,* 108**,** 243-52.
ROCHE, C. D., LIN, H., HUANG, Y., DE BOCK, C. E., BECK, D., XUE, M. & GENTILE, C. 2023. 3D bioprinted alginate-gelatin hydrogel patches containing cardiac spheroids recover heart function in a mouse model of myocardial infarction. *Bioprinting,* 30**,** e00263.
SANKAR, M., KARTHIKEYAN, R. & VIGNESHKUMAR, S. 2023. Synthesis and Characterization of Chitosan Acetylcholine Nanoparticles for Neural Disorders Associated with Cancer Treatment. *Journal of Inorganic and Organometallic Polymers and Materials,* 33**,** 2465-2484.
SAW, E. L., PEARSON, J. T., SCHWENKE, D. O., MUNASINGHE, P. E., TSUCHIMOCHI, H., RAWAL, S., COFFEY, S., DAVIS, P., BUNTON, R., VAN HOUT, I., KAI, Y., WILLIAMS, M. J. A., KAKINUMA, Y., FRONIUS, M. & KATARE, R. 2021. Activation of the cardiac non-neuronal cholinergic system prevents the development of diabetes-associated cardiovascular complications. *Cardiovascular Diabetology,* 20**,** 50.
SEBASTIÃO, M. J., SERRA, M., PEREIRA, R., PALACIOS, I., GOMES-ALVES, P. & ALVES, P. M. 2019. Human cardiac progenitor cell activation and regeneration mechanisms: exploring a novel myocardial ischemia/reperfusion in vitro model. *Stem Cell Research & Therapy,* 10**,** 77.
SENA, E. S., CURRIE, G. L., MCCANN, S. K., MACLEOD, M. R. & HOWELLS, D. W. 2014. Systematic reviews and meta-analysis of preclinical studies: why perform them and how to appraise them critically. *J Cereb Blood Flow Metab,* 34**,** 737-42.
SHARMA, P., MING, C. L. C., WANG, X., BIENVENU, L. A., BECK, D., FIGTREE, G. A., BOYLE, A. & GENTILE, C. 2022. Biofabrication of advanced in vitro 3D models to study ischaemic and doxorubicin-induced myocardial damage. *Biofabrication*.
SIRIPAKKAPHANT, C., ONGNOK, B., PRATHUMSAP, N., KHUANJING, T., CHUNCHAI, T., ARUNSAK, B., PANTIYA, P., CHATTIPAKORN, N. & CHATTIPAKORN, S. C. 2023. Vagus Nerve Stimulation Provides Neuroprotection Against Doxorubicin-induced Chemobrain Via Activations of Both Muscarinic and Nicotinic Acetylcholine Receptors. *Alzheimer's & Dementia,* 19**,** e073548.
SULHEIM, E., BAGHIROV, H., VON HAARTMAN, E., BØE, A., ÅSLUND, A. K., MØRCH, Y. & DAVIES, C. D. L. 2016. Cellular uptake and intracellular degradation of poly (alkyl cyanoacrylate) nanoparticles. *Journal of nanobiotechnology,* 14**,** 1-14.
VIEIRA-ALVES, I., COIMBRA-CAMPOS, L. M. C., SANCHO, M., DA SILVA, R. F., CORTES, S. F. & LEMOS, V. S. 2020. Role of the α7 Nicotinic Acetylcholine Receptor in the Pathophysiology of Atherosclerosis. *Frontiers in Physiology,* 11.
VOLKOVA, M. & RUSSELL, R. 2011. Anthracycline cardiotoxicity: prevalence, pathogenesis and treatment. *Current cardiology reviews,* 7**,** 214-220.
WANG, C., JIANG, H., ZHU, J. & JIN, Y. 2024. A new agent for contrast-enhanced intravascular ultrasound imaging in vitro: polybutylcyanoacrylate nanoparticles with drug-carrying capacity. *Artificial Cells, Nanomedicine, and Biotechnology,* 52**,** 218-228.
WEDN, A. M., EL-BASSOSSY, H. M., EID, A. H. & EL-MAS, M. M. 2021. Modulation of preeclampsia by the cholinergic anti-inflammatory pathway: Therapeutic perspectives. *Biochemical Pharmacology,* 192**,** 114703.

XU, H., SHI, Q., MO, Y., WU, L., GU, J. & XU, Y. 2019. Downregulation of α7 nicotinic acetylcholine receptors in peripheral blood monocytes is associated with enhanced inflammation in preeclampsia. *BMC Pregnancy Childbirth,* 19**,** 188.

ZAFEIROPOULOS, S., AHMED, U., BIKOU, A., MUGHRABI, I. T., STAVRAKIS, S. & ZANOS, S. 2023. Vagus nerve stimulation for cardiovascular diseases: Is there light at the end of the tunnel? *Trends in Cardiovascular Medicine*.